

AD-774 051

DEVELOPMENT OF ENGINEERING DATA ON
THICK-SECTION ELECTRON BEAM WELDED
TITANIUM

John G. Bjeletich

Lockheed Missiles and Space Company,
Incorporated

Prepared for:

Air Force Materials Laboratory

August 1973

DISTRIBUTED BY:

NTIS

National Technical Information Service
U. S. DEPARTMENT OF COMMERCE
5285 Port Royal Road, Springfield Va. 22151

20050203230

Best Available Copy

Security Classification

AD-774051

DOCUMENT CONTROL DATA - R & D

(Security classification of title, body of abstract and indexing annotation must be entered when the overall report is classified)

1. ORIGINATING ACTIVITY (Corporate author) Lockheed Palo Alto Research Laboratory Lockheed Missiles & Space Co., Inc. ✓ Palo Alto, Calif. 94304		2a. REPORT SECURITY CLASSIFICATION Unclassified	
2. REPORT TITLE Development of Engineering Data on Thick-Section Electron Beam Welded Titanium		2b. GROUP	
4. DESCRIPTIVE NOTES (Type of report and inclusive dates) Final Report			
5. AUTHOR(S) (First name, middle initial, last name) John G. Bjeletich			
6. REPORT DATE August 1973		7a. TOTAL NO. OF PAGES 25/99	7b. NO. OF REFS 15
8a. CONTRACT OR GRANT NO. F33615-71-C-1338		8b. ORIGINATOR'S REPORT NUMBER(S) LMSC D352462 ✓	
8c. PROJECT NO. 7381		9d. OTHER REPORT NO(S) (Any other numbers that may be assigned this report) AFML-TR-73-197 ✓	
10. DISTRIBUTION STATEMENT Approved for public release; distribution unlimited			
11. SUPPLEMENTARY NOTES		12. SPONSORING MILITARY ACTIVITY Air Force Materials Laboratory Wright-Patterson Air Force Base, Ohio	
13. ABSTRACT Some high performance aerospace structures are fabricated of titanium plate. Presently, Ti-6Al-4V, in the mill-annealed condition, is the titanium alloy most commonly used for this application. A potential choice is the recently developed alloy, Beta III, in the solution treated and aged condition. This report provides a vital portion of the basic engineering data necessary for the design of reliable and efficient airframe structures involving electron-beam weldments in the two alloys. Tensile, fracture toughness, and subcritical crack growth properties of both base metal and weldments have been obtained for 1- and 2-in. Ti-6Al-4V and 1-in. Beta III plate. Test temperatures ranged from -65°F to 175°F and the test environments included laboratory air, water, salt water and JP-4 jet fuel. The concept of stress intensity factors from linear elastic fracture mechanics is used to quantitatively assess the load carrying capacity and crack growth resistance of the test materials. Fracture toughness results, K_{IC} , K_C , and K_{IE} , and tensile properties are tabulated while the fatigue crack propagation and stress corrosion cracking rates, da/dN and da/dt , respectively, are presented in a graphic format.			

DD FORM 1473

Best Available Copy

Security Classification

UNCLASSIFIED

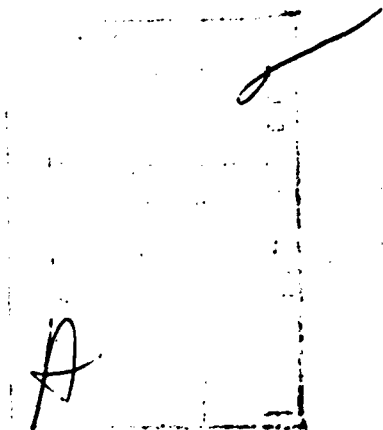
Security Classification

14. KEY WORDS	LINK A		LINK B		LINK C	
	ROLE	WT	ROLE	WT	ROLE	WT
<p>Titanium, Ti-6Al-4V (MA), Beta III (STA) Thick Section, Weldments, Electron Beam, Tensile Properties, Fracture Toughness, Compact-Tension, Single Edge Notch, Part- Through Thickness, Surface-Flaw, da/dN, da/dt, K_{ISCC}, K_{IC}, K_{IC}, 3.5% NaCl, H₂O, JP4</p>						

ia

NOTICE

When Government drawings, specifications, or other data are used for any purpose other than in connection with a definitely related Government operation, the United States Government thereby incurs no responsibility nor any obligation whatsoever; and the fact that the government may have formulated, furnished, or in any way supplied the said drawings, specifications, or other data, is not to be regarded by implication or otherwise as in any manner licensing the holder or any other person or corporation, or conveying any rights or permission to manufacture, use, or sell any patented invention that may in any way be related thereto.



Copies of this report should not be returned unless return is required by security considerations, contractual obligations, or notice on a specific document.

ic

DEVELOPMENT OF ENGINEERING DATA
ON THICK-SECTION ELECTRON BEAM
WELDED TITANIUM

J. G. Bjeletich

Approved for public release; distribution unlimited


ic

PREFACE

This report was prepared by the Lockheed Palo Alto Research Laboratory, Palo Alto, California, under Contract F33615-71-C-1338. This contract was performed in the period of March 1971 to June 1973 under Project No. 7381, "Materials Applications," Task No. 738106, "Engineering and Design Data." The work was administered under the direction of the Air Force Materials Laboratory, Air Force Systems Command, Wright-Patterson Air Force Base, Ohio, by Mr. Clayton Harnsworth (AFML/MXE), technical manager.

The program was conducted by the Metallurgy and Composites Laboratory, T. E. Tietz, Manager, under the direction of Mr. John G. Bjeletich, Project Leader. Individuals participating in this investigation and the areas of their contributions were: John G. Bjeletich, Project Leader; T. M. Morton, Data Analysis; and R. M. Harrington, Testing. Other contributors included: A. T. Devinroy and R. L. Boorn, Testing; A. R. Hansen, Metallography; G. W. Martin, Microprobe Analysis; D. Andrade, Jr., and R. J. Galvez, Jr., Non-Destructive Inspection; and W. P. McGregor, Solar Aircraft, Div. of International Harvester Co., San Diego, Calif., Electron Beam Welding. Program supervision was provided by R. E. Lewis of the Fracture Behavior Group.

This technical report has been reviewed and is approved.


A. Olevitch
Chief, Materials Engineering Branch
Materials Support Division
Air Force Materials Laboratory

SUMMARY

Some high performance aerospace structures are fabricated of titanium plate. Presently, Ti-6Al-4V, in the mill annealed condition, is the titanium alloy most commonly used for this application. A potential choice is the recently developed alloy, Beta III, in the solution treated and aged condition. This report provides a vital portion of the basic engineering data necessary for the design of reliable and efficient airframe structures involving electron beam weldments in the two alloys. Tensile, fracture toughness, and sub-critical crack growth properties of both base metal and weldments have been obtained for 1- and 2-in. Ti-6Al-4V plate and 1-in. Beta III plate.

In Ti-6Al-4V, the 2-in. plate was found to be substantially tougher than the 1-in. plate. This disparity in fracture resistance is principally attributed to microstructural differences in the two plates. The microstructure in the 2-in. plate consists of coarse acicular α while fine equiaxed α predominates in the microstructure of the 1-in. plate.

For the two alloys, the fracture toughness, K_{IC} , ranges from a discouragingly low value of 26 ksi-in^{1/2} in Beta III electron beam weldments to unusually high values in excess of 100 ksi-in^{1/2} in the 2-in thick Ti-6Al-4V base metal.

At ΔK values from approximately 10 to 12 ksi-in^{1/2} and above, lowering the frequency of cyclic loading in salt water from 10 to 0.1 Hz significantly increases da/dN in the 1-in Ti-6Al-4V base metal. This same material, which is crystallographically textured, is susceptible to stress corrosion cracking in JP4 jet fuel.

In tests duplicated at test temperatures of -65°F, room, and 175°F much of the da/dN , da/dt and K_{ISCC} data appear to be more directly dependent upon the toughness of the specific specimen being evaluated than upon temperature.

In similar environments, the 1-in Beta III base metal exhibits a substantial advantage over the 1-in Ti-6Al-4V base metal in strength, toughness and resistance to crack growth. When joined by electron beam welding, Beta III, while maintaining nearly all of its base metal strength, has poor flaw tolerance and undesirable crack growth characteristics due to the formation of a microstructural imperfection during weld zone solidification.

Part-through thickness fatigue crack growth rate data are successfully correlated with the results obtained from tests of compact tension specimens. Based upon this correlation, a reasonable analysis of spectrum fatigue loaded surface-flawed specimens is attained. The analysis is based on the da/dN data from compact tension specimens and an empirical equation to describe crack propagation at all stress ratios.

Methods of using the appropriate toughness, da/dN , da/dt and K_{ISCC} data to formulate improved specifications are appended, with particular concern for flaws or defects in electron beam weldments.

TABLE OF CONTENTS

Section	Page
I INTRODUCTION	1
II MATERIALS PROCESSING	2
1. Materials	2
a. Ti-6Al-4V Alloy	2
b. Beta III Titanium	3
2. Weldment Preparation	3
3. Repair Welding	5
4. Nondestructive Inspection	5
5. Thermal Treatments	7
III TESTING	9
1. Specimen Preparation	9
2. Test Schedule	10
3. Test Equipment	11
4. Test Procedures	12
a. Tensile Property Tests	13
b. Axial Fatigue Tests	13
c. Fracture Toughness Tests	14
(1) Compact Tension	14
(2) Single-Edge Notch	14
(3) Part-Through Thickness	15
d. Fatigue Crack Growth	15
(1) Compact Tension Specimens	15
(2) Part-Through Thickness Specimens	17
e. Environmental Crack Growth	17

Section	Page
f. Spectrum Fatigue	18
g. Natural Defect	18
IV RESULTS AND DISCUSSION	19
1. Materials	19
2. Tensile Property Tests	20
3. Axial Fatigue Property Tests	22
4. Fracture Toughness	22
a. Compact Tension Specimens	22
b. Single-Edge Notch	26
c. Part-Through Thickness Specimens	27
5. Fatigue Crack Growth Tests	29
a. Compact Tension Specimens	29
b. Part-Through Thickness Specimens	39
6. Environmental Crack Growth and Threshold Stress Intensity	40
7. Spectrum Fatigue	45
8. Natural Defects	47
V CONCLUSIONS	48
VI RECOMMENDATIONS	49
REFERENCES	50
APPENDIX	173

LIST OF ILLUSTRATIONS

FIGURE		Page
1	Microstructure of 1-In.-Thick Ti-6Al-4V Mill Annealed Plate	52
2	Microstructure of 2-In.-Thick Ti-6Al-4V Mill Annealed Plate	53
3	Microstructure of 1-In.-Thick Beta III Titanium Solution-Treated Plate	54
4	Cross-Section of 1-In.-Thick Weldments of Ti-6Al-4V Alloy	55
5	Tensile Test Specimen Configuration	56
6	Axial Fatigue Test Specimen Configuration	57
7	Compact Tension Test Specimen Configuration for K_{IC} Testing	58
8	Wedge Opening Load Test Specimen Configuration for Crack Growth Rate Tests	59
9	Single-Edge Notch Specimen Configuration for K_C Testing	60
10	Part-Through Thickness Specimen Configuration for K_{IC} and da/dt Testing	61
11	Test Specimen for Natural Defect Evaluation	62
12	Compact Tension K_{IC} Test Record	63
13	Typical Load-Crack Opening Displacement Record, Specimen 4-2, 2-In.-Thick Ti-6Al-4V Base Metal, T-L Orientation	65
14	A da/dN Test Specimen with Automatic Crack Follower in Place	66
15	Typical Autographic Plot of Crack Length vs. Cycles	67
16	A da/dt Test Specimen with Manual Crack Follower in Place	68

FIGURE		Page
17	Fatigue Load Spectrum	69
18	Microstructures of Ti-6Al-4V Electron Beam Weldments	70
19	Typical Microstructures of 1-In.-Thick Ti-6Al-4V E. B. Weldments with Single Joining Pass	71
20	Typical Microstructures of 1-In.-Thick Ti-6Al-4V E. B. Weldments with Multiple Passes	72
21	Heat-Affected Zone Hardness Survey Results and Locations	73
22	Microstructure of Beta III Electron Beam Weldment	74
23	Microstructure of Fusion Zone Centerline in E. B. Weld Beta III	75
24	Average Tensile Properties of Starting Test Materials at Room Temperature	76
25	Variation of the Average Longitudinal Tensile Properties of Ti-6Al-4V 1-In. Plate (MA) Base Metal with Test Temperature	77
26	Variation of the Average Transverse Tensile Properties of Ti-6Al-4V 1-In. Plate (MA) Base Metal with Test Temperature	78
27	Variation of the Average Tensile Properties of Ti-6Al-4V 1-In. Plate E. B. Weldments with Test Temperature	79
28	Variation of the Average Transverse Tensile Properties of Beta III Titanium 1-In. Plate (STA) Base Metal with Test Temperature	80
29	Variation of the Average Tensile Properties of Beta III Titanium 1-In. Plate (STA) E. B. Weldments with Test Temperature	81
30	S-N Curve for Ti-6Al-4V 1-In. Plate (MA) Base Metal	82
31	S-N Curve for E. B. Welded Ti-6Al-4V 1-In. Plate	83

FIGURE

Page

32	Weld Zone Single-Edge Notch Fracture Toughness of E. B. Welded Ti-6Al-4V 1-In. Plate vs. Test Specimen Thickness at Room Temperature	84
33	Weld Zone Single-Edge Notch Fracture Toughness of E. B. Welded Ti-6Al-4V 1-In. Plate vs. Test Specimen Thickness at -65°F	85
34	Weld Zone Single-Edge Notch Fracture Toughness of E. B. Welded Beta III Titanium 1-In. Plate (STA) vs. Test Specimen Thickness at Room Temperature	86
35	Weld Zone Single-Edge Notch Fracture Toughness of E. B. Welded Beta III Titanium 1-In. Plate (STA) vs. Test Specimen Thickness at -65°F	87
36	Ti-6Al-4V Base Metal, 1.0-In. MA Plate, T-L Direction, CTT Specimens, Room Temperature, Laboratory Air and Salt Water Environments	88
37	Ti-6Al-4V Base Metal, 1.0-In. MA Plate, T-L Direction, CTT Specimens, -65° Laboratory Air Environment	89
38	Ti-6Al-4V Base Metal, 1.0-In. MA Plate, T-L Direction, CTT Specimens, 175° Laboratory Air and Salt Water Environments	90
39	Ti-6Al-4V E. B. Weldment, 1.0-In. Plate, HAZ, T-L Direction, CTT Specimens, Room Temperature Laboratory Air Environment	91
40	Ti-6Al-4V E. B. Weldment, SR, 1.0-In. Plate, HAZ, T-L Direction, CTT Specimens, Room Temperature Water and Salt Water Environments	92
41	Ti-6Al-4V E. B. Weldment, SR, 1.0-In. Plate, HAZ, T-L Direction, CTT Specimens, Room Temperature JP4 Environment	93
42	Ti-6Al-4V E. B. Weldment, SR, 1.0-In. Plate, HAZ, T-L Direction, CTT Specimens, -65°F Laboratory Air Environment	94
43	Ti-6Al-4V E. B. Weldment, SR, 1.0-In. Plate, HAZ, T-L Direction, CTT Specimens, 175°F Laboratory Air Environment	95

FIGURE

Page

44	Ti-6Al-4V E. B. Weldment, SR, 1.0-In. Plate, HAZ, T-L Direction, CTT Specimens, 175°F Water and Salt Water Environments	96
45	Ti-6Al-4V E. B. Weldment, 1.0-In. Plate, WZ, T-L Plate Directions, CTT Specimens, Room Temperature Laboratory Air Environment	97
46	Ti-6Al-4V E. B. Weldment, SR, 1.0-In. Plate, WZ, T-L Plate Directions, CTT Specimens, Room Temperature Water Environment	98
47	Ti-6Al-4V E. B. Weldment, SR, 1.0-In. Plate, WZ, T-L Plate Directions, CTT Specimens, Room Temperature Salt Water Environment	99
48	Ti-6Al-4V E. B. Weldment, SR, 1.0-In. Plate, WZ, T-L Plate Directions, CTT Specimens, Room Temperature JP4 Environment	100
49	Ti-6Al-4V E. B. Weldment, SR, 1.0-In. Plate, WZ, T-L Plate Directions, CTT Specimens, -65°F Laboratory Air Environment	101
50	Ti-6Al-4V E. B. Weldment, SR, 1.0-In. Plate, WZ, T-L Plate Directions, CTT Specimens, 175°F Laboratory Air Environment	102
51	Ti-6Al-4V E. B. Weldment, SR, 1.0-In. Plate, WZ, T-L Plate Directions, CTT Specimens, 175°F Water and Salt Water Environments	103
52	Beta III Titanium Base Metal, 1.0-In. STA Plate, T-L Direction, CTT Specimen, Room Temperature Laboratory Air Environment	104
53	Beta III Titanium Base Metal, 1.0-In. STA Plate, T-L Direction, CTT Specimen, Room Temperature 3.5% NaCl Solution Environment	105
54	Beta III Titanium Base Metal, 1.0-In. STA Plate, T-L Direction, CTT Specimen, -65°F Laboratory Air Environment	106
55	Beta III Titanium Base Metal, 1.0-In. STA Plate, T-L Direction, CTT Specimen, 175°F Laboratory Air Environment	107

FIGURE

Page

56	Beta III Titanium E. B. Weldment, STA, 1.0-In. Plate, HAZ, T-L Direction, CTT Specimen, Room Temperature Laboratory Air Environment	108
57	Beta III Titanium E. B. Weldment, STA, 1.0-In. Plate, HAZ, T-L Direction, CTT Specimen, -65°F Laboratory Air Environment	109
58	Beta III Titanium E. B. Weldment, STA, 1.0-In. Plate, HAZ, T-L Direction, CTT Specimen, 175°F Laboratory Air Environment	110
59	Beta III Titanium E. B. Weldment, STA, 1.0-In. Plate, WZ, T-L Plate Directions, CTT Specimen, Room Temperature Laboratory Air Environment	111
60	Beta III Titanium E. B. Weldment, STA, 1.0-In. Plate, WZ, T-L Plate Directions, CTT Specimen, Room Temperature 3.5% NaCl Solution Environment	112
61	Beta III Titanium E. B. Weldment, STA, 1.0-In. Plate Directions, CTT Specimen, -65°F Laboratory Air Environment	113
62	Beta III Titanium E. B. Weldment, STA, 1.0-In. Plate, WZ, T-L Plate Directions, CTT Specimen, 175°F Laboratory Air Environment	114
63	Ti-6Al-4V Base Metal, 1.0-In. MA Plate, T-S Direction, PTT Specimens, Room Temperature Laboratory Air and Salt Water Environments	115
64	Ti-6Al-4V E. B. Weldment, AW, 1.0-In. Plate, HAZ, T-S Direction, PTT Specimens, Room Temperature Laboratory Air and Salt Water Environments	116
65	Ti-6Al-4V E. B. Weldment, AW, 1.0-In. Plate, WZ, T-S Plate Directions, PTT Specimens, Room Temperature Laboratory Air and Salt Water Environments	117
66	Environmental Crack Growth Rate Data for Ti-6Al-4V Base Metal, 1.0-In. MA Plate, T-L Direction, in 3.5 % NaCl at Room Temperature	118

FIGURE		Page
67	Environmental Crack Growth Rate Data for Ti-6Al-4V Base Metal, 1.0-In. MA Plate, T-L Direction, in 3.5% NaCl at 175°F	119
68	Environmental Crack Growth Rate Data for Ti-6Al-4V Base Metal, 1.0-In. MA Plate, T-L Direction, in JP4 at Room Temperature	120
69	Environmental Crack Growth Rate Data for Ti-6Al-4V E. B. Weldment, SR, 1.0-In. Plate, HAZ, T-L Direction, in 3.5% NaCl at Room Temperature	121
70	Environmental Crack Growth Rate Data for Ti-6Al-4V E. B. Weldment, SR, 1.0-In. Plate, HAZ, T-L Direction, in 3.5% NaCl at 175°F	122
71	Environmental Crack Growth Rate Data for Ti-6Al-4V E. B. Weldment, SR, 1.0-In. Plate, WZ, T-L Plate Directions, in 3.5% NaCl at Room Temperature	123
72	Environmental Crack Growth Rate Data for Ti-6Al-4V E. B. Weldment, SR, 1.0-In. Plate, WZ, T-L Plate Directions, in 3.5% NaCl at 175°F	124
73	Environmental Crack Growth Rate Data for Beta III Titanium Base Metal, 1.0-In. STA Plate, T-L Direction, in 3.5% NaCl at Room Temperature	125
74	Environmental Crack Growth Rate Data for Beta III Titanium Base Metal, 1.0-In. STA Plate, T-L Direction, in 3.5% NaCl at 175°F	126
75	Environmental Crack Growth Rate Data for Beta III Titanium E. B. Weldment, ST, 1.0-In. Plate, WZ, T-L Directions, in 3.5% NaCl at Room Temperature	127
76	Fracture Surfaces and Spectrum Fatigue Results for Ti-6Al-4V E. B. Weldment, SR, 1.0-In. Plate, Heat-Affected Zone, T-S Direction, PTT Specimens	128
77	Fracture Surfaces and Spectrum Fatigue Results for Ti-6Al-4V E. B. Weldment, SR, 1.0-In. Plate, Weld Fusion Zone, T-S Direction, Shallow, Precracked PTT Specimens	129

FIGURE		Page
78	Fracture Surfaces and Spectrum Fatigue Results for Ti-6Al-4V E. B. Weldments, SR, 1.0-In. Plate, Weld Fusion Zone, T-S Direction, Deep Precracked PTT Specimens, Precracks	130
79	Spectrum Fatigue Results with Predicted Life Curves	131
80	Crack Growth Rate Equation for Fatigue Life Prediction Model in Heat-Affected Zone	132
81	Crack Growth Rate Equation for Fatigue Life Prediction Model in Weld-Fusion Zone	133

LIST OF ILLUSTRATIONS - APPENDIX

A-1	Allowable Flaw Sizes in 1-in. Thick Ti-6Al-4V E. B. Weldments for Inert Service Environments	177
A-2	Allowable Flaw Sizes in 1-in. Thick Ti-6Al-4V E. B. Weldments for a Service Environment of 3.5 Percent NaCl	178

LIST OF TABLES

TABLE		Page
I	Vendor's Certification Data of Test Materials	134
II	Schedule for Electron Beam Welding of Ti-6Al-4V and Beta III Alloy 1-In. Plate	135
III	Schedule for Electron Beam Welding of Ti-6Al-4V 2-In. Plate	136
IV	Aging Response of 1-In.-Thick Beta III Titanium Plate	137
V	Schedule of Specimens Tested	138
VI	Tensile Properties of Ti-6Al-4V Two-Inch Plate (MA) Base Metal at R.T.	139
VII	Tensile Properties of Ti-6Al-4V Two-Inch Plate (MA) E. B. Weldments at R.T.	140
VIII	Tensile Properties of Ti-6Al-4V One-Inch Plate (MA) Base Metal at R.T.	141
IX	Tensile Properties of Ti-6Al-4V One-Inch Plate (MA) Base Metal at -65°F	142
X	Tensile Properties of Ti-6Al-4V One-Inch Plate (MA) Base Metal at 175°F	143
XI	Tensile Properties of Ti-6Al-4V One-Inch Plate E. B. Weldments at R.T.	144
XII	Tensile Properties of Ti-6Al-4V One-Inch Plate E. B. Weldments at -65°F	145
XIII	Tensile Properties of Ti-6Al-4V One-Inch Plate E. B. Weldments at 175°F	146
XIV	Tensile Properties of Beta III Titanium One-Inch Plate (STA) Base Metal at R.T.	147
XV	Tensile Properties of Beta III Titanium One-Inch Plate (STA) Base Metal at -65°F	148

TABLE		Page
XVI	Tensile Properties of Beta III Titanium One-Inch Plate (STA) Base Metal at 175°F	149
XVII	Tensile Properties of Beta III Titanium One-Inch Plate (STA) E. B. Weldments at R.T.	150
XVIII	Tensile Properties of Beta III Titanium One-Inch Plate (STA) E. B. Weldments at -65°F	151
XIX	Tensile Properties of Beta III Titanium One-Inch Plate (STA) E. B. Weldments at 175°F	152
XX	Axial Fatigue Life of Ti-6Al-4V One-Inch Plate (MA) Base Metal	153
XXI	Axial Fatigue Life of E. B. Welded Ti-6Al-4V One-Inch Plate	154
XXII	ASTM E399-72 Criteria for a Valid Plane Strain Fracture Toughness Result	155
XXIII	Fracture Toughness of Ti-6Al-4V Two-Inch Plate (MA) Base Metal at R.T.	156
XXIV	Fracture Toughness of Ti-6Al-4V Two-Inch Plate (MA) Base Metal at -65°F	157
XXV	Fracture Toughness of Ti-6Al-4V Two-Inch Plate (MA) Base Metal at 175°F	158
XXVI	Heat-Affected Zone Fracture Toughness of E. B. Welded Ti-6Al-4V Two-Inch Plate at R.T.	159
XXVII	Heat-Affected Zone Fracture Toughness of E. B. Welded Ti-6Al-4V Two-Inch Plate at -65°F	160
XXVIII	Heat-Affected Zone Fracture Toughness of E. B. Welded Ti-6Al-4V Two-Inch Plate at 175°F	161
XXIX	Weld Zone Fracture Toughness of E. B. Welded Ti-6Al-4V Two-Inch Plate at R.T.	162
XXX	Weld Zone Fracture Toughness of E. B. Welded Ti-6Al-4V Two-Inch Plate at -65°F	163
XXXI	Weld Zone Fracture Toughness of E. B. Welded Ti-6Al-4V Two-Inch Plate at 175°F	164

TABLE		Page
XXXII	Weld Zone Fracture Toughness of E. B. Welded Ti-6Al-4V One-Inch Plate at R.T.	165
XXXIII	Fracture Toughness of Beta III Titanium One-Inch Plate (STA) Base Metal and E. B. Weldments at R.T.	166
XXXIV	Weld Zone Single-Edge Notch Fracture Toughness of E. B. Welded Ti-6Al-4V One-Inch Plate at R.T.	167
XXXV	Weld Zone Single-Edge Notch Fracture Toughness of E. B. Welded Ti-6Al-4V One-Inch Plate at -65°F	168
XXXVI	Weld Zone Single-Edge Notch Fracture Toughness of E. B. Welded Beta III Titanium One-Inch Plate at R.T.	169
XXXVII	Weld Zone Single-Edge Notch Fracture Toughness of E. B. Welded Beta III Titanium One-Inch Plate at -65°F	170
XXXVIII	Part-Through Thickness Fracture Toughness of Ti-6Al-4V One-Inch Plate Base Metal and E. B. Weldments at R.T.	171
XXXIX	Natural Defect Results	172

LIST OF TABLES - APPENDIX

A-I	Fatigue Crack Growth Parameters in Inert Environments	179
A-II	Fatigue Crack Growth Parameters in 3.5 Percent NaCl Solution	180

SECTION I

INTRODUCTION

The objective of this program is to develop the basic tensile and fracture toughness data necessary for the design of an electron-beam-welded primary airframe structure of titanium using mill-annealed (MA) Ti-6Al-4V and solution-treated and aged (STA) Beta III (Ti-11.5 Mo-6Zr-4.5 Sn) alloys. Useful values of the fracture resistance characteristics of these materials could also serve as the basis for the revision of existing specifications or the drafting of new specifications for electron-beam-welded titanium airframe structures.

In fabricated structural members, particularly those joined by welding, the presence of pre-existing defects is not an unlikely occurrence. Flaw-like defects behave as cracks and can readily extend under the influence of cyclic loads or at certain combinations of load and environment. Even defects with relatively large root radii require only a small number of cyclic load excursions to generate a fatigue crack (1).^{*} Consequently, to insure a safe operating lifetime, provisions in the design philosophy must account for potentially detrimental defects or pre-existing flaws and their behavior. This requires a knowledge of the load-carrying capacity and crack propagation resistance of the structural material in the presence of flaws. These material characteristics must be quantified in engineering terms and known over the entire range of operating conditions; i.e., temperature, stress, and environment.

In the work reported herein, fracture mechanics criteria and the concept of stress intensity factors are used to assess the fracture resistance and subcritical crack growth behavior in the two titanium alloys. Test temperatures range from -65°F to 175°F and the test environments include laboratory air, water, salt water and JP4 jet fuel. Tensile, fracture and crack growth properties evaluated in the program are the following:

o Yield Strength	F _{TY}
o Ultimate Strength	F _{TU}
o Elongation	E _L
o Reduction of Area	R of A
o Modulus of Elasticity	E
o Plane Strain Fracture Toughness	K _{IC}
o Part-Through Thickness Fracture Toughness	K _{IE}
o Single Edge Notch Fracture Toughness	K _{IC}
o Threshold Stress Intensity Factor	K _{ISCC}
o Fatigue Crack Propagation Rate	da/dN
o Stress Corrosion Crack Growth Rate	da/dt

The data from these tests are essential, also, in the formulation of meaningful accept-reject criteria for electron beam weldments of the titanium alloys. A discussion of how the data may be used for this purpose is included in the appendix.

^{*} Numbers in parenthesis refer to references.

SECTION II

MATERIALS PROCESSING

1. MATERIALS

The test materials consisted of the alpha-beta titanium alloy, Ti-6Al-4V, and the beta titanium alloy, Ti-11.5 Mo-6 Zr, 4.5 Sn (trade name Beta III). This section describes the processing history of the materials prior to their incorporation into the scheduled test plan.

a. Ti-6Al-4V Alloy

The primary test material (1- and 2-in. plate of mill annealed Ti-6Al-4V) was purchased from G. O. Carlson, Inc., Thorndale, Pa. All of the 1-in. plate was from a single heat, A41642-1, and all of the 2-in. plate was from another heat, HC-442-1B.

The vendor's certification report lists the composition and properties given in Table I. The processing history, as certified and reported by the vendor, is as follows:

- o Heat A/1642-1. A 30-in.-diameter ingot, approximately 90-in. long, was rolled into a slab having cross-sectional dimensions of 45-in. by 8-in. The slab was conditioned, then cut to the following dimensions: 50-in. long, 45-in. wide, and 8-in. thick. The slab weight was 2885 lb. Finally, the slab was rolled into one piece of 1-in. plate, 192-in. long and 72-in. wide.
- o Heat HC-442-1B. A 34-in.-diameter ingot, approximately 90-in. long, was rolled into a slab having cross-sectional dimensions of 45-in. by 6-in. The slab was conditioned, then cut to the following dimensions: 96-in. long, 45-in. wide, and 6-in. thick. The slab weight was 4360 lb. Finally, the slab was rolled into one piece of 2-in. plate, 260-in. long and 72-in. wide.

In both heats, the starting temperature for rolling the ingot was 2025°F \pm 25° and the starting temperature for rolling the slab was 2000°F \pm 25°. Prior to heat treating, the plates were hot flattened at a uniform temperature of 1650°F. The annealing temperature was 1325°F \pm 25°. Final reduction was accomplished in a 4-high mill. No reheats were required in the processing.

The plates were cut by the material distributor into 24-in. panels for con-

venience in preparation of weldments and in widths varying from 1.5 to 9.5 inches to accommodate the subsequent extraction of test specimens. Each panel was identified with an alphanumeric code and forwarded to NDI processing for nondestructive inspection. Representative samples were removed from one selected panel of each thickness for metallographic evaluation. The representative microstructures of the two plate thicknesses are shown in Figures 1 and 2.

b. Beta III Titanium Alloy

The second test material - Beta III titanium alloy - was provided by Colt Industries Crucible, Inc., Stainless Steel Division, Midland, Pa. In the quantities required for the test program, the maximum thickness plate available from the producer was 1-in. Consequently, all of the Beta III test material was 1-in.-thick plate from one heat (K-50776) and in the solution treated condition.

- o Heat K-50776. The starting ingot, 32-in. in diameter and weighing 9660 lbs., was forged into a 20-in. by 20-in. bloom. A segment was parted from the parent bloom and forged to a slab, 38-in. by 4.0-in. by slab length. After forging, the slab was hot rolled to 38-in. by 1.00-in. by slab length. The hot-rolled plate was solution treated at 1350°F, then water quenched. Prior to and following the solution treating and quenching operations, the plate was grit blasted to remove any developed scale.

For convenience in weldment preparation, the material was furnished by the supplier in 24-in. long panels. The panels varied in width from 1.5 to 9.5 inches to accommodate the subsequent extraction of test specimens. The as-received test panels exhibited considerable distortion. Panel components of subsequent weldments were straightened by reverse three-point loading prior to joining by electron beam welding. After strengthening, each panel was identified with an alphanumeric code and forwarded to NDI processing for nondestructive inspection. A representative sample was removed from one panel for metallographic evaluation. The representative microstructure is shown in Figure 3.

2. WELDMENT PREPARATION

Electron beam welding of panels to provide weldment test specimens of the Ti-6Al-4V and Beta III titanium test materials was performed by the Solar Aircraft Division of International Harvester Co. at San Diego, California.

The requirements and specifications for performing the electron beam welding included: (1) a Sciaky 60KV-30KW unit, preferably with a triode gun design; (2) a vacuum chamber capable of accepting the largest weldment (24-in. in the weld direction by 19-in.) and capable of maintaining a pressure of 10^{-5} to 10^{-4} mm of mercury; (3) welding to be from one side only; (4) under-

cutting to be limited on both the face and root surfaces to less than 10 mils; and (5) drop-through to be controlled by some adequate method; e.g., a backup of chips or a strip of similar material. In addition, the performer was instructed to strive for a quality of weldment that is acceptable for application as a high-integrity, highly stressed airplane wing box frame component in all the welded panels except one. The excepted panel was to have defects deliberately introduced during joining. These defects were to typify those most likely to be encountered in an electron beam weldment.

a. One-Inch-Thick Test Material

Procedure and welding conditions were the same for joining 1-in. thickness of both test materials, Ti-6Al-4V and Beta III. Welding was performed at an applied voltage of 36.5 kilovolts and a beam current of 375 milliamps. Run-on and run-off tabs as well as backup strips of the same material as the panels were tack-welded to the plates prior to performing the joining pass with the electron beam gun. The Ti-6Al-4V backup strips were 1/4-in. thick and 1-in. wide, and the Beta III backup strips were 1/8-in. thick and 1-in. wide. All faying surfaces were previously milled flat. All components were cleaned with an acetone wipe before welding. After the joining pass, a wash or cosmetic pass was performed at the welding voltage of 25 kilovolts and a beam current of 200 milliamps. The complete welding schedule for the electron beam joining of the 1-in.-thick test materials is given in Table II.

b. Two-Inch-Thick Test Material

The 2-in.-thick Ti-6Al-4V plate was welded at an applied voltage of 45 kilovolts and a beam current of 450 milliamps. Run-on and run-off tabs as well as 1/4-in.-thick and 1-in.-wide backup strips all of Ti-6Al-4V were tack-welded to the plates prior to performing the joining pass with the electron beam gun. The faying surfaces of the plate panels were milled flat prior to shipment to Solar. Before welding, all the components, including tabs and backup strips, were cleaned with an acetone wipe. No wash pass was performed. The complete welding schedule for the electron beam joining of 2-in.-thick Ti-6Al-4V is given in Table III.

c. One-Inch-Thick Defective Weldment

In an attempt to supply a weldment intentionally containing a variety of natural defects, the weldment procedure was varied during the fabrication of one weldment of 1-in.-thick Ti-6Al-4V. The basic welding conditions remained the same as those previously described for 1-in.-thick test material. However, various materials (i.e., grease, a steel shim, and grit) were placed between the faying surfaces along various segments of the weld length and welded over. In addition, one segment of weld length contained "arc outs", where the electron beam current was intentionally shut off momentarily.

3. REPAIR WELDING

After 100% radiographic inspection, 10 electron beam welded Ti-6Al-4V test panels - seven, 1-in.-thick, two 2-in.-thick, and one short transverse panel - were found to be defective and unusable for specimen preparation. These panels were supposedly representative of aircraft quality weldments. To salvage the defective weldments, methods of sectioning the 1- and 2-in.-thick panels along the 24 in. of weld length were explored and found to be economically impractical. Likewise, obtaining new base metal panels to be joined by electron beam welding was also undesirable. In addition to its economic disadvantage, the introduction of metallurgical variables associated with a different lot of material could lead to objectionable effects in the test data. As a result, the most viable decision was to repair the weldments by eliminating the defects with an additional pass or passes of the electron beam.

During the exploration of economically feasible sectioning methods, one of the unintentionally defective weldments was bisected along its entire weld length. The bisected panels, with their outside edges milled flat to act as faying surfaces, were submitted for rejoining along with the nine defective weldments to be repaired. The two panels were joined with the same welding procedures used in the original joining. Subsequent radiographic inspection showed this weldment to be defect free.

The additional welding pass or passes on the other nine unintentionally defective weldments was also accomplished with the same welding parameters as the original joining (see Tables II and III). Upon completion of the first repair pass, the welds were radiographically inspected for defects. Of the nine weldments repaired, four were found to be defective. A second repair pass, again with the same welding parameters as the original, was performed on the four weldments still containing flaws. Subsequently, these weldments were radiographed and deemed to be free of defects. After the final repair passes, a wash or cosmetic pass was performed at a welding voltage of 25 kilovolts and a beam current of 200 milliamperes. The wash pass parameters are shown on the bottom portion of Table II.

Arc-outs occurred during the repair welding of one of the weldments that required only one complete repair pass. When this happened, the weld was restored and the arc-out region was welded over to repair any defect.

4. NONDESTRUCTIVE INSPECTION

a. Base Metal

All of the as-received base metal plates of both Ti-6Al-4V and Beta III were ultrasonically inspected using the pulse-echo method. Results of the individual plate inspections were compared with the ultrasonic signatures obtained from previously prepared standards. The standards consisted of 1- and 2-in.-thick plates of Ti-6Al-4V and 1-in.-thick plate of Beta III with a series of strategically positioned flat-bottomed holes of constant depth and

various diameters. Holes with diameters of 0.016, 0.047, and 0.078-in. were introduced into one face of the 1- and 2-in. standards at 1/4 thickness, 1/2 thickness, and 3/4 thickness locations by electrochemical machining. This scheme of hole size and placement provides a comparative basis for determining the effective size of ultrasonic mismatch regions as well as their relative location within each plate.

(1) Ti-6Al-4V Alloy.

Ultrasonic inspection of the Ti-6Al-4V plates indicated some noise that can be attributed to the microstructural nature of the alloy. The resulting attenuation of the ultrasonic pulses traversing the material thickness is responsible for an estimated 5% decrease in sensitivity. Nevertheless, no structural discontinuities were detected in any of the Ti-6Al-4V plates.

(2) Beta III Alloy.

The inspection sensitivity in the Beta III plates was decreased by 10% due to a relatively high background noise level. Two of the Beta III panels exhibited anomalous responses over large, continuous portions of the examined surface areas. A comparison with the 1-in. standard suggested that the material regions below these surface areas contained a multitude of discontinuities effectively greater than a hole of 0.078-in. diameter. In both plates, the "defective" regions were remote from the edges to be joined by electron beam welding. Subsequent to their incorporation into electron beam weldments, the two plates were radiographically inspected. Examination of the x-rays showed the presence of no defects in the suspect regions. The ultrasonic indications were probably the result of localized inhomogeneities or segregation in the material's microstructure.

b. Weldments

All of the weldments of both Ti-6Al-4V and Beta III were 100% radiographically inspected. The weldments were radiographed with a 300 kV Norelco beryllium window type x-ray unit with a tungsten target. For better delineation of radiographic details, the small focal spot size, 2.0 mm², was employed. In all cases, the source-film distance was 48 in. For the 1-in.-thick weldments of both test materials, the settings were 170 kV and 4mA for a period of 8 minutes. Settings of 220 kV and 4 mA for 8 minutes were used to radiograph the 2-in.-thick weldments.

A Class 2 radiographic double-coated film (i.e., Gevaert Industrial Film Type D4 with lead screens) was used. The lead screens are 0.001-in.-thick and are positioned on the front and back of the film. The film was processed in standard Eastman Kodak X-Ray developed for a period of 8 minutes at 68°F.

(1) Ti-6Al-4V Alloy.

Of the 17 1-in.-thick Ti-6Al-4V weldments inspected, all but three showed

some radiographic indications of defects. Only one of the seven 2-in-thick Ti-6Al-4V weldments was found to be free of radiographic evidence of defects. Most of the evidence of defects is in the form of linear indications. These range in photographic intensity from very pronounced and continuous dark lines to subtle, discontinuous traces. In some instances, the evidence extends over almost the entire weld length, while in others it exists as short isolated linear segments or a series of isolated short linear segments.

Examination of a weldment cross-section corresponding to a location intersecting a subtle linear indication on its radiograph showed the source of the indication to be a lack of fusion of the faying surfaces near the weld root. After etching the cross-section, the region exhibiting the lack of fusion extended to nearly 30% of the weldment thickness (see Figure 4(a)).

The extent of defect indications in those weldments returned for repair welding was verified by a second radiographic inspection performed by Solar at their electron beam welding facility. These weldments were also subjected to additional radiographic inspections following each repair welding pass. A cross-section of a repaired weldment is shown in Figure 4(b).

(2) Beta III Alloy

Radiographs of the 1-in.-thick Beta III weldments also showed evidence indicating a lack of fusion. In two of the four Beta III weldments, the radiographic traces of defective areas were limited in extent to about 1-in. of weld length. Radiographs of the other two exhibited several traces. However, the traces were quite short, 0.8 to 1.3 inches. By the selective positioning of specimens, the Beta III weldments could be used without repair welding.

5. THERMAL TREATMENTS

a. Aging of Beta III

The desired yield strength in the Beta III titanium was set in the range of 150 to 160 ksi. This strength level represents an improvement of about 30% in yield strength and approximately 15% in the strength-to-density ratio over mill-annealed Ti-6Al-4V. It was assumed that Beta III must exhibit at least this level of mechanical property improvement in combination with fracture properties comparable to those of mill-annealed Ti-6Al-4V to remain a viable candidate material for major applications in airframe structures.

The Beta III material was aged at 1045°F for 8 hours. The aging temperature was selected on the basis of mechanical property tests of material samples aged for 8 hours at one of the four recommended temperatures - 950°, 1000°, 1050°, and 1100°F. The properties obtained are listed in Table V.

A mysterious discrepancy of about 33 ksi exists between the obtained yield strength of the as-received material in the transverse direction and those

provided by the vendor (Table I.) Also, the material lacked the aging response suggested by the properties published by the developers of this alloy (2). Metallographic examination of the aged material at 500 and 3000 diameters reveals a microstructure very similar to that exhibited by the as-received material in Figure 3.

b. Stress-Relieving of 1-in.-Thick Ti-6Al-4V Alloy

During the fatigue precracking of 2-in.-thick compact tension specimens of as-welded Ti-6Al-4V, many difficulties were encountered in obtaining a uniform single crack that stayed relatively in plane. The residual stresses produced by the electron beam welding operation were the suspected cause. Prior to conducting a crack follower calibration test, one of the extra weldment specimens was post-weld annealed at 1300°F for 5 hours. Propagation of the fatigue crack was very uniform through the specimen thickness and the crack continued to grow along the plane of the starter slot. As a result, all of the compact tension specimens from 1-in.-thick Ti-6Al-4V weldments except four were subjected to a similar post-weld annealing treatment. The four excepted specimens were left in the as-welded condition to evaluate the effect of this condition on the fatigue crack growth resistance characteristics.

SECTION III

TESTING

1. SPECIMEN PREPARATION

The plan for removal of test specimens from the base metal panels of both test materials (Ti-6Al-4V and Beta III) was implemented as originally scheduled. In weldment panels of both materials that exhibited no radiographic evidence of defects, test specimens were also removed in accordance with the original plan. However, in weldments where the amount and location of radiographic defect indications did not jeopardize the yield of test specimens originally intended, the specimen removal plans were modified. The modifications consisted of rearranging specimen locations to avoid defects; changing the direction of the starter notch by 180° in some compact tension specimens; and transposing some specimen configurations from one panel to another. Weldments in which the extent of radiographic indications of defects was too great to provide a reasonable length of sound weld were repaired. The plans for specimen removal from the required weldments were implemented as originally intended.

All the test specimens were removed from their parent panels in blank form and the blanks machined to the final test configurations. After machining, the specimens were cleaned to remove machining grease and then packaged.

a. Tensile

The specimen configuration for the tension tests was the standard ASTM round specimen with threaded ends and a 5-in. overall length. The configuration is shown in Figure 5. Specimens were taken from both the longitudinal and transverse directions in the base metal plates of the two test materials. Weldment test specimens came only from those weldments joined with their parent panel rolling directions parallel to the weld length. All three weldment types - 1-in. and 2-in.-thick Ti-6Al-4V and 1-in.-thick Beta III - were represented.

b. Axial Fatigue

Axial fatigue specimens were fabricated from 1-in.-thick Ti-6Al-4V base metal and weldments only. All the specimens were for the transverse orientation in base metal and weldments. The specimen configuration used in these tests is shown in Figure 6.

c. Compact Tension Type

Compact tension-type specimens were used to evaluate the plane strain

fracture toughness of the 2-in.-thick Ti-6Al-4V base metal and weldments, the 1-in.-thick Ti-6Al-4V weldments, and the 1-in.-thick Beta III base metal and weldments. The test specimen configuration with an $H/W = 0.6$ is that recommended in ASTM E399-72, the standard method of test for plane-strain fracture toughness of metallic materials. The test specimen configuration is shown in Figure 7.

d. Wedge Opening Load

To measure the rate of crack growth during fatigue testing and under the combined influence of sustained load and environment, a specimen of the same genre as above but better known as a wedge opening load specimen (WOL) was employed. This specimen has an H/W ratio of 0.486, permitting a longer useful range of crack extension, and, thus, is better suited for subcritical crack growth studies as well as for the determination of the threshold stress intensity factor, K_{ISCC} . The specimen's configuration is displayed in Figure 8.

e. Single-Edge Notch

Determination of the critical value of stress intensity of 1-in.-thick weldments of Ti-6Al-4V and Beta III in specimen thicknesses of 1-in. and less was accomplished with the use of a single-edge notch type specimen. The use of this specimen, whose configuration is shown in Figure 9, for material thicknesses in which a mixed mode state of stress usually prevails is justified by its efficiency. The material necessary to fabricate a specimen, its preparation time, and its loading capacity are all less than for any of the other commonly used specimen types for K_C testing.

f. Part-Through Thickness

Although this type of specimen is the least efficient from the standpoint of material utilization, failure load requirements, and analytical tractability, it does model a crack situation that is prevalent in thick-section structures in service. Consequently, 24 specimens were fabricated and used to evaluate the fracture resistance and the fatigue crack growth resistance (both constant amplitude and spectrum loading) of different weld regions in 1-in.-thick Ti-6Al-4V weldments. The weld location to be evaluated was positioned along the specimen's midlength. The specimen configuration is shown in Figure 10. The panels in all the parent weldments were joined with their rolling directions parallel to the fusion plane.

A rectangular-shaped starter notch approximately 0.050-in. deep and 0.100-in. wide was placed in the specimen at midlength symmetric with its long axis by electrical discharge machining. After notching, each specimen was cleaned in acetone and thoroughly dried. The notch was sharpened to natural acuity by subjecting the specimen to sinusoidal loads at a constant amplitude of 25,000 lbs. The precrack was extended to various surface lengths up to a maximum of 0.25-in. The precrack surface length in most of the specimens was in the vicinity of the maximum.

g. Natural Defect

The specimen configuration shown in Figure 11 was used to evaluate the effect of the "natural" defects intentionally incorporated in one weldment of 1-in.-thick Ti-6Al-4V.

2. TEST SCHEDULE

The schedule of specimens tested in this program, including material, material condition, plate thickness, type of specimen, specimen orientation, test environment, and test temperature, is given in Table V.

3. TEST EQUIPMENT

a. Loading Apparatus

Loads in the tensile, K_{IC} , K_{IC} , K_{IE} , and natural defect tests were applied with a Tinius Ossen multirange 120,000-lb capacity Universal Hydraulic Testing Machine. The accuracy of the machine meets or exceeds the accepted ASTM standard of 1% of indicated load.

Cyclic loads for precracking, da/dN testing, spectrum fatigue, and axial fatigue were applied with various closed-loop, servo-actuated hydraulic rams. These rams are situated in loading frames with fatigue rated capacities ranging from 25,000 to 50,000 lb.

Loading of the specimens in environmental crack growth and K_{ISCC} tests was provided by load frames specially designed for this purpose. The frames consist of a reacting yoke and a strain-gage-instrumented bolt that acts as a load cell. The bolt is threaded into one beam of the WOL specimen. The yoke passes over the bolt and is secured with a loading pin to the opposite beam. To load the specimen, a tensile load is applied to the bolt by the Tinius Olsen test machine and reacted against the yoke. When the desired load or crack-opening displacement is achieved, the testing machine's function is transferred to the load frame by a securing nut that is threaded on the bolt against the yoke. The crack-opening force is provided by the residual strain energy stored in the loading bolt and yoke. The load cell permits continual monitoring of this crack-opening force.

b. Thermal Chamber

Specimens tested at -65°F and $+175^{\circ}\text{F}$ were brought to the required test temperature in a Missimer Environmental Chamber. The circulating air chamber utilizes dry ice for cooling and is capable of maintaining the two test temperatures within $\pm 3^{\circ}\text{F}$.

c. Programmable Function Generator

A digital programmable arbitrary function generator manufactured by Weston Instruments was used to command the servo-actuated hydraulic loading ram in

the spectrum fatigue tests. The instrument has an analog output of -10V to +10V with 0.1% FS accuracy and 0.5% resolution. Also, it has the capability of data input by paper tape and can assimilate 120 characters per second. With the included options, cycle counting, both block count and tape mark are possible.

d. Crack Following Instruments

Ultrasonic crack followers, designed and built by LMSC, were used to measure the crack length during da/dN and da/dt tests. The devices utilize a Sperry UM721 ultrasonic reflectoscope with a dual transgate. A 5-MHz lead zirconate titanate transducer is placed on top of the specimen in a traveling frame. When the transducer is just over the crack tip, the reflected signal from the crack is compared to the reflected signal from the back surface. Crack growth is then easily determined by measuring the transducer displacement required to maintain the same ratio of the two signals. The displacement is measured optically by a vernier or electrically from the output of a linear voltage potentiometer attached to the transducer carriage. A manually driven crack follower was used to measure the growth rates in the da/dt tests, and an automatic crack follower was used to measure growth rates in the da/dN tests. The automatic follower is equipped with a servo-controlled electric motor which maintains the transducer over the crack tip throughout the tests. Electrical output of the linear voltage potentiometer versus the number of cycles was autographically recorded on an X-Y plotter.

e. Digital Counter with Analog Output

This specially designed multirange counter permitted direct recording of the cumulative cycle count on an X-Y plotter. Combined with the automatic crack follower, a crack length versus cycles curve was plotted directly and continuously for each da/dN specimen.

f. Metallographic Equipment

A Bausch & Lomb Research Metallograph was used to examine the microstructures of the test materials.

4. TEST PROCEDURES

Room temperature tests were conducted in the ambient conditions of temperature and humidity prevailing at the time of the test. The laboratory in which the tests were performed is air conditioned. Typical conditions in this room are $78^{\circ} \pm 5^{\circ}\text{F}$ and 40 ± 10 percent relative humidity.

Prior to conducting the tests scheduled for temperatures of -65°F and $+175^{\circ}\text{F}$, a thermocouple-instrumented "dummy" specimen of the configuration to be tested was used to determine the time required for temperature stabilization within the specimen. Subsequently, each specimen was allowed to "soak" in the environmental chamber for a time period in excess of that required for

for thermal equilibrium before commencing the test.

a. Tensile Property Tests

The tensile property tests were performed on the standard size specimens in accordance with the recommendations specified in ASTM E8-69. Specimens were loaded at a strain rate of 0.5% per minute through the 0.2% offset yield point and to fracture. Strains in the gage section of base metal specimens were measured with an ASTM class B-1, 2-in. LVDT extensometer. An ASTM class B-1, 1/2-in. LVDT extensometer positioned to span the weld zone was used to sense strains in weldment samples. In addition, SR-4 electrical resistance strain gages with a gage length of 0.125-in. were applied over the weld zone in these specimens. Individual load-strain curves were automatically recorded for each base metal specimen tested.

Two load-strain curves, one reflecting the output of the 1/2-in. LVDT and the other the output of the SR-4 gage, were recorded for each weldment specimen tested. Yield loads were determined from these records by drawing a line parallel to the elastic or initial linear portion of the curve from a point representing a strain of 0.2% on the zero load axis. Tensile yield strength was computed by dividing the determined yield load by the original cross-sectional area of the corresponding specimen's gage section. Similarly, ultimate strength was computed using the ultimate load attained during the tensile test of each specimen. Modulus of elasticity values for each specimen was obtained by taking the slope of the initial straight line portion of the load-strain curve and converting it to a stress-strain ratio.

Upon fracture of the individual tensile specimens, the two pieces of the original specimen were removed from the test assembly and fitted together. The separation between gage marks placed on the specimen's gage length prior to testing as well as the diameter of the specimen in the necked region were measured to the nearest 0.001 in. These measurements were used to calculate the percent elongation and percent reduction of area, respectively. A gage mark separation of 2 in. was used on all specimens. In addition, a gage mark separation of 0.5 in. was placed symmetrically across the weld zone in weldment samples to determine its contribution to the specimen's percent elongation.

b. Axial Fatigue Tests

The fatigue tests were conducted in an axial load frame with a fatigue rating of 50 Kips. Prior to testing, the load train of the test machine was carefully aligned with a test specimen in place. To minimize any extraneous bending moments, an Ormond flexure fixture was included in the load train as well as spherical loading links above and below the specimen.

All specimens were subjected to a stress ratio* of 0.1. Frequency of the constant amplitude loading varied from 4 Hz, for specimens stressed near the

*Stress Ratio, $R = (\text{min. stress}/\text{max. stress})$

ultimate strength, to 30 Hz, for specimens stressed at about 50% of the ultimate strength. The number of cycles to failure were automatically tabulated by a counter that is an integral component of the electronic control instrumentation. The entire system was programmed to shut down when the test specimen failed. Original cross-sectional dimensions were used to compute the fatigue stress.

c. Fracture Toughness Tests

All fracture toughness tests were performed on precracked specimens whose starter notch was sharpened to fatigue crack acuity by constant-amplitude cyclic loads.

(1) Compact Tension

The fracture toughness tests utilizing the 1-in.- and 2-in.-thick compact tension specimens were conducted in accordance with the recommendations of the standard method of test for Plane-Strain Fracture Toughness of Metallic Materials, ASTM E399-72. The procedures for this test are somewhat involved and can be summarized best by the test records for a valid K_{IC} result of a 2-in.-thick specimen. These records are typical and are included as Figures 12 and 13. In all tests, the crack opening displacement was measured with a linear voltage differential transformer spanning the specimen's starter notch. A schematic representation of this arrangement is shown in the sketch included in Figure 13.

(2) Single-Edge Notch

All of the single-edge notched specimens scheduled for testing were fabricated from weldments of both 1-in.-thick test materials, Ti-6Al-4V and Beta III. A 1/16-in.-thick abrasive saw of silicon carbide was used to introduce the starter notches. All specimens were notched in their weld fusion zones. Cyclic loads initiated fatigue cracks and extended them to a/W ratios ranging from 0.3 to approximately 0.6. In all cases, the maximum stress intensity during precracking was kept below a value of 30 ksi-in.^{1/2}. Loading of the specimens was at a rate of approximately 30 ksi-in.^{1/2}/min. A linear voltage differential transformer positioned across the starter notch recorded the crack-opening displacement. Individual load vs. crack-opening displacement curves were obtained for each specimen tested. Two critical load values were taken from each record. One, the maximum or failure load; the second, a 5% offset secant load. In some instances, a distinct "popin" load was observed. This value was also recorded.

Post test critical crack size measurements were made. The critical stress intensity values were computed for each combination of critical load and crack length for each specimen. The solution for the stress intensity is expressed as (3):

$$K_C = Y \cdot \frac{P \sqrt{a}}{BW} \quad (1)$$

where a is the critical crack length, P is the critical load, B is the specimen thickness, W is the specimen width, and Y is a compliance constant. Expressed in polynomial form, Y can be represented as:

$$1.99 - 0.41(a/W) + 18.70(a/W)^2 - 38.48(a/W)^3 + 53.85(a/W)^4$$

(3) Part-Through Thickness

The specimens, precracked to a surface length of about 0.25-in., were secured with clevises in the load train of a testing machine and the load applied at rate of 20,000 lb/min. Only the ultimate failure load was recorded. Measurement of the critical crack sizes were made upon completion of the test.

The conventional expression for the stress intensity factor in part-through thickness specimens and the one used in this program is that formulated by Irwin (4):

$$K_{IC} = 1.1\sigma\sqrt{a/Q} \quad (2)$$

where a is the depth of the crack, σ is the gross section stress, and Q is a normalizing factor that depends upon the ratio of flaw depth to half length and on a correction term for plastic zone size.

d. Fatigue Crack Growth

(1) Compact Tension Specimens

All compact tension specimens were notched to an a/W ratio of about 0.3. Precracking was accomplished at room temperature in a manner similar to the procedure described in ASTM E399-72.

A traveling microscope was used to monitor crack extension in eight specimens scheduled for testing in a room temperature laboratory air environment. Four of these specimens were precracked in the heat affected zone (HAZ) and four were precracked in the weld zone (WZ). The specimen sizes were polished and a graduated scale affixed to facilitate the optical measurement of crack length. With this method, surface indications of crack length were measured on a periodic basis. Measurement was to the nearest ± 0.003 in.

An ultrasonic crack follower was used to monitor the crack length in all other fatigue crack growth specimens. This device, which has a resolution of 0.002 in., senses the midthickness crack extension. In a number of the room temperature tests, growth was monitored by the periodic measurement of crack length with the manually operated crack follower. Crack extension in most of the specimens was continually sensed with the automatic crack follower. A test specimen with the servo-controlled crack follower in place is shown in Figure 14. In many of the room temperature specimens, periodic verification of the crack follower results was performed by optical measurement of surface traces.

Small clear plastic chambers with a peripheral molded silicone rubber seal positioned on the specimen sides and surrounding the crack were used to contain the test environments. The gap between the two chambers created by the specimen notch was sealed with a long narrow cylindrical rubber gasket. This arrangement provides a fluid-tight seal around the entire usable crack growth range of the test specimen. For tests at 175°F, the plastic chambers were replaced with copper ones that were electrically insulated from the specimen.

After a precrack was initiated and extended approximately 0.02 to 0.1 in., the fatigue load was reduced to a value corresponding to an initial stress intensity yielding a crack growth rate between 10^{-6} to 10^{-5} in./cycle. At this cyclic load level, the crack was extended until the length reached the limit of the specimen's useful range ($a/W = 0.75$) or failure occurred. To cover a broader range of stress intensities, in many of the specimens the cyclic load was increased before test termination. The stress ratio in all cases was 0.1.

For each specimen on which the automatic crack follower was used, individual crack length versus cycles records were autographically plotted. An example of such a curve is included as Figure 15. In other instances, specific data points from either optical readings or manual crack follower measurements were plotted and a smooth curve fitted to the data points. Crack growth rates were determined by taking slopes of these curves at designated crack lengths. Corresponding stress intensity ranges were computed from the minimum and maximum cyclic loads and the designated crack length. Subsequently, the crack growth rates, da/dN , were plotted as a function of the applied stress intensity range, ΔK .

Crack growth rate data were not obtained from the initial portion of the crack length versus cycles record until the curve exhibited no effects of load history and notch proximity. In most cases, this amounted to a crack extension of approximately $2.5 (K_{I_1}/F_{TY})^2$, where K_{I_1} is the stress intensity for the combination of maximum fatigue load and crack length (see Figure 15).

Data were acquired at frequencies of 0.1 and 10. Hz to show the effect of environmental exposure time during peak loads on the crack growth rate. Much of the crack extension occurred at a frequency of 10 Hz. Periodically, a specimen was subjected to a frequency of 0.1 Hz to establish any principal differences that may exist with the 10 Hz information. Cyclic loading at the lower frequency was only for durations sufficient to establish a growth rate. In general, cyclic loading at the lower frequency was performed at relatively high values of stress intensity (see Figure 15). If a principal difference (a factor at 2.5 or more) from the 10 Hz data was noted, the 0.1 Hz cyclic loading was performed at much lower stress intensities in the duplicate specimen. In cases where a duplicate was not available, the stress intensity was decreased by lowering the cyclic load. Before subsequent data acquisition, the crack was extended until no effects of load history were observed.

Following the completion of each test, crack follower accuracy was verified by comparison with known actual crack length; e.g., fracture surface markings

due to load or frequency changes. Because of crack front bowing, optical measurements taken on the specimen surface and crack follower crack length indications, in many instances, differed slightly.

Stress intensity values were calculated using the expressions (5):

$$K_I = \frac{P}{B\sqrt{a}} \cdot Y \quad (3)$$

where a is the crack length, P is the applied load, B is the specimen thickness, and Y is a compliance constant. Expressed in polynomial form, Y can be represented as

$$30.95(a/w) - 195.6(a/w)^2 + 370.6(a/w)^3 - 1186.3(a/w)^4 + 754.6(a/w)^5 .$$

(2) Part-Through Thickness Specimens

Specimen surfaces in the vicinity of the notch were polished and a linear scale affixed to permit optical measurement of the surface crack length. Precracked specimens were subjected to cyclic loads of constant amplitude and surface crack lengths recorded. Measurements were made at optical magnifications of 10 to 50 diameters using a binocular microscope.

In environmental tests, a small clear plastic chamber with molded silicone rubber seals was mounted over the crack growth area including the graduated scale to contain the salt water.

In all cases, cracks were extended to about 50% of the specimen thickness and the test terminated. The stress ratio in all specimens was 0.1. Individual specimens were cyclically loaded at a frequency of either 10 Hz or 0.1 Hz.

After completion of the da/dN tests, the specimens were monotonically loaded to fracture. Fatigue crack growth data was determined in a post-test examination of the specimen by measuring the crack extension in both the a and c directions. Surface markings were used to gage the amount of crack extension. Growth rates were calculated by dividing the amount of extension by the number of cycles. Stress intensities were calculated for the range of fatigue crack growth using the Irwin equation previously described.

e. Environmental Crack Growth

All test specimens were notched to a a/W ratio of about 0.3 and all were previously stress relieved. Specimens were fatigue precracked at room temperature with maximum cyclic loads corresponding to stress intensities less than one-half of the initial crack-opening loaded stress intensity.

Originally, six specimens secured in their respective load frames were crack-opening loaded at room temperature in lab. air to near K_{IC} . Proximity of the

applied load to the critical load was gaged by the rate at which stress waves (acoustic emissions) were being emitted from the vicinity of the crack front. At this point, the load frame was activated to transfer the crack-opening load from the test machine to the fixture. Subsequently, the specimens with load frames attached were immersed in 3.5 percent solution of salt water.

With no signs of crack growth after a prolonged period, even in specimens thought to be susceptible, all of the tests were dismantled. The next loading was performed in the presence of the test environment. Loads were increased until evidence of crack growth was observed. At this time, the load frames were secured and clear plastic chambers containing the environment were positioned over the crack growth area. The load cells in the fixture were periodically monitored and the crack length was measured with the hand driven ultrasonic crack follower. A photograph of the test setup is shown in Figure 16.

Specimens for elevated temperature tests were also loaded at room temperature then placed in the Missimer's Environmental Chamber at 175°F.

Specimens were exposed in their respective environments until the crack had progressed through the usable range or until the extension of the crack had stopped. Load and crack length versus time measurements were gathered during the course of the tests. From this information, crack growth rates were determined, and stress intensities calculated using the same equation that applied in the da/dN tests. The stress intensity below which the crack growth rate became diminishingly small was identified as the threshold value, K_{ISCC} .

f. Spectrum Fatigue

Six previously precracked part-through thickness specimens were continuously subjected to repetitions of the 59-layer fatigue spectrum, shown in Figure 17. Four of the specimens were precracked in the weld zone (weld centerline) and two in the heat-affected zone (~0.020 in. from edge of weld fusion zone). The servo-actuated hydraulic loading ram of the test machine was commanded by a programmable function generator. A paper tape containing the spectrum shown in Figure 17 was fed through the function generator in a closed loop for continuous operation. The specimens were fatigued to failure in all cases, and the required number of spectrum repetitions (blocks) and the layer number responsible were recorded.

g. Natural Defect

Specimens containing the natural defects were monotonically loaded to failure and the failure load noted. Also examined and measured was the defect area through which failure occurred.

SECTION IV

RESULTS AND DISCUSSION

1. MATERIALS

a. Base Metal

(1) Ti-6Al-4V

The materials in the 1-in. and 2-in. thickness are from different heats and exhibit strikingly different microstructures. Compare Figures 1 and 2. The microstructure of the thicker plate, shown in Figure 2, is consistent with Ti-6Al-4V worked in the vicinity of the beta transus; that is, where the end of working occurs above or very near the beta-to-alpha transformation temperature. The prominent features include the classical Widmanstätten pattern of acicular alpha grains. On the other hand, the microstructure of the 1-in. plate appears more typical of Ti-6Al-4V receiving a larger degree of work at a lower temperature. This microstructure, Figure 1, is predominantly fine, equiaxed alpha and beta grains with some residual Widmanstätten alpha grains. The processing histories reveal that, indeed, the 1-in. plate received more work, and presumably much of it at lower temperatures.

(2) Beta III

The microstructure of the Beta III alloy in the as-received condition, Figure 3, appears more typical of solution treated and aged material than of solution treated and quenched. No significant differences were noted in the microstructure of the material after it was submitted to an aging treatment of 1045°F for 8 hours. The enhanced transverse strength of the as-received material (Table IV) over that certified by the vendor (Table I) substantiates the metallographic evidence of an aged structure. Apparently, the material was subjected by the vendor to an extraneous (and unreported) thermal treatment following its certification and before receipt for testing in the present program.

b. Weldments

(1) Ti-6Al-4V

Since it was necessary to repair many of the 1-in.-thick Ti-6Al-4V weldments by remelting their fusion zones with additional passes of the electron beam, the microstructures of two weldments exemplifying welding condition extremes were subjected to a comparative metallographic analysis. One sample contained a single pass, the standard joining technique; and the other contained, in addition to its initial joining pass, two repair passes. The purpose of

the analysis was to illustrate the metallurgical differences or similarities in the heat-affected zones of the two conditions. Cross-sections of the two weldments are shown in Figure 4. Higher magnification views of an area traversing the transition between the base metal, heat-affected zone, and the fusion zone of the weldments are exhibited in Figure 18. A comparison of the photomicrographs in Figure 18 reveals the similarity in width of the heat-affected zones. Microstructures of the weldment components (i.e., base metal, heat-affected zone, and fusion zone) at a magnification of 500 diameters are included in Figure 19 for a single pass weldment and Figure 20 for the repair weldment. As expected, the appearance of the weld fusion zone and base metal microstructures are very similar. A comparison of the heat-affected zone microstructures, Figures 19(b) and 20(b), reveals some disparities; however, a detailed examination of much of the heat-affected zones of the two weldments reveals a predominance of microstructural similarities. A microhardness survey of the base metal-weld fusion zone transition regions was conducted. The results are shown in Figure 21. The agreement of readings across the heat-affected zones and the similarities in heat-affected zone size and microstructure suggests that no obvious metallurgical differences exist between the two conditions.

(2) Beta III

The microstructure of an electron beam weldment in 1-in.-thick Beta III plate joined with a single pass is exhibited in Figure 22. The principal characteristic of the weldment is the almost perfectly planar alignment of contiguous grain boundaries along the weldment centerline. A metallographic examination of the grains whose boundaries form the planar alignment reveals pronounced coring (see Figure 23). A microprobe scan of a sample that parted along the centerline alignment of grain boundaries showed a hundred fold increase in iron concentration on the surface. No anomalous concentrations of constituents were found during a microprobe scan across the centerline of the specimen shown in Figure 22. Apparently the segregation of iron is confined to the centerline plane; and in a layer significantly less than 1 in., the nominal microprobe beam diameter. This finding, however, is suspect. Although the sample was cleaned prior to performing the microprobe scan, it is possible that the cleaning operation lacked the necessary rigor to remove all traces of any contamination acquired during the sample's test history.

2. TENSILE PROPERTY TESTS

Tensile properties determined include the 0.2% offset yield strength, the ultimate strength, percent elongation, percent reduction of area, and modulus of elasticity. Individual results and their average values are tabulated for each material condition and test temperature. The yield strength, elongation and modulus of elasticity columns for weldments contain two entries for each specimen. The first entry is the yield and modulus determination from strain data obtained with a 1/8-in. SR-4 electrical resistance gage in the weld fusion zone; and the percent elongation in 2 inches. The second entry is the yield and modulus determinations from strain data obtained with a 1/2-in.,

B-1, LVDT extensometer placed symmetrically across the weld zone; and percent elongation in 1/2-in. across the weld fusion zone.

In addition the average result of each tensile property has been plotted as a function of the test temperature.

Average tensile properties of all the starting test materials, both base metal and weldments, are represented in Figure 24 for comparative analysis. The significantly different values of the elastic modulus in the longitudinal and transverse directions of the 1-in.-thick Ti-6Al-4V, and approximately the same value for the two directions in 2-in.-thick Ti-6Al-4V is additional evidence of the metallurgical disparity in the two materials. Anisotropic elastic moduli signify a crystallographically textured structure and this condition is indicative of cold working (working below the Beta transus).

a. Ti-6Al-4V

(1) 2-Inch-Thick Plate

(a) Base Metal (Mill Annealed)

Room temperature properties are given in Table VI.

(b) Weldment (As Welded)

Room temperature properties are given in Table VII.

(2) 1-Inch-Thick Plate

(a) Base Metal (Mill Annealed)

Tensile properties at room temperature (-65°F and 175°F) are given in Tables VIII, IX, and X, respectively. Plots of the variation of the average tensile properties with test temperature are shown in Figures 25 and 26.

(b) Weldments (As Welded)

Tensile properties at room temperature (-65°F and 175°F) are given in Tables XI, XII, and XIII, respectively. A plot of the variation of the average tensile properties with test temperature is shown in Figure 27.

b. Beta III

(1) 1-Inch-Thick Plate

(a) Base Metal (Solution Treated and Aged)

Tensile properties at room temperature (-65°F and 175°F) are given in Tables XIV, XV, and XVI, respectively. A plot of the variation of the average transverse tensile properties with test temperature is shown in Figure 28.

(b) Weldments (Solution Treated and Aged)

Tensile properties at room temperature (-65°F and 175°F) are given in Tables XVII, XVIII, and XIX, respectively. A plot of the variation of the average tensile properties with test temperature is shown in Figure 29.

3. AXIAL FATIGUE PROPERTY TESTS

Due to the shape of the axial fatigue test specimen, the highest uniaxial tensile stress during loading occurs in the minimum cross-section located at the specimen's mid-gage length. Therefore, to determine the weld fusion zone ultimate strength, one of the weldment axial fatigue specimens was monotonically loaded to failure. The maximum stress required to rupture the specimen, 169.7 ksi, is considerably greater than the average ultimate strengths of the base metal, 148.5 ksi, and weldment, 147.9 ksi, obtained in tests with the standard tensile specimen of uniform cross-section.

Of the 10 weldment specimens exposed to axial fatigue loads, eight failed outside of the minimum cross-section and outside of the weld fusion zone. Failure in these eight specimens appeared to have initiated in the base metal immediately adjacent to the weld fusion zone (near heat-affected zone).

Failure in all of the base metal specimens was in the vicinity of the minimum cross-section.

a. Ti-6Al-4V, 1-In.-Thick Plate, Base Metal (Mill Annealed)

A tabulation of the specimens tested, the maximum stress, stress ratio, frequency, and number of cycles to failure is presented in Table XX. A plot of the maximum stress versus the number of cycles to failure (S-N curve) is shown in Figure 30.

b. Ti-6Al-4V, 1-Inch-Thick Plate, Weldments (As Welded)

A tabulation of the specimen tested, the maximum stress, stress ratio, frequency and number of cycles to failure is presented in Table XXI. A plot of the maximum stress versus the number of cycles to failure (S-N curve) is shown in Figure 31.

4. FRACTURE TOUGHNESS

a. Compact Tension Specimens

The tests were conducted in accordance with ASTM E399-72, and the criteria for validity described in this standard were applied to the test results. A listing of these criteria and their appropriate section designation within the ASTM standard are shown in Table XXII. Also shown in the table is a code letter used in the subsequent tables of the test results to identify violations.

The individual test results as well as average values of replicate tests of compact tension specimens are given in Tables XIII through XXXIII. Included are tabulations of specimen identification, orientation, thickness, crack

length, $K_{f(max)}$ - the maximum stress intensity during fatigue precracking, K_Q - the conditional fracture toughness, K_{IC} - the plane strain fracture toughness, $2.5 (K_{IC}/F_{TY})^2$ - the ASTM size criterion for validity, and a column for the code letters of any violations of ASTM validity criteria.

Judging from much of the published fracture toughness results, the principal and in some cases the sole condition for the validity of the result is the ASTM size criterion; i.e., a and $B \geq 2.5 (K_Q/F_{TY})^2$. Consequently, in the present report, the conditional fracture toughness result, K_Q , from any test specimen that satisfies the above size condition has been included in the K_{IC} column of the test results. If other conditions are not satisfied, the code letter of the violated criterion still appears in the appropriate column.

(1) Ti-6Al-4V

(a) 2-Inch-Thick Plate

Base Metal (Mill Annealed). The fracture toughness values of the material were evaluated in three directions (T-L, L-T, and S-L)* at room temperature in laboratory air. The results are given in Table XXIII. The average fracture toughness values of the two in-plane orientations are within 3 percent, and both are above 100 ksi-in^{3/2}. The relative agreement in the two directions confirms the material's planar isotropy established by the tensile properties. The level of toughness obtained for this material may appear to be higher than that normally associated with this alloy. Much of the published results were obtained in the more common plate thicknesses of 1-in. or less. In these sizes, the structure of the alloy can differ markedly from that found in thicker sections (compare Figures 1 and 2). The test results in Figure 24 also reflect this difference. Some recent results on 3-in.-thick Ti-6Al-4V plate with a yield strength comparable to that of the test material show comparable fracture toughness values (6).

Although the tests performed in the short transverse direction did not yield valid results, the conditional values indicate a fracture toughness in excess of 75% of the in-plane toughness.

Fracture toughness results of the plate's T-L orientation at -65°F and 175°F are given in Tables XXIV and XXV, respectively. Toughnesses at -65°F are valid and show a decrease of about 17% from the average value at room temperature. The results obtained at 175°F are beyond the valid measurement capability of the specimens. Nevertheless, the conditional values indicate an enhancement of at least 11% over the room temperature average. The general relationship between toughness and temperature is as expected.

Weldments (As Welded). Difficulty was encountered in growing fatigue precracks in the weld zone and the heat-affected zone. Most of the specimens, particularly those in which the precrack was intended to propagate in the heat-affected zone, behaved in an anomalous manner. The precracks either refused to extend in plane, refused to grow uniformly through the thickness,

* Descriptions of orientation code contained in ASTM E399-72.

or would initiate on more than one crack plane. All three abnormal types of behavior prevailed in some specimens. In one instance, a precrack failed to initiate along a 0.15-in. segment of the starter notch adjacent to one surface, extended 0.75-in. beyond the starter notch at midthickness, and was retarded to 0.45-in. extension along the opposite surface. In all of the as-welded specimens, the cycles required for precracking exceeded the amount necessary to precrack base metal specimens; in some cases, by as much as an order of magnitude.

As a result of the anomalous precracking behavior, none of the weldment results satisfy all of the ASTM conditions for validity. All are either bowed too severely, too long at midthickness due to bowing, lacking uniform precrack extension, or too far out of plane. Most display various combinations of these conditions.

Fracture toughness in the heat-affected zone was evaluated at room temperature for three different weldment orientations (L-T, T-L, and S-L). The results are presented in Table XXVI. Three specimens of each orientation were tested. Panels joined with their rolling directions normal to the fusion plane provided the L-T specimens. The T-L specimens were taken from weldments composed of panels with their rolling directions parallel to the fusion plane. Two narrow plates, joined with their short transverse directions normal to the fusion plane, provided the S-L specimens.

Four of the six in-plane oriented specimens reveal conditional fracture toughness values that are exceedingly high. The cause stems mainly from the large deviation of the crack plane from the normal path. In each case, the crack deviated from the heat-affected zone into the base metal. At the critical load, unstable propagation continued at a large angle to the load axis. The remaining two specimens, 1-2 and 3, satisfy the ASTM size criterion and are guilty of only minor violations of the other validity conditions. The K_{IC} values listed for these two specimens are probably indicative of the valid plane strain results. These values closely reflect the base metal results in Table XXIII. Likewise, the toughness of the three short transverse oriented specimens are similar to their base metal counterparts. In all likelihood, the toughness in the S-L direction bears a relationship to the in-plane oriented toughnesses similar to that found in base metal.

Heat-affected zone fracture toughness results in the T-L direction at -65°F and 175°F are given in Tables XXVII and XXVIII. Again, the out-of-plane extension of the precracks and their unstable propagation into the base metal at a large angle to the load axis results in toughness values of excessive quantity at -65°F . The toughness values at 175°F are well beyond the measurement capacity of the test specimens.

Weld fusion zone fracture toughness results obtained for the T-L orientation at room temperature (-65°F and 175°F) are given in Tables XXIX, XXX, and XXXI, respectively.

All three of the room temperature test specimens were of adequate dimensions

for a valid result. The listed violations of the other validity conditions probably have only a minor influence on the conditional values. As a result, the average toughness value given in the table is probably representative of the weld fusion zone plane strain fracture toughness.

One of the specimens tested at -65°F, 3-2, propagated out of the weld zone across the heat-affected zone and fractured through the base metal. Consequently, it exhibits an unrealistic toughness value. Specimens 3-4 and 4-4 satisfy the ASTM size criterion and only exhibit minor violations. The average value of their toughness results is probably a very fair estimate of the valid plane-strain result.

The toughness values obtained at 175°F exceed the measurement potential of the 2-in. compact tension specimen.

(b) 1-Inch-Thick Plate

Weldments (As Welded). Three specimens in the T-L direction were tested at room temperature. The results are given in Table XXXII. The same precracking problems described above in the 2-in.-thick weldments were encountered. All three of the specimens were of sufficient size for valid plane-strain fracture toughness measurement. The violations noted in the table were minor and probably of little consequence in their effect on the conditional result. The average fracture toughness value given in the table is probably well within the scatter limit of the actual valid plane-strain result.

The abnormal precracking behavior that plague the as-welded fracture toughness results can be attributed to the presence of residual stresses in these specimens.

Confirmation of this was obtained in subsequent fatigue tests on specimens removed from the same weldments. After a post-weld annealing treatment at 1300°F for 5 hours, the anomalous precracking patterns were eliminated.

(2) Beta III. 1-Inch-Thick Plate

(a) Base Metal (STA). One specimen was tested at room temperature in the T-L orientation. The result is given in Table XXXIII. The test result and specimen dimensions satisfy all of the ASTM criteria for validity. The value obtained indicates that Beta III base metal has an excellent combination of fracture toughness and yield strength.

(b) Weldments (STA). One specimen precracked in the heat-affected zone and one specimen precracked in the weld zone, both in the T-L orientation, were tested at room temperature. Their results are included in Table XXXIII. No difficulties were encountered in the precracking operation. Undoubtedly, because the magnitude of the residual stresses produced by the electron beam joining process were diminished during the 8-hour aging treatment. Both tests - heat-affected zone and weld zone - completely satisfied all of the ASTM conditions for a valid plane-strain fracture toughness determination.

While the heat-affected zone shows excellent tolerance to flaws, the weld zone toughness is decreased to less than one-half that of the base metal. Obviously, the planar alignment of grain boundaries present in the weld fusion (see Figures 22 and 23) is an undesirable condition for resistance to fracture.

b. Single-Edge Notch

Ti-6Al-4V and Beta III weldment specimens of 1-in., 1/2-in., and 1/4-in.-thickness were tested at room temperature and -65°F. All specimens were from the T-L orientation. Replicate determinations were performed on the Ti-6Al-4V weldments while only one Beta III specimen of each thickness was evaluated at each test temperature. The results are tabulated as well as exhibited in plots displaying the variation in the average critical stress intensity factor as a function of specimen thickness.

Tabulation columns include: specimen identification, orientation, thickness, width, crack length, three different categories of critical stress intensities and one, headed "Fracture Path", that identifies the weldment region in which unstable crack propagation predominated. The three categories of critical stress intensities listed in the table are K_{popin} , K_Q , and K_{max} . An abrupt crack-opening displacement (COD) at relatively constant load in the autographic load vs. COD curve is usually indicative of crack popin; i.e., a short unstable extension of the central portion of the crack front. The observed load level of this phenomena was used to calculate the K_{popin} value. The K_Q value was obtained from a 5% secant offset load - a method similar to that described in ASTM E399 for the empirical determination of the critical load. The maximum load required to fracture the test specimens resulted in the K_{max} value. Critical crack lengths were determined during post-test examination of the fracture surfaces.

Included in the plots of the average critical stress intensity factor vs. thickness is the ASTM recommended specimen thickness that qualifies the result for validity. The critical stress intensity factors in these plots is the average K_Q value.

(1) Ti-6Al-4V, 1-Inch Thick Plate, Weldments (As Welded)

Although precracks stayed in plane, the residual stresses present caused non-uniform crack fronts in all the specimens.

Room temperature test results are given in Table XXXIV, and the -65°F test results are included in Table XXXV. The dependency of the fracture toughness on specimen thickness is shown in Figure 32 for room temperature and in Figure 33 for -65°F. The 1-in.-thick specimens at both temperatures have sufficient thickness to qualify as valid test results. Also, the room temperature value shows excellent agreement with that obtained in compact tension specimens. At both temperatures, the 1-in. thickness of the test specimens provides adequate elastic constraint to cause a planar fracture path that remains in the fusion zone. Judging from the fracture path, which extends into

base metal, and their higher toughnesses, a mixed mode state-of-stress prevails in the thinner specimens.

The classical dependency of fracture toughness with material thickness is exhibited by the curve in Figure 32. Although the same general trend is revealed in Figure 33 for the test material at -65°F , the toughness in the 1/4-in. specimens is slightly less than that in the 1/2-in. specimens.

(2) Beta III, 1-Inch-Thick Plate, Weldments (Solution Treated and Aged)

Room temperature test results are given in Table XXXVI, and the -65°F test results are included in Table XXXVII. The variation of fracture toughness with specimen thickness at room temperature is illustrated in Figure 34 and at -65°F in Figure 35. The 1-in.-thick room temperature specimen broke during fatigue precracking after 7680 cycles at a maximum cyclic load of 15,000 lb. The combination of maximum load and crack length corresponded to a stress intensity factor of only 28.7 ksi-in.^{1/2}. The fracture plane was almost perfectly flat and coincided with the contiguous alignment of grain boundaries found along the centerline of Beta III weldments. Failure in the 1/4-in. specimen was also along the weld centerline, and the fracture surface exhibited an appearance similar to that observed in the 1-in.-thick specimen. The fracture path in the 1/2-in.-thick specimen was partially through material away from the weld centerline. Consequently, the toughness of this specimen was considerably greater than that of the other two thicknesses. As shown in Figure 34, the plane-strain fracture toughness values in the two types of specimens - compact tension and single edge notched - do not show good agreement.

All three specimen thicknesses tested at -65°F revealed a very flat fracture surface appearance with their paths along the weld centerline. Almost identical toughnesses were obtained for the 1-in. and 1/4-in. thicknesses. As in the room temperature tests of Beta III and the -65°F tests of Ti-6Al-4V, the highest toughness is exhibited by the 1/2-in. specimen.

Obviously, the fracture resistance of Beta III weldments is greatly diminished by the metallurgical conditions existing at the centerline.

c. Part-Through Thickness, Ti-6Al-4V, 1-Inch-Thick Plate

Although the part-through thickness (PTT) specimen models a crack situation that is the most realistic in actual thick-sectioned aircraft structures, it is not well understood analytically. Presently, there is no accepted standard method of conducting the test or evaluating fracture toughness results with this specimen. Consequently, various expressions exist for relating the fracture stress and critical flaw size. Most are modifications of Eq. (2) to account for the effects of free surface proximity and have met with limited success (7, 8, and 9). However, in the crack depth range of the PTT fracture toughness specimens tested in this program - 40 to 50 percent of specimen thickness - the inadequacy of Eq. (2) has not been demonstrated. For this

stated range of crack depths, most of the existing expressions yield approximately the same toughness results.

Among many aerospace and airframe workers in the field of fracture, criteria for judging the validity of toughness results obtained with PTT specimens have evolved. The validity conditions are: (1) the net stress must be equal to or less than 90 percent of the yield stress; (2) the surface length of the crack must be one-fourth or less than the specimen width; and (3) the uncracked ligament portion of the specimen thickness at the deepest penetration of the precrack must be equal to or greater than $\pi/16 (K_{IE}/F_{TY})^2$.

The tabulation of part-through thickness fracture toughness results includes a column for entries indicating which of the three criteria, if any, were violated in the test. Also included in the tabulations are the specimen identification, crack location, thickness, width, crack depth, crack length, gross failure stress, net failure stress, and the fracture toughness result calculated from Eq. (2). To prevent confusion with the valid plane-strain fracture toughness obtained in accordance with ASTM E-399, the toughness calculated from Eq. (2) is designated K_{IE} .

All the test specimens - base metal, heat-affected zone, and weld fusion zone - were loaded normal to the parent plate's rolling direction with the plane of the precrack parallel to the rolling direction. However, the path of the precrack in its deepest penetration coincided with the parent plate's short transverse direction. Although the accepted ASTM crack plane orientation identification code was not intended for PTT specimens, the above described alignment of load axis, rolling direction and crack plane is probably analogous to the T-S orientation in the more common test specimen configurations.

(1) Base Metal (Mill Annealed)

One PTT specimen with the starting precrack in the base metal was tested at room temperature in laboratory air. The result is given in Table XXXVIII. This toughness result is invalid because the ratio of the specimen's net failure stress to material yield stress - 0.96 - is about 6 percent greater than the validity limit. Fracture toughness tests of the 1-in.-thick base metal with other types of specimen configuration were not performed. Consequently, the merit of the value obtained with the PTT specimen cannot be directly ascertained. Judging from the relationship between the toughnesses of the weld zone and base metal in 2-in.-thick plate, it appears that in this case the PTT result underestimates the valid plane-strain value by 10 to 15 percent.

(2) Weldments (As Welded)

The fracture toughness results from three specimens precracked in the heat-affected zone and one precracked in the weld zone are also included in Table XXXVIII. One of the heat-affected zone toughness values and the sole weld zone value are valid according to the criteria adopted. The weld zone PTT

toughness is about 28 percent less than the valid plane-strain results obtained with compact tension and single-edge notch specimens. As with the base metal, no direct comparison is available for the heat-affected zone. By reasoning similar to that employed in evaluating the base metal result, in this case, the average PTT toughness appears to underestimate the valid plane strain fracture toughness by as much as 20 percent.

It should be mentioned that the purpose in performing these tests was not to measure an inherent characteristic of the test material, but rather to determine the parameter, K_{IE} , that relates the critical part-through thickness flaw size and fracture stress in this test material. Knowledge of the K_{IE} factor, even though it is somewhat parametric in nature, is essential in providing practical and reliable safe-life predictions in real situations.

5. FATIGUE CRACK GROWTH TESTS

Fatigue crack growth data were obtained with compact tension type specimens and part-through thickness specimens. Compact tension specimens were employed to determine the fatigue crack propagation rates in both test materials at three temperatures (room, -65°F, and 175°F) and in environments including laboratory air, water, 3.5-percent NaCl solution, and the jet engine fuel JP4. Only the Ti-6Al-4V base metal and weldments were tested in the part-through thickness configuration. Test conditions consisted of laboratory air and salt water environments at room temperature only. Water for the test environments, as well as that used to prepare the salt solution, was commercially purchased deionized water.

The 3.5-percent salt solution was prepared with reagent grade crystalline sodium chloride provided by the J. T. Baker Chemical Company. The reagent is certified to meet ACS specifications. An approximate 5-gal. quantity of the solution was prepared and stored in a polyethylene container.

The JP4 jet fuel used in this test program was freshly siphoned from a flight tank at the NASA-Ames facility located at Moffett Naval Air Station, Mountain View, Calif. The fuel was stored in an airtight amber-colored, glass bottle for a period of time less than two weeks before its utilization in the test program. Upon completion of the program, the water content of the JP-4 fuel was analyzed by Karl Fischer titration and found to be 63 parts per million.

All of the test data are shown in log-log plots with the fatigue crack propagation rate, da/dN , as the ordinate and the stress intensity factor range, ΔK , as the abscissa.

a. Compact Tension Specimens

Most of the fatigue crack growth rate data presented in this report was obtained using an automatic ultrasonic crack follower. This device, in conjunction with the cycle counter, permits autographic plotting of crack length and number of cycles for each test specimen. After each test, the results are

verified for accuracy by comparing the recorded measurements with known actual crack lengths; e.g., surface markings (from load or frequency changes).

This technique of crack length measurement and recording provides several advantages over the other two more common methods; i.e., optical and step-advanced ultrasonic. Two of the principal ones are [1] continuous monitoring of the crack extension and [2] autographic recording of an X-Y plot of the crack length and number of cycles. The continuous monitoring aspect of the self-averaging autographic crack follower permits the detection of localized changes in crack resistance due to metallurgical variations present in the test material. Consequently, graphical differentiation of the actual X-Y plot of the crack length and number of cycles yields a truly representative crack growth rate at each appropriate stress intensity value. To some extent, this variability in crack growth rate, characteristic of the metallurgical inhomogeneity found in all commercial alloys, is inherently filtered out of the da/dN data obtained from a curve fitted to intermittent points from either optical measurements or a step-advanced ultrasonic record.

Some presentations of fatigue crack growth data list the number of data points that comprise a given plot (10). It is assumed that this quantity reflects the number of crack length observations actually made to provide the plotted data points. The number of data points possible from the autographically plotted crack length versus cycles curves generated in this test program is theoretically infinite. Pragmatically, a continuous line or a series of continuous lines that represent the differentiation of the autographic curves could be drawn. Such an endeavor is a laborious one and can lead to plots that are difficult to interpret. Therefore, to avoid confusion and save time only a representative sampling of the autographic record's continuous slope has been included in the data plots provided in this report.

(1) Ti-6Al-4V - 1-In.-Thick Plate

(a) Base Metal Metal (Mill Annealed)

Room Temperature

- o Laboratory Air. The data are shown in Figure 36. The predominance of a linear relationship usually exhibited by metallic materials in log-log plots is not readily apparent. Below a ΔK of about 9 ksi-in.^{1/2}, the crack growth rate becomes negligible. This is probably in the vicinity of the fatigue crack growth threshold. At slightly higher levels, the growth rate increases rapidly and, as expected, increases very rapidly as the applied maximum stress intensity approaches the material's fracture toughness. The data show good agreement with that exhibited by 1.25-in. mill-annealed plate in the same orientation and specimen type (10).
- o Salt Water. Also included in Figure 36 are the data obtained in an environment of 3.5 percent NaCl. The most salient feature of this data is the starting crack growth rate increase in salt water at

0.1 Hz. Manifestation of the detrimental effect of the 3.5-percent NaCl environment at this frequency appears almost immediately at a ΔK at about 10 to 12 ksi-in.^{1/2}. For an increase of stress intensity to approximately 15 to 20 ksi-in.^{1/2}, the accompanying crack growth rate increases by three orders of magnitude. In this same span of ΔK (from 10 to 20 ksi-in.^{1/2}), the da/dN at 10 Hz does not appear to differ a great deal from the baseline laboratory air data.

-65°F

- o Laboratory Air. The data are displayed in Figure 37. Also included in the figure are broken line curves defining the limits of the room temperature laboratory air data from Figure 36. Except at the higher values of stress intensity, the data are in good accord with that obtained at room temperature. Where the -65°F data display greater rates of crack growth, the maximum applied stress intensity factor is closer to the temperature decreased critical value. Only one specimen was tested.

175°F

- o Laboratory Air. The data obtained at frequencies of 0.1 Hz and 10 Hz are shown in Figure 38. For comparative purposes, the limits of the room temperature laboratory air data have been superimposed as a broken-line band. A frequency effect was not observed. At a ΔK of 40 ksi-in.^{1/2} and less, the data coincide with the lower-bound of the room temperature data. Above this level of stress intensity range, the increase in crack growth rate is slower than that measured at room temperature. The obvious reason for this observation is the greater difference between the maximum applied stress intensity and the critical value at the elevated test temperature.
- o Salt Water. The data from tests performed in salt water at the two frequencies are also included in Figure 38. At a ΔK of 20 ksi-in.^{1/2}, the growth rate is independent of both environment and frequency. However, at a slightly greater ΔK , both the environmental influence and the effect of frequency become pronounced. At 10 Hz, three to four-fold increase over the baseline laboratory air data is maintained over the span of stress intensity ranges examined. Meanwhile, the crack growth rate at 0.1 Hz increases by three orders of magnitude. The limits of the room temperature laboratory air and salt water data are included in Figure 38 for comparison. As can be seen in this figure, the laboratory air and salt water data bear a relationship similar to that observed at room temperature. It appears that the data would approximate the room temperature data except for a small shift to the right. Only one specimen was tested.

(b) Weldments (As Welded)

To obviate the precracking anomalies resulting from the residual stress

patterns in as-welded specimens, all were stress-relieved save four, two pre-cracked in the heat-affected zone and two precracked in the weld fusion zone. These four specimens were tested at room temperature in laboratory air to determine any gross effects of residual stresses. The data are included in plots along with the data from their stress-relieved counterparts.

(c) Weldments Stress-Relieved - Heat-Affected Zone (HAZ)

Room Temperature

- o Laboratory Air. The data from both stress-relieved and as-welded specimens are shown in Figure 39. At lower ΔK values, the as-welded specimens exhibit slightly slower cracking rates than those that are stress-relieved. The decreased growth rate probably results from the residual stresses present in the as-welded specimens. At increased ΔK levels, however, this slight advantage disappears. Also, at stress intensity ranges below about 30 ksi-in.^{1/2}, the heat-affected zone and base metal data overlap. Since the heat-affected zone is probably not as tough as the base metal (see Table XXXVIII), the more rapid increase in the propagation rate of the HAZ data as it approaches its critical value, prior to the base metal, is to be expected.

Crack length determinations on these specimens were made by optical measurement of the surface crack traces. The rather regular alignment of data points is a consequence of this method of crack growth data collection. Four specimens were tested.

- o Water and Salt Water. The results of the fatigue crack growth tests performed in water and 3.5 percent salt solution are shown in Figure 40. Up to a ΔK of 30 ksi-in.^{1/2}, the data for all test conditions correspond fairly well with the laboratory air data, indicating an independence of environmental and frequency effects. The upper and lower limits of the laboratory air data have been included in the figure. The 10 Hz data in both water and salt water environments remain within the bounds of the laboratory air results to the maximum ΔK at which growth rates at this frequency were examined. Above a ΔK of 30 ksi-in.^{1/2}, the growth rates in both liquid environments are accelerated at the 0.1 Hz frequency. The acceleration is more pronounced in the salt water environment with the greatest difference in growth rates occurring as the applied stress intensity approaches the critical stress intensity value.
- o JP4. Two specimens precracked in the heat-affected zone were tested in an environment of JP4 jet fuel; the obtained results are displayed in Figure 41. Included in the figure for comparison are the limits of the room temperature laboratory air data. It appears that the JP4 environment does not have any effect on the baseline laboratory air fatigue crack propagation rate.

-65°F

- o Laboratory Air. The -65°F data are shown in Figure 42. Also included in the figure are the upper and lower bounds of the data obtained in room temperature laboratory air for the same weldment location. As indicated in Figure 42, the 10 Hz data agree very well with those obtained at room temperature. The same is true for the 0.1-Hz data to a ΔK just below 40 ksi-in.^{1/2}. Above this value, the extended exposure time in the vicinity of the peak loads that occur at the lower frequency results in increased crack propagation rates. At applied maximum stress intensity factors in the proximity of the critical value, the alloy Ti-6Al-4V exhibits a sustained load cracking (SLC) phenomenon (11). Consequently, the accelerated rate of crack extension at relatively high values of ΔK during low frequency cyclic loads can be expected.

175°F

- o Laboratory Air. The data for 175°F are exhibited in Figure 43. Frequency effects were not discernible. The upper and lower limits of the room temperature, laboratory air data have been superimposed. As shown in the figure, the propagation rates at the elevated temperature, generally, are lower than at room temperature. A similar relationship existed with the base metal.
- o Water and Salt Water. Results of tests performed on water and salt water environments are plotted in Figure 44. Also included are the limits defining the baseline laboratory air data at 175°F. At a cyclic load frequency of 10 Hz in both the H₂O and 3.5 percent NaCl solution environment, a significant effect on the baseline data was noted. For the lower frequency, however, deviation from the baseline data was observed at a ΔK of about 30 ksi-in.^{1/2}. As in the case of room temperature behavior, acceleration of the crack propagation rate is greater in the salt solution.

(d) Weldments Stress-Relieved - Weld-Fusion Zone (WZ)

Room Temperature

- o Laboratory Air. Results from stress-relieved and as-welded specimens, precracked in the weld fusion-zone and tested at room temperature in laboratory air, are presented in Figure 45. At ΔK values of less than 20 ksi-in.^{1/2}, the data from as-welded specimens indicate a slightly slower fatigue crack propagation rate. Residual stresses in these specimens appear to be responsible for the retarded growth rate. Above 20 ksi-in.^{1/2}, a difference in the growth rates between welded and stress-relieved conditions was not discernible. Compared to similarly tested base metal (Figure 36), the weld-zone propagation rates are lower when below a ΔK of 30 ksi-in.^{1/2} and slightly higher when above a ΔK of 30 ksi-in.^{1/2}. The difference in rates at the lower ΔK values probably results from the difference in the

metallurgical structures of the two locations. The faster rates prevail in the crystallographically textured microstructure of the base metal, and the slower rates in the as-cast microstructure of the weld-fusion zone. The increased propagation rates of the weld-fusion zone above 30 ksi-in.² can be attributed to the proximity of the critical stress intensity factor, which is lower than that of the base metal. (See Table XXXVIII).

The data were determined by taking slopes of curves fitted to points obtained either from the optical measurement of surface traces or from the periodic measurement of the crack progression by a manually operated ultrasonic crack follower. A total of four specimens were tested.

- o Water. The data are shown in Figure 46. The upper and lower bounds of the room temperature baseline laboratory air data are shown as dashed lines in Figure 46. Below a ΔK of 40 ksi-in.², the data lie adjacent, for the most part, to the lower bound of the baseline data. Above the 40 ksi-in.² ΔK value, the data from specimens tested in the two environments - water and laboratory air - coincide. In contrast to the heat-affected zone results (Figure 40), effects due to frequency are not readily distinguishable.

A manually operated ultrasonic crack follower was used to measure crack extension.

- o Salt Water. Results from specimens precracked in the weld zone and fatigue tested in 3.5 percent NaCl solution are shown in Figure 47. For a baseline comparison, the laboratory air data boundaries have been shown as dashed lines. Cyclic loads applied at a frequency of 10 Hz do not have any effect, and the associated crack growth rates are similar to the laboratory air data. This also applies to fatigue loads at 0.1 Hz, up to a ΔK of approximately 25 ksi-in.². Above this ΔK value, the 0.1-Hz data deviate from the baseline results and exhibit an increased rate of crack propagation. This 0.1-Hz salt water corrosion fatigue threshold of 25-ksi-in.² is slightly less than that found in the heat-affected zone; i.e., 30 ksi-in.², but considerably greater than the salt-water corrosion-fatigue threshold observed in base metal; i.e., 10 to 12 ksi-in.². The principal metallurgical differences between these three regions - base metal, heat-affected zone, and weld-fusion zone - is microstructural. Basically, the crystallographically textured microstructure of the base metal is altered slightly by thermal energy in the heat-affected zone and completely by melting and resolidification in the weld-fusion zone. The three different values of the salt-water-corrosion fatigue threshold given above for a material of essentially the same composition are yet another example of the influence of metallurgical variables on the crack growth behavior of a given material.

- o JP4. The crack growth data for specimens tested in JP4 are given in Figure 48. The data coincide fairly well with the superimposed dashed-line plot of the laboratory air data limits. When variations in individual test specimens are considered, no influence of frequency on the test data can be detected.

-65°F.

- o Laboratory Air. The data are presented in Figure 49. The dashed lines represent the room temperature laboratory air data band. A frequency effect is not obvious to a stress intensity range of 40 ksi-in.². The data fall along the lower bound of the room temperature results. As can be seen from the extent of the data points, the toughness of these specimens exceeds that obtained in other tests at both room temperature and -65°F. (See Tables XXXIV and XXXV.) The propagation rates, below a ΔK of 40 ksi-in.² follow the lower bound of the room temperature rates. Above this ΔK value, the rates, all obtained at 0.1 Hz, increase markedly. This increase in fatigue crack propagation rate as the applied maximum stress intensity factor approaches is to be expected.

175°F

- o Laboratory Air. The results of these tests are shown in Figure 50. Included in the figure are dashed lines showing limits of the room temperature laboratory air data. The tests indicate rates that are comparable to the slowest rates obtained in room temperature laboratory air.
- o Water and Salt Water. The data from tests in both environments are presented in Figure 51. The band of laboratory air data, also at 175°F, has been superimposed as dashed lines.

With the exception of those measured at ΔK values less than 20 ksi-in.², rates of specimens tested in salt water at 10 Hz and of specimens tested in water at both 10 and 0.1 Hz do not show a significant increase over the laboratory air results. In fact, at some levels of stress intensity range, retardation is indicated in the water environment. As in the other material conditions, a frequency effect in the salt water environment is evident. Above a corrosion fatigue threshold of approximately 30 ksi-in.², the propagation rate at 0.1 Hz increases rapidly.

The general trend of the laboratory air fatigue crack data in the three Ti-6Al-4V locations - base metal, heat-affected zone, and weld-fusion zone - indicates increased growth at decreased temperature and decreased growth at increased temperature. (See Figures 37, 38, 42, 43, 49, and 50.) However, this trend is not sufficiently consistent to serve as a firm basis for defining the direct influence of tempera-

ture on crack propagation rate. Rather, the cracking rates in specific specimens appear to be more directly related to the ratio of the stress intensity factor range to the specimen fracture toughness. With respect to temperature, the fatigue crack propagation rate behavior parallels that of the material fracture toughness. Specimens that exhibit anomalous fatigue crack growth rates also reveal an anomalous value of fracture toughness or vice versa. For each of the material locations, it appears that the crack growth rates at all three test temperatures, plotted against $\Delta K/K_{IC}$ on a common set of axes, would almost coincide, that is, fall within a relatively narrow band. Similar situations appear to exist for corrosion fatigue crack propagation behavior, including the corrosion fatigue threshold.

(2) Beta III Titanium - 1-In.-Thick Plate

(a) Base Metal (Solution Treated and Aged)

Room Temperature

- o Laboratory Air. The results of the Beta III base metal fatigue tested in laboratory air are given in Figure 52. Frequency effects were not readily apparent. Between ΔK values of 30 and 40 ksi-in.^{1/2}, the crack growth rates correspond to the lower bound of the Ti-6Al-4V laboratory air data. Because of its higher room-temperature fracture toughness, the Beta III crack growth rates above a ΔK value of 40 ksi-in.^{1/2} are markedly slower than those of Ti-6Al-4V.
- o Salt Water. The data are shown in Figure 53. The upper and lower bounds of the laboratory air data are included for comparative purposes. The data are quite erratic; nevertheless, they reveal a general tendency to follow the behavior of the laboratory air results up to a ΔK value of 40 ksi-in.^{1/2}. Up to this level of stress intensity factor range, frequency effects are not evident. The corrosion fatigue threshold appears to be near a ΔK value of 45 ksi-in.^{1/2}. Above this threshold value, the growth rate at 0.1 Hz frequency shows a steep rise.

-65°F

- o Laboratory Air. A graphical presentation of the data is given in Figure 54. The growth rate appears to be unaffected by the cyclic load frequency. To relatively high values of ΔK , the data coincides fairly well with the room temperature results shown as dashed lines. The increased crack growth rate above a ΔK of 60 ksi-in.^{1/2} results from the proximity of the maximum applied stress intensity factor to the temperature-decreased critical stress intensity value.

175°F

- o Laboratory Air. The results of the fatigue tests performed at 175°F

in a laboratory air environment are shown in Figure 55. Frequency effects are not apparent. Included in the figure as dashed lines are the upper and lower limits of the room temperature results. Good agreement with the room temperature fatigue crack propagation rates is indicated.

The fatigue crack growth resistance of the Beta III base metal in laboratory air is, for the most part, independent of the test temperature. The proximity of the applied maximum stress intensity factor to the critical value, however, has a significant influence on the crack growth rate. At lower temperature, the critical value; i.e., fracture toughness, is decreased; therefore, at relatively high values of ΔK the associated crack growth rate is greater.

(b) Weldments (Solution-Treated and Aged)

Heat-Affected Zone (HAZ)

o Room Temperature.

- Laboratory Air. The data from the heat-affected zone specimen fatigue tested in room temperature laboratory air is shown in Figure 56. The boundaries of the base metal room temperature data are included for purposes of comparison. When the crack remains in the heat-affected zone, as represented by the data points in the figure, the crack growth rates are similar to the base metal.
- Salt Water. The precrack in the heat-affected zone specimen scheduled to be tested in a salt-water environment almost immediately grew into the weld-fusion zone and to the center-line where unstable fracture ensued at a ΔK of 28 ksi-in.^{1/2}. Except for one data point, a growth rate of 3.5×10^{-4} in./cycle at a ΔK of 25 ksi-in.^{1/2} and a frequency of 10 Hz, no other fatigue crack propagation rate data were obtained for the heat-affected zone in salt water.

o -65°F

- Laboratory Air. The data for a laboratory air environment at -65°F are shown in Figure 57. For a comparative analysis, the room temperature, laboratory air, and base-metal data limits have been included in the figure as dashed lines. In general, the crack growth rate appears to be insensitive to frequency. The anomalous data points at relatively low values of ΔK result when the crack plane and the fusion plane either converge to a point of very small separation or actually intersect for a very short interval of crack length. The high crack growth rate at a ΔK value in excess of 60 ksi-in.^{1/2} can

be attributed to the propinquity of the critical value of stress intensity.

o 175°F

- Laboratory Air. The data are shown in Figure 58. As in the Figures 56 and 57, the room temperature laboratory air, and base-metal data limits have been superimposed as dashed lines. There is no evidence of a frequency effect. Good agreement with the room temperature and the 175°F laboratory air data is indicated.

When the fatigue crack is truly situated in the heat-affected zone, the material behavior approximates that of the base metal very satisfactorily. Increased crack growth rates result when the crack deviates from the heat-affected zone and propagates in the microstructure that constitutes the transition region with the weld-fusion zone.

Weld Fusion Zone (WZ)

o Room Temperature

- Laboratory Air. Crack propagation rates for a specimen pre-cracked in the weld-fusion zone and fatigue tested in room temperature laboratory air are shown as a function of the stress intensity factor range in Figure 59. The limits of the room temperature, laboratory air and base-metal data have been superimposed as dashed lines for comparison. It appears that cyclic load frequency does not have any effect on the crack propagation rates. At low ΔK levels, the data agree with the base metal results. However, there is a pronounced upswing in the weld-zone, fatigue cracking rates at a ΔK of approximately 25 ksi-in.^{1/2}. The weld-zone toughness is a fraction of that of the base metal. Obviously, the marked increase in cracking rate is due to the nearness of conditions leading to unstable crack propagation.
- Salt Water. The crack growth behavior of a specimen pre-cracked in the weld-fusion zone and fatigue-tested in salt water is highly erratic. (See Figure 60.) Growth rates at the same ΔK level can vary as much as three orders of magnitude. The crack plane in this specimen coincided with the contiguous alignment of grain boundaries along the weld-fusion centerline. Once exposed to salt, a crack in the weld-fusion zone has an affinity for the continuous microstructural discontinuity at the centerline. Crack growth rates along this centerline plane of grain boundaries appear to be independent of the stress intensity factor range. Propagation rates in the range of 0.0025 to 0.04 in./cycle prevail over the entire range of applied ΔK values.

o -65°F

- Laboratory Air. The data for laboratory air are presented in Figure 61. Included in the figure as dashed lines are the upper and lower bounds of the room temperature laboratory air data. Much of the data are within the boundaries of the room temperature results, with most of the data adjoining the lower boundary. A significant effect of frequency is not indicated.

o 175°F

- Laboratory Air. The weld-zone fatigue crack growth data at 175°F is shown in Figure 62. Frequency appears to have no influence on the test results. Crack growth rates are considerably slower than those measured at room temperature, as shown by the dashed lines in Figure 62.

Much of the data generated in weld-zone specimens was obtained from specimens where the crack propagated in the fusion zone but not along the centerline where the grain boundaries are aligned. Cracks that find their way to the centerline usually cause failure at low stress intensity values. In the presence of salt solution, the preferential propagation direction of precracks is to the weld centerline and then along it. With the absence of salt water, a precrack, not already situated in the "superboundary", will continue to grow in the fusion zone without any preference for the centerline. As in the case of Ti-6Al-4V, the crack propagation rates in the Beta III weld zone exhibit, at the different test temperatures, a strong dependence upon the value of ΔK in relation to the toughness of the specimen being tested.

Over much of the stress intensity factor range, the fatigue crack growth is strongly influenced by the toughness of the specimen being evaluated. This influence is quite obvious above a stress intensity factor range corresponding to about 70 percent of the specimen's toughness. It appears that scatter in the test results is reduced if da/dN is considered a function of $\Delta K/K_{IC}$ rather than ΔK alone. Further, da/dN for a given material condition may be shown to be a single function of $\Delta K/K_{IC}$ for the three test temperatures investigated.

b. Part-Through Thickness Specimens

The shape of a part-through thickness crack is usually semielliptical or semicircular. The (c) location along the crack front is the intersection of the crack plane with the surface or the extremity of the semimajor axis of the semielliptical flaw. The crack front (a) location is the deepest penetration of a symmetrically shaped flaw or the extreme position of the semiminor axis of a semielliptical flaw.

All of the crack growth data at the (a) location were obtained by end-point analysis. Crack extensions at the (c) location were optically measured periodically with a traveling microscope. Growth rates were derived from the slope of a curve fitted to points on a plot of crack length versus cycles.

The data are represented as plots of the fatigue crack propagation rate and the stress intensity factor range. Fatigue crack growth rates are indicated for the propagation in both the (a) and (c) directions.

(1) Ti-6Al-4V - 1-in.-Thick Plate

(a) Base Metal (MA)

Room Temperature

- o Laboratory Air and Salt Water. The data are shown in Figure 63. The upper and lower limits of the data obtained with compact tension type specimens in similar environments are included in the figure. As shown in the figure, excellent agreement exists between the results from the two different types of specimens.

(b) Weldments (AW) - Heat-Affected Zone (HAZ)

Room Temperature

- o Laboratory Air and Salt Water. The data for these tests are given in Figure 64 which includes dashed lines representing the data trends from compact tension type specimens in laboratory air and salt water environments. Except for some disparity at a ΔK of 12 ksi-in.^{1/2}, agreement between the two specimen types is quite good.

(c) Weldments (AW) - Weld-Fusion Zone (WZ)

Room Temperature

- o Laboratory Air and Salt Water. The data are exhibited in Figure 65. The dashed lines represent the upper and lower bounds of the laboratory air data obtained with compact tension specimens. As is the case of the base-metal and heat-affected zone results, the weld-zone data from compact tension type and part-through thickness specimens agree very well.

6. ENVIRONMENTAL CRACK GROWTH AND THRESHOLD STRESS INTENSITY

All tests on both materials - Ti-6Al-4V and Beta III titanium - were performed on precracked compact tension specimens. The test environments included a 3.5 percent sodium chloride (NaCl) solution at room temperature and 175°F and JP4 jet fuel at room temperature.

The 3.5 percent NaCl solution was prepared with reagent-grade crystalline sodium chloride and commercially purchased deionized water. The NaCl, processed by the J. T. Baker Chemical Company, is certified to meet ACS specifications. The salt water was previously prepared and stored in a poly-

ethylene container until utilized in testing. To maintain the salt concentration at 3.5-percent during tests, evaporation losses in the test chambers were replenished with deionized water only.

The JP4 for the jet fuel environment was freshly siphoned from a flight storage tank at the NASA-Ames facility, Moffett Naval Air Station, Mountain View, Calif. The fuel was stored in an airtight, amber-colored bottle for a period of time less than two weeks before its utilization in the tests. The water content of the fuel was 63 ppm as determined by Karl Fischer titration.

The stress corrosion crack growth rates are presented in graphical format. The logarithm of the growth rate, da/dt , appears as the ordinate and the stress intensity factor, K , as the abscissa. Growth rate data are representative slopes of curves fitted to periodic determinations of crack length. The individual graphs also carry identification of the environmental crack growth threshold stress intensity factor, K_{ISCC} .

Initially, one specimen each of Beta III base metal and Beta III weld-zone and heat-affected zone weldments, and Ti-6Al-4V weld-zone and heat-affected zone weldments were sustain-loaded to approximately 75 to 90 percent of their K_{IC} values. After about 3 days storage in laboratory air, these specimens were exposed to the NaCl solution. After a 3-week exposure period, there was no indication of crack growth.

The specimens were removed from the test environment, dried, reloaded to a higher stress intensity value, and immediately exposed to the NaCl solution. During reloading, the crack in the Beta III heat-affected zone specimen started to propagate on the application of load. The load application was about 200 lb. greater than the sustained value and about 400 lb. less than the original load applied to secure the specimen in its self-stressing fixture. The crack continued to grow along the entire usable range of the specimen at an average velocity of about 6 in./hr. Post-test examination of the specimen revealed that the crack, following initiation, propagated to the weld centerline and continued growing along the centerline. This location corresponds to the contiguous alignment of grain boundaries that is typical in the Beta III weldments of this program. (See Figures 22 and 23.)

The remaining four specimens, after an additional three weeks' exposure to the salt solution, still did not exhibit any evidence of crack growth. These experiments were interrupted, the specimens unloaded, and then precracked a second time. Following the precracking operations, the environmental crack growth test procedures were repeated except that the crack tip was inoculated with salt water while the load was being increased. Load application was continued until either crack growth could be immediately observed or approximately 95 percent of the specimen's K_{IC} value was attained. Upon completion of the procedures to maintain a stressed condition, each specimen was left in its own NaCl environment.

The observed stress corrosion cracking immunity of the specimens loaded in laboratory air appears to be a consequence of the combination of a specimen's immediate load history and some type of chemical passivity that occurs in laboratory air at the crack tip. As a result of these findings, all subse-

quent specimens were loaded in the test environment as described.

a. Ti-6Al-4V - 1-In.-Thick Plate

(1) Base Metal (Mill-Annealed)

(a) Salt Water

Room Temperature. The data are shown in Figure 66. The stress intensity factor at which the crack growth rate becomes negligible (K_{ISCC}) is 30-ksi-in.²

175°F. These data are presented in Figure 67. The threshold stress intensity factor, K_{ISCC} , is at 33 ksi-in.² An interesting aspect of these data is the increased value of the environmental crack growth threshold. The higher threshold level was consistent with fatigue crack growth results where the analogous corrosion fatigue threshold was at a higher level in the 175°F tests. At the two test temperatures, a not-unexpected disparity exists between the threshold values for environmental crack growth and corrosion fatigue. The magnitude of the disparity, however, is surprising.

(b) JP4

Room Temperature. The data are shown in Figure 68. Once the crack started propagating, it grew through the entire usable range of the specimen. Since an appreciable slowdown in growth rate did not occur, there was no indication of the environmental crack growth threshold value of stress intensity. Little or no effect was anticipated from the JP4. Consequently, loads were applied to very near the critical load level corresponding to the specimen K_{IC} value before the JP4 was injected into the crack tip region. As a result, the initial stress intensity of the specimen was beyond the limit necessary to achieve crack arrest.

At the higher stress intensity factors, the measured rate in JP4 may contain a crack growth contribution that appears to be an inherent characteristic of the Ti-6Al-4V material. During the loading of some of the Ti-6Al-4V specimens by the procedures already described, a sustained load cracking (SLC) threshold was indicated. Above an undetermined but relatively high value of stress intensity, crack propagation, in the absence of any environment other than laboratory air, was observed. Measurement of this propagation rate was not attempted. Upon detection of the first indications of this type of crack extension, the crack tip was inoculated with the intended environment, and the application of load was terminated; these were almost simultaneous actions.

The susceptibility of Ti-6Al-4V base metal to environmental crack growth in JP4 represented behavior completely unexpected by the investigators.

(2) Weldments Stress-Relieved - Heat-Affected Zone (HAZ)

(a) Salt Water

Room Temperature. The growth rate data are displayed in Figure 69. The plateau crack velocity is less, and the threshold stress intensity factor is 10 percent greater than that observed in base metal.

175°F. Crack growth rates are shown in Figure 70. The two specimens were precracked in slightly different locations in the heat-affected zone. One was precracked in the far heat-affected zone at a point very close to base metal; the other was precracked nearer the weld-fusion plane. As shown in Figure 70, the crack velocity in the far HAZ specimen increased with decreasing stress intensity as the crack propagated into the base metal. The maximum velocity roughly corresponds with the plateau velocity measured in base metal at 175°F. In addition, the threshold stress intensity agrees with that observed in base metal.

In the heat-affected zone specimen precracked closer to the weld-fusion zone, the plateau velocity is almost two orders of magnitude slower, and the threshold value of stress intensity is about 20 percent greater. The above observations indicate a transitory role - between the responses in base metal and weld fusion zone - in the mechanical behavior of the heat-affected zone.

(b) JP4

Room Temperature. The specimen intended for testing in JP4 jet fuel was defective due to a lack of penetration along much of its usable length. Failure analysis of the specimen revealed evidence of some growth. The crack front was irregular; therefore, meaningful data were not obtained from this specimen and an estimate of the threshold value of stress intensity could not be made.

(3) Weld Fusion Zone (WZ)

(a) Salt Water

Room Temperature. The stress corrosion crack growth rate data are shown in Figure 71. Although the specimen was loaded beyond the sustained-load cracking threshold, it did not exhibit a distinct plateau region. The environmental crack growth threshold stress intensity is about 20 percent greater than its counterpart in base metal under similar testing conditions.

175°F. Crack growth data at this temperature are shown in Figure 72. The lowest value of stress intensity at which crack growth was observed is identified as the threshold. As seen in Figure 72, the corresponding value in the duplicate test specimen was at about 59 ksi-in.^{1/2}. Both specimens were probably immune to the influences of the elevated temperature salt water, and the stress intensities below which the crack growth rates became negligible correspond to the sustained-load cracking threshold of each sample.

(b) JP4

Room Temperature. A somewhat similar situation existed in the weld-zone specimen when loaded and exposed to an environment of JP4. The one data point obtained in the test is included in Figure 68 with the base metal results. The stress intensity at which a minimal amount of crack extension occurred is identified as the K_{ISCC} value for JP4. In all probability, the weld zone is immune to the JP4 environment, and the recorded threshold value represents the sustained-load cracking threshold of the specimen.

The Ti-6Al-4V material appears to be most vulnerable to stress corrosion cracking when the constant deflection mode specimens are loaded above the sustained load crack threshold (SLC) in the presence of a potentially aggressive environment.

b. Beta III Titanium - 1-in.-Thick Plate

(1) Base Metal (Solution Treated and Annealed)

(a) Salt Water - Room Temperature

Beta III titanium base metal did not exhibit detectable crack growth at three different stress intensity factors. (See Figure 73.) Each time the immunity of the material was established at a given value, the stress intensity was increased. In between loadings, the specimen was freshly precracked. Since evidence of growth was not detected at a stress intensity factor of 86 ksi-in.^{1/2}, the test was terminated.

(b) Salt Water - 175°F

Beta III titanium base metal exposed to salt water at 175°F also revealed immunity to stress corrosion cracking. After two loadings - the last one at a stress intensity factor of 86 ksi-in.^{1/2} - crack growth was not evident. (See Figure 74.)

(2) Weldments - Heat-Affected Zone (HAZ)

(a) Salt Water - Room Temperature

The behavior of this specimen was described in the introductory paragraphs of this portion of Section III. (See III, 6.)

(b) Salt Water - 175°F

The specimen selected for evaluation at the 175°F temperature failed during loading. The precrack was in the heat-affected zone immediately adjacent to the weld-fusion zone. On loading, the crack initiated and propagated down the weld centerline. As in all the other cases of weld-centerline failure, the fracture surface had a 100-percent flat appearance.

(3) Weldments - Weld-Fusion Zone (WZ)

(a) Salt Water - Room Temperature

Due to the highly erratic behavior of the Beta III weld centerline in all of the other fracture tests performed previously, both specimens - the one scheduled for room temperature testing and the one intended for testing at 175°F - were tested at room temperature. The crack growth rate results are shown in Figure 75.

The precrack front in one of the specimens was located in the weld zone but very near the fusion plane. After loading, the crack extended for a short distance and was then arrested. This crack growth rate and stress intensity at crack arrest are shown in Figure 75. Because of this precrack location, this value of stress intensity, 50 ksi-in.^{1/2}, appears to a good estimate of the minimum threshold stress intensity in the heat-affected zone. On subsequent reloading, the crack in the above specimen extended to the centerline and started propagating at the rates shown. The precrack for the second specimen was initially situated in the weld zone, and then began propagating immediately. The minimum stress intensity at which a crack growth was obtained in the weld centerline was 14 ksi-in.^{1/2}.

The Beta III titanium base metal attribute of immunity to stress corrosion cracking is offset by the considerable lack of crack tolerance along the centerline of its electron beam weld fusion zone.

7. SPECTRUM FATIGUE

Six part-through thickness specimens (Figure 10), four precracked in the weld-fusion zone and two precracked in the heat-affected zone, were subjected to continuous repetition of the loading spectrum (see Figure 17) until failure. During spectrum loading, the frequency of cyclic stress corresponded to a loading rate of 400 ksi/sec with a limiting frequency of 20 Hz.

The precrack depths in the two heat-affected zone specimens were 46 and 32 percent of the specimen thickness, respectively. In the four weld-zone specimens, the depths of precracking were 46, 45, 29 and 21 percent, respectively, of the specimen thickness.

Photographs of the fracture surfaces, pertinent specimen dimensions, and layer and block numbers in which failure occurred are included in Figure 76 for the heat-affected zone specimens and Figures 77 and 78 for the weld zone specimens. A block is one complete spectrum cycle consisting of 59 layers.

In Figure 76, the surface markings, due to the various amplitudes and frequencies of the individual layers, are readily discernible. The fractographic signatures of the spectrum's varying loads and frequencies are also evident in Figures 77 and 78 but are not as clearly distinguished. Each set of surface markings can be correlated with one spectrum fatigue block; for example, in Figure 76(a), there are 21 distinct sets of surface markings.

All precracks were intentionally made to be nearly semicircular. To a large extent, the growing cracks retained this semicircular shape to about

75 percent of the specimen thickness in the heat-affected zone specimens and up to nearly 90 percent in some of the weld-zone specimens. Retardation of crack growth is apparent along the crack surface length and in the proximity of the far free surface. A large plastic zone from high amplitude loads in previous blocks acts to retard crack growth. Because of the lack of adequate elastic constraint, the sizes of plastic zone where the crack front either intersects or approaches the free surfaces are larger than the sizes of plastic zones associated with the crack front near mid-thickness. This crack-retarding "skin effect" results in flaw shapes that have a winged appearance such as that shown in Figure 76(a). Since the yield strength is greater in the weld-fusion metal with, therefore, the degree of elastic constraint also greater, the winged appearance is not as pronounced in these specimens.

An iterative computer program was used to predict failure in the spectrum fatigue loaded part-through thickness specimens. The predicted failure curves for the heat-affected zone and the weld zone, as well as the results from the test specimens, are shown in Figure 79. Considering the complexity of loading spectrum and the variability in material fracture toughness, a remarkable correlation was obtained.

The computer program is based on the following assumptions:

- o Irwin's equation adequately described the stress intensity.
- o The flaw is semicircular and remains so to failure.
- o At all stress ratios, the crack growth is accurately described by an empirical modification of the Forman equation (12).
- o Failure occurs at the validated fracture toughness value obtained with part-through thickness specimens; i.e., at 46 ksi-in.^{1/2} for the heat-affected zone and 41 ksi-in.^{1/2} for the weld-fusion zone.

The modified equation is

$$da/dN = C \Delta K^n / (1-R)(K_{IE} - \Delta K) \quad (4)$$

The constant, C, and exponent, n, are determined from fatigue crack propagation data obtained with compact tension specimens. The similarity in crack growth rates in the two types of specimens, CTT and PTT, is shown in Figures 63, 64, and 65. The adequacy of the modified Forman equation in describing the fastest rates obtained in actual compact tension tests is exhibited in Figures 80 and 81 for the heat-affected zone and weld zone, respectively. At stress ratios other than zero, equation (4) above provides slower crack growth rates, particularly at high ΔK values, than does the Foreman equation. With the mixed loading sequence in any spectrum, this appears to be a more realistic approach.

Computer simulation of crack growth is attained by the successive addition of the calculated crack extension that occurs during an individual spectrum layer. The growth resulting from each layer is computed - a product of growth rate times the number of cycles within the layer - after the determination of the layer's stress intensity factor, ΔK , and stress ratio, R . Growth in each layer is accumulated until failure occurs when $K_{max} = K_{IE}$. The total number of blocks, the layer and number of cycles at failure, and the initial and final crack sizes are printed.

The actual cross-sectional areas of the specimens were equal to or greater than the area given to the computer model. The specimen WZ-2, which had the greatest difference in cross-sectional area (about 11 percent), also exhibited the greatest deviation from its predicted life. In addition, the fracture toughness value used for the heat-affected zone predictions was the lowest of the three given in Table XXXVIII. Adjustments for the variations in cross-sectional areas and fracture toughness of the individual specimens would result in even more accurate failure predictions. Regardless of the foregoing observations, the correlations viewed in Figure 79 are encouraging.

8. NATURAL DEFECTS

Of the six natural defect specimens, three failed at loads at a fraction of the yield and three did not fail at loads corresponding to 90 percent of the yield. The results are given in Table XXXIX.

The results from these tests were disappointing. Defect sizes were either too gross or too small to be tractable analytically by fracture mechanics techniques.

Intentional incorporation of defects during welding proves to be a very inefficient method of providing flawed material for testing. Except where very large capacity loading facilities are available, the method is also an impractical one. One of the major contributing factors is the inability of the welding operator to control defect size adequately. This inability is of particular significance with respect to thick-section weldments where the dimensions of a subsequent test specimen impose a limitation on the length of weldment in which the flaw is to be incorporated.

The procedures followed to encourage the formation of defects produced chemical and metallurgical alterations that are not truly representative of the normally welded structure. Additionally, the intentional defects most easily produced and controlled were not the type of defect most readily encountered in production weldments. In this entire program, the only type of gross defect found in the production weldments was the lack of fusion in the vicinity of the root face. In this region, the narrow pencil-shaped profile of fused metal at times failed to encompass a portion of the faying surface junction. The result was a linear crack-like defect.

SECTION V CONCLUSIONS

The test results demonstrate the following:

- o Ti-6Al-4V weldments are superior to Beta III weldments in toughness, fatigue crack growth resistance, corrosion fatigue crack growth resistance, and resistance to stress corrosion cracking.
- o Beta III electron beam weldments contain an inherent microstructural imperfection that accounts for their lack of crack tolerance and crack growth resistance.
- o In the 1-in. thicknesses tested in this program, Beta III base metal exhibits higher strength and greater subcritical crack growth resistance in the various test media than does the Ti-6Al-4V base metal.
- o A sustained load crack threshold (SLC), i.e., a value of stress intensity near K_{IC} above which subcritical crack propagation occurs in the absence of any environment other than laboratory air, is present in the 1-in. Ti-6Al-4V alloy.
- o When 1-in. Ti-6Al-4V alloy is loaded in a constant deflection mode above the sustained load crack threshold in the presence of a potentially aggressive environment, vulnerability to stress corrosion cracking is enhanced.
- o Microstructure is one of the principal influences on the fracture properties of Ti-6Al-4V alloy.
- o Crystallographically textured, 1-in. Ti-6Al-4V plate is susceptible to stress corrosion cracking in the JP-4 jet fuel. The water content of the fuel is 63 ppm.
- o The salt water stress corrosion crack threshold, K_{ISCC} , in the 1-in. thickness of both titanium alloys increases with increased test temperature.
- o The fatigue crack growth behavior of a given titanium alloy at ΔK values above about 20 ksi-in.^{1/2} exhibits a strong dependency on the specific toughness of the individual specimen being evaluated.
- o Fatigue crack growth data from compact tension specimens can be used to provide safe-life predictions in spectrum loaded part-through thickness specimens.
- o Testing of thick section weldments with intentionally included natural defects to assess the influence of the defects on material fracture behavior is inefficient, and at times can cause a misleading evaluation.

SECTION VI

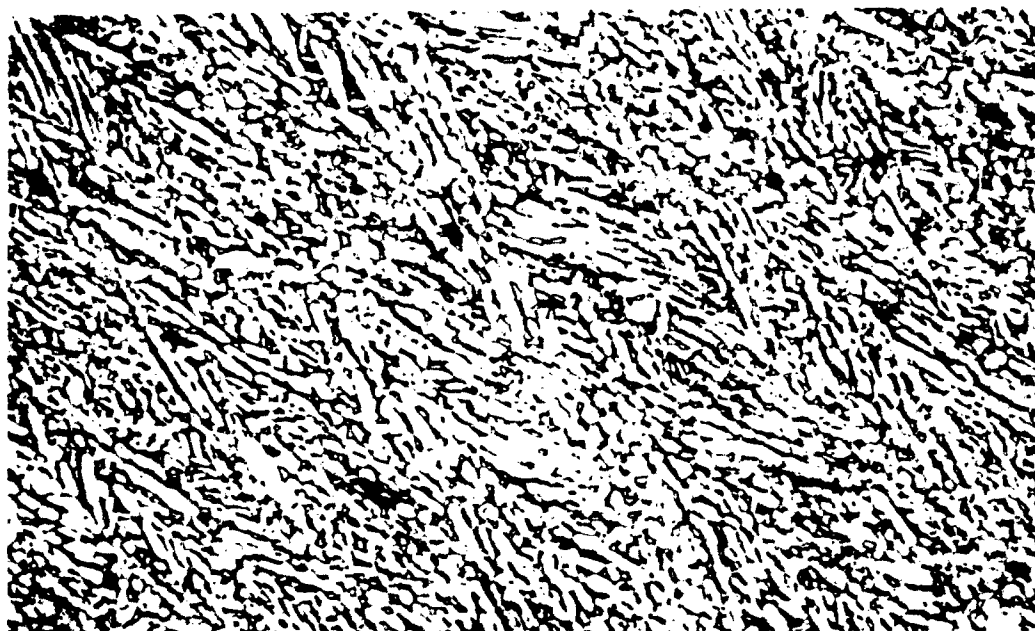
RECOMMENDATIONS

1. Until different welding techniques for Beta III are developed, or the existing one improved, thick section electron beam weldments of the alloy should not be used in any structural application.
2. Nondestructive inspectability of weldments to detect lack of fusion in thick section titanium alloy butt joints must be improved. Possibly, the means to accomplish the improvement might be incorporated into the weldment itself. For example, serrated profiles can be machined into the faying surfaces. Regardless of the intimacy of main surface contact, the serration or serrations in any unfused segment of the junction would result in more easily resolved radiographic images.
3. The role of the sustained load crack threshold (SLC) in Ti-6Al-4V alloy, when present, appears to be a very important one. For example, in the present program, the 1-in. Ti-6Al-4V constant deflection mode test specimens exhibited immunity to all room temperature test environments until they had been loaded beyond the SLC threshold during exposure to the test media. Since the SLC threshold appears to be so near the material's critical value of stress intensity, the probability of encountering in service the same susceptibility observed in the laboratory appears to be quite low. Consequently, consideration of the SLC threshold as the failure criterion in design instead of K_{IC} could lead to more reliable and efficient utilization of the material. Further research in the causes of a SLC threshold in Ti-6Al-4V and its effect on the stress corrosion susceptibility of the alloy is recommended.
4. To obtain more realistic subcritical crack growth data, techniques that continually monitor either the effective crack length or the crack length at the specimen midthickness should be strongly encouraged or made a requirement. This is particularly the case if: (1) reliable engineering information for design purposes is required, and (2) correlations between a material's microstructure and its subcritical crack growth behavior is desired.
5. Evaluation of the effects of cracks in weldments on mechanical behavior should be restricted to the testing of specimens of common configuration containing mechanically synthesized flaws; i.e., flaws with fatigue crack acuity.

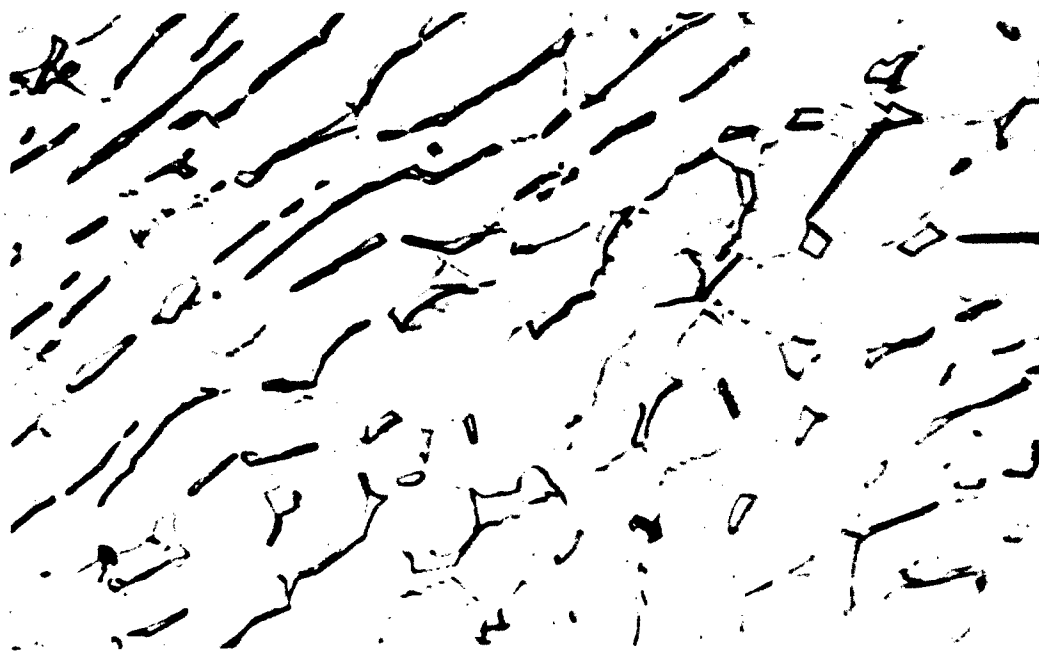
REFERENCES

1. R. G. Forman, "Study of Fatigue Crack Initiation From Flaws Using Fracture Mechanics Theory," presented at the Fourth International Symposium on Fracture Mechanics, Pittsburgh, Pa., Aug 1970
2. V. C. Peterson, J. B. Guernsey, and H. A. Johnson, "Beta III Titanium Properties and Applications," AIA Paper No. 68-976
3. W. F. Brown, Jr., and J. E. Srawley, Plane Strain Crack Toughness Testing of High Strength Metallic Materials, American Society for Testing Materials, Special Technical Publication 410, 1966, p. 12
4. G. R. Irwin, "Crack Extension Force for a Part-Through Crack in a Plate," J. Appl. Mech., Vol. 84, 1962, pp. 651-654
5. W. K. Wilson, Review of Analysis and Development of the WOL Specimen, Westinghouse Research Report 67-707-BTLPV-R1, MDR 8, 1967
6. R. W. Judy, C. N. Freed, and R. T. Goode, A Characterization of Fracture Resistance of Thick Section Titanium Alloy, NRL Report 7427, Jul 5, 1972
7. A. S. Kobayashi, On the Magnification Factors of Deep Surface Flaws, Structural Development Research Memo No. 16, The Boeing Company, Dec 1965
8. F. W. Smith, Stress Intensity Factors for a Semi-Elliptical Surface Flaw, Structural Development Research Memo No. 17, The Boeing Company, Aug 1966
9. P. N. Randall, Discussion in "Plane Strain Crack Toughness Testing of High Strength Metallic Materials," by W. F. Brown, Jr. and J. E. Srawley, ASTM STP 410, 1966, pp. 88-125
10. Damage Tolerant Design Handbook, A Compilation of Fracture and Crack-Growth Data for High Strength Alloys, MC1C-HB-01, Metals and Ceramics Information Center, Battelle, Columbus Laboratories, Dec 1972
11. D. A. Meyn, "Effect of Hydrogen Content on Sustained Load Cracking in Ti-6Al-4V," Report on NRL Progress, Jun 1972, pp. 17-19
12. R. C. Forman et al., "Numerical Analysis of Crack Propagation in Cyclic Loaded Structures," Transactions of ASME, J. of Basic Engineering, Vol. 89, No. 3, Sep 1967

13. C. F. Tiffany, Fracture Control of Metallic Pressure Vessels, NASA SP-8040, May 1970
14. NASA/Industry Working Group, Preliminary Criteria for the Fracture Control of Space Shuttle Structures, prepared at Langley Research Center, Hampton, Va., Jun 1971
15. J. G. Bjeletich, and T. M. Morton, "Fracture Mechanics Technology and Optimum Pressure Vessel Design," to be published in ASTM STP 536, American Society for Testing and Materials, Philadelphia, Pa., 1973

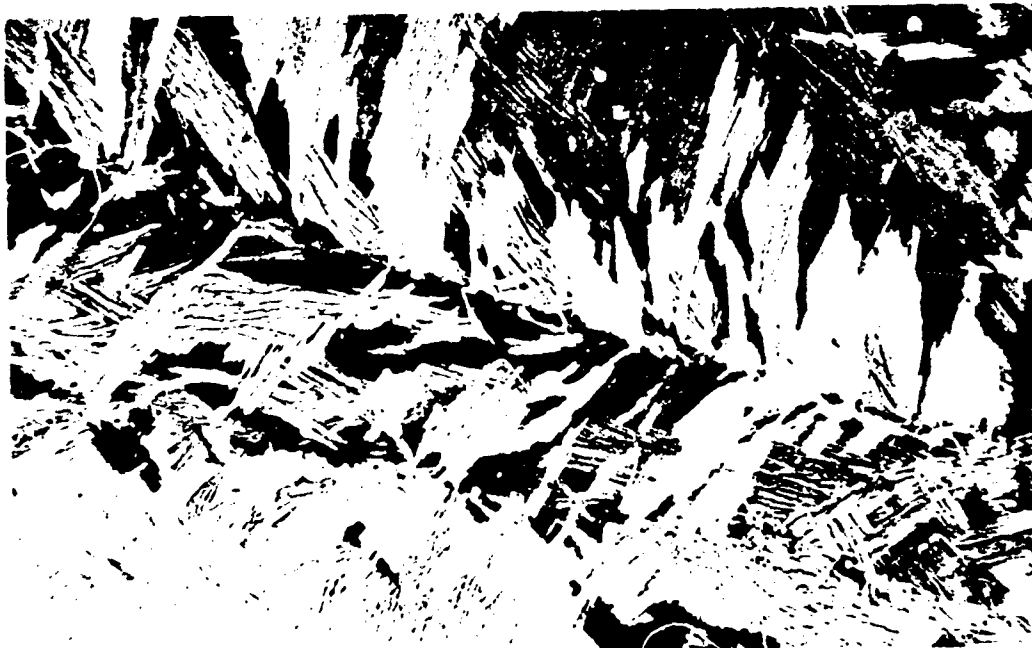


(a) 500x



(b) 3000x

Figure 1 Microstructure of 1-in.-Thick Ti-6Al-4V Mill Annealed Plate

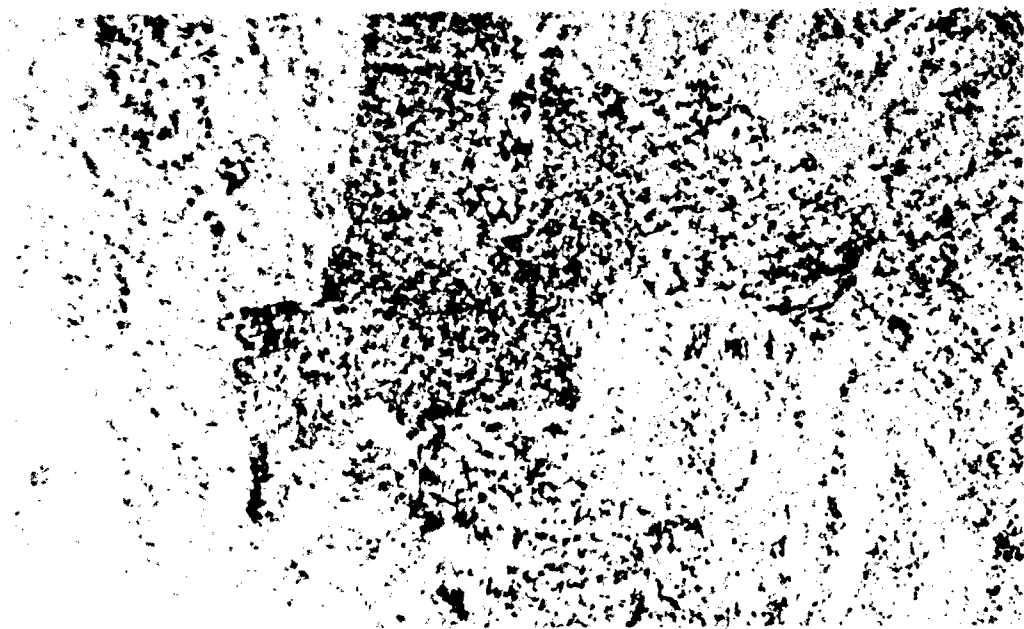


(a) 200x

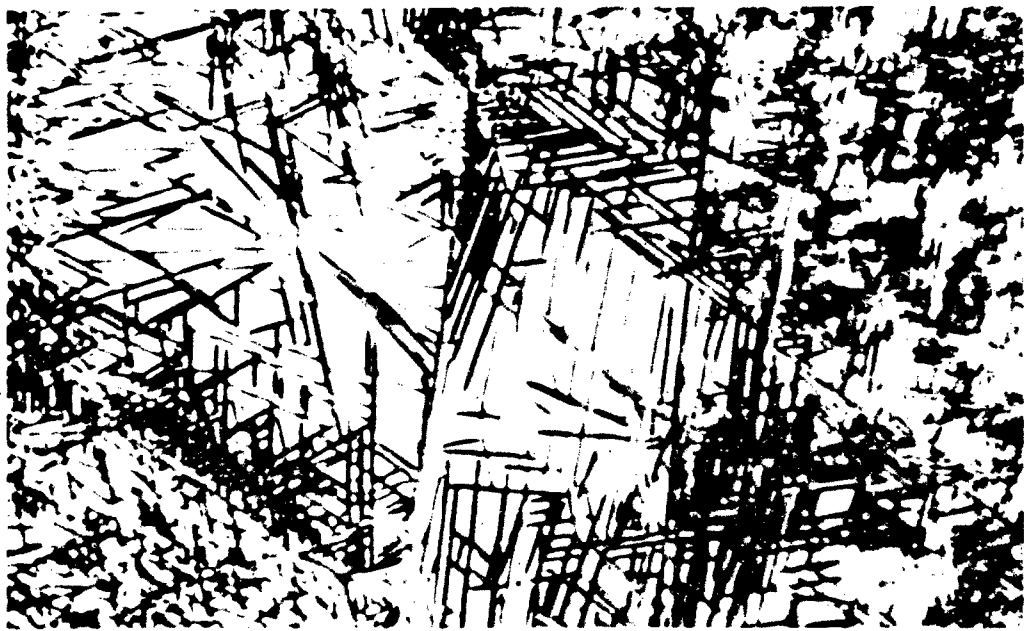


(b) 3000x

Figure 2 Microstructure of 2-in.-Thick Ti-6Al-4V Mill Annealed Plate

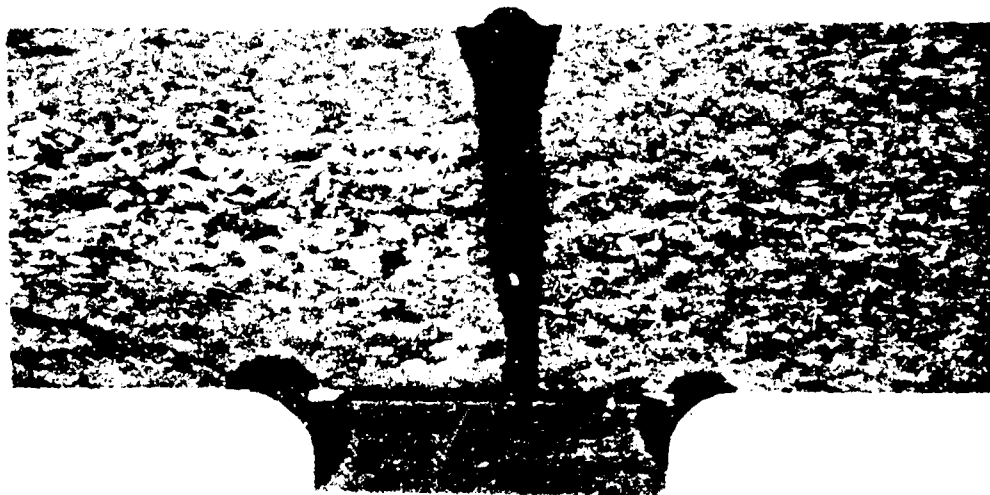


(a) 500x

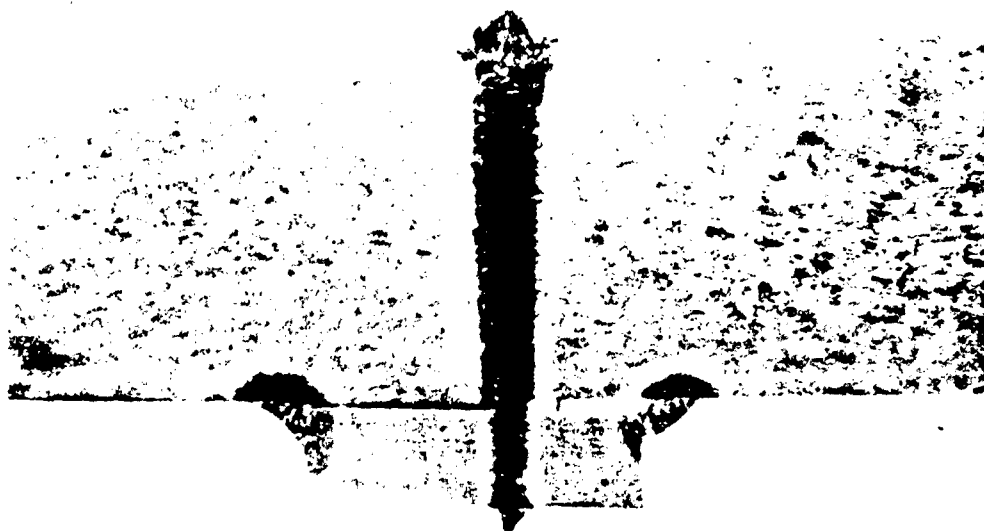


(b) 3000x

Figure 3 Microstructure of 1-in.-Thick Beta III Titanium Solution-Treated Plate (As-Received Condition)

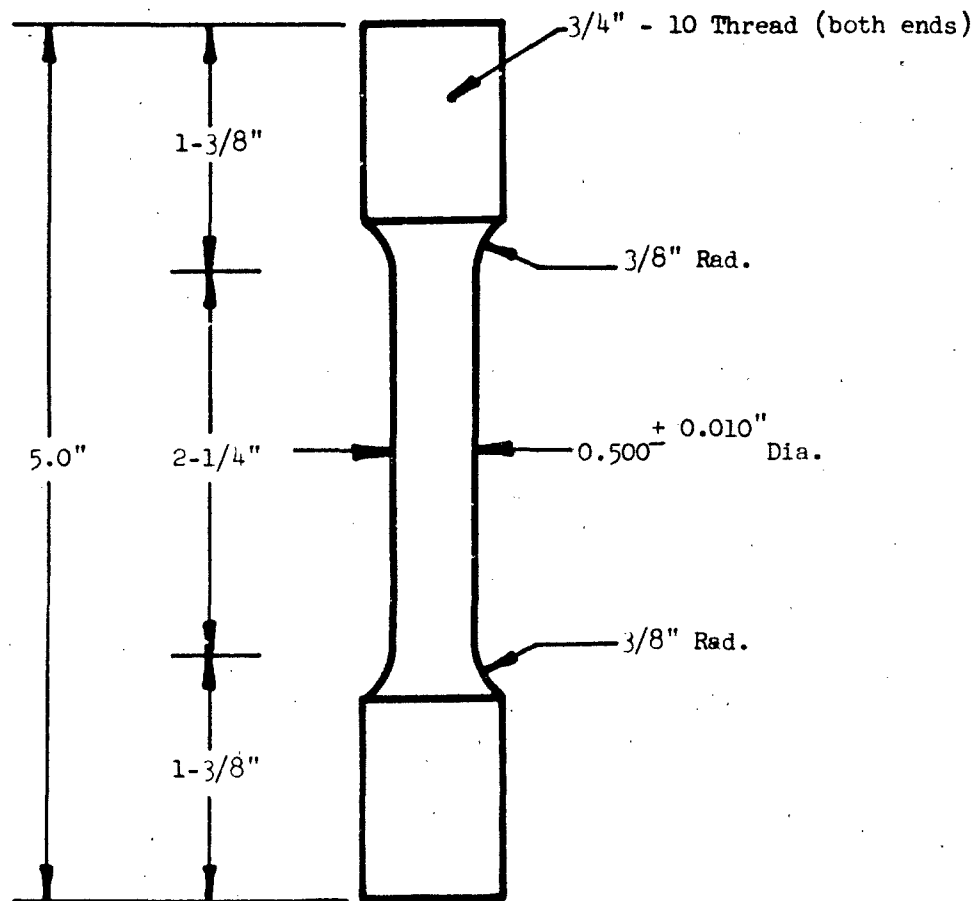


(a) 2x



(b) 2x

Figure 4 Cross-Section of 1-in.-Thick Weldments of Ti-6Al-4V Alloy: (a) Panels welded by a single electron beam joining pass. The butt facing surfaces adjacent to the weldment's root face were not joined metallurgically; (b) Panels welded by a single electron beam joining pass plus two additional repair passes to completely eliminate all radiographic traces of defects.



NOTE: Dia. at center of reduced section not to be greater than at either end. Difference in dia. anywhere in reduced section not to exceed 1% of dia. at center.

Figure 5 Tensile Test Specimen Configuration

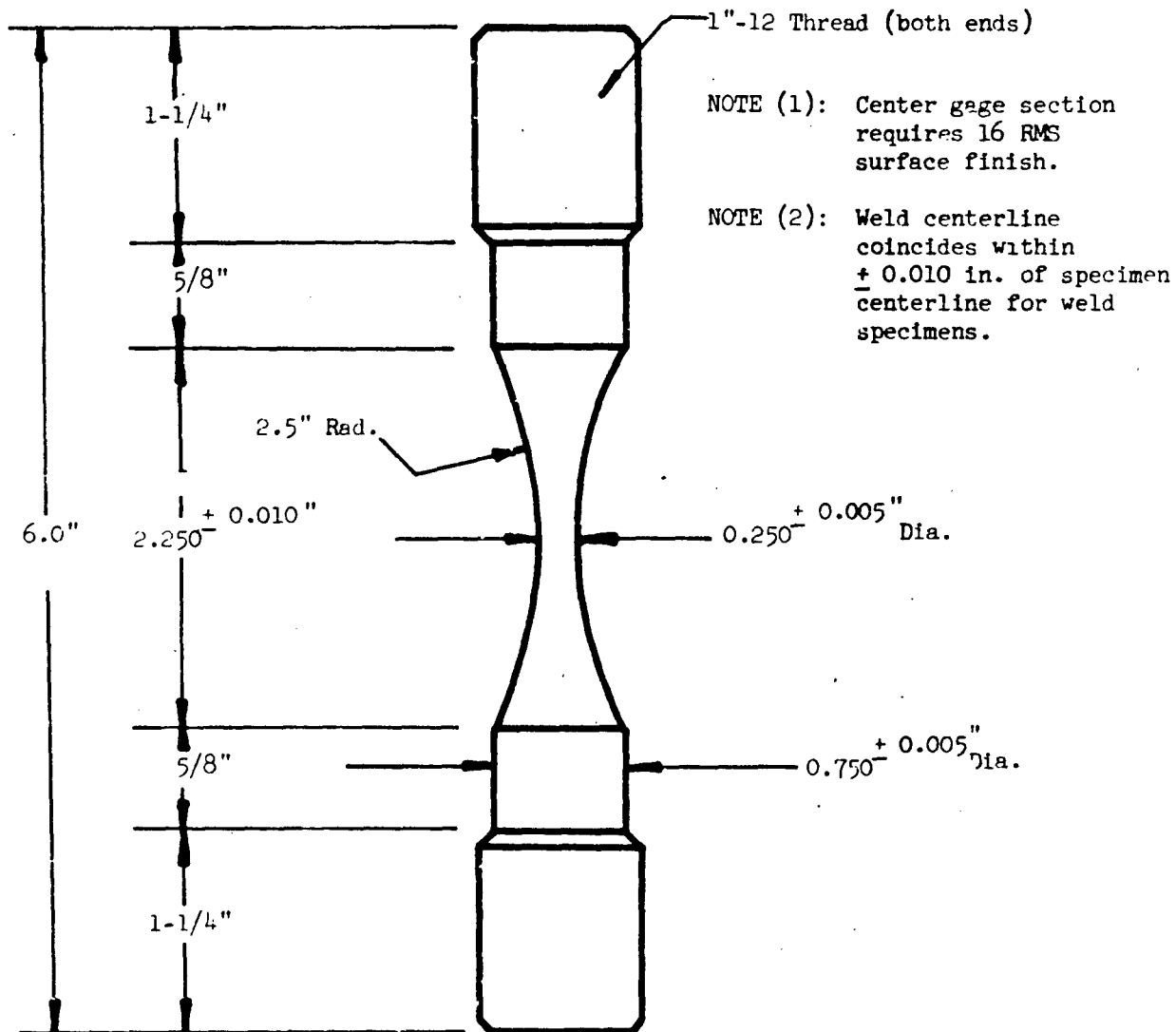


Figure 6 Axial Fatigue Test Specimen Configuration

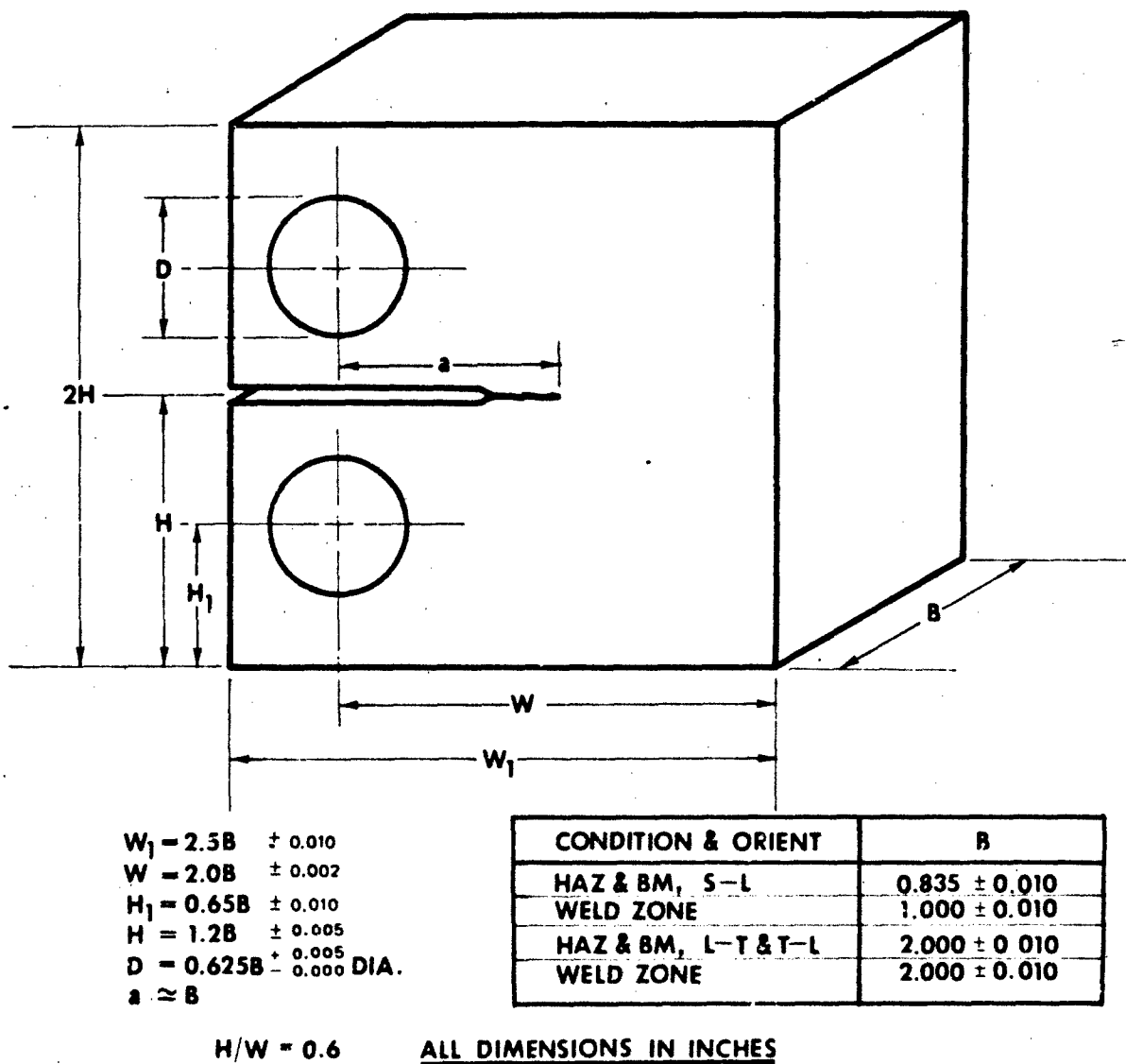
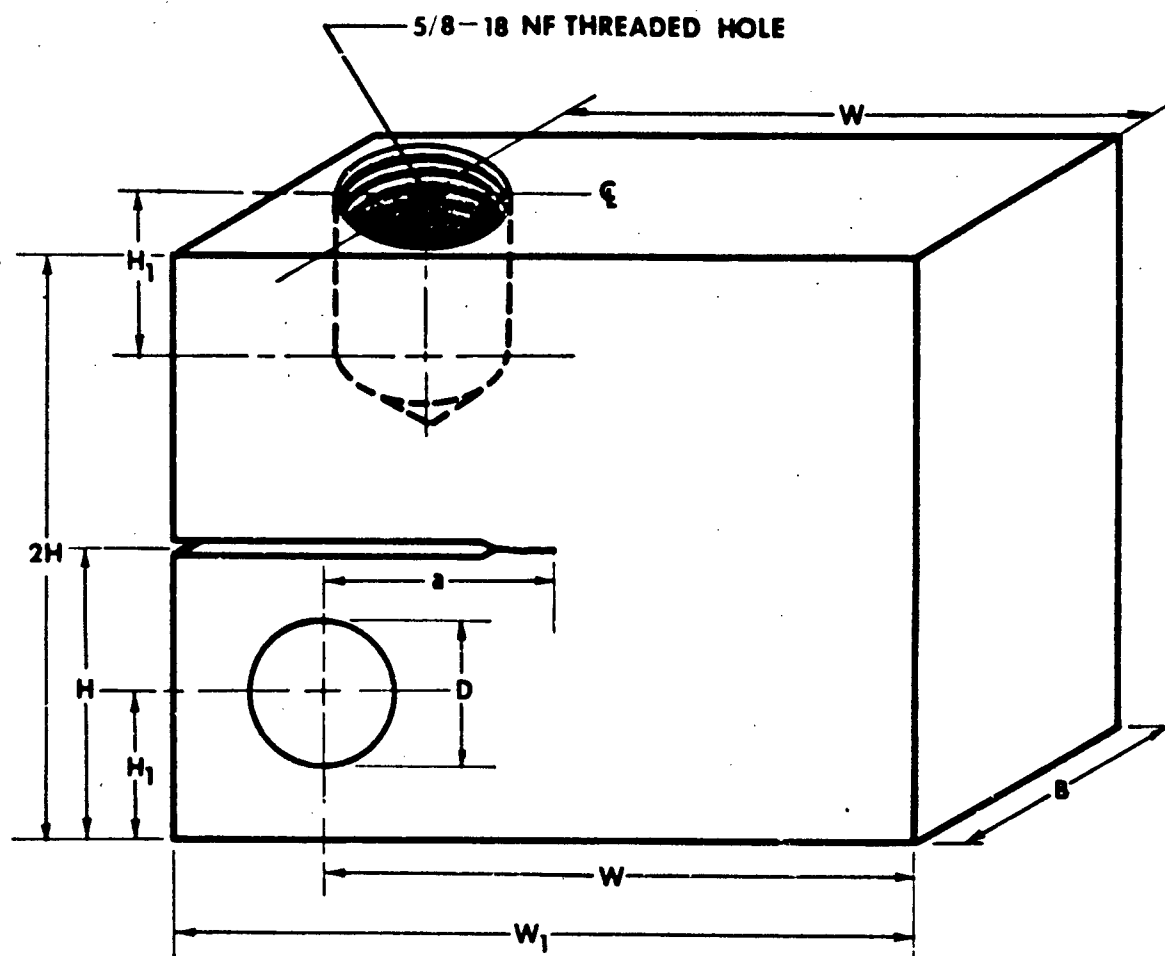


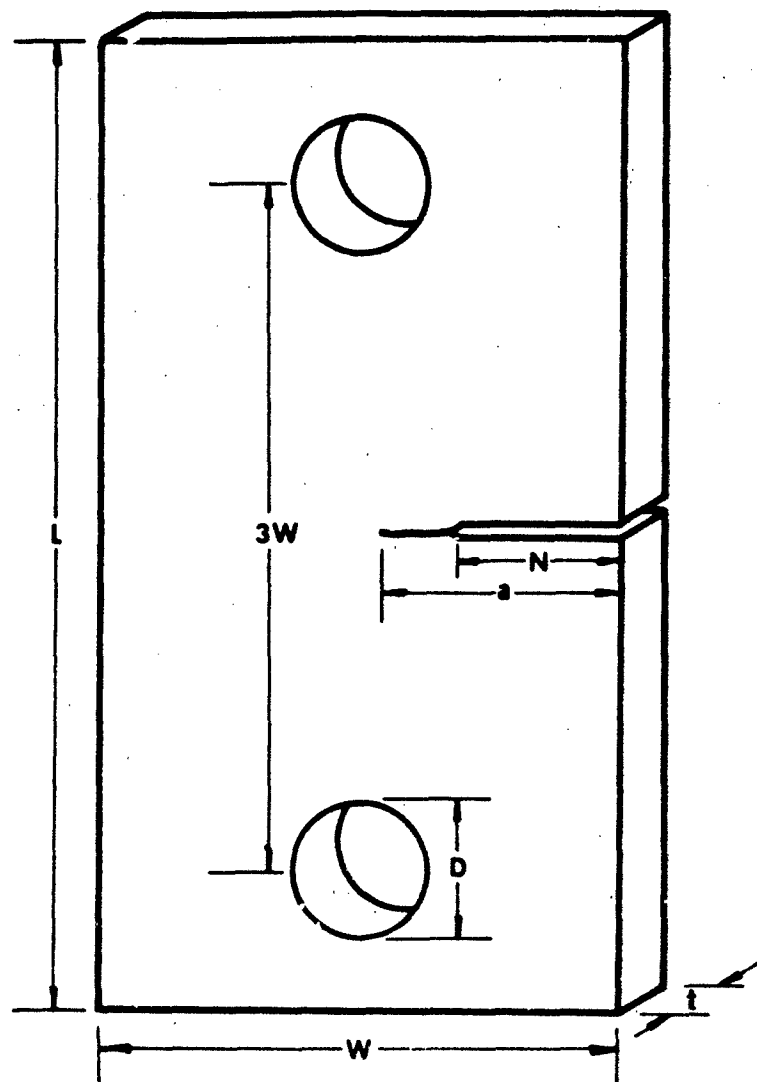
Figure 7 Compact Tension Test Specimen Configuration for K_{IC} Testing.



ALL DIMENSIONS IN INCHES

B	1.000 ± 0.010	
H	1.240 ± 0.005	H/W = 0.486
H₁	0.650 ± 0.010	
W	2.550 ± 0.002	
W₁	3.200 ± 0.005	
D	0.625 ± 0.005 - 0.000 DIA.	
a	1.00 MIN.	

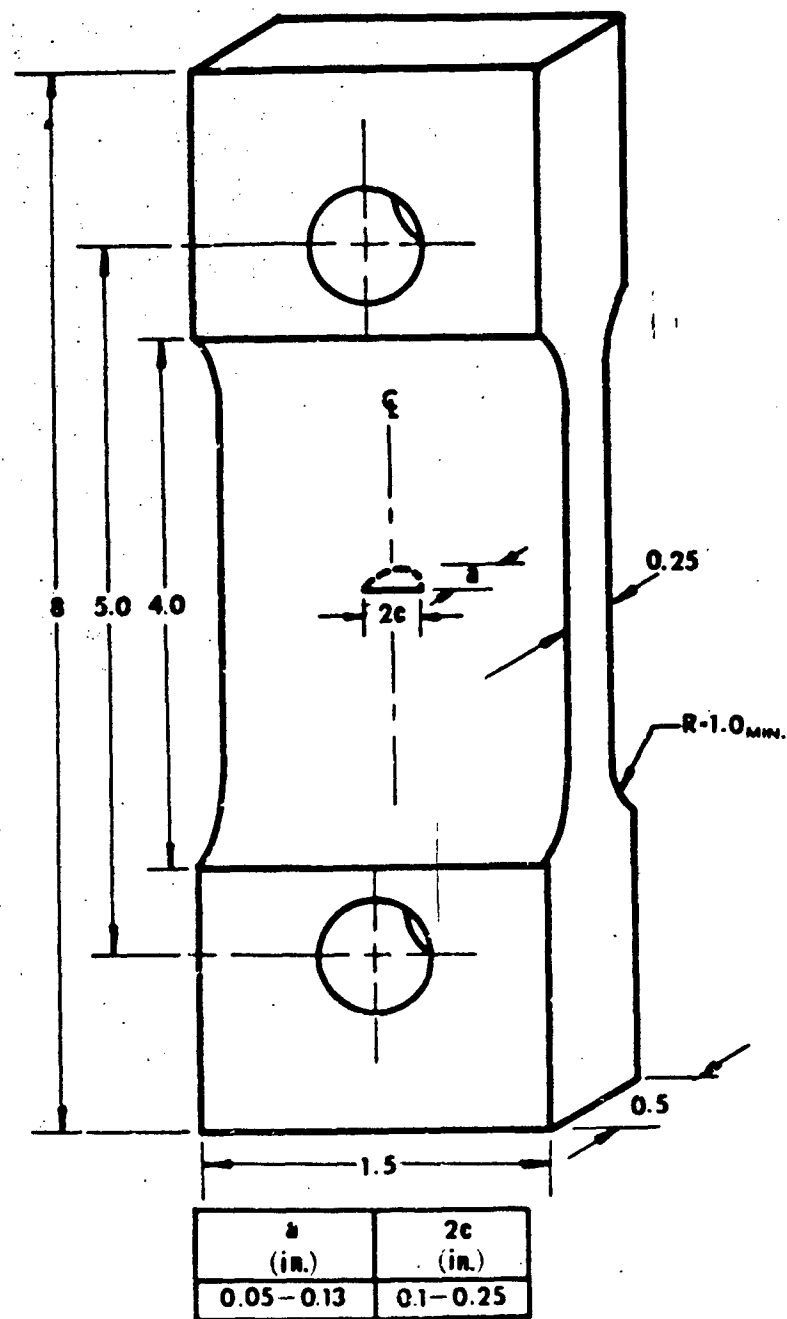
Figure 8 Wedge Opening Load Test Specimen Configuration for Crack Growth Rate Tests



ALL DIMENSIONS IN INCHES

t	W	L	a	N	D
1/4	5	19	1-2.5	0.8	1
1/2	5	19	1-2.5	0.8	1
1	3	13	1-1.5	0.8	1

Figure 9 Single-Edge Notch Specimen Configuration for K_{IC} Testing



ALL DIMENSIONS IN INCHES

Figure 10 Part-Through Thickness Specimen Configuration for K_{Ic} and da/dt Testing

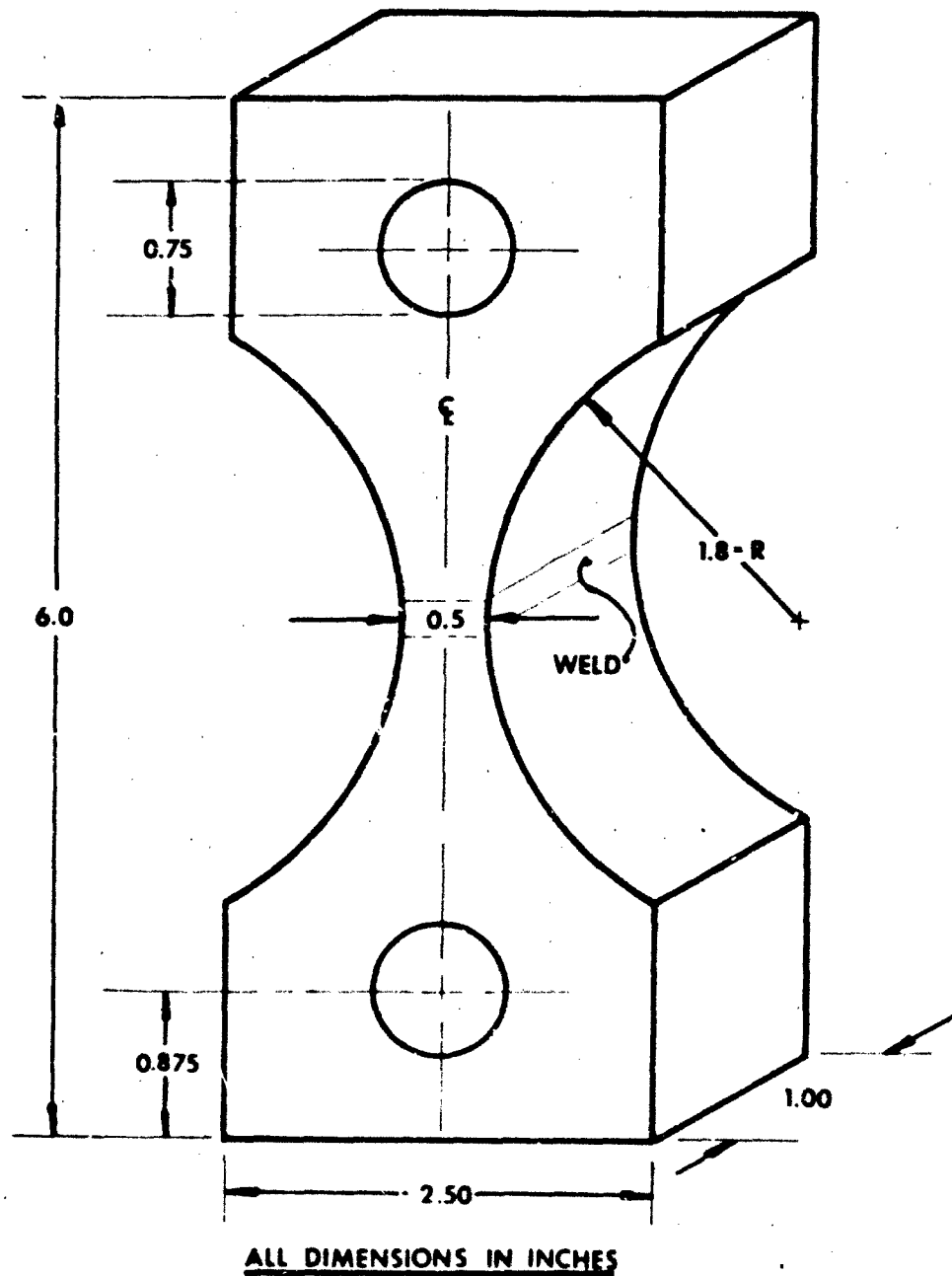


Figure 11 Test Specimen for Natural Defect Evaluation

COMPACT TENSION K_{Ic} TEST RECORD

Fracture Behavior Laboratory
Dept. 52-31, Bldg. 204
Materials and Structures Lab.

SUMMARY	
Material <u>T-6Al-4V</u>	Tests by <u>ROY HARRINGTON</u> Date <u>7-25-72</u>
Specimen No. <u>4-2</u>	Calculations by <u>R.H.</u> Date <u>9-20-72</u>
$K_I(\max)$ <u>20.68</u> ksi-in ^{3/2}	Checked by <u>T.M. HAZEN</u> Date <u>9-22-72</u>
ΔK_I at a_c <u>18.61</u> ksi-in ^{3/2}	<u>J.G. BYELETKA</u> Date <u>11-15-72</u>
$K_I(\max)/a_c$ <u>0.00122</u> in ^{1/2}	
K_{Ic} <u>112.4</u> ksi-in ^{3/2}	Precracking Temperature (T_1) <u>72</u> °F
P_{max}/P_Q <u>1.018</u>	Test Temperature (T_2) <u>72</u> °F
$2.5(K_Q/P_{ty})^2$ <u>2.072</u>	Relative Humidity <u>20</u> %
K_{Ic} <u>112.4</u> ksi-in ^{3/2}	Fracture Appearance <u>10</u> % Oblique
R_{sc} <u>NA</u>	ASTM E399-72

1. Material: T-6Al-4V, 2-INCH PLATE BASE METAL

- 1.1 Heat Treatment: MILL ANNEALED
- 1.2 Process History: HEAT HC-42-1B
- 1.3 Properties: P_{tu} 136.1 ksi; P_{ty} 125.6 ksi; E 17.0 10^6 psi; δ 8.9 % Elong.;
9.7 % RL; — Ft-lbs. CVM at — °F

2. Specimen:

- 2.1 Thickness, B: 2.002 in. 2.4 R/W 0.6008
- 2.2 Depth, W: 4.000 in. 2.5 Notch length, a_c : 1.810/1.815 in.
- 2.3 Height, PH: 4.806 in. 2.6 Orientation: T-L

3. Fatigue Precracking:

Run No.	a_i (l) (in.)	a_i (r) (in.)	P_{max} (lbs.)	P_{min} (lbs.)	N Cycles	a_f (l) (in.)	a_f (r) (in.)	$K_I(\max)^{**}$ (ksi-in ^{3/2})	ΔK_I at a_c (ksi-in ^{3/2})	Frequency (Hz)
1	1.810	1.815	14,000	1,000	7,000	1.840	1.870	30.3	27.5	8
2	1.840	1.870	11,000	1,100	4,000	1.850	1.910	24.2	22.0	8
3	1.910	1.850	11,000	1,100	3,000	1.950	1.870	24.4	22.0	8
4	1.950	1.870	8,000	800	17,000	2.010	1.880	18.4	16.2	8
5	2.010	1.880	8,000	800	9,000	2.020	1.920	18.7	16.8	8
6	END FATIGUE PRECRACKING TEST					40,000				
7										
8										

* a_i and a_f are measured at the specimens left (l) and right (r) face surfaces.
 ** K_I stress intensity calculated using the average value of a_f [$(a_i(l) + a_i(r))/2$].
 Note: Stress intensity values in the summary calculated using the post-test final crack size a_c (see test 4.4).

+ SAMPLE BRUISED IN LOADING LIFTING

Figure 12 Compact Tension K_{Ic} Test Record

COMPACT TENSION K_{Ic} TEST RECORD (continued)

4. Final Crack Measurements:

4.1 a_1 :	2.090 ± 0.010 in.	4.5 a_c/w :	0.524
4.2 a_2 :	2.110 ± 0.011 in.	4.6 (a_{left}):	2.030 ± 0.010 in.)
4.3 $a_{3/4}$:	2.090 ± 0.010 in.	4.7 (a_{right}):	1.940 ± 0.010 in.)
4.4 $a_{avg} = a_c$:	2.097 ± 0.010 in.	4.8 crack plane, θ :	$3-5$ degrees

5. Tension Testing:

(Load vs. Crack Opening Displacement Record Attached)	
5.1 COD Gage No.:	CAGE CALIBRATED FORCE
5.2 Loading rate:	TEST
5.3 Loading rate in terms of K_{Ic} :	$43,000$ lbs./min.
5.4 Elastic compliance (v/P):	111.1 ksi-in ² /min.
5.5 Load at 5% Secant Intercept, P_5 :	1.74 μ -in/lb.
5.6 Maximum load, P_{max} :	$43,500$ lbs.
5.7 Load at onset of unstable crack growth, P_Q :	$44,300$ lbs.
5.8 P_{max}/P_Q :	$43,500$ lbs.
5.9 $r (a/w)$:	1.016
5.10 $K_{Ic} = (P_Q/BW^{3/2}) r (a/w)$:	10.34
	112.4 ksi-in ^{1/2}

6. Fracture Appearance:

6.1 Width of flat fracture, f :	1.8 in.
6.2 Oblique fracture, $(B-f)/B \times 100$:	10 %

7. $K_{Ic} = K_{Ic}$ if following criteria not violated:

	E399 Section	Not Violated	Violated
a. a_c and $B \geq 2.5 (K_{Ic}/\sigma_{ys})^2$ $2,002$	7.1.1	<input checked="" type="checkbox"/>	<input type="checkbox"/>
b. $0.45 \leq a/w \leq 0.55$	7.2.1	<input checked="" type="checkbox"/>	<input type="checkbox"/>
c. $W \leq W/16$	7.2.2	<input checked="" type="checkbox"/>	<input type="checkbox"/>
d. $(a_f - a_i) \geq 0.05 a_c$ or 0.05 in.	7.2.3	<input checked="" type="checkbox"/>	<input type="checkbox"/>
e. $K_{Ic, max}/E \leq 0.002$ in ^{1/2}	7.4.2	<input checked="" type="checkbox"/>	<input type="checkbox"/>
f. $K_{Ic, max} \leq 0.6 K_{Ic}$ (last $0.025(a_c)$)	7.4.2	<input checked="" type="checkbox"/>	<input type="checkbox"/>
g. $\Delta K_{Ic} \geq .9 K_{Ic}$	7.4.3	<input checked="" type="checkbox"/>	<input type="checkbox"/>
h. $K_{Ic(max)} \leq 0.6 (\sigma_{Y.S.T1} / \sigma_{Y.S.T2}) K_{IcT2}$	7.4.4	<input checked="" type="checkbox"/>	<input checked="" type="checkbox"/>
i. Size tolerances	8.2	<input checked="" type="checkbox"/>	<input type="checkbox"/>
j. $ a_1 - a_2 , a_1 - a_{3/4} , a_2 - a_{3/4} \leq 0.05(a_c)$	8.2.1	<input checked="" type="checkbox"/>	<input type="checkbox"/>
k. $(a_{avg} - a_o) \leq$ larger of $0.05 a_{avg}$ or 0.05 in.	8.2.2	<input checked="" type="checkbox"/>	<input type="checkbox"/>
l. a_1 or $a_2 \leq 0.9 a_{avg}$	8.2.3	<input checked="" type="checkbox"/>	<input type="checkbox"/>
m. $\theta \leq 10^\circ$	8.2.4	<input checked="" type="checkbox"/>	<input type="checkbox"/>
n. 30 ksi-in ^{1/2} /min. $\leq K/At \leq 150$ ksi-in ^{1/2}	8.4	<input checked="" type="checkbox"/>	<input type="checkbox"/>
o. Alignment	8.4	<input checked="" type="checkbox"/>	<input type="checkbox"/>
p. $P_{max}/P_Q \leq 1.1$	9.1.2	<input checked="" type="checkbox"/>	<input type="checkbox"/>

8. If no only violation, then:

$$K_{Ic} = P_{max} / (W + a) \sqrt{(W-a)} \sigma_{ys}$$

N/A

9. Comments:

Figure 12 (Continued)

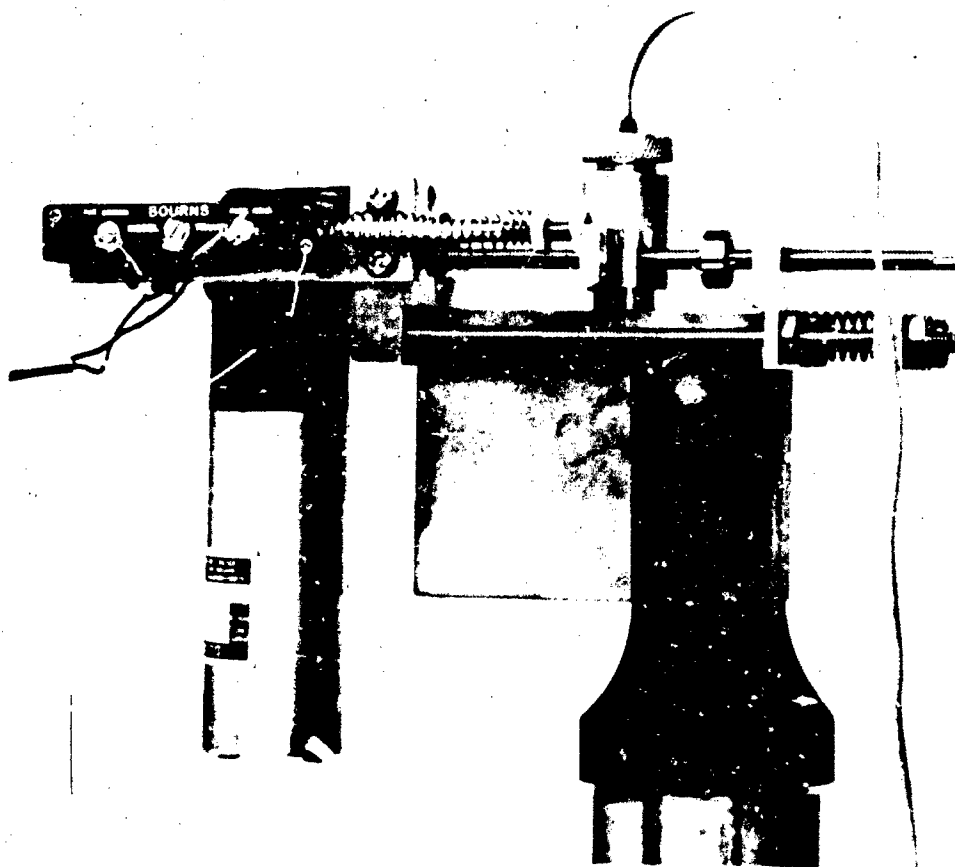


Figure 14 A da/dN Test Specimen With Automatic Crack
Follower in Place

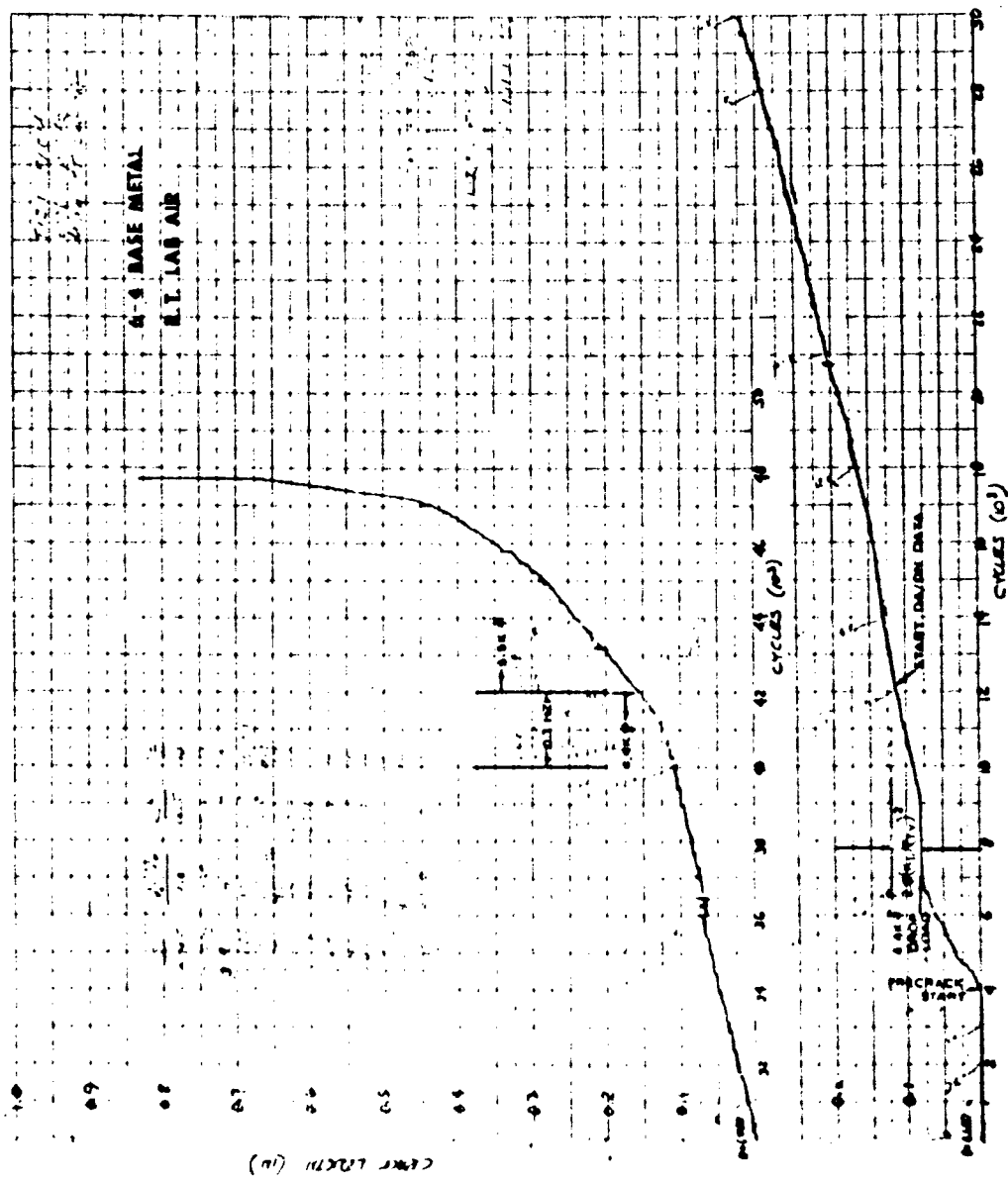


Figure 15 Typical Autographic Plot of Crack Length Vs. Cycles. The Curve is for a Ti-6Al-4V Specimen Tested in Laboratory Air at Room Temperature.

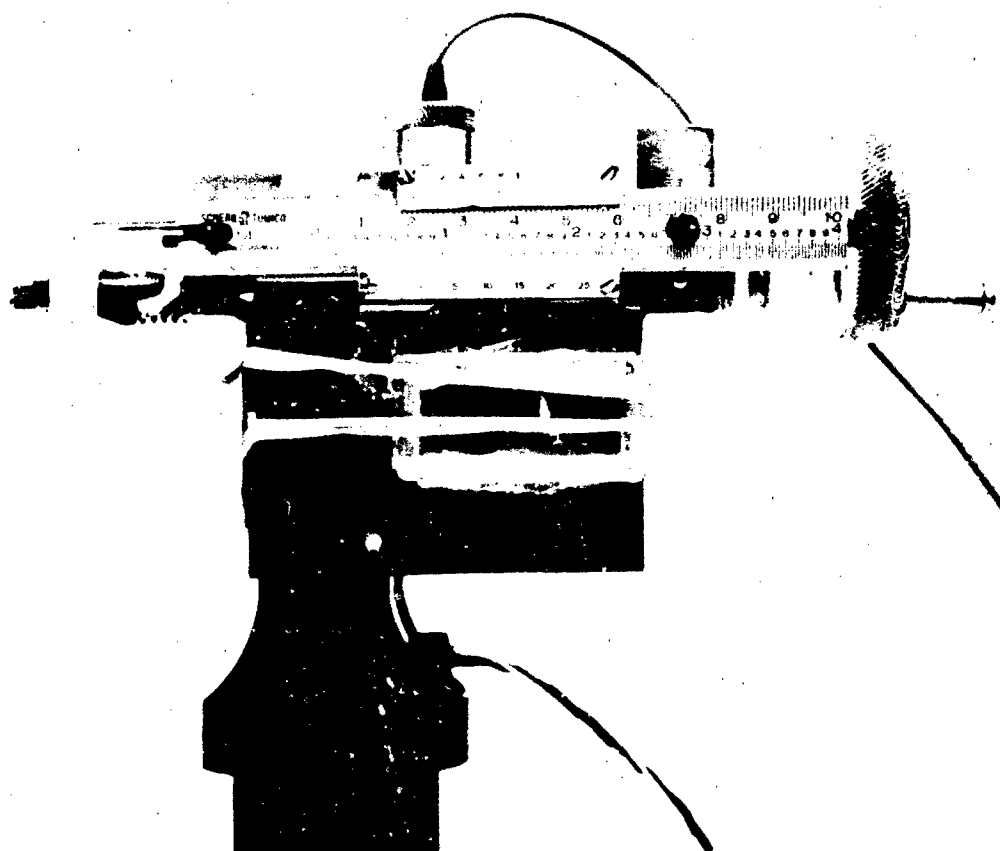
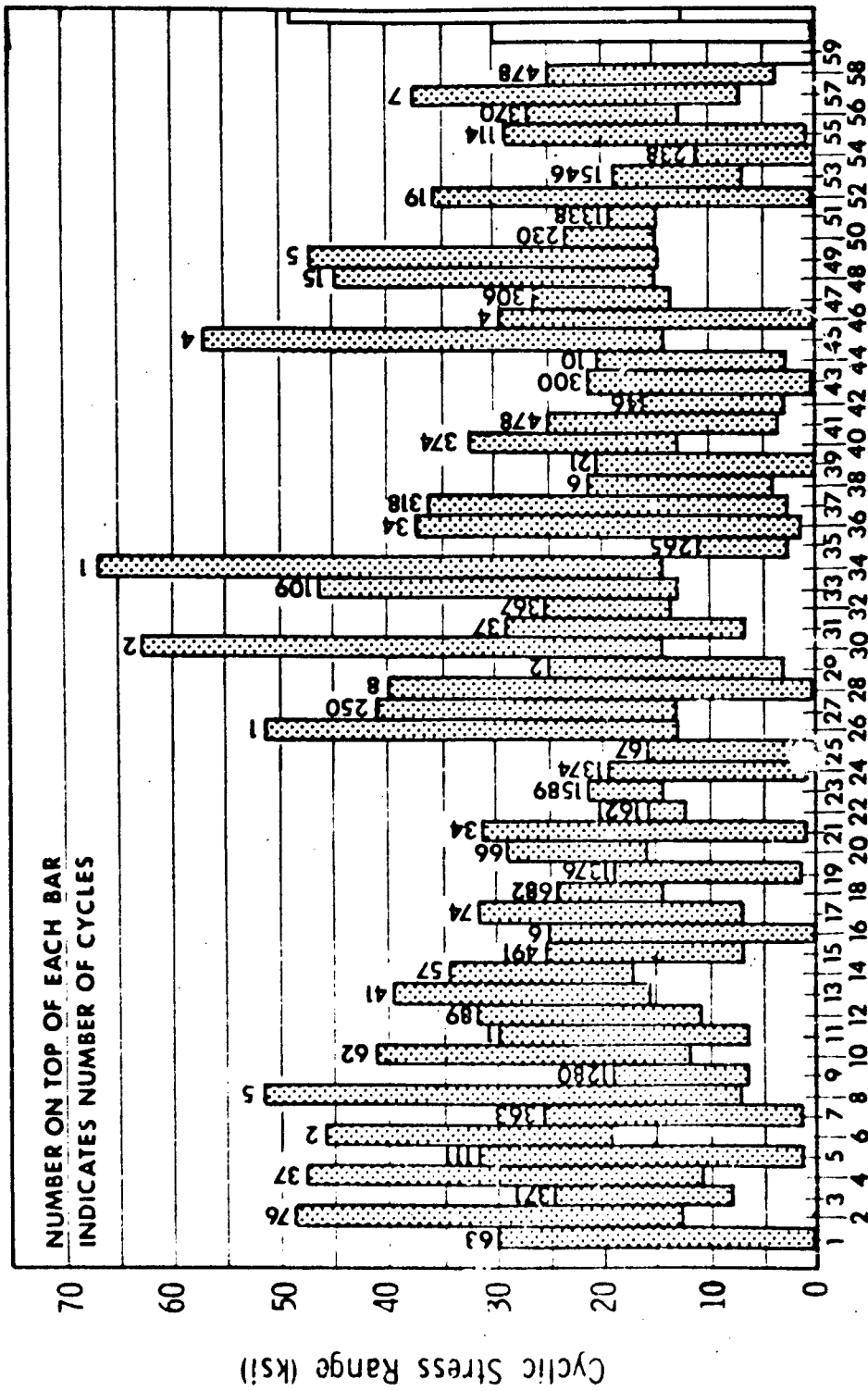


Figure 16 A da/dt Test Specimen With Manual Crack
Follower in Place



Spectrum Layer Number

Figure 17 Fatigue Load Spectrum

(a)



WELD FUSION ZONE

HEAT-AFFECTED ZONE

BASE METAL

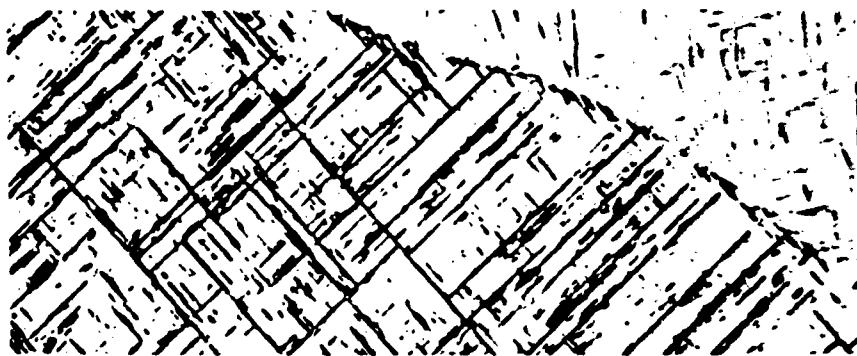
65x

(b)



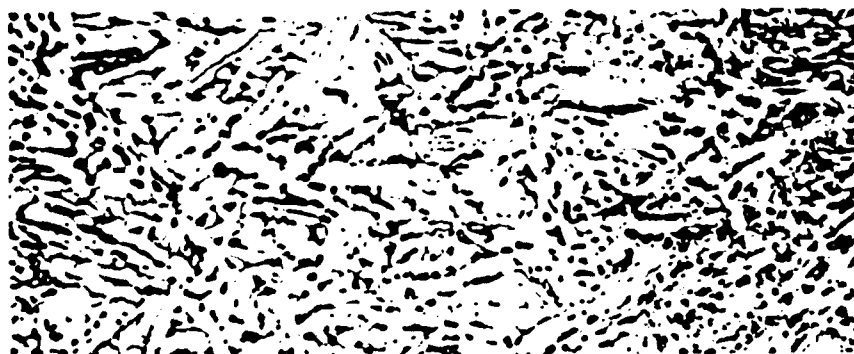
65x

Figure 18 Microstructures of Ti-6Al-4V Electron Beam Weldments (65x): (a) Single-Pass Weldment; (b) Repair Weldment



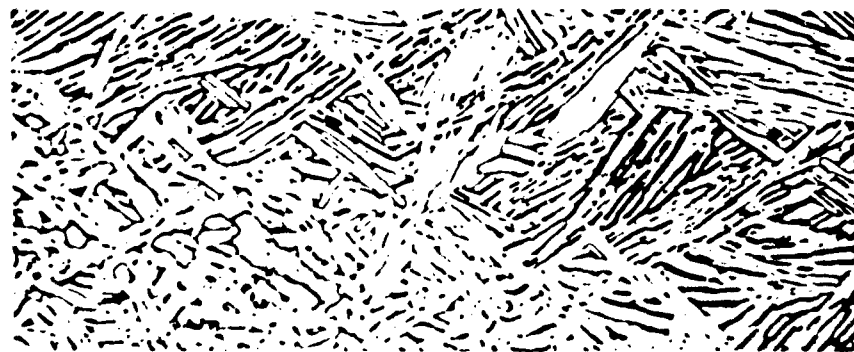
(a) WELD FUSION ZONE

500X



(b) HEAT-AFFECTED ZONE

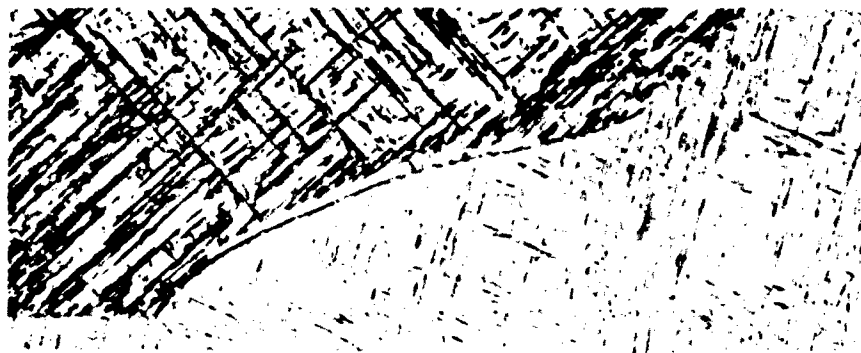
500X



(c) BASE METAL

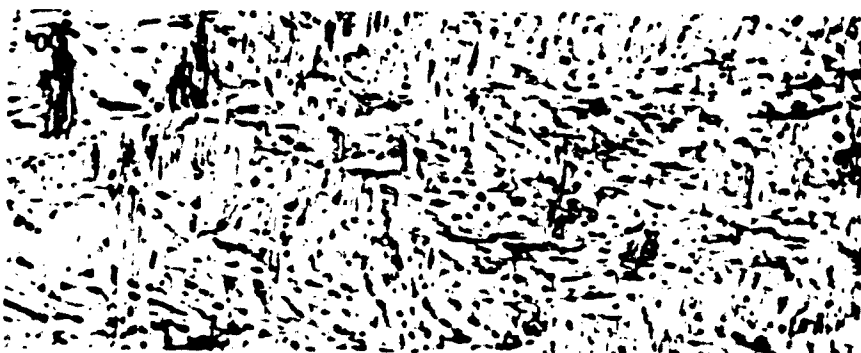
500X

Figure 19 Typical Microstructures of 1-in.-Thick Ti-6Al-4V E. B. Weldments With Single Joining Pass: (a) Weld Fusion Zone; (b) Heat-Affected Zone; (c) Base Metal



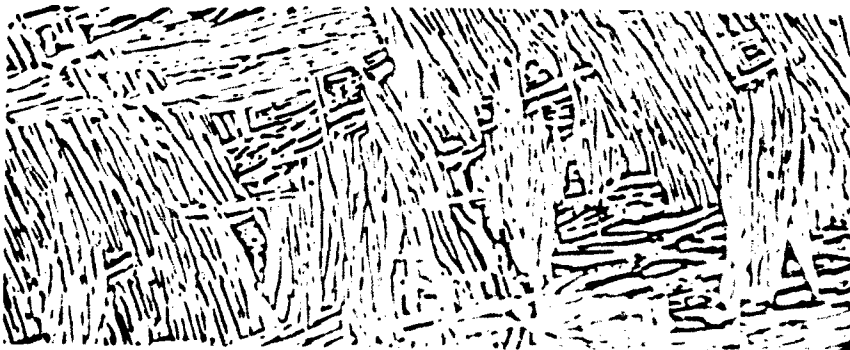
(a) WELD FUSION ZONE

500X



(b) HEAT-AFFECTED ZONE

500X



(c) BASE METAL

500X

Figure 20 Typical Microstructures of 1-in.-Thick Ti-6Al-4V E.B. Weldment With Multiple Passes: (a) Weld Fusion Zone; (b) Heat-Affected Zone; (c) Base Metal

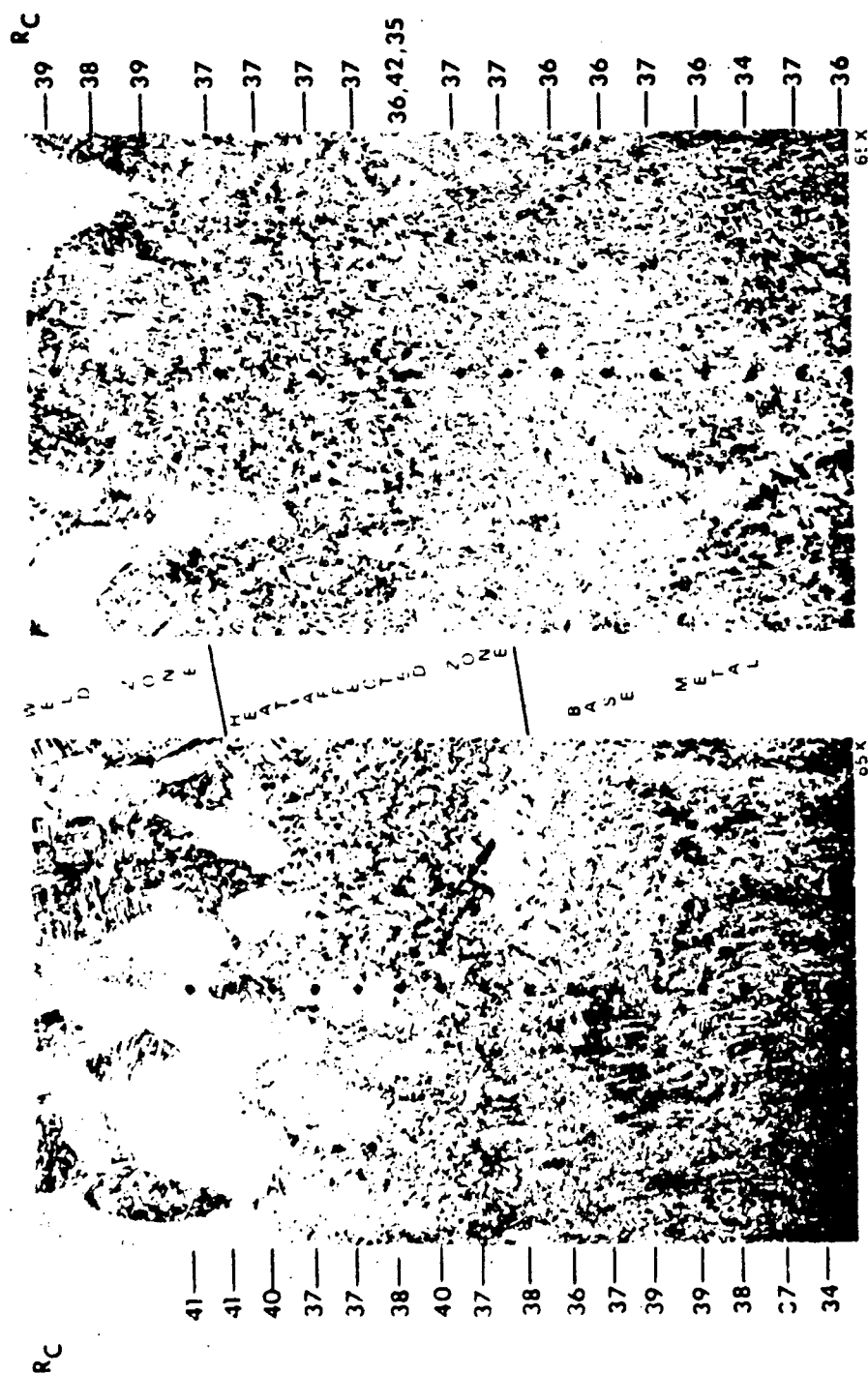


Figure 21 Heat-Affected Zone Hardness Survey Results and Locations. (Hardness Readings Converted to R_C.)



7X

Figure 22 Microstructure of Beta III Electron Beam Weldment. Notice the planar alignment of contiguous grain boundaries coincident with the centerline of the weld fusion zone.



200X

Figure 23 Microstructure of Fusion Zone Centerline in E.B. Weld Beta III. Grains exhibit a highly dendritic or cored structure.

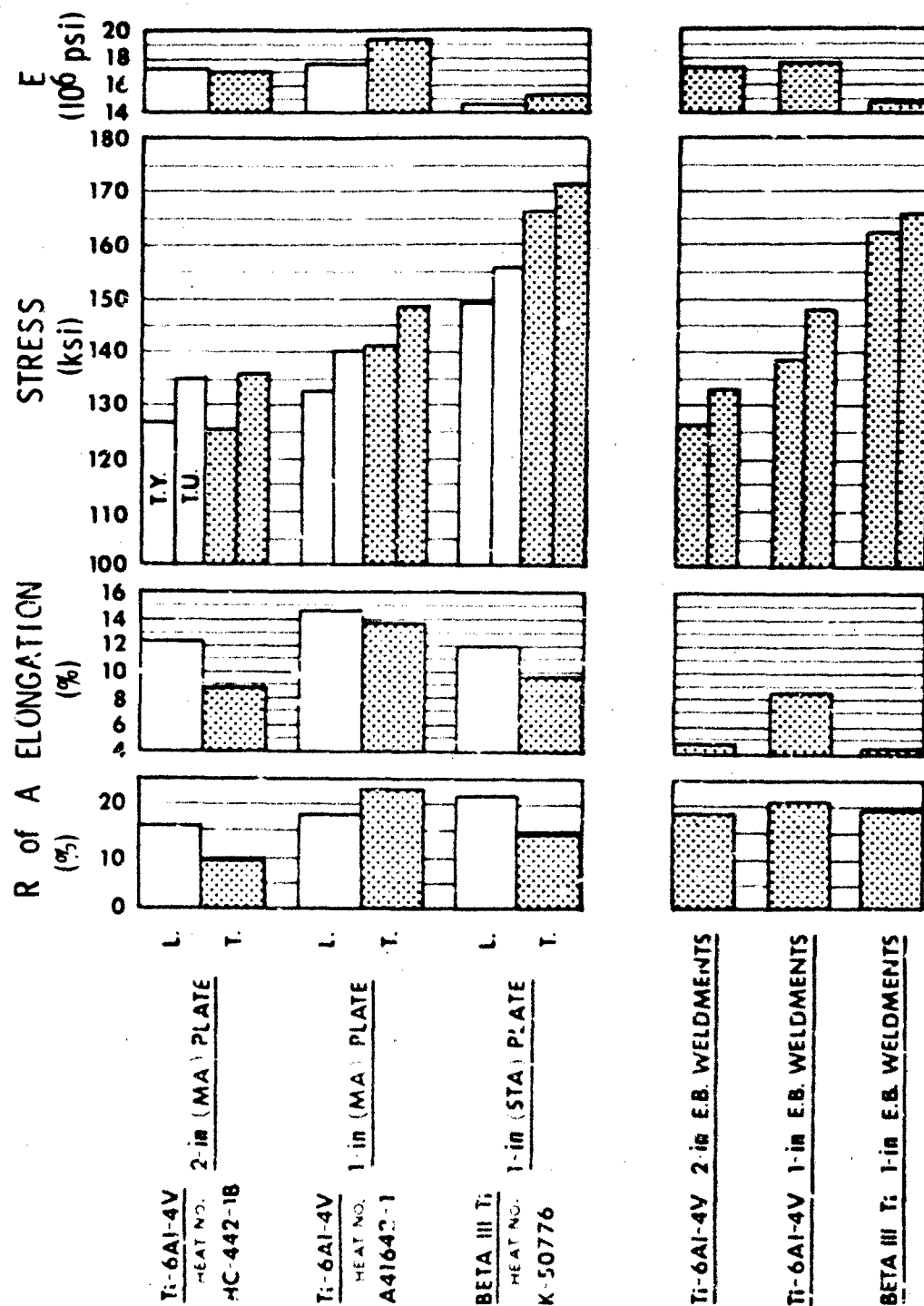


Figure 24 Average Tensile Properties of Starting Test Materials at Room Temperature

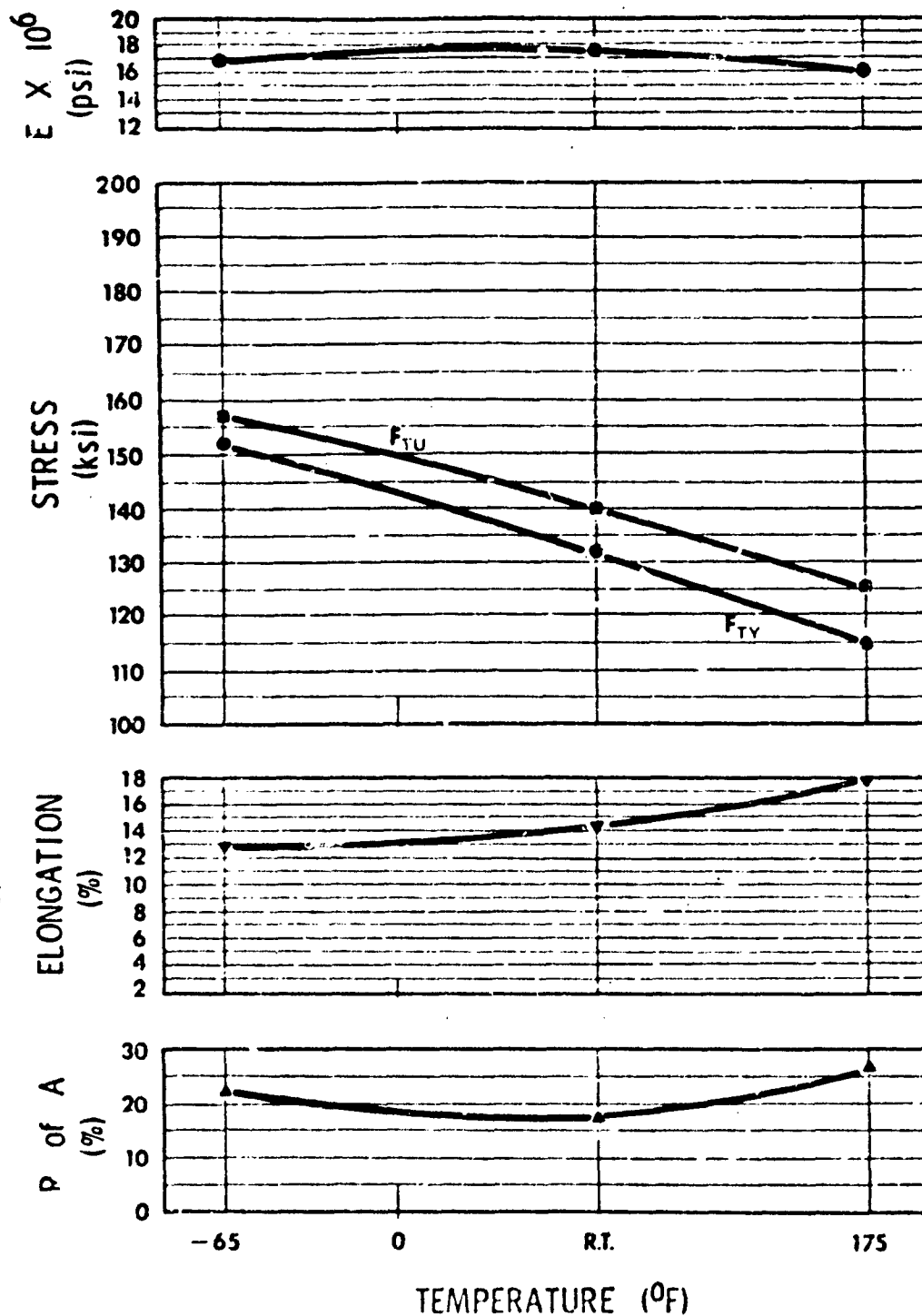


Figure 25 Variation of The Average Longitudinal Tensile Properties of Ti-6Al-4V 1-in. Plate (MA) Base Metal With Test Temperature

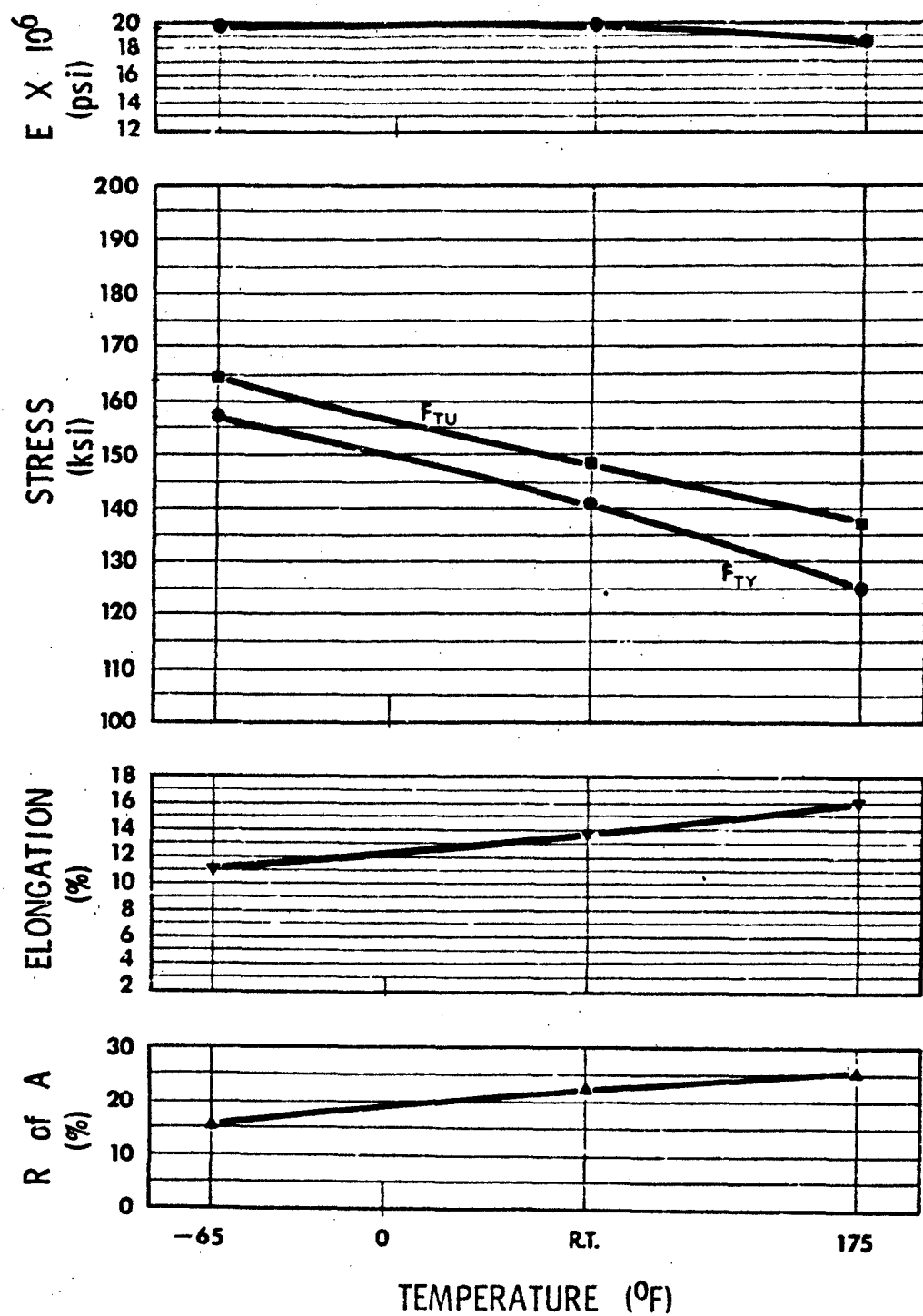


Figure 26 Variation of The Average Transverse Tensile Properties of Ti-6Al-4V 1-in. Plate (MA) Base Metal With Test Temperature

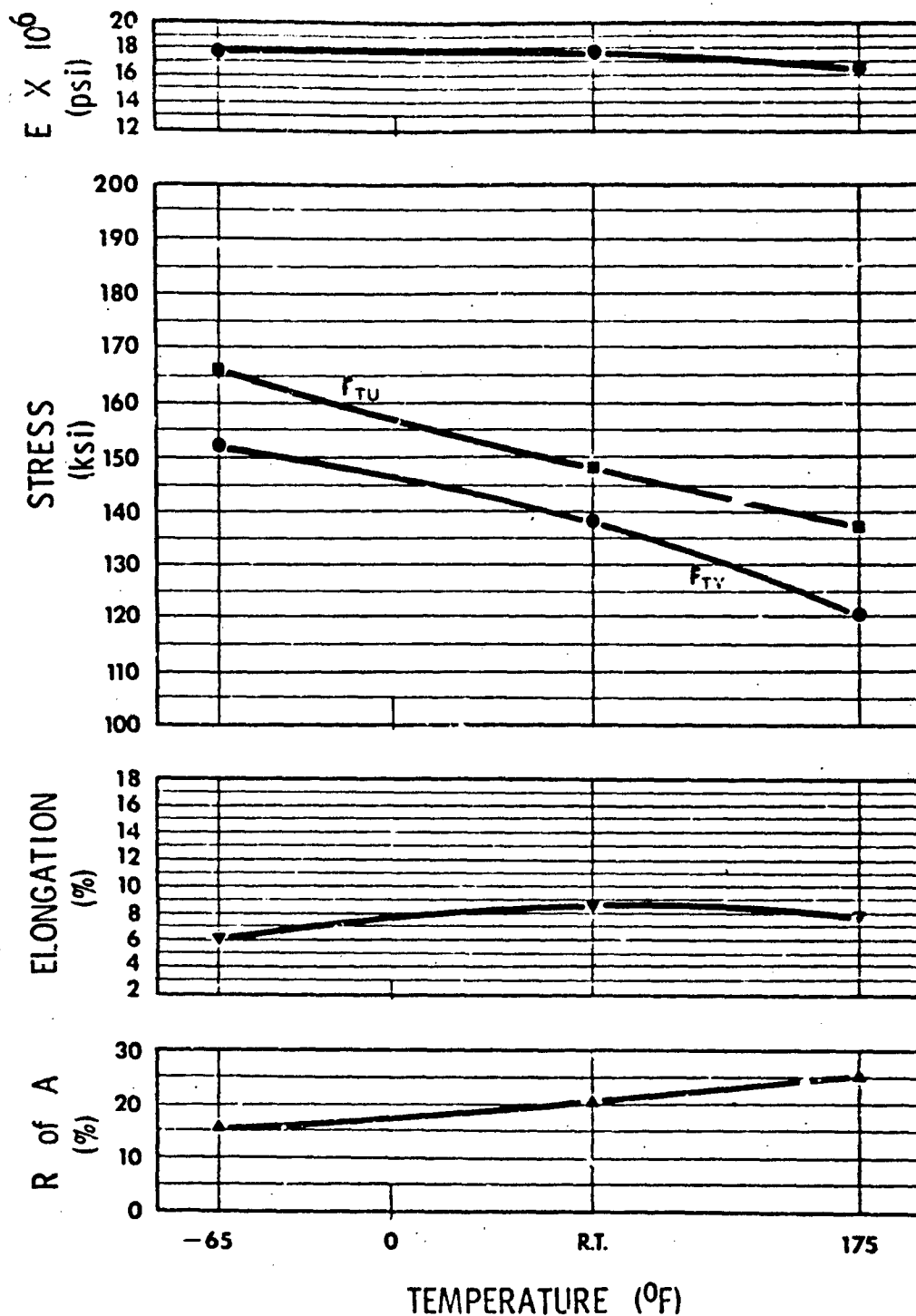


Figure 27 Variation of The Average Tensile Properties of Ti-6Al-4V 1-in. Plate E.B. Weldments With Test Temperature

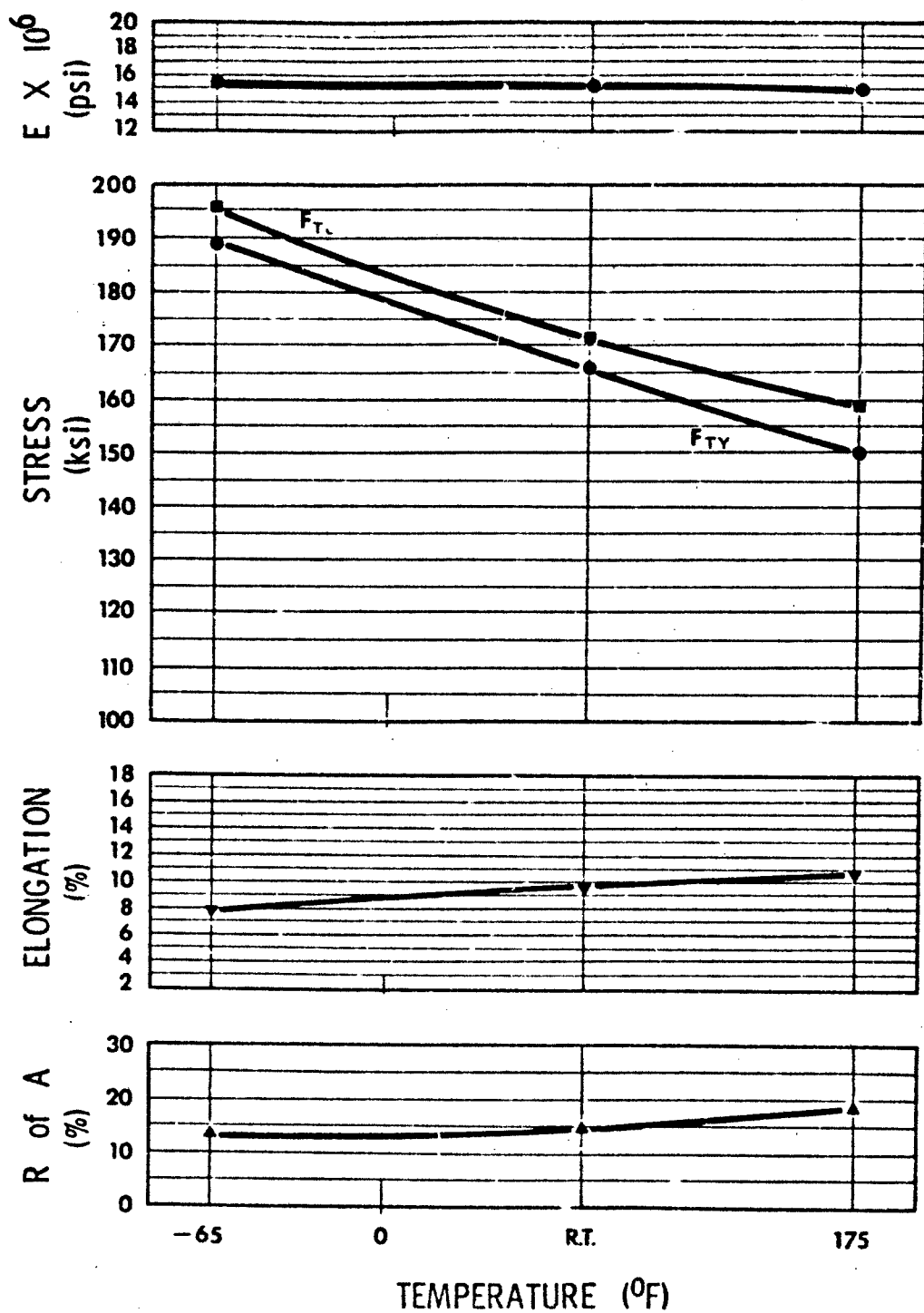


Figure 28 Variation of The Average Transverse Tensile Properties of Beta III Titanium 1-in. Plate (STA) Base Metal With Test Temperature

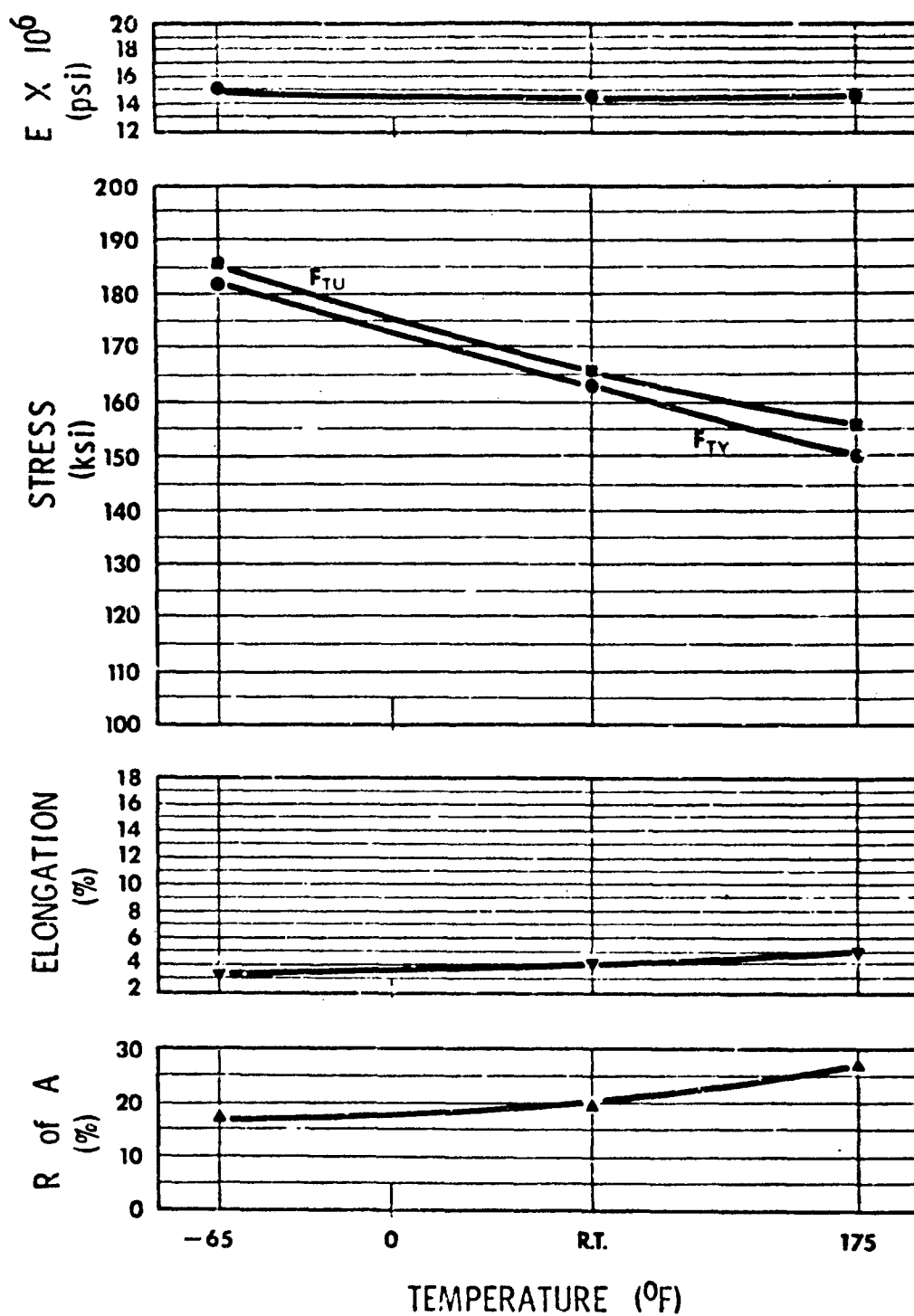


Figure 29 Variation of The Average Tensile Properties of Beta III Titanium 1-in. Plate (STA) E.B. Weldments With Test Temperature

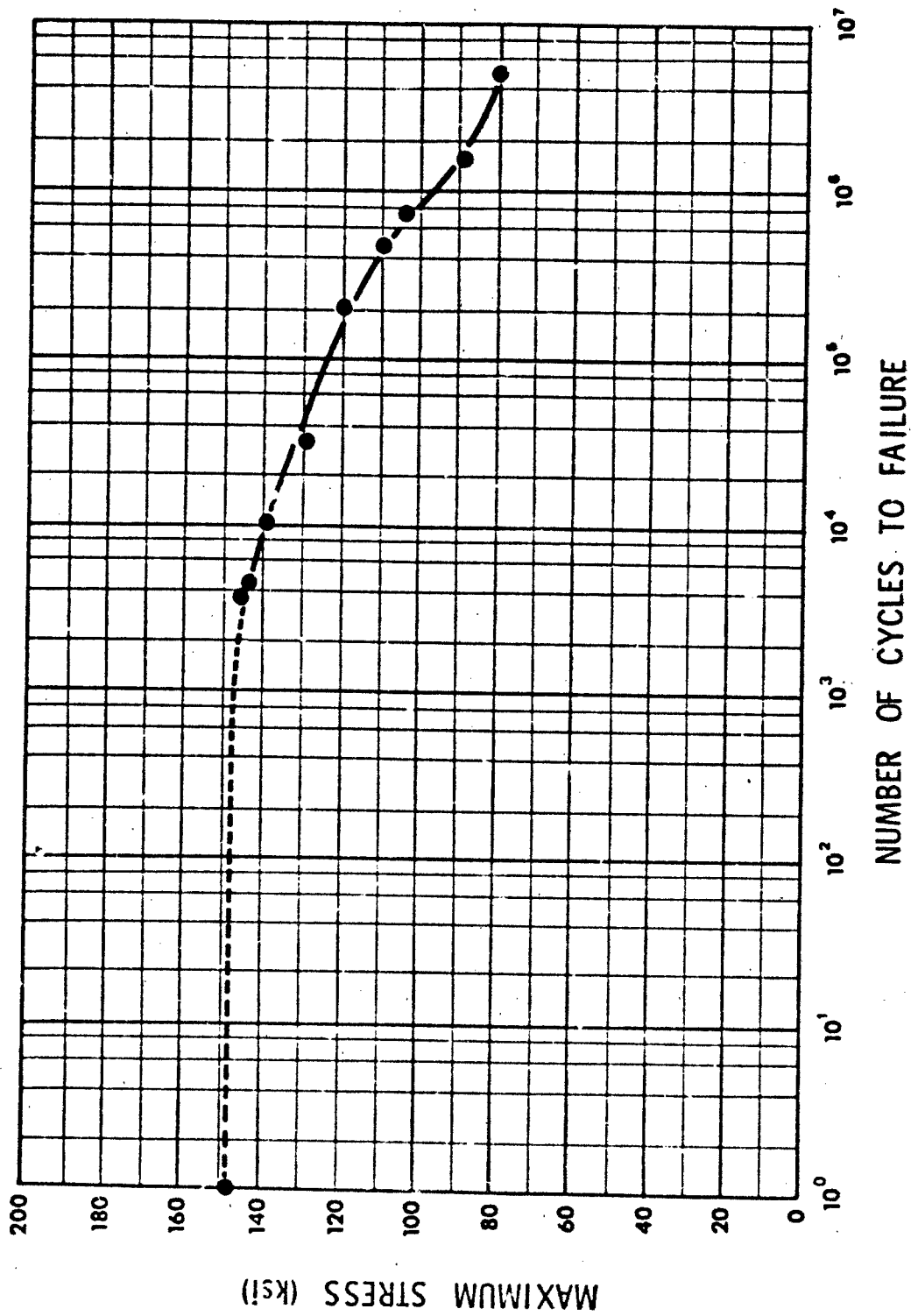


Figure 30 S-N Curve For Ti-6Al-4V 1-in. Plate (MA) Base Metal
(Stress Ratio = 0.1)

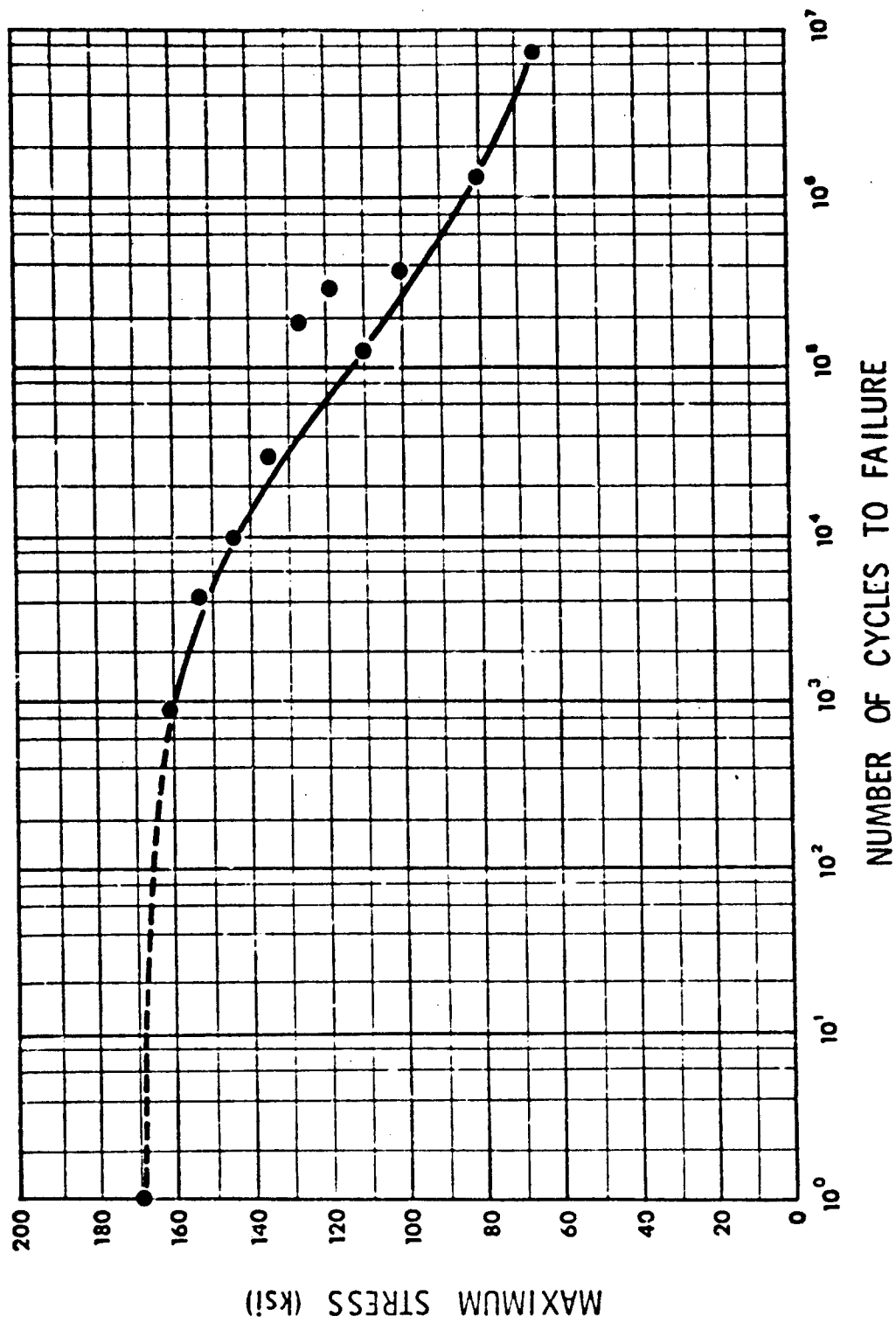


Figure 31 S-N Curve For E.B. Welded Tl-6Al-4V 1-in. Plate
(Stress Ratio = 0.1)

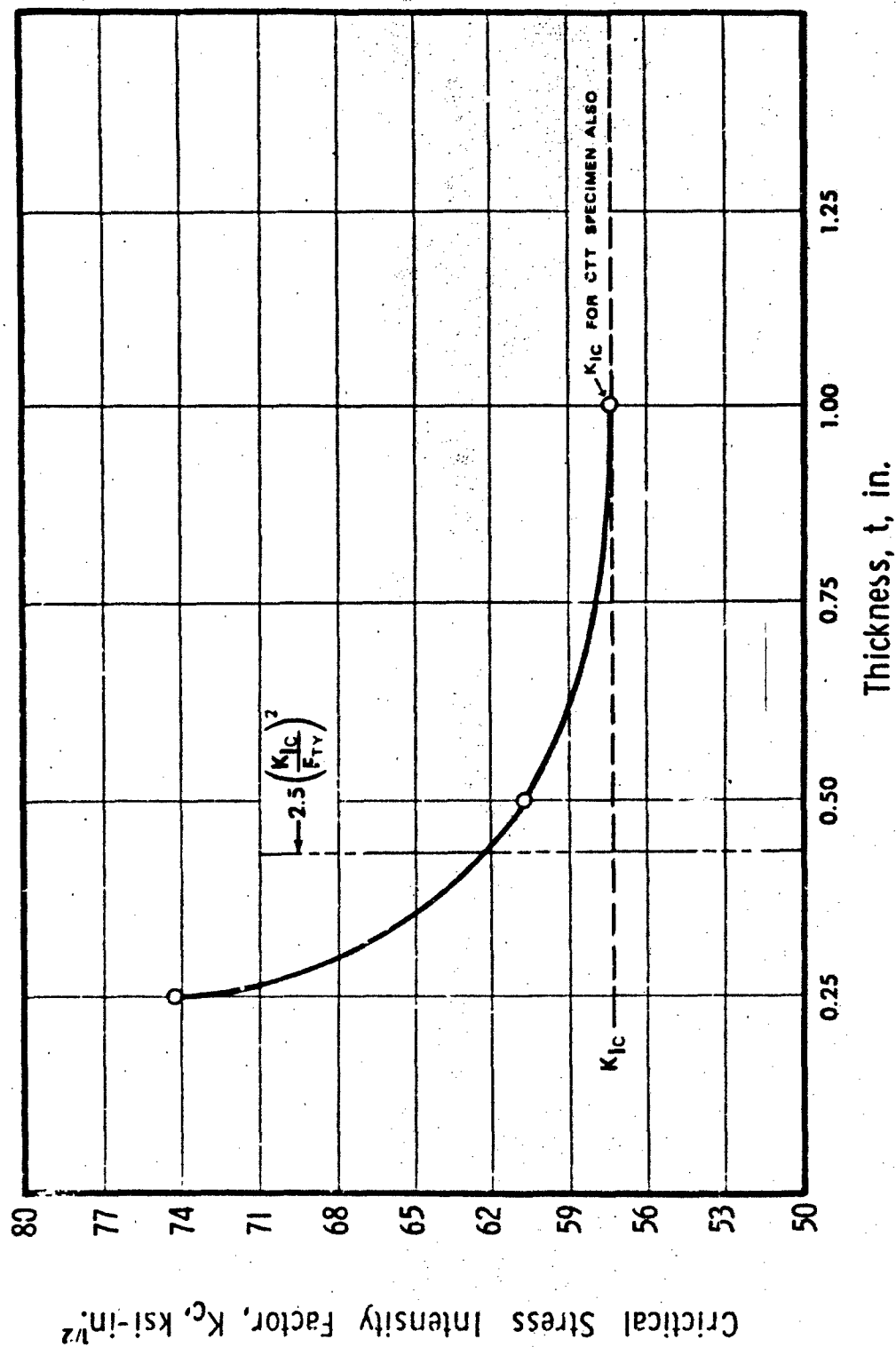


Figure 32 Weld Zone Single-Edge Notch Fracture Toughness of E.B. Welded T1-6A1-4V 1-in. Plate Vs. Test Specimen Thickness at Room Temperature (Material in As-Welded Condition)

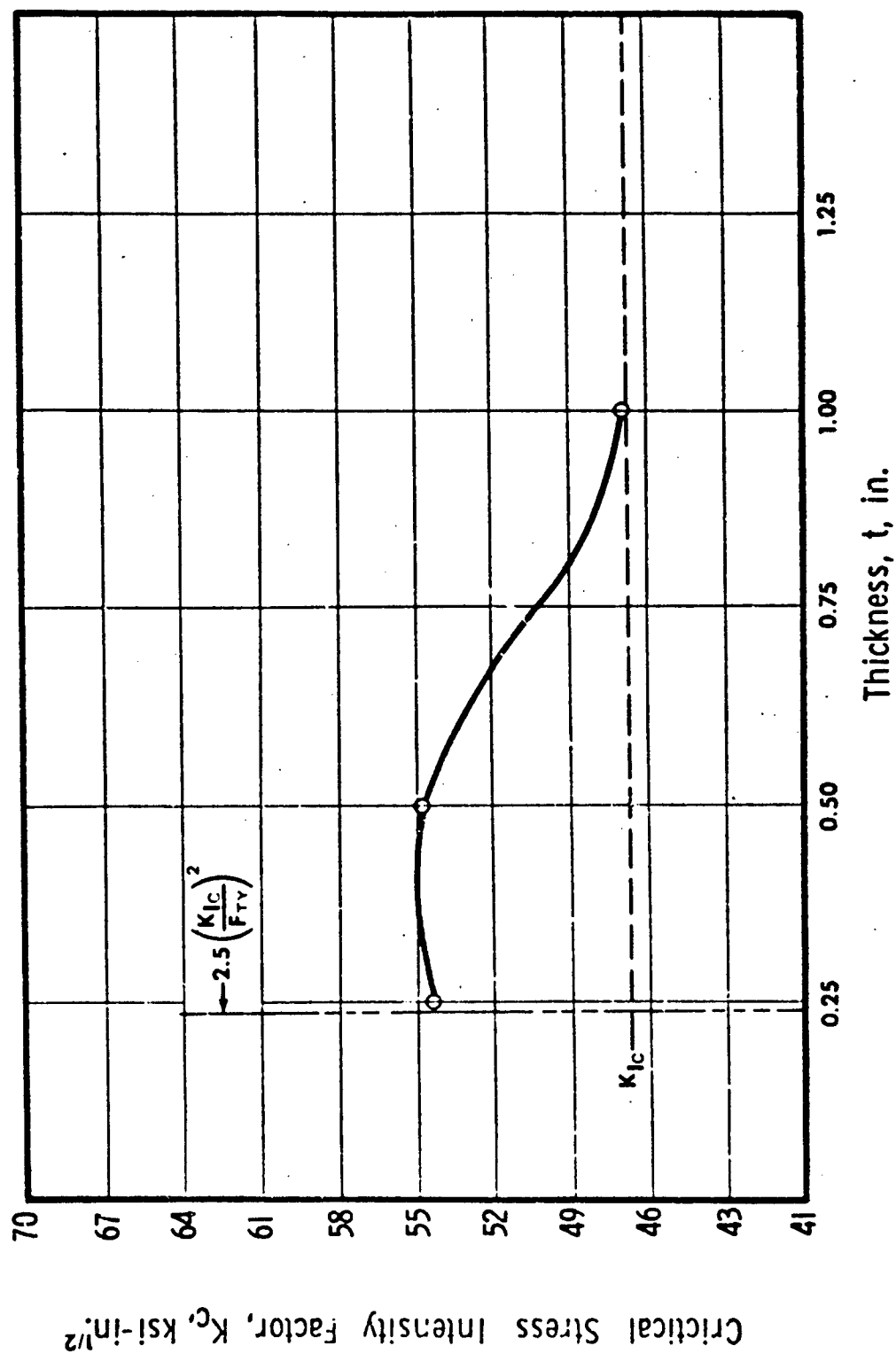


Figure 33 Weld Zone Single-Edge Notch Fracture Toughness of E.B. Welded TI-6Al-4V 1-lr. Plate Vs. Test Specimen Thickness at -65°F (Material in As-Welded Condition)

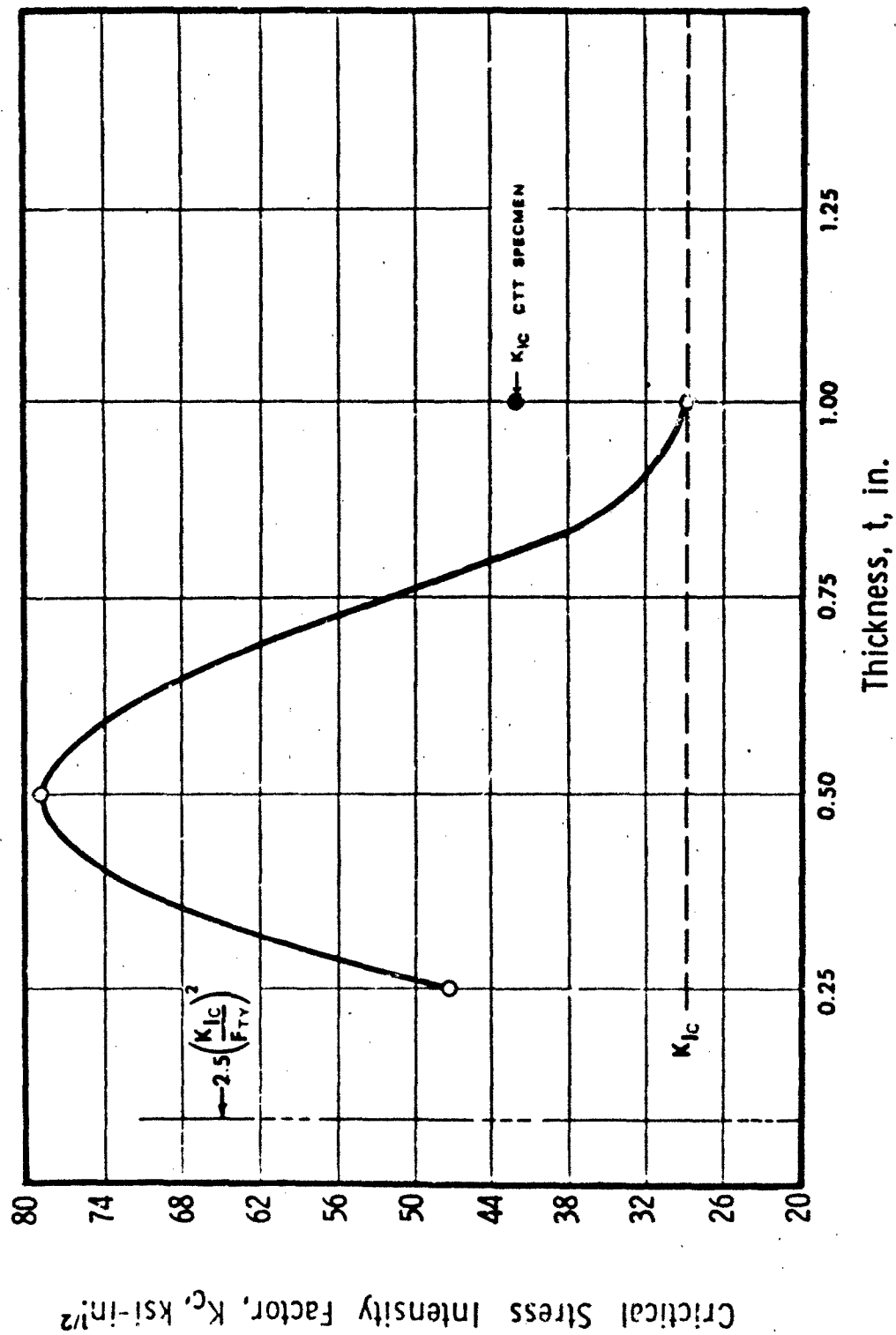


Figure 34 Weld Zone Single-Edge Notch Fracture Toughness of E.B. Welded Beta III Titanium 1-in. Plate (STA) Vs. Test Specimen Thickness at Room Temperature

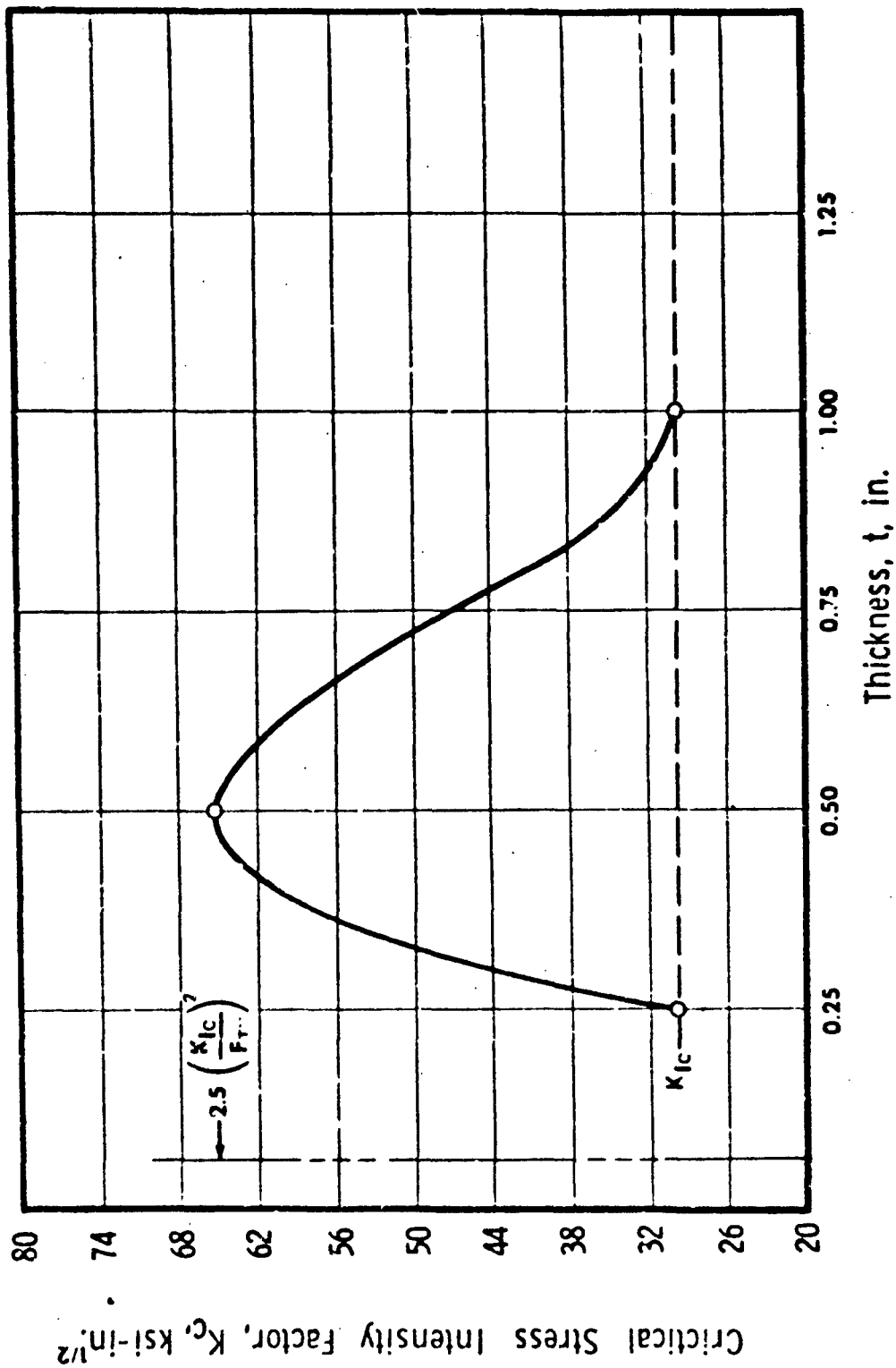


Figure 35 Weld Zone Single-Edge Notch Fracture Toughness of E.B. Welded Beta III Titanium
1-in. Plate (STA) Vs. Test Specimen Thickness at -65°F

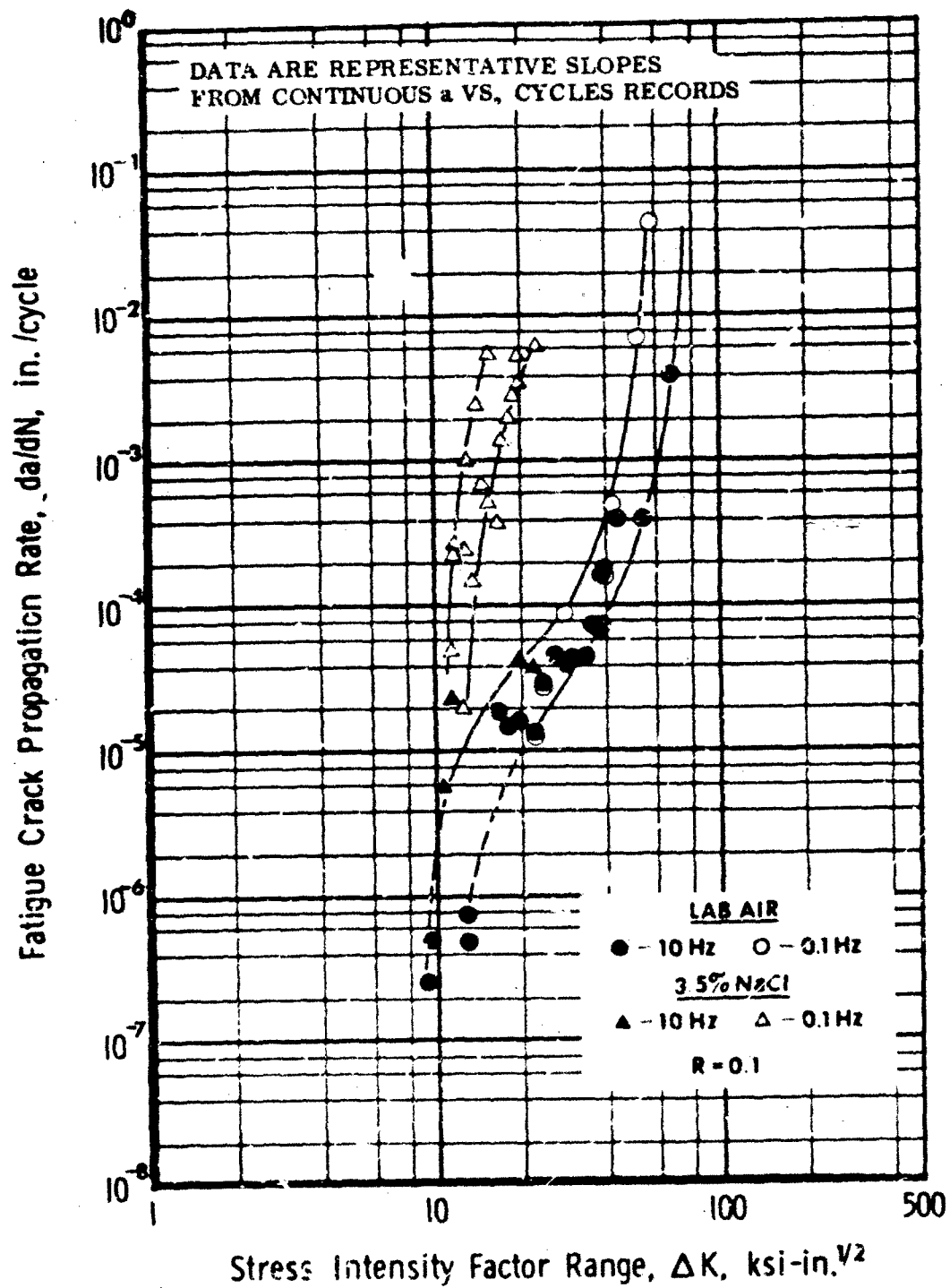


Figure 36 Ti-6Al-4V Base Metal 1.0-in. MA Plate, T-L Direction, CTT Specimens, Room Temperature, Laboratory Air and Salt Water Environments (Specimen Thickness: 1.00 in.; Width: 2.55 in.; H/W = 0.486)

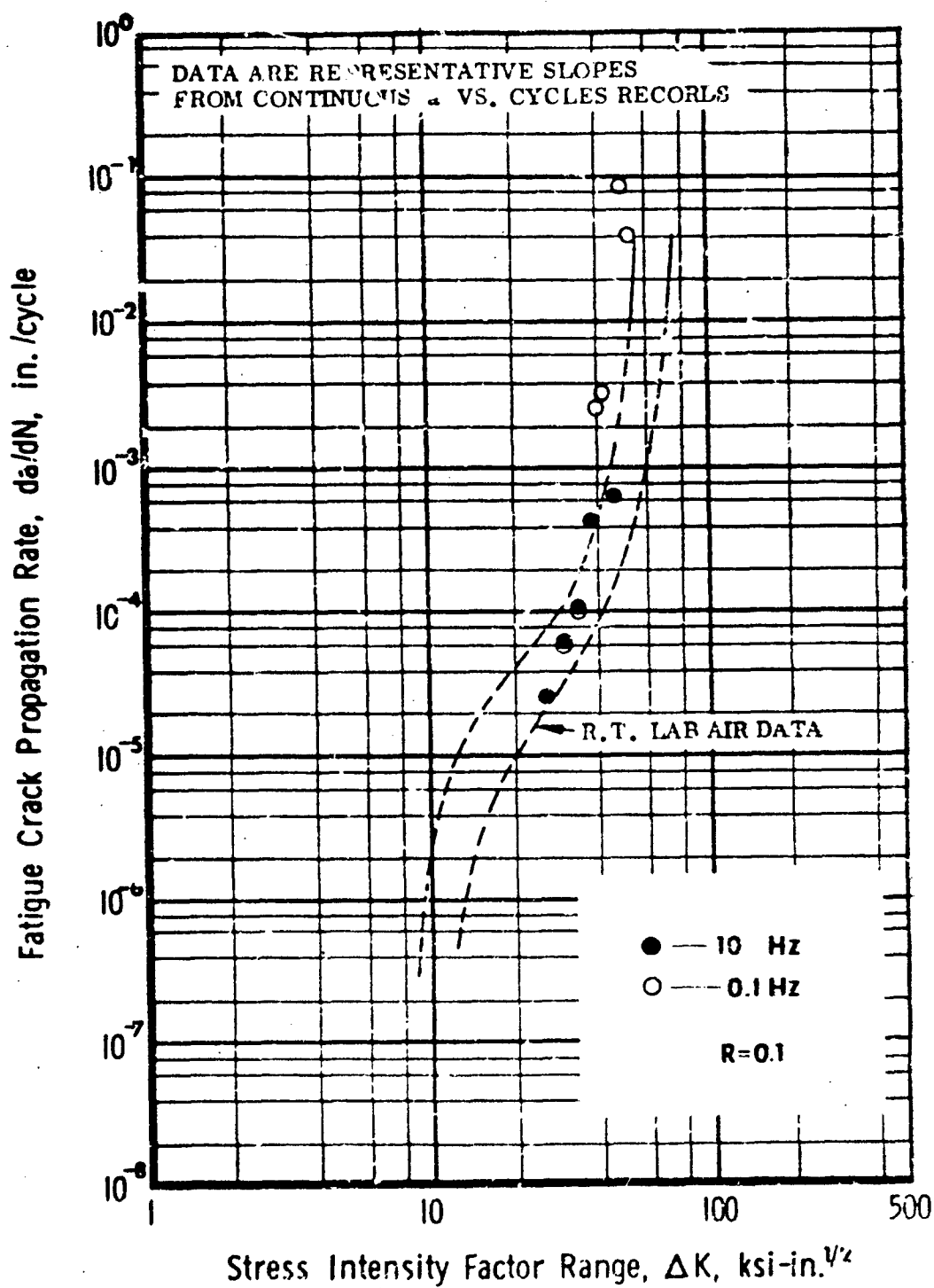


Figure 37 TI-6Al-4V Base Metal, 1.0 in. MA Plate, T-L Direction, CTT Specimens, -65°F Laboratory Air Environment (Specimen Thickness: 1.00 in.; Width: 2.55 in.; H/W = 0.486)

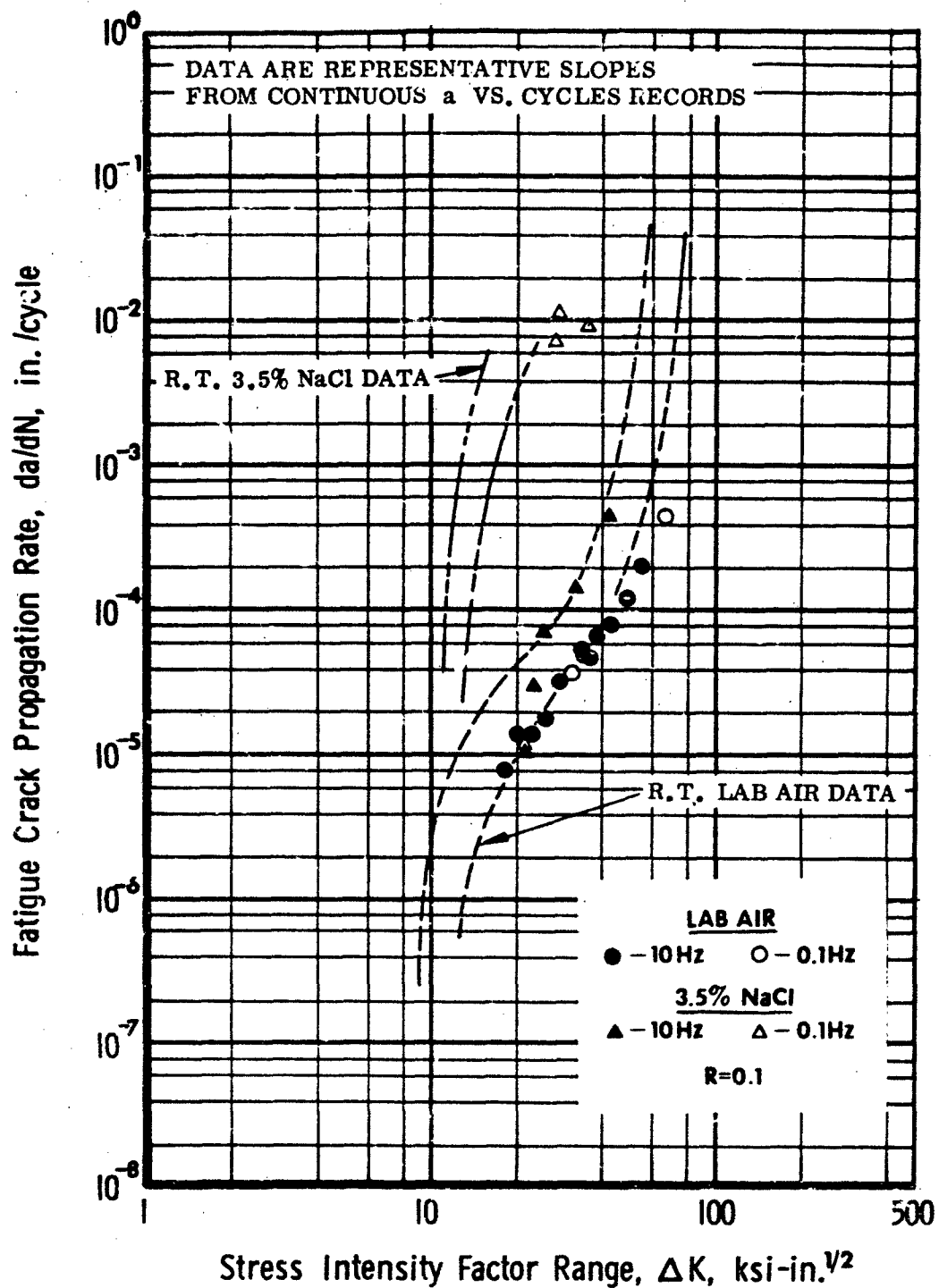


Figure 38 Ti-6Al-4V Base Metal, 1.0-in. MA Plate, T-L Direction, CTT Specimens, 175°F Laboratory Air and Salt Water Environments (Specimen Thickness: 1.0 in.; Width: 2.55 in.; H/W = 0.486)

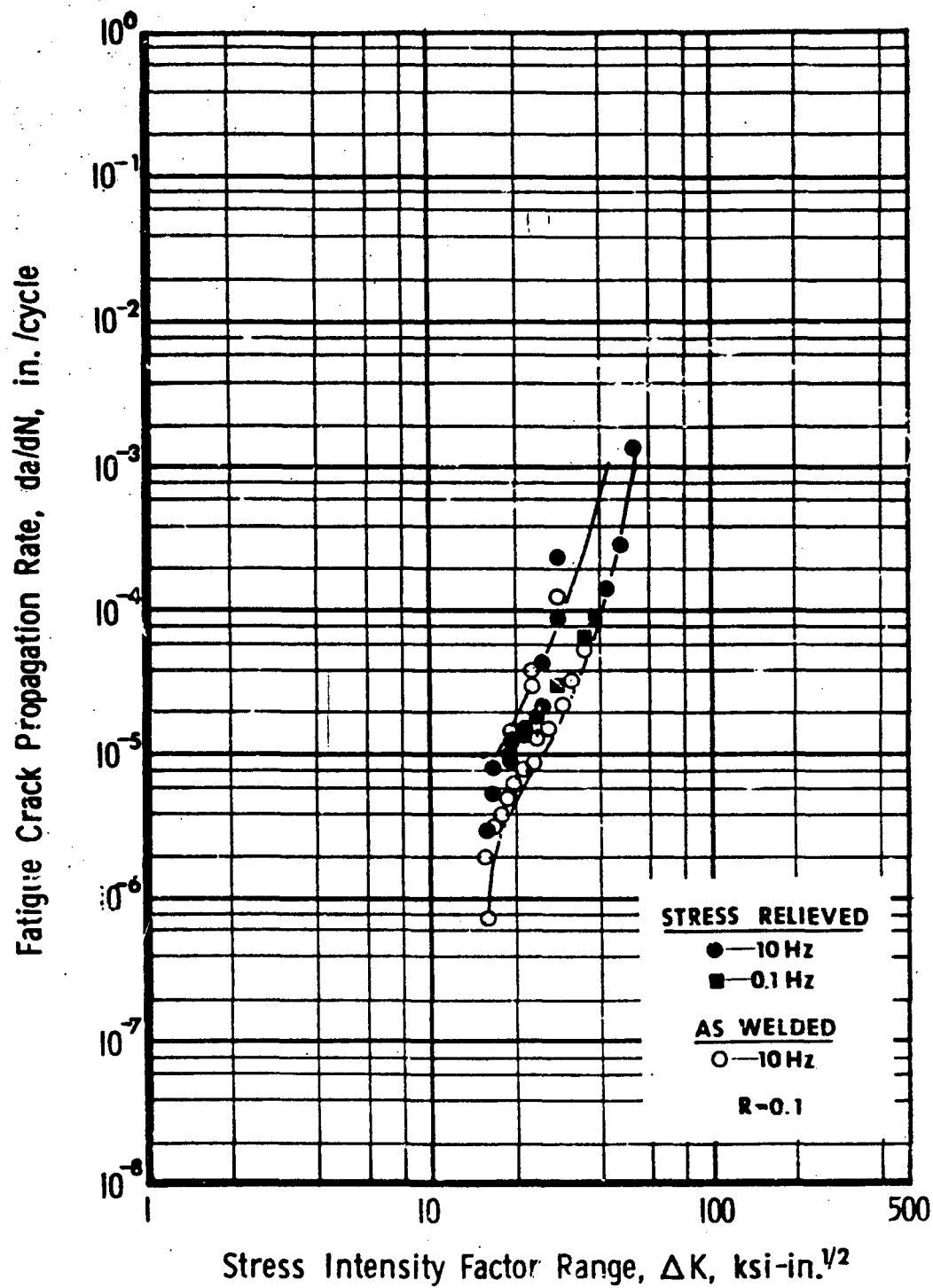


Figure 39 Ti-6Al-4V E.B. Weldment, 1.0-in. Plate, HAZ, T-L Direction, CTT Specimens, Room Temperature Laboratory Air Environment (Specimen Thickness: 1.00 in.; Width: 2.00 in.; H/W = 0.6)

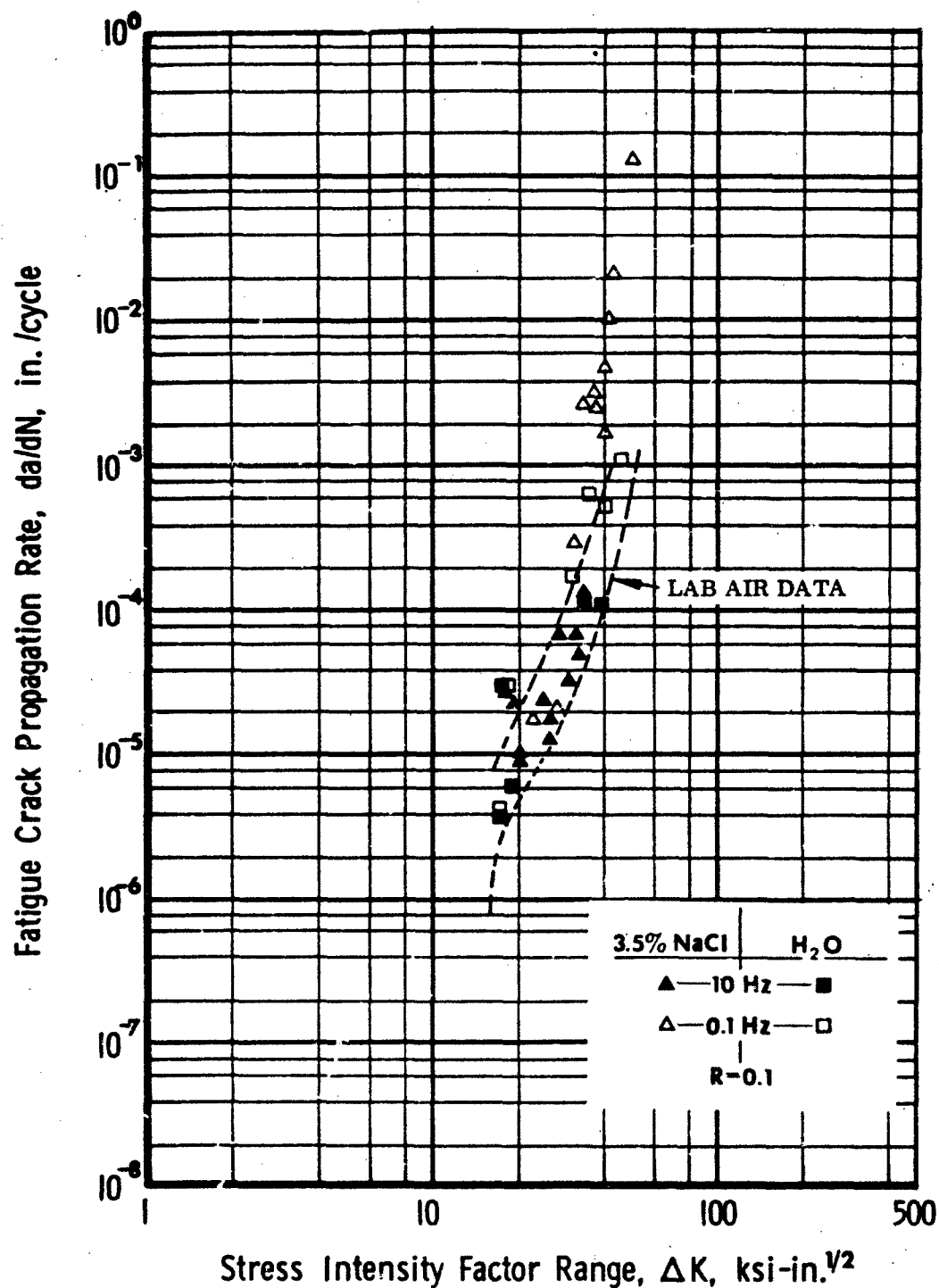


Figure 40 Ti-6Al-4V E.B. Weldment, SR, 1.0-in. Plate, HAZ, T-L Direction, CTT Specimens, Room Temperature Water and Salt Water Environments. (H₂O Specimen Thickness: 1.00 in.; Width: 2.00 in.; H/W = 0.6) (3.5% NaCl Specimen Thickness: 1.00 in.; Width: 2.55 in.; H/W = 0.486)

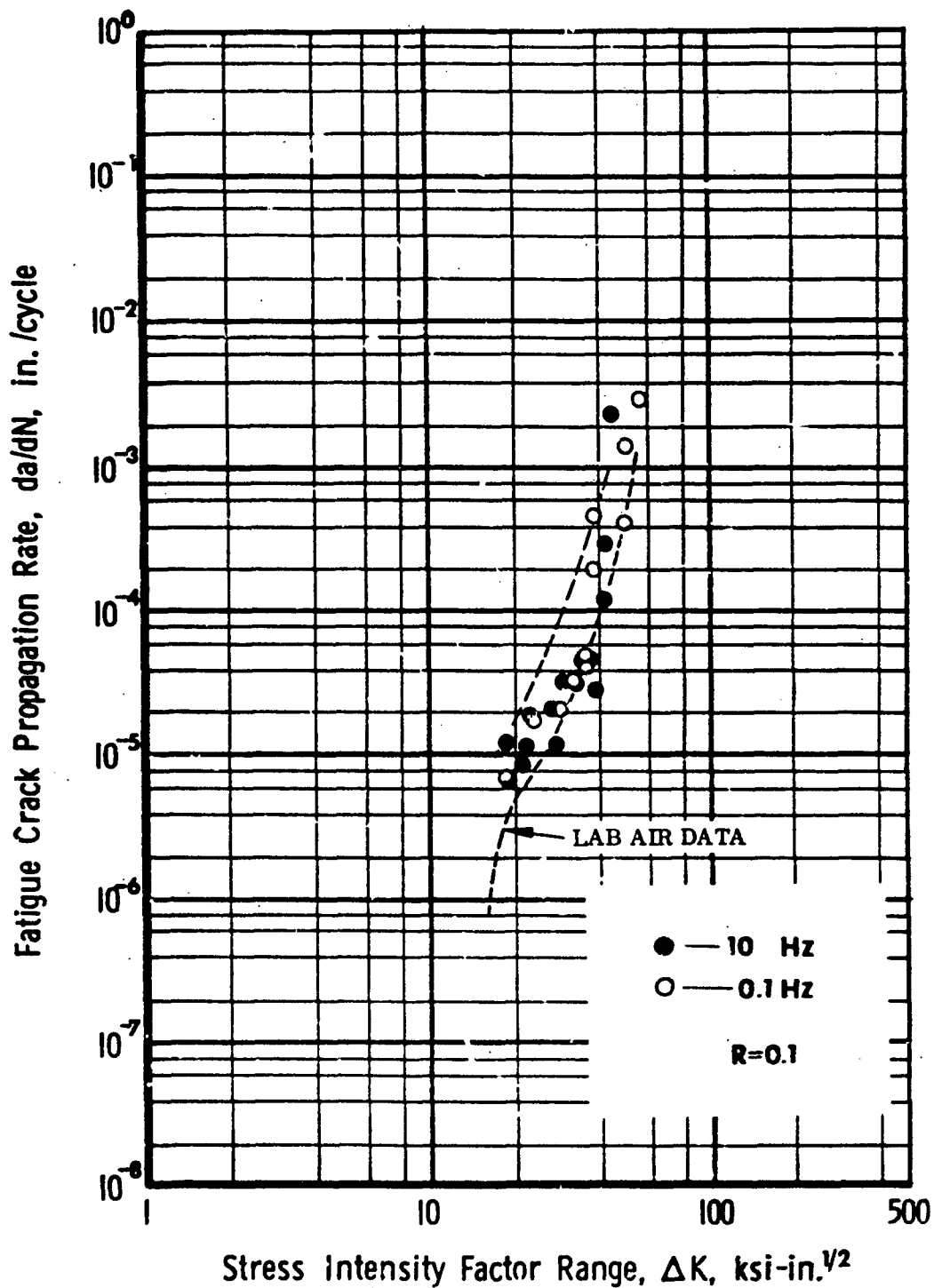


Figure 41 Ti-6Al-4V E.B. Weldment, SR, 1.0-in. Plate, HAZ, T-L Direction, CTT Specimens, Room Temperature JP4 Environment (Specimen Thickness: 1.00 in.; Width: 2.55 in.; H/W = 0.486)

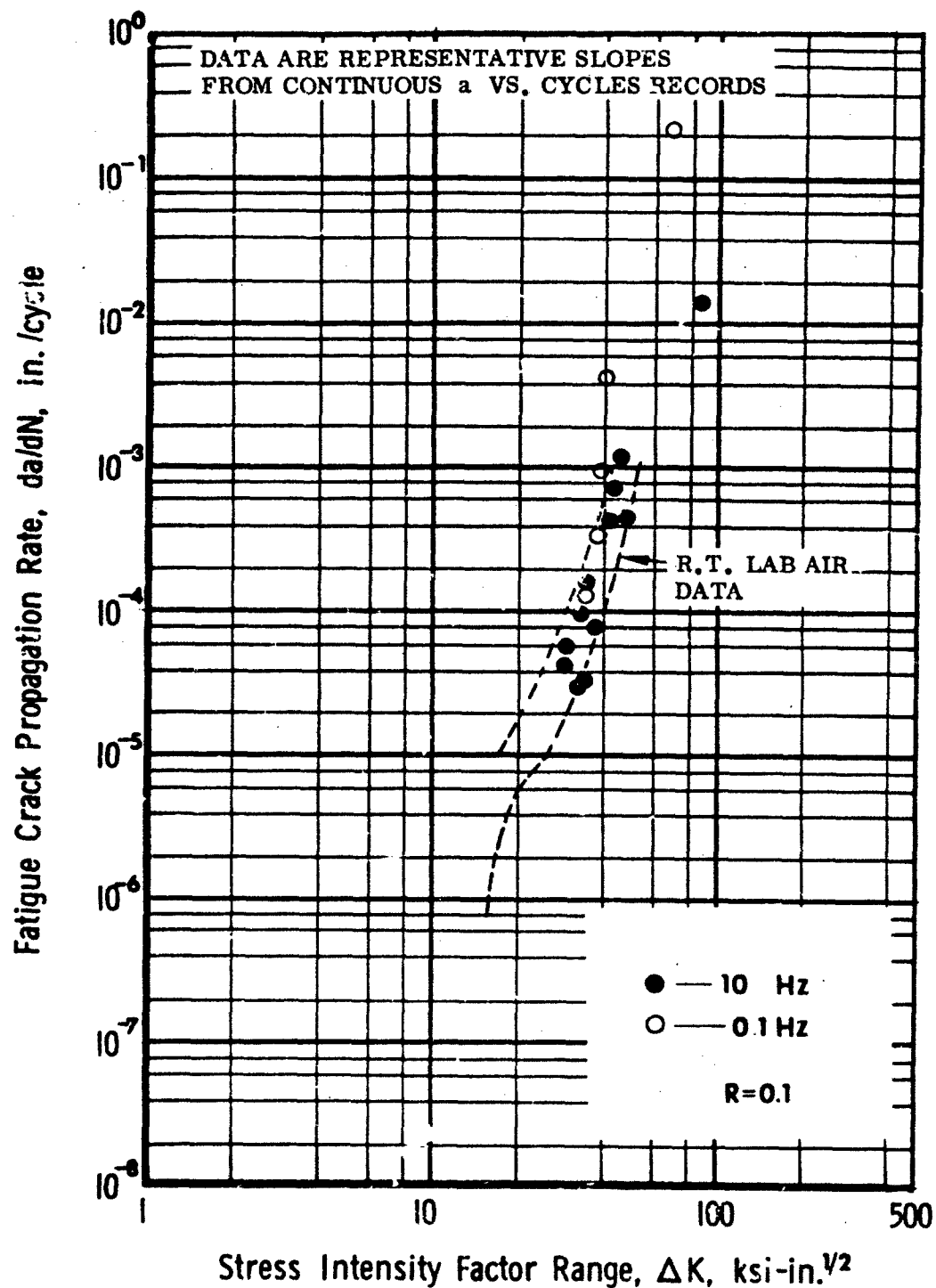


Figure 42 Ti-6Al-4V E.B. Weldment, SR, 1.0-in. Plate, HAZ T-L Direction, CTT Specimens, -65°F Laboratory Air Environment (Specimen Thickness: 1.00 in.; Width: 2.55 in.; H/W = 0.486)

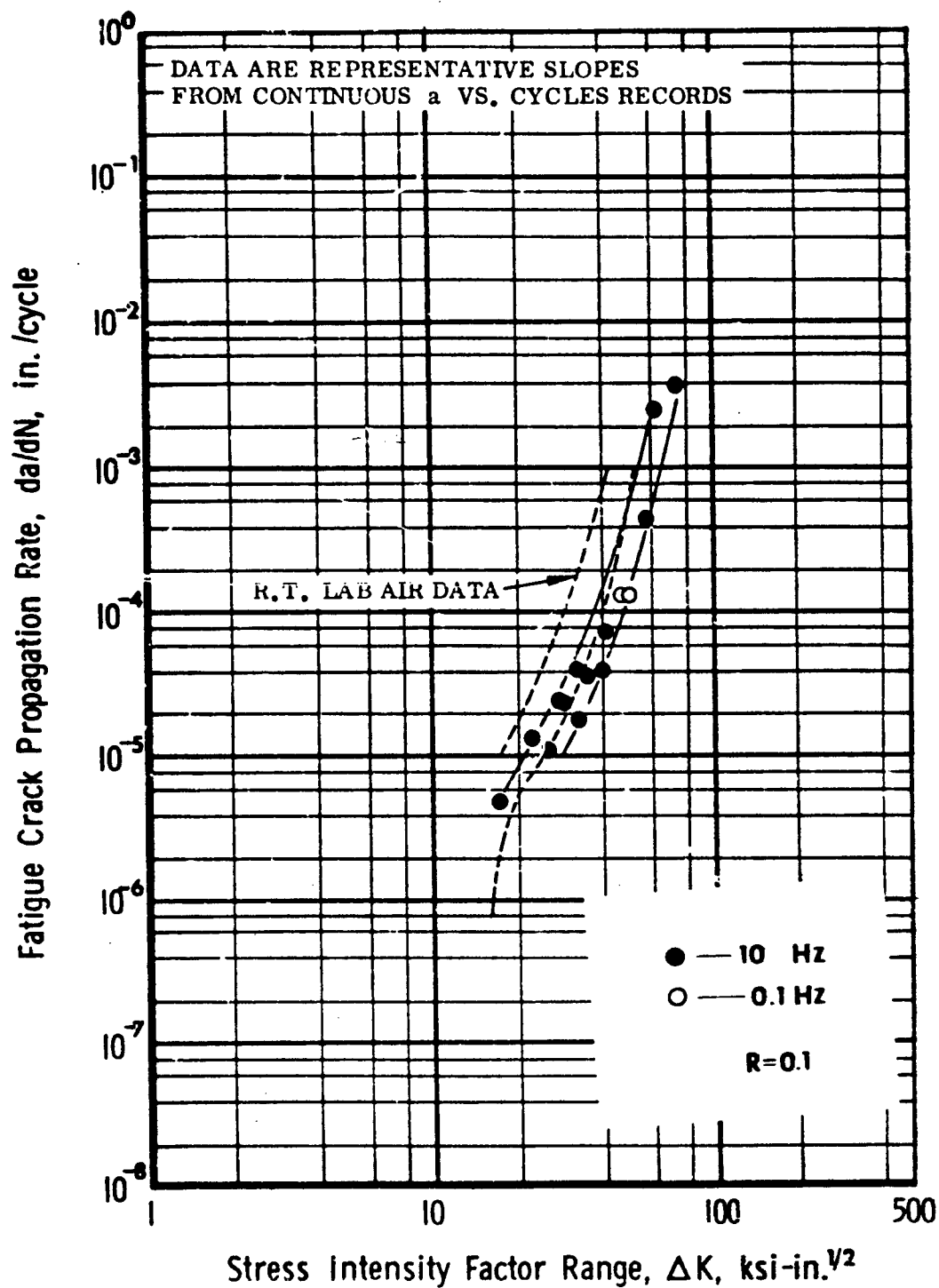


Figure 43 T1-6A1-4V F.B. Weldment, SR, 1.0-in. Plate, HAZ, T-L Direction, CTT Specimens, 175°F Laboratory Air Environment (Specimen Thickness: 1.00 in.; Width: 2.55 in.; H/W = 0.486)

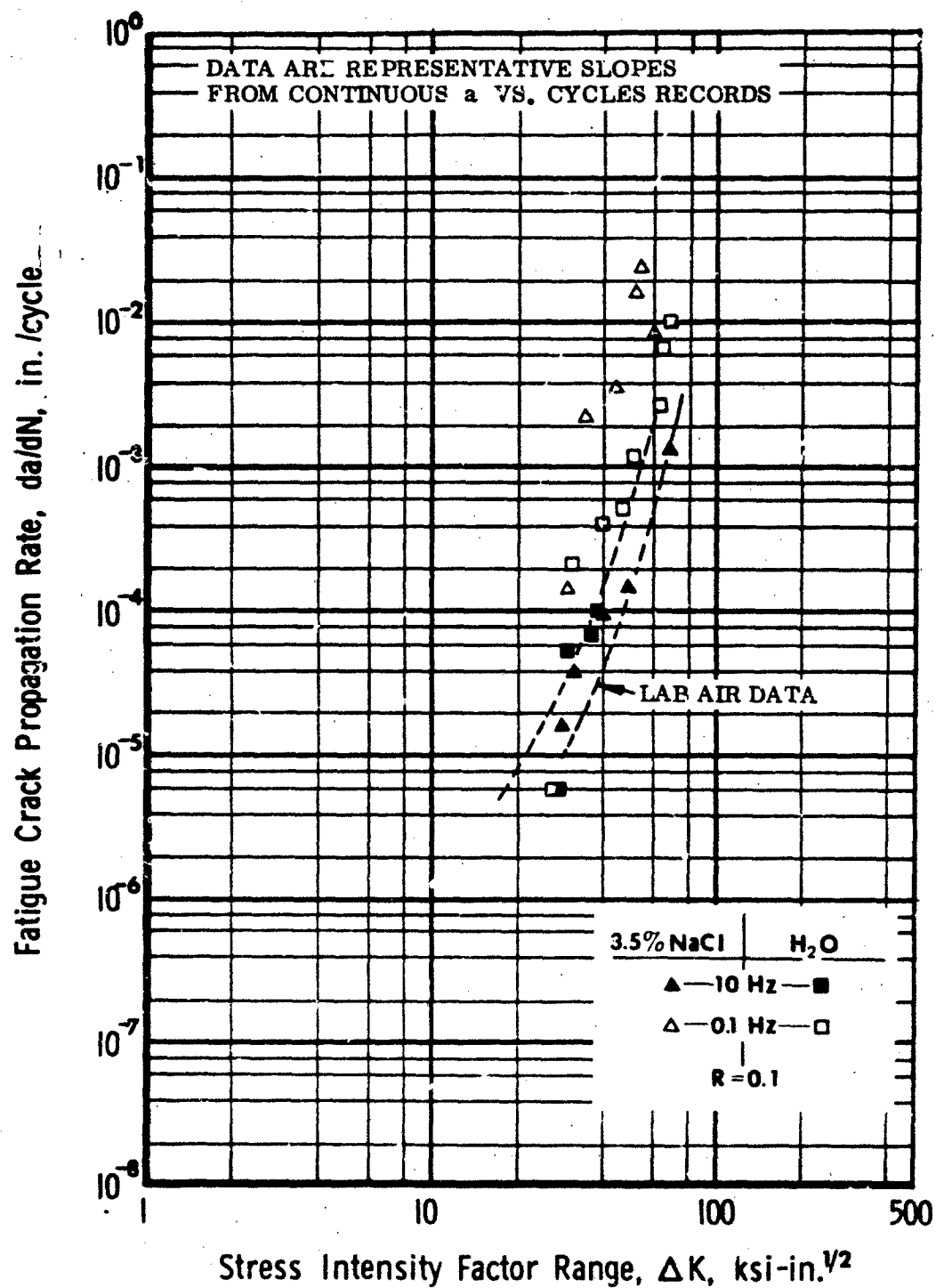


Figure 44 Ti-6Al-4V E.B. Weldment, SR, 1.0-in. Plate, HAZ, T-L Direction, CTT Specimens, 175°F Water and Salt Water Environments (Specimen Thickness: 1.00 in.; Width: 2.55; H/W = 0.486)

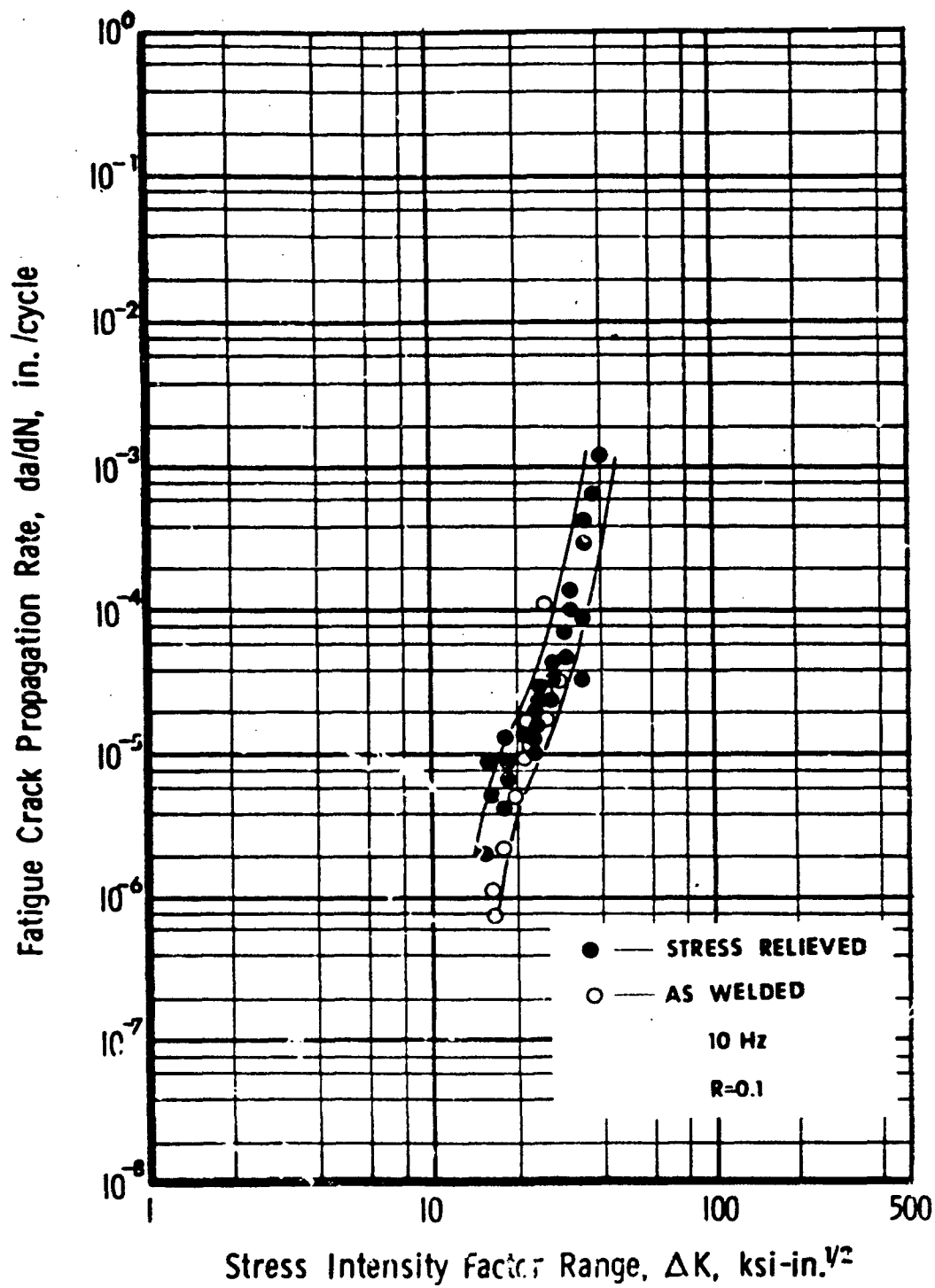


Figure 45 Ti-6Al-4V E.B. Weldment, 1.0-in. Plate, WZ, T-J, Plate Directions, CTT Specimens, Room Temperature Laboratory Air Environment (Specimen Thickness: 1.00 in.; Width: 2.00 in.; H/W = 0.6)

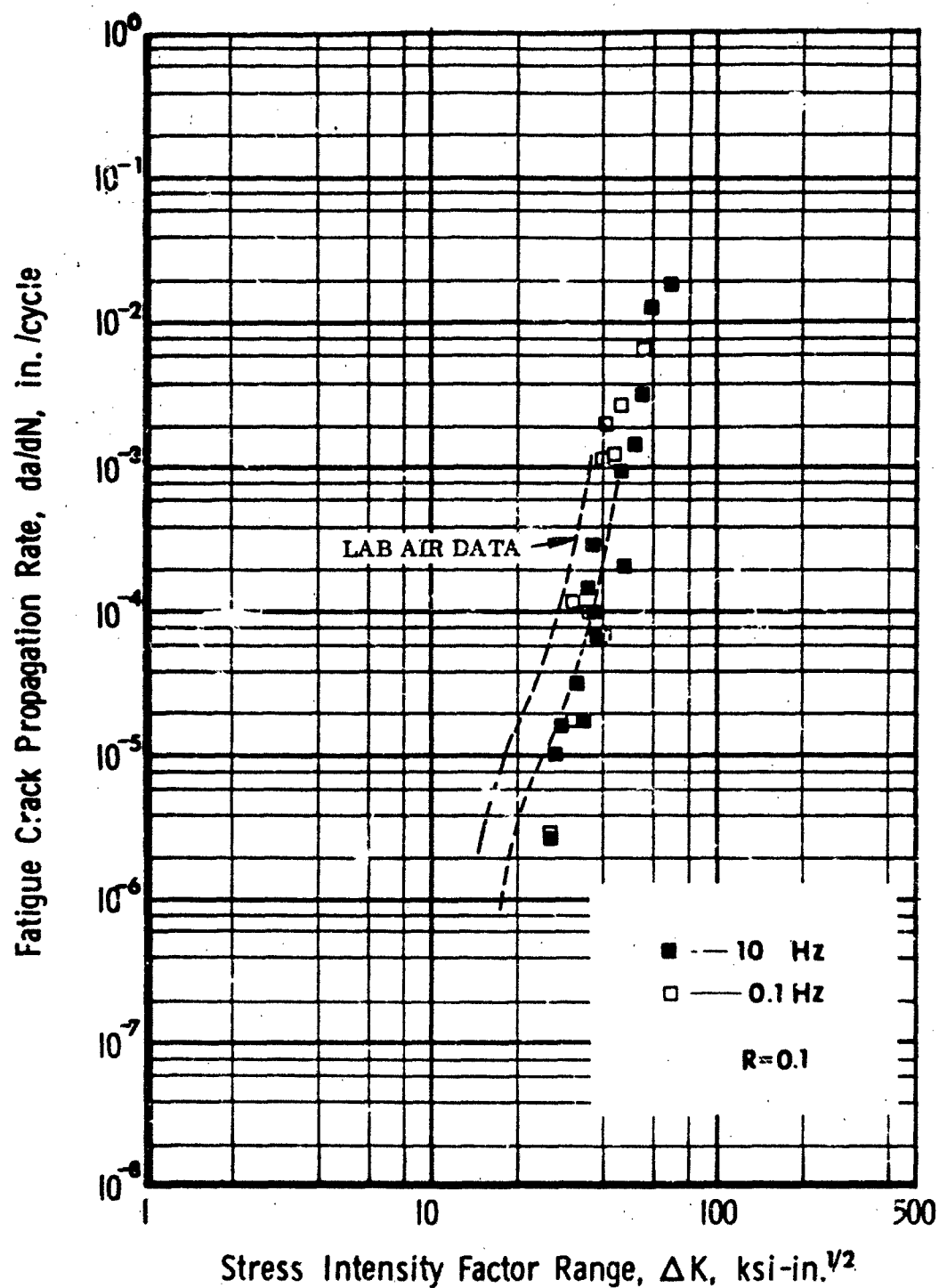


Figure 46 Ti-6Al-4V E.B. Weldment, SR, 1.0-in. Plate, WZ, T-L Plate Directions, CTT Specimens, Room Temperature Water Environment (Specimen Thickness: 1.0 in. Width: 2.00 in.; $H/W = 0.6$)

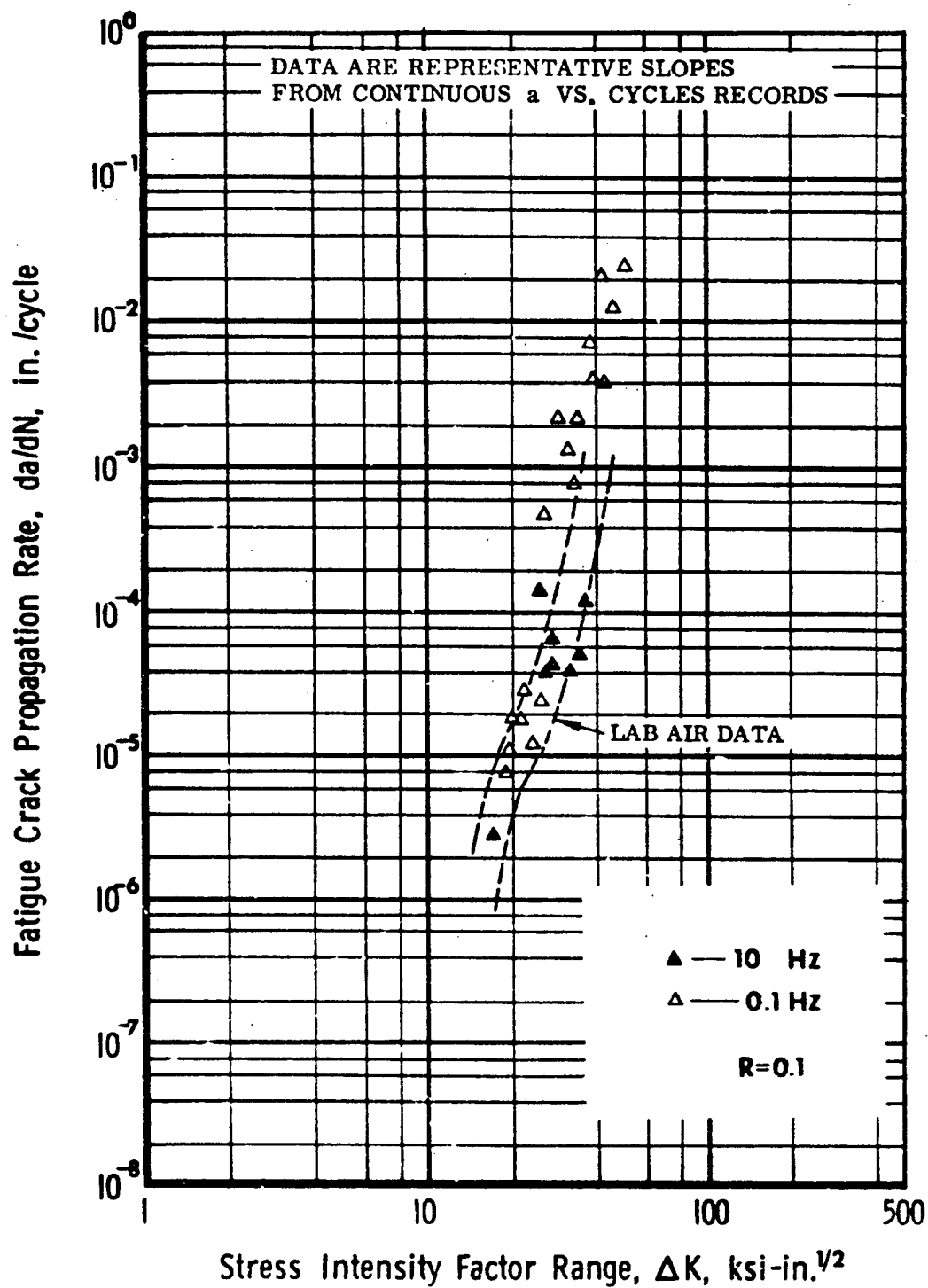


Figure 47 Ti-6Al-4V E.B. Weldment, SR, 1.0-in. Plate, WZ T-L Plate Directions, CTT Specimens, Room Temperature Salt Water Environment (Specimen Thickness: 1.00 in.; Width 2.55 in.; H/W = 0.486)

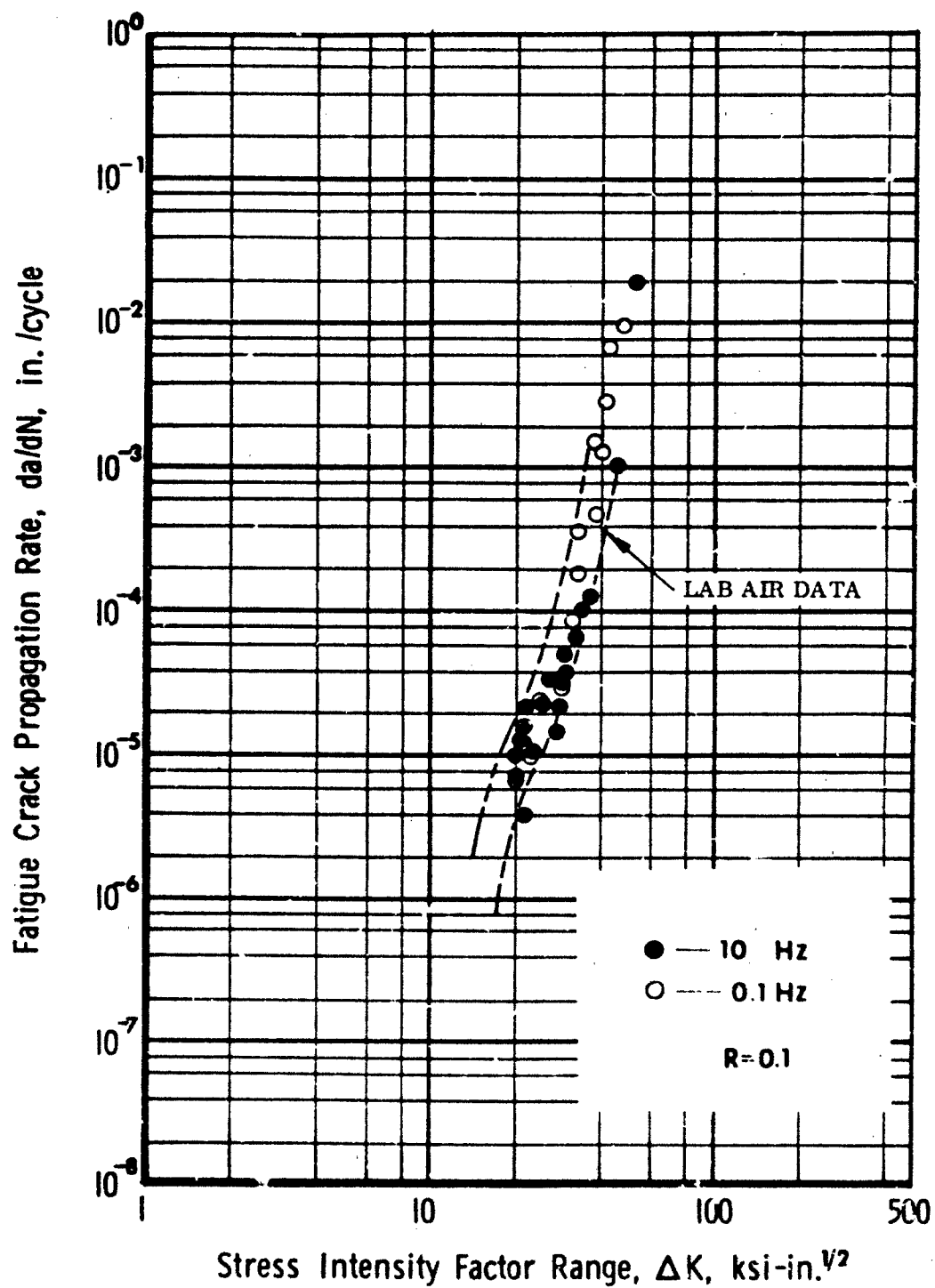


Figure 48 Ti-6Al-4V E.B. Weldment, SR, 1.0-in. Plate, WZ, T-L Plate Directions, CTT Specimens, Room Temperature JP4 Environment, (Specimen Thickness: 1.00 in.; Width: 2.55 in.; $h/W = 0.486$)

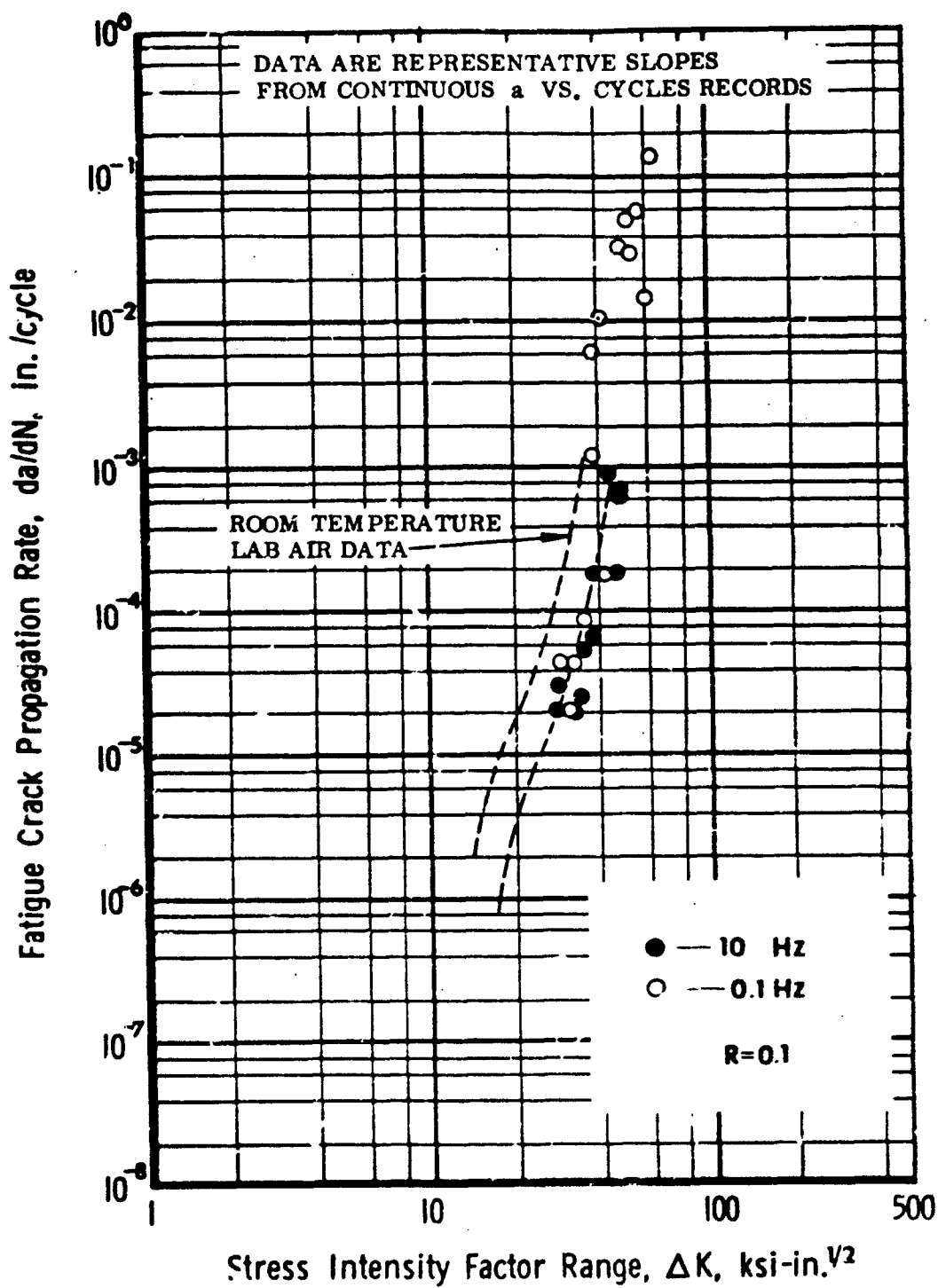


Figure 49 Ti-6Al-4V E.B. Weldment, SR, 1.0-in. Plate, WZ, T-L Plate Directions, C'T Specimens, -65°F Laboratory Air Environment (Specimen Thickness: 1.00 in.; Width: 2.55 in.; H/W = 0.486)

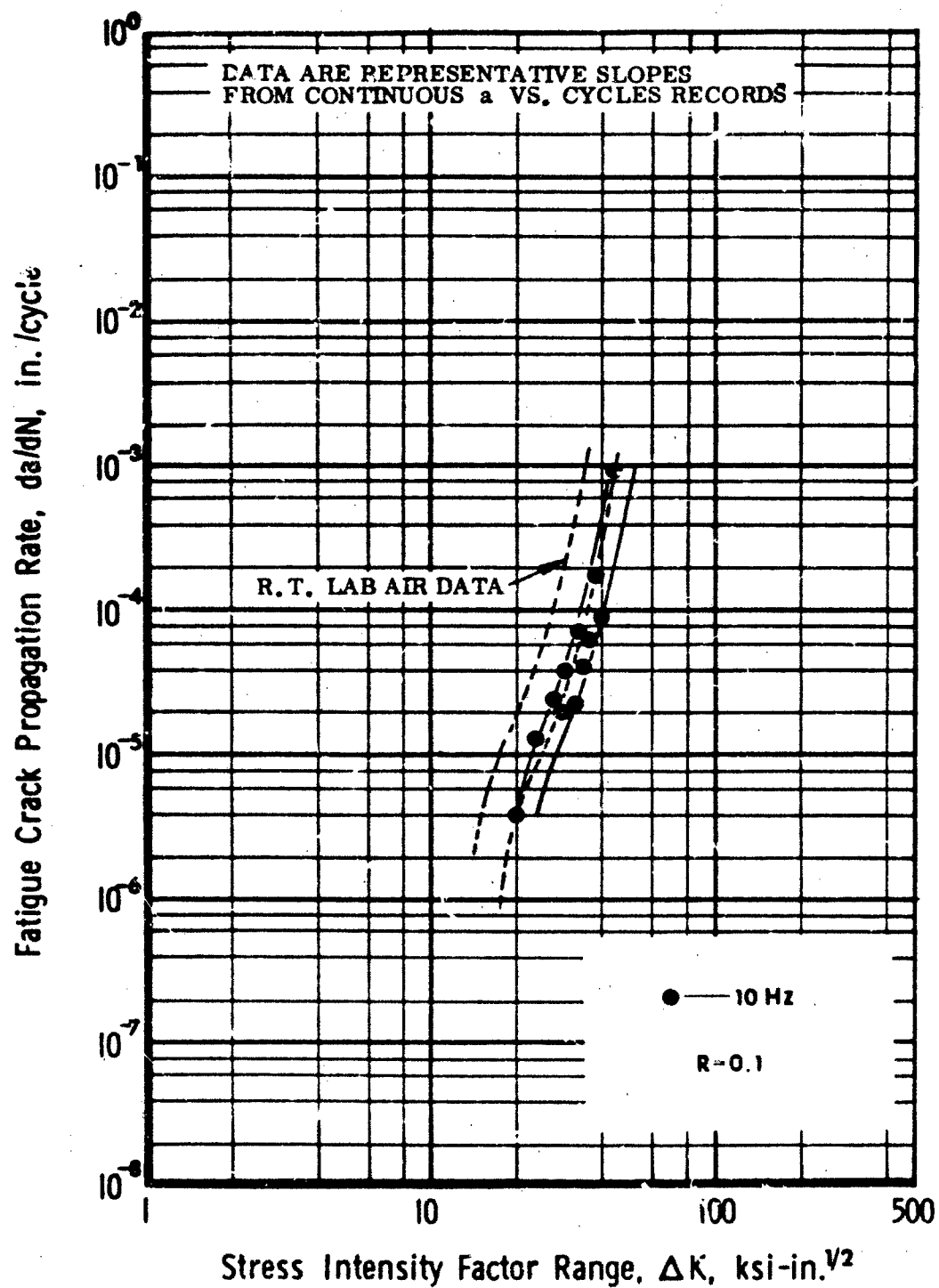


Figure 50 Ti-6Al-4V E.B. Weldment, SR, 1.0-in. Plate, WZ, T-L Plate Directions, CTT Specimens, 175°F Laboratory Air Environment (Specimen Thickness: 1.00 in.; Width: 2.55 in.; H/W = 0.486)

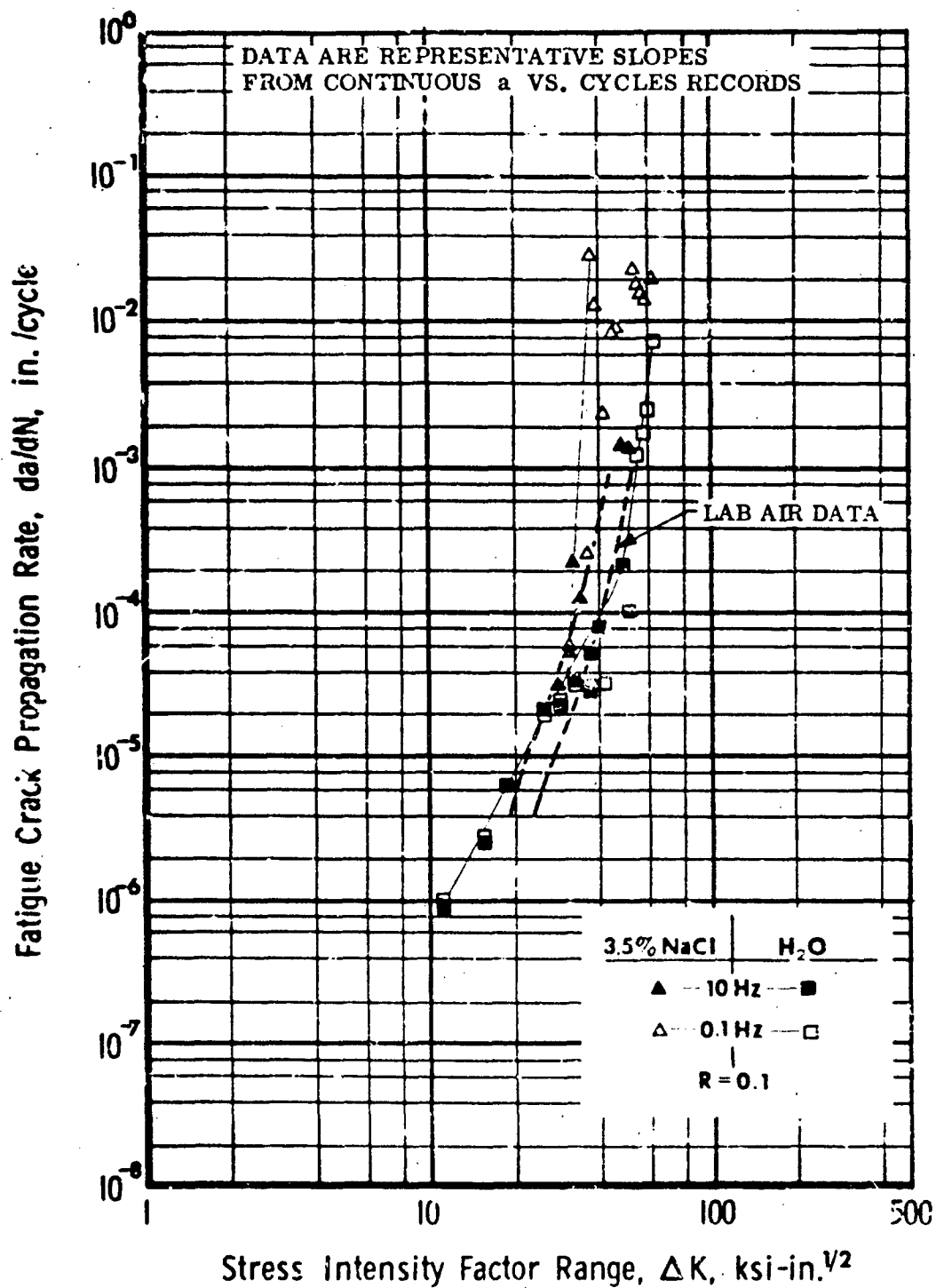


Figure 51 Ti-6Al-4V E.B. Weldment, SR, 1.0-in. Plate, WZ, T-L Plate Directions, CTT Specimens, 175°F Water and Salt Water Environments (Specimen Thickness: 1.00 in.; Width: 2.55 in.; H/W = 0.486)

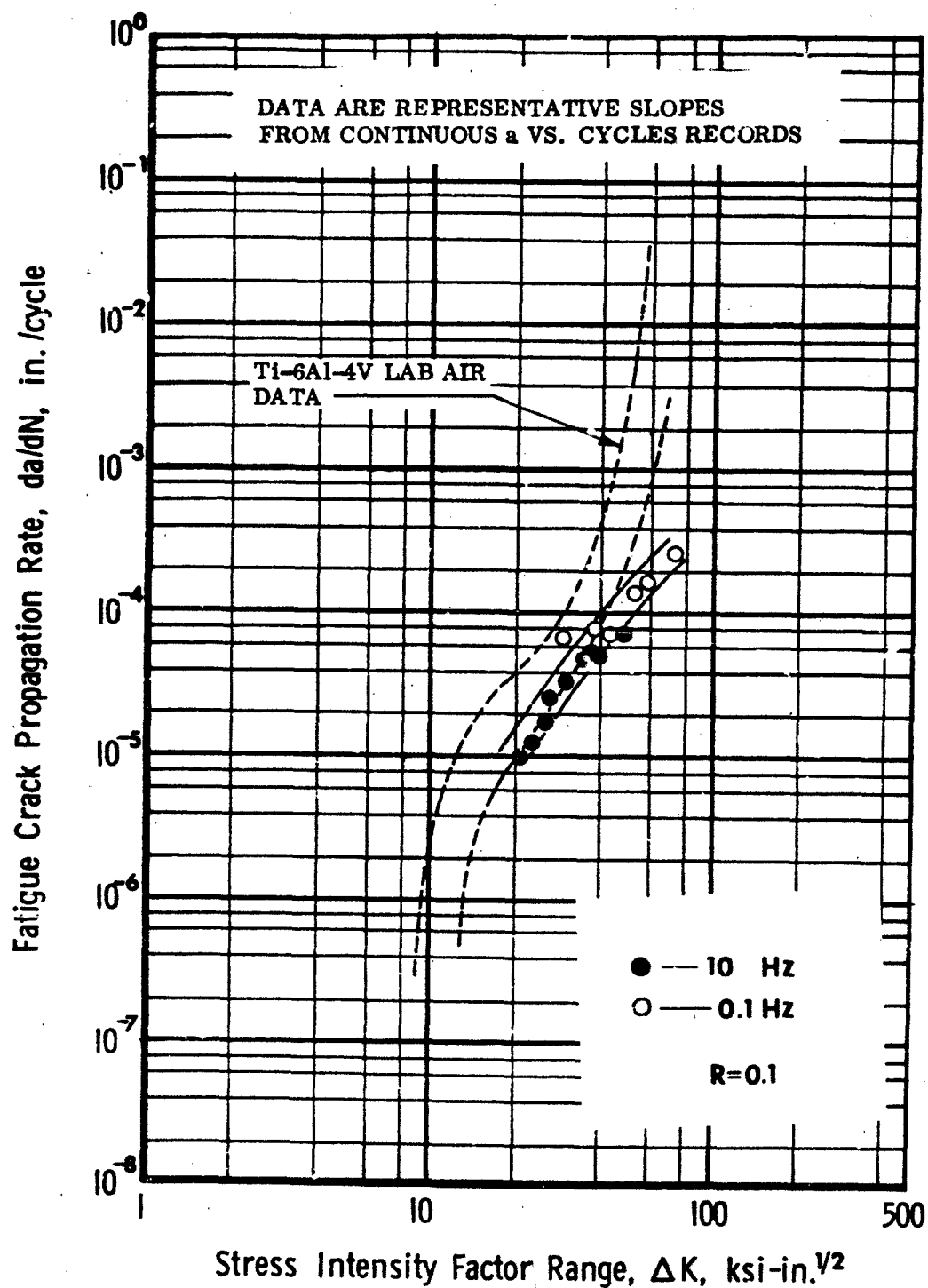


Figure 52 Beta III Titanium Base Metal, 1.0-in. STA Plate, T-L Direction, CTT Specimen, Room Temperature Laboratory Air Environment (Specimen Thickness: 1.00 in.; Width: 2.55 in.; H/W = 0.486)

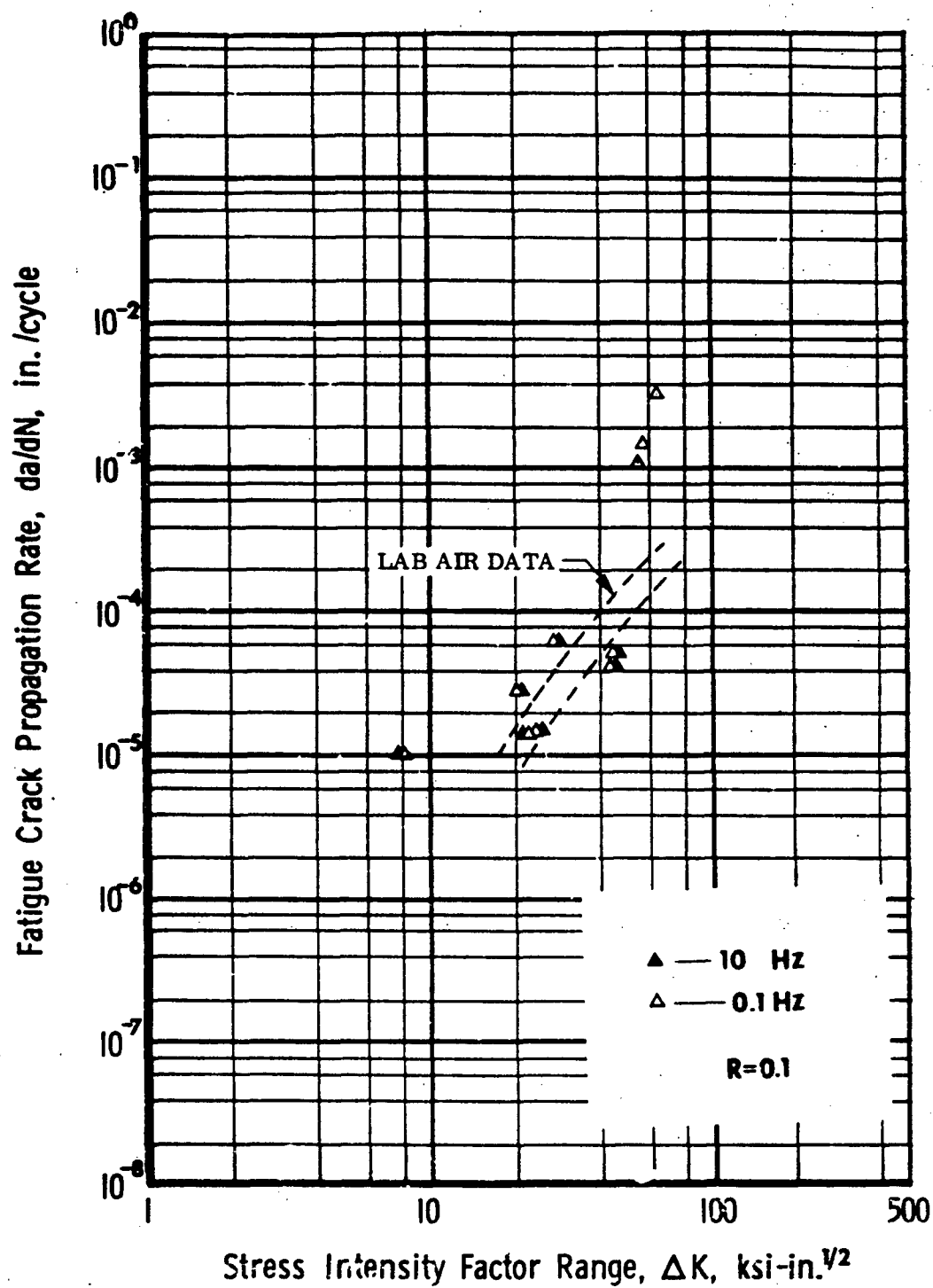


Figure 53 Beta III Titanium Base Metal, 1.0-in. STA Plate, T-L Direction, CTT Specimen, Room Temperature 3.5% NaCl Solution Environment (Specimen Thickness: 1.00 in.; Width: 2.55 in.; H/W = 0.486)

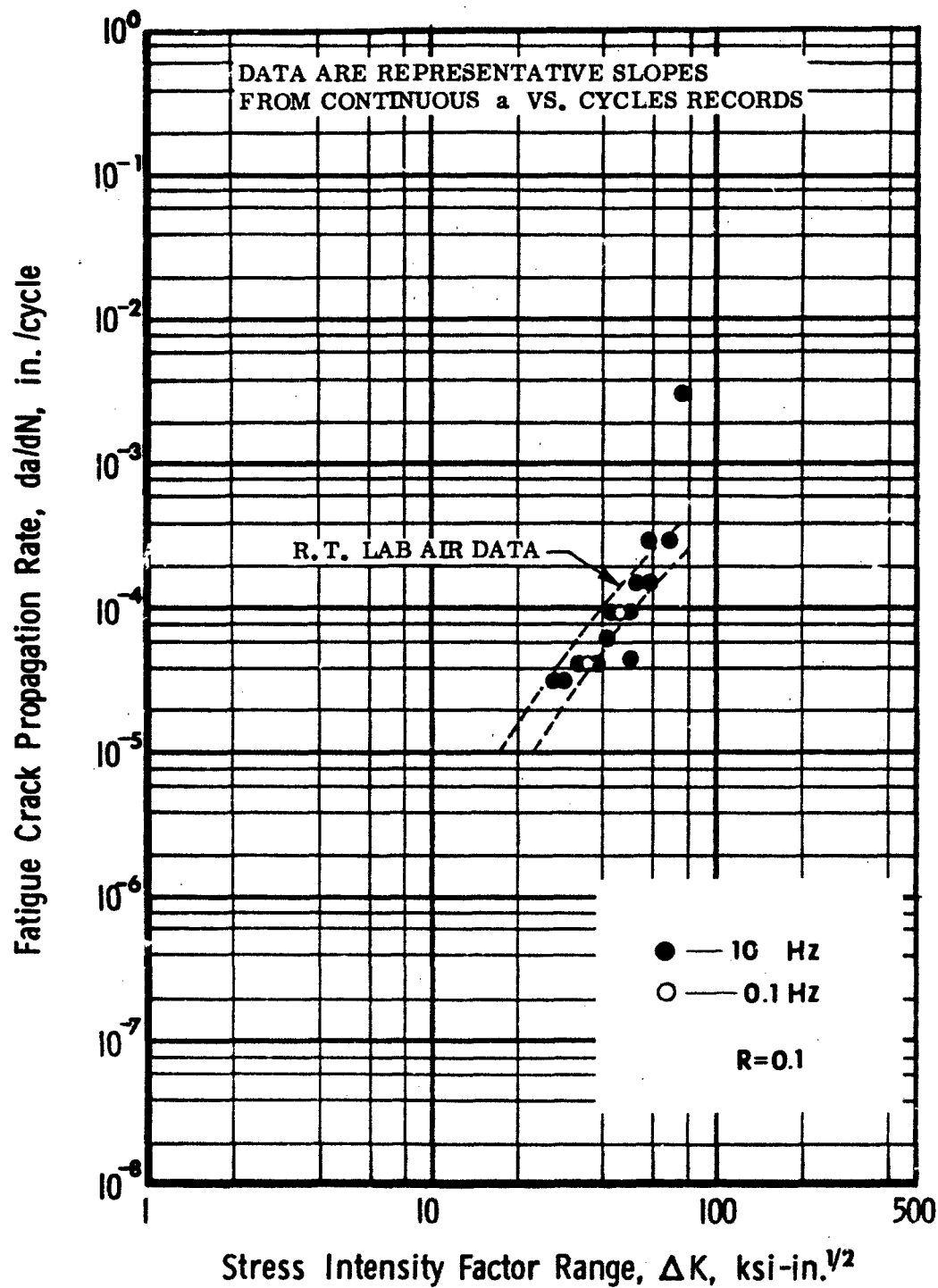


Figure 54 Beta III Titanium Base Metal, 1.0-in. STA Plate, T-L Direction, CTT Specimen, -65°F Laboratory Air Environment (Specimen Thickness: 1.00 in.; Width: 2.55 in.; H/W = 0.486)

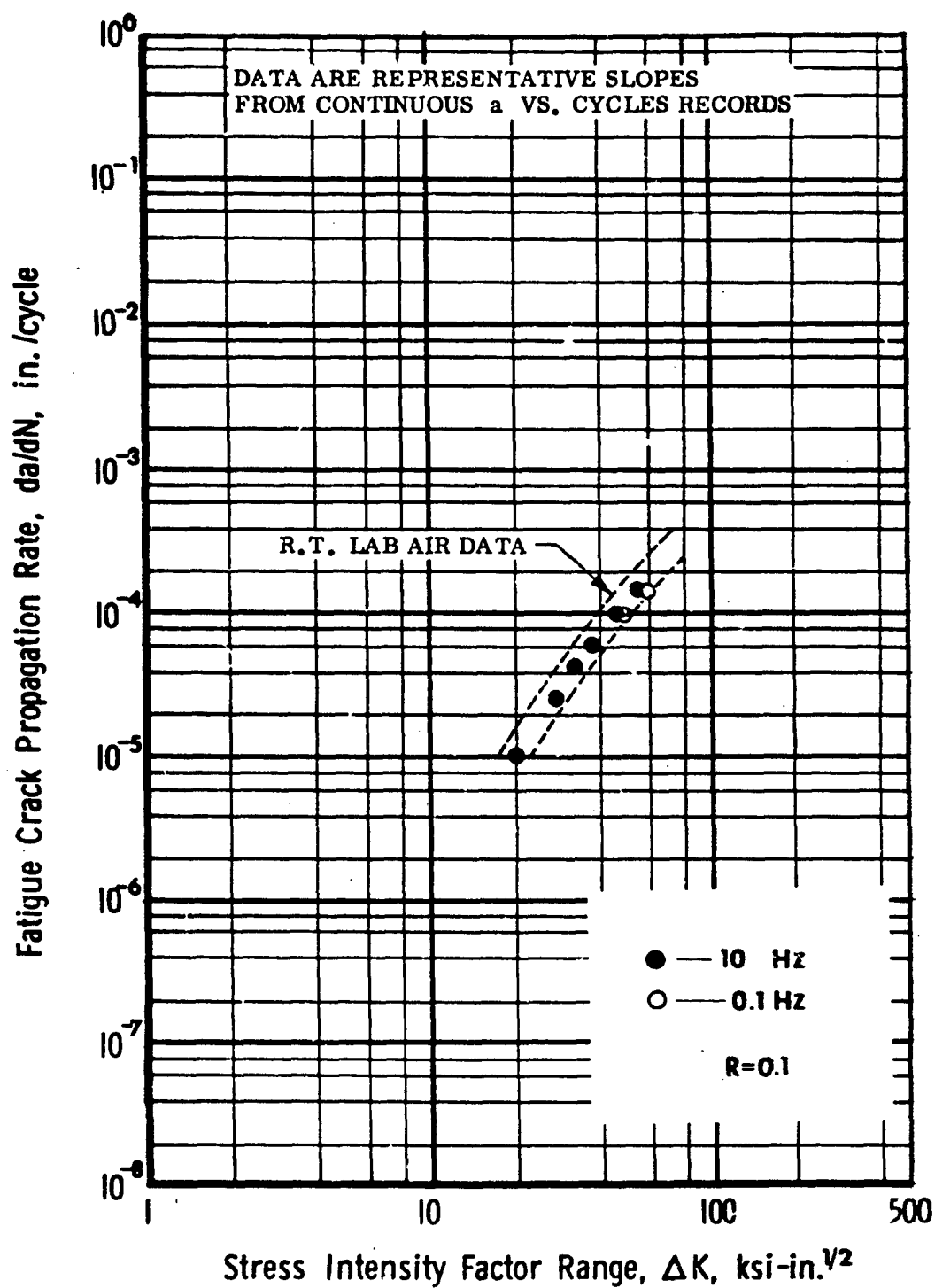


Figure 55 Beta III Titanium Base Metal, 1.0-in. STA Plate, T-L Direction, CTT Specimen, 175°F Laboratory Air Environment (Specimen Thickness: 1.00 in.; Width: 2.55 in.; H/W = 0.486)

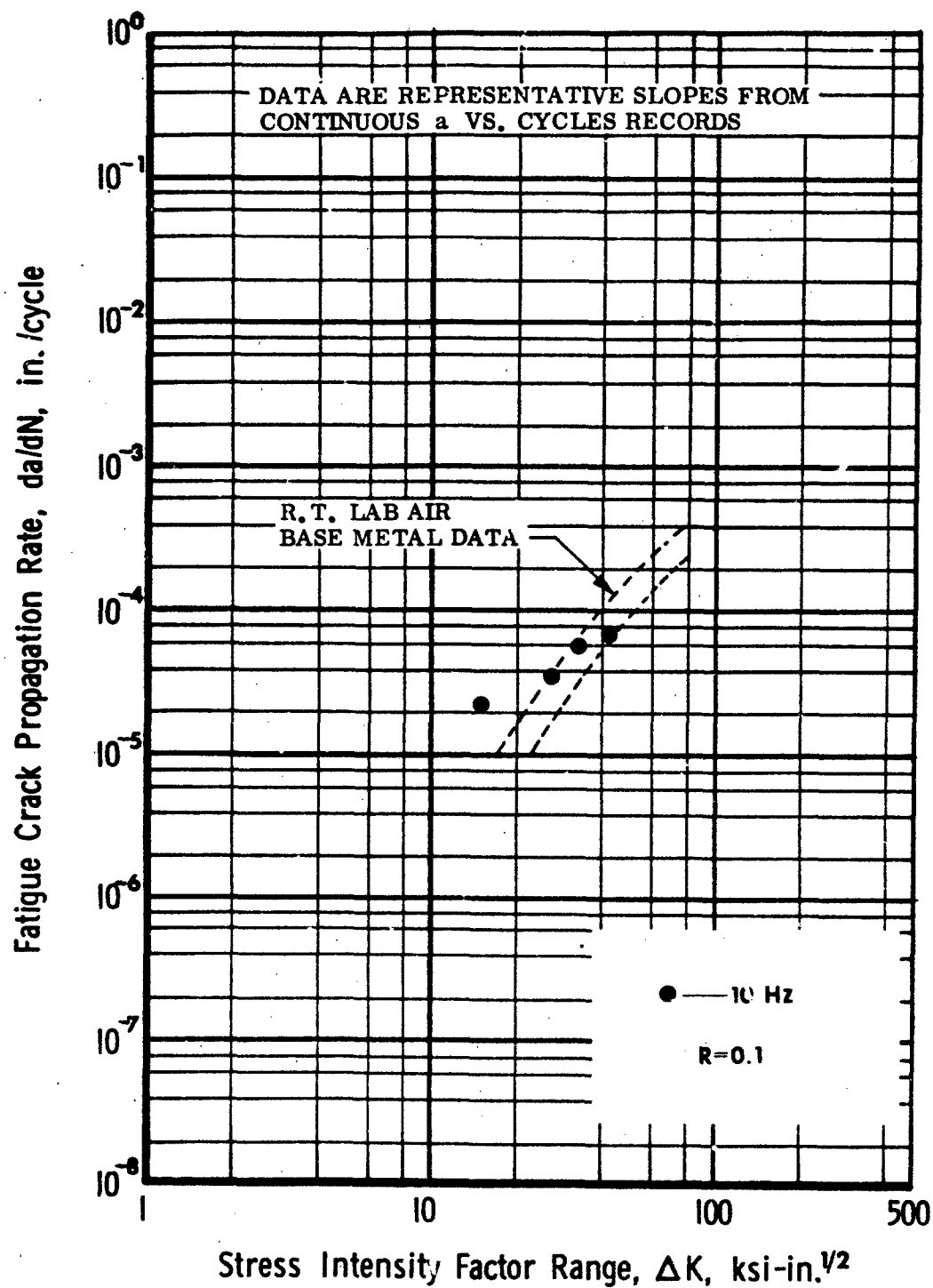


Figure 56 Beta III Titanium E.B. Weldment, STA, 1.0-in. Plate, HAZ, T-L Direction, CTT Specimen, Room Temperature Laboratory Air Environment (Specimen Thickness: 1.00 in.; Width: 2.55 in.; H/W = 0.486)

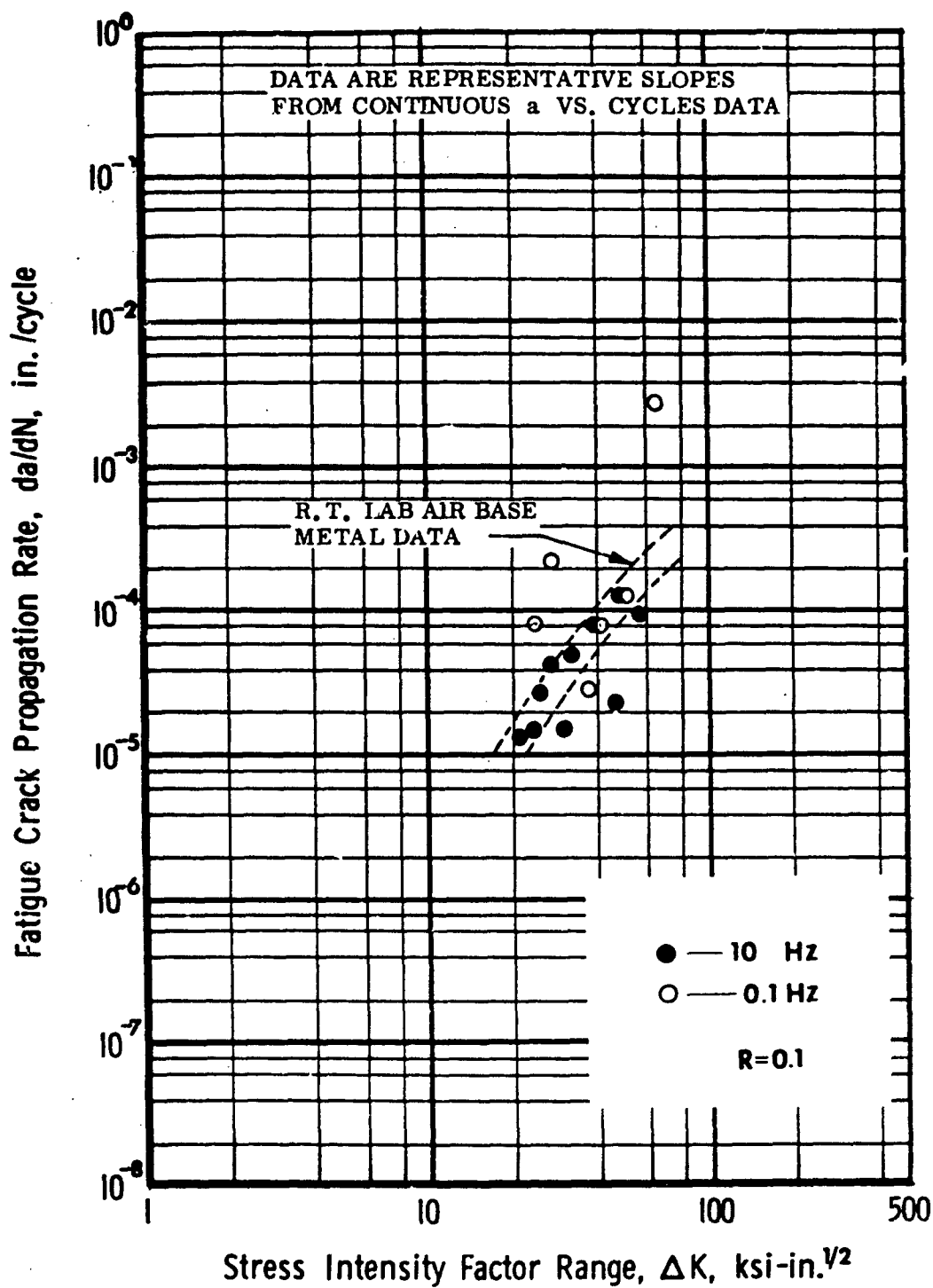


Figure 57 Beta III Titanium E.B. Weldment, STA, 1.0-in. Plate, HAZ, T-L Direction, CTT Specimen, -65°F Laboratory Air Environment (Specimen Thickness: 1.00 in.; Width: 2.55 in.; H/W = 0.486)

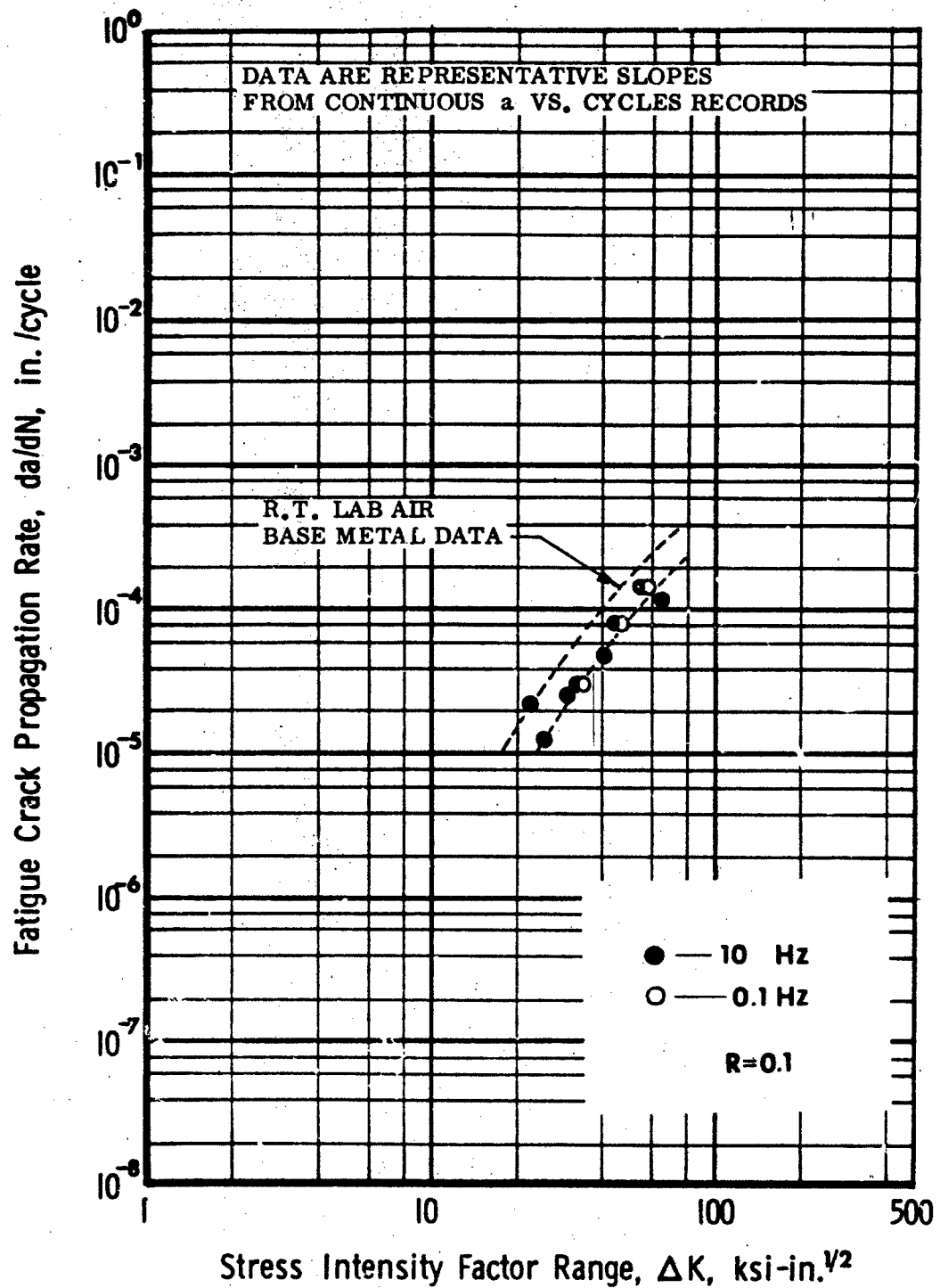


Figure 58 Beta III Titanium E.B. Weldment, STA, 1.0-in. Plate HAZ, T-L Direction, CTT Specimen, 175° F Laboratory Air Environment (Specimen Thickness 1.00 in.; Width: 2.55 in.; H/W = 0.486)

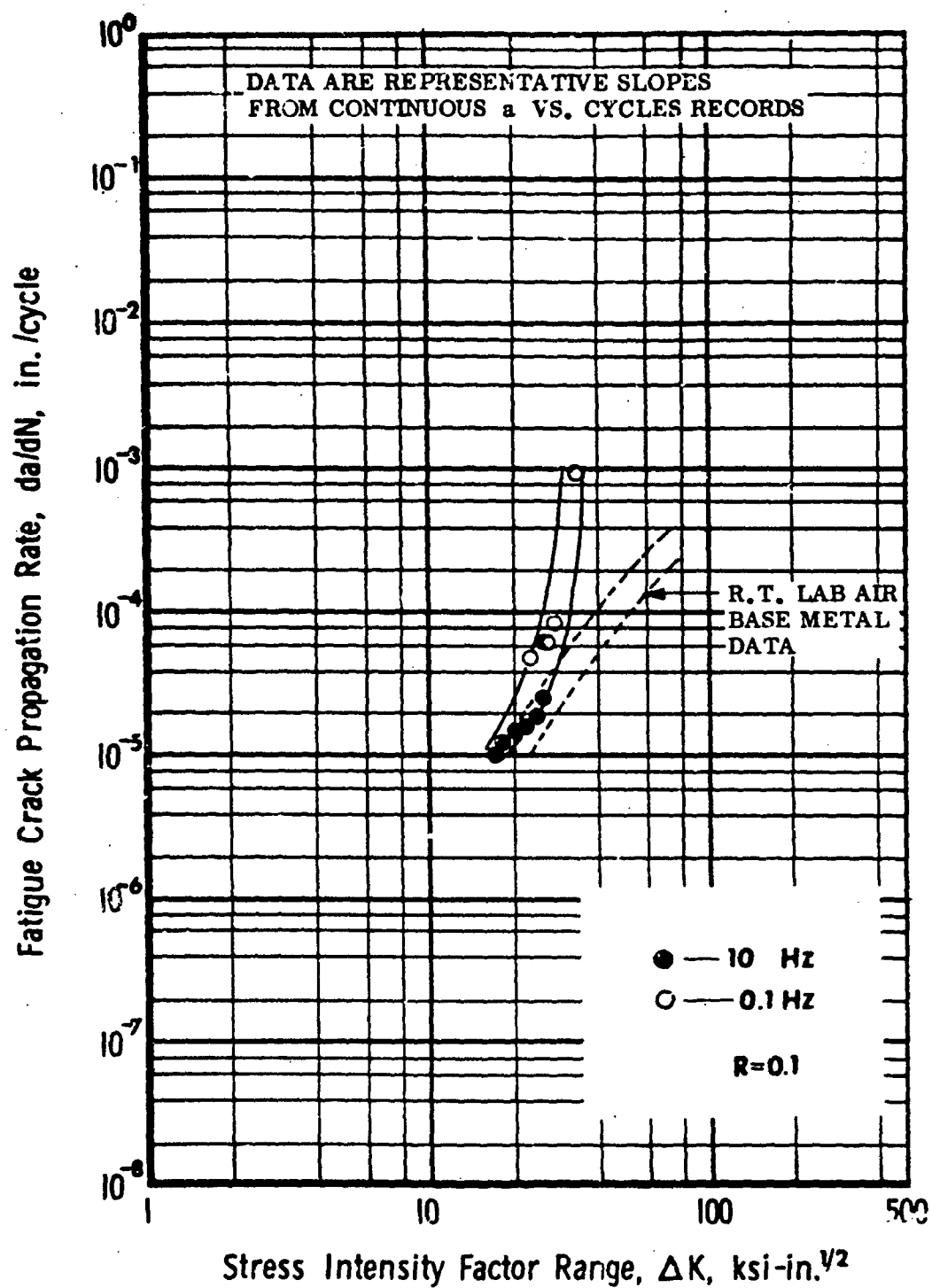


Figure 59 Beta III Titanium E.B. Weldment, STA, 1.0-in. Plate, WZ, T-L Plate Directions, CTT Specimen, Room Temperature Laboratory Air Environment (Specimen Thickness: 1.00 in.; Width: 2.55 in.; H/W = 0.486)

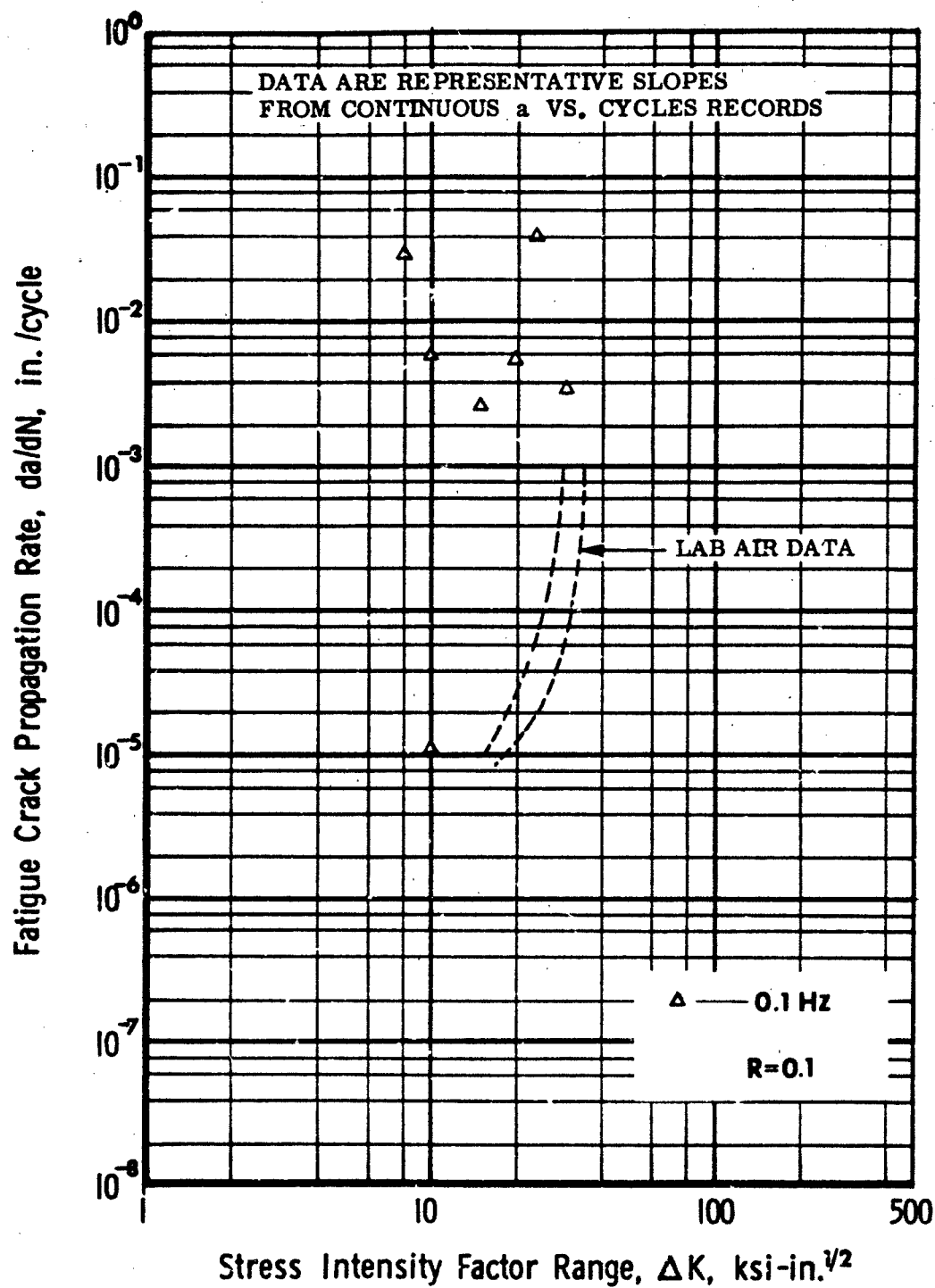


Figure 60 Beta III Titanium E.B. Weldment, STA, 1.0-in. Plate, WZ, T-L Plate Directions, CTT Specimen, Room Temperature 3.5% NaCl Solution Environment (Specimen Thickness: 1.00 in.; Width: 2.55 in.; H/W = 0.486)

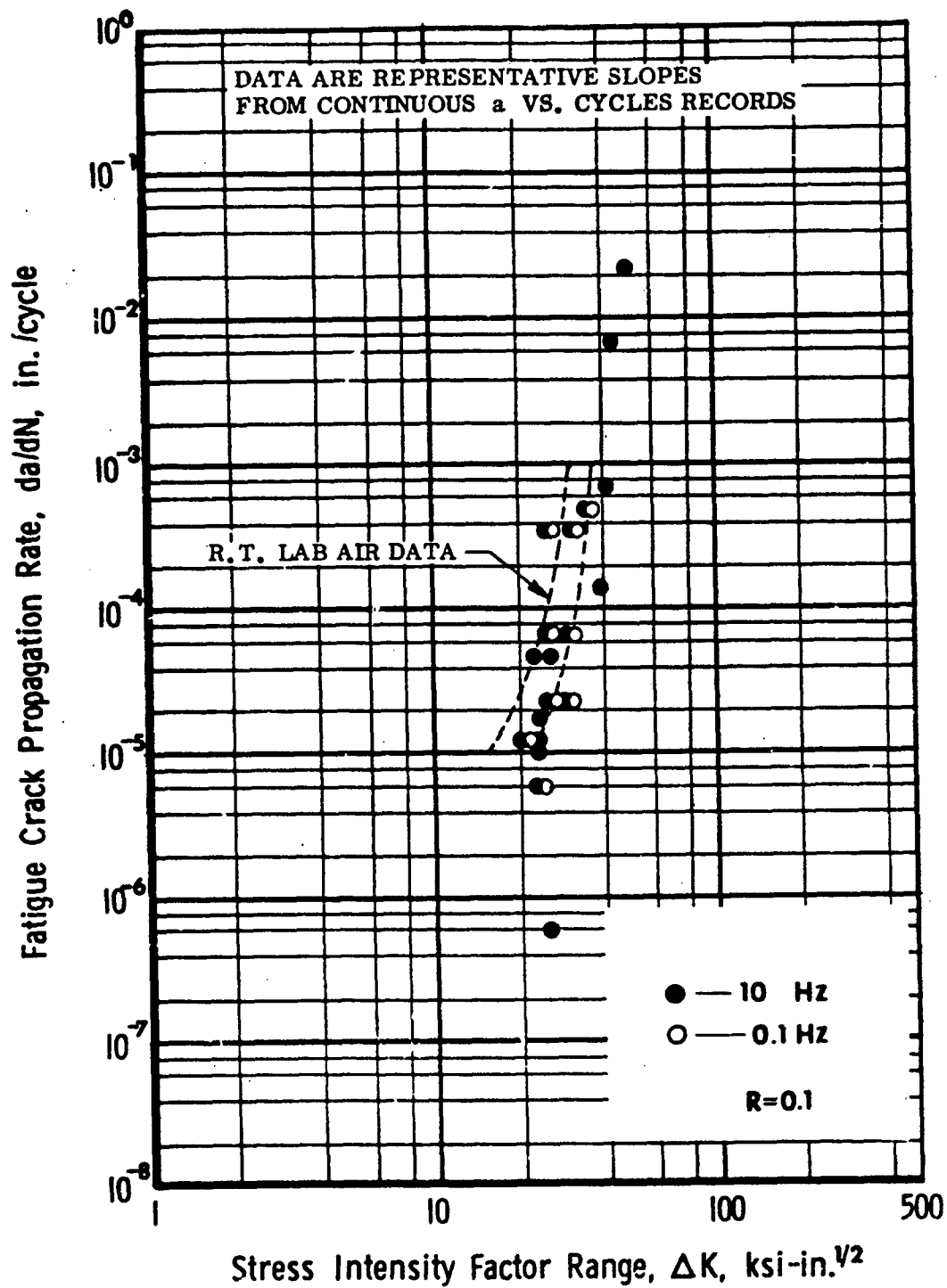


Figure 61 Beta III Titanium E.B. Weldment, STA, 1.0-in. Plate, WZ, T-L Plate Directions, CTT Specimen, -65°F Laboratory Air Environment (Specimen Thickness: 1.00 in.; Width: 2.55 in.; $H/W = 0.486$)

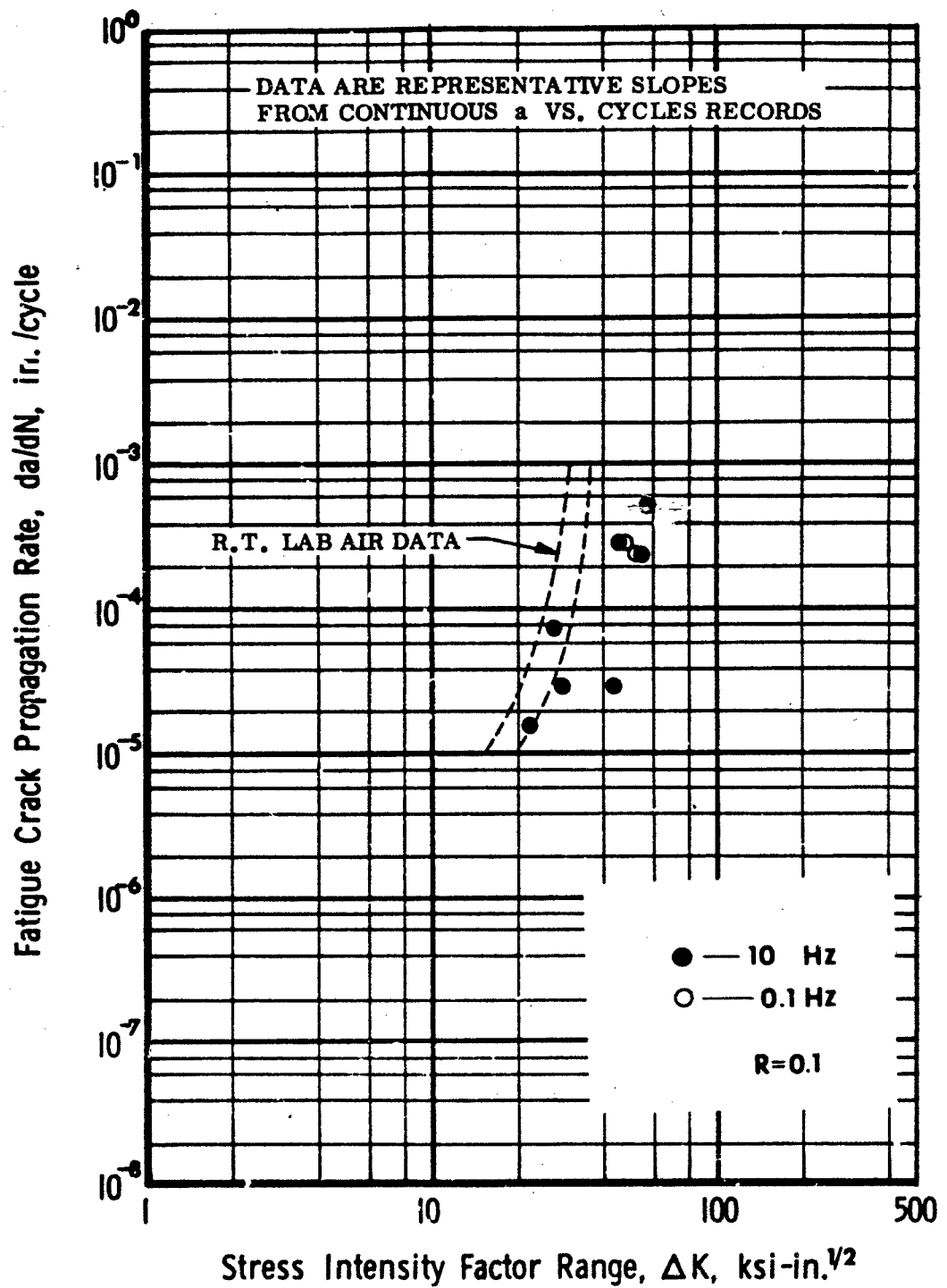


Figure 62 Beta III Titanium E.B. Weldment, STA, 1.0-in. Plate, WZ, T-L Plate Directions, CTT Specimen, 175°F Laboratory Air Environment (Specimen Thickness: 1.00 in.; Width: 2.55 in.; H/W = 0.486)

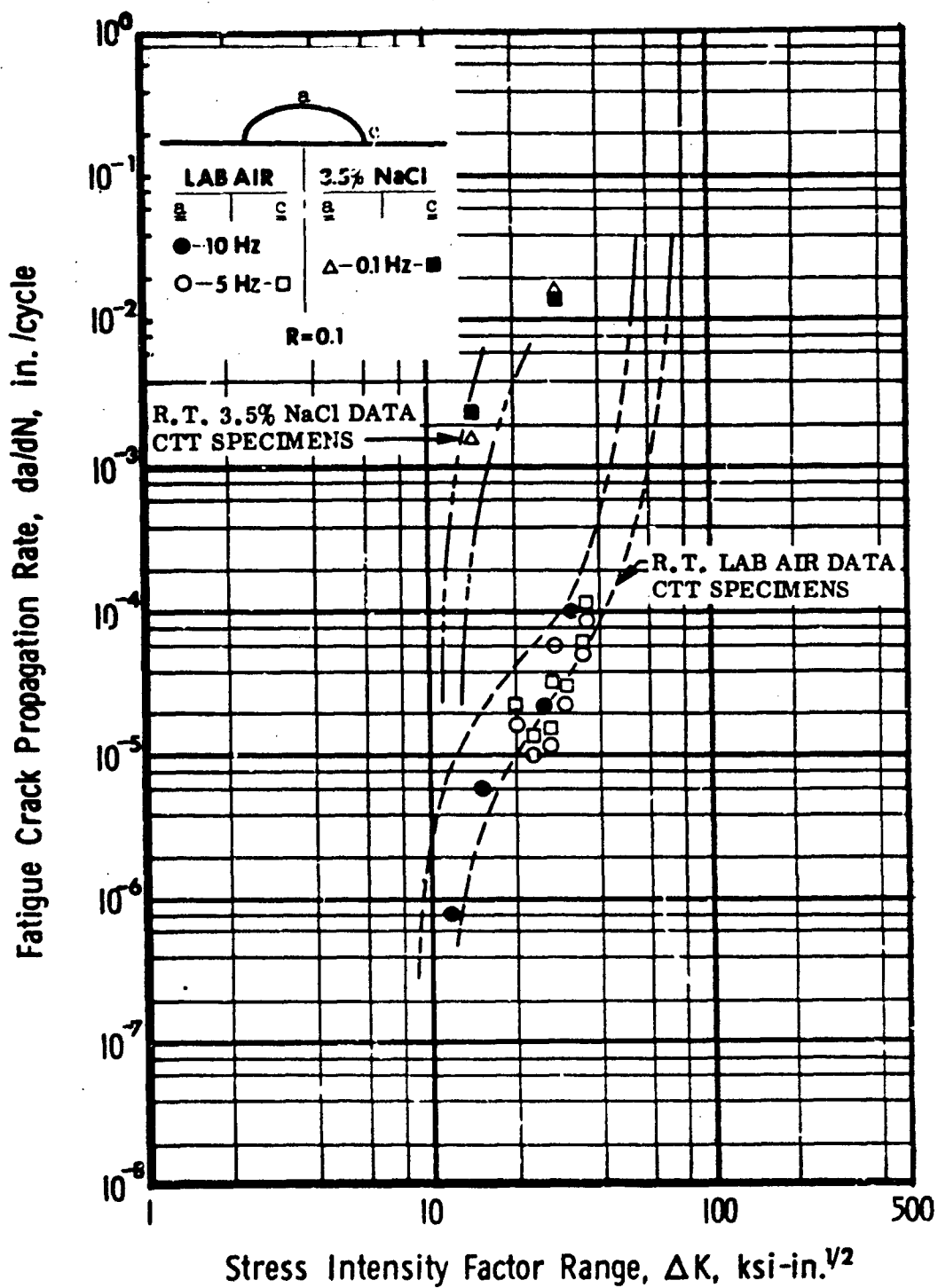


Figure 63 Ti-6Al-4V Base Metal, 1.0-in. MA Plate, T-S Direction, PTT Specimens, Room Temperature Laboratory Air and Salt Water Environments (Specimen Thickness: 0.250 in.; Width: 1.5 in.)

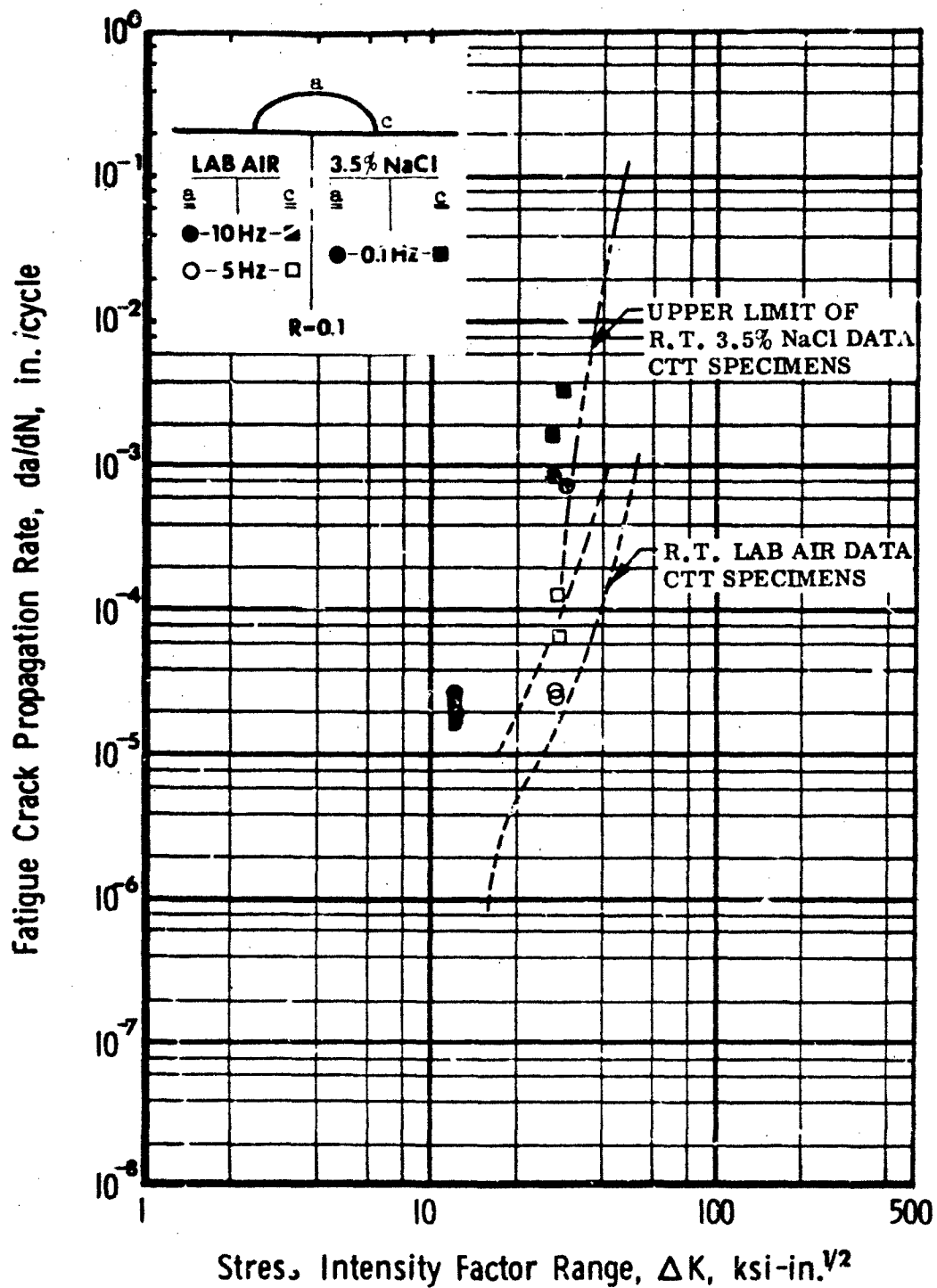


Figure 64 Ti-6Al-4V E.B. Weldment, AW, 1.0-in. Plate, HAZ, T-S Direction, PTT Specimens, Room Temperature Laboratory Air and Salt Water Environments (Specimen Thickness: 0.250 in.; Width: 1.5 in.)

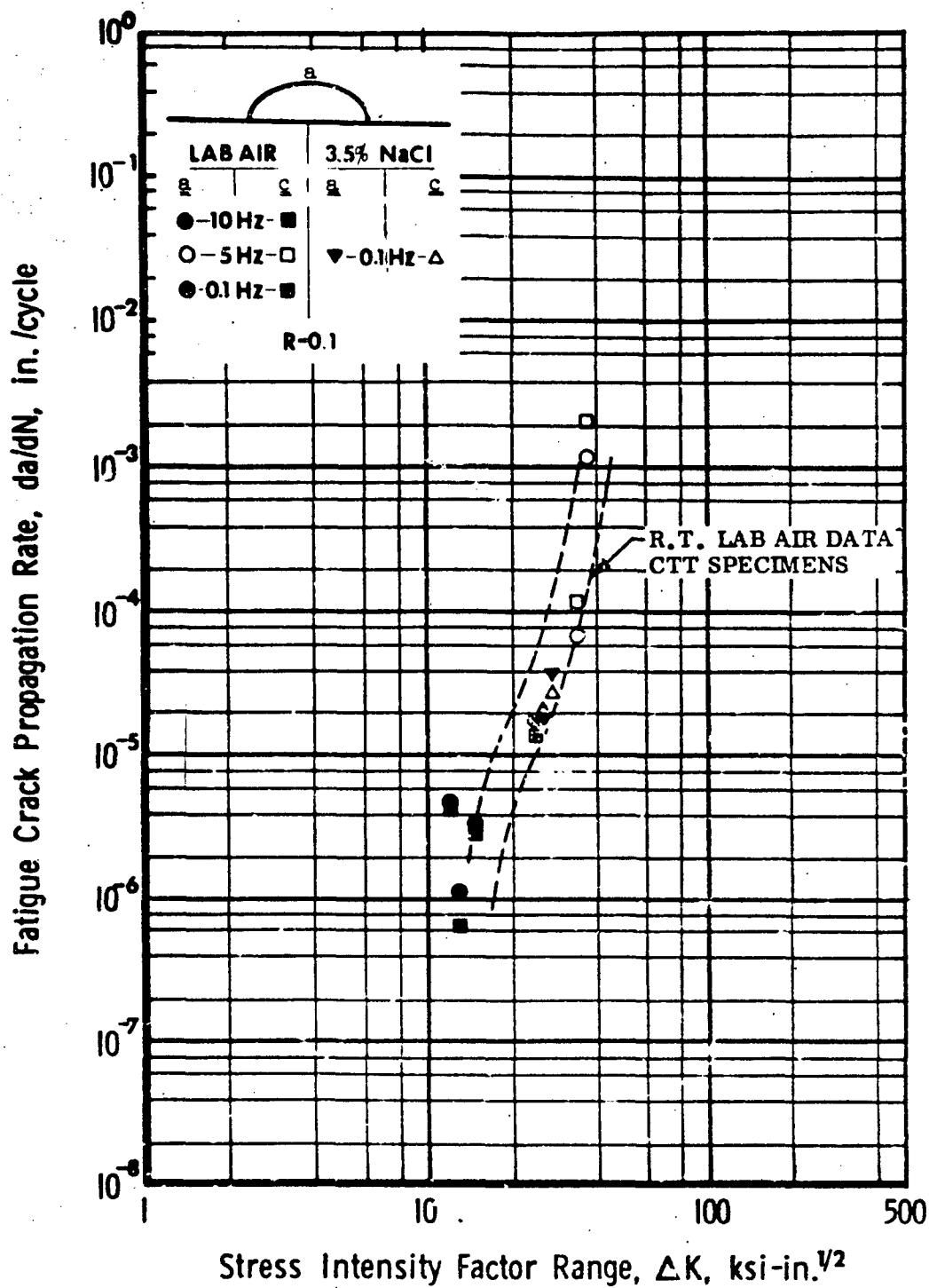


Figure 65 Ti-6Al-4V E.B. Weldment, AW, 1.0-in. Plate, WZ, T-S Plate Directions, PTT Specimens, Room Temperature Laboratory Air and Salt Water Environments (Specimen Thickness: 0.250 in.; Width: 1.5 in.)

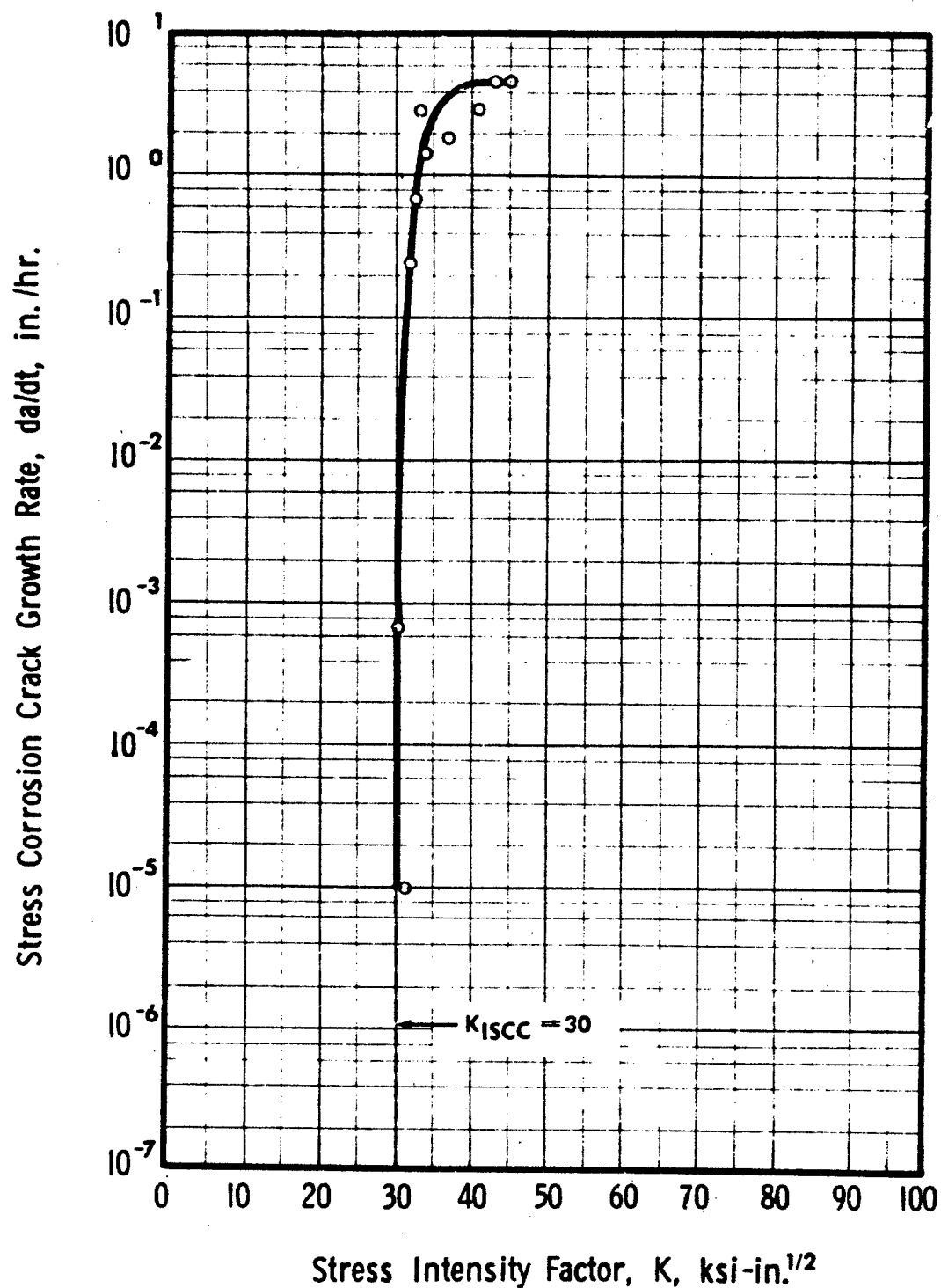


Figure 66 Environmental Crack Growth Rate Data for Ti-6Al-4V Base Metal, 1.0-in. MA Plate, T-L Direction, in 3.5 Percent NaCl at Room Temperature (CTT Specimen; $B = 1.00$ in.; $W = 2.55$ in.; $H/W = 0.486$)

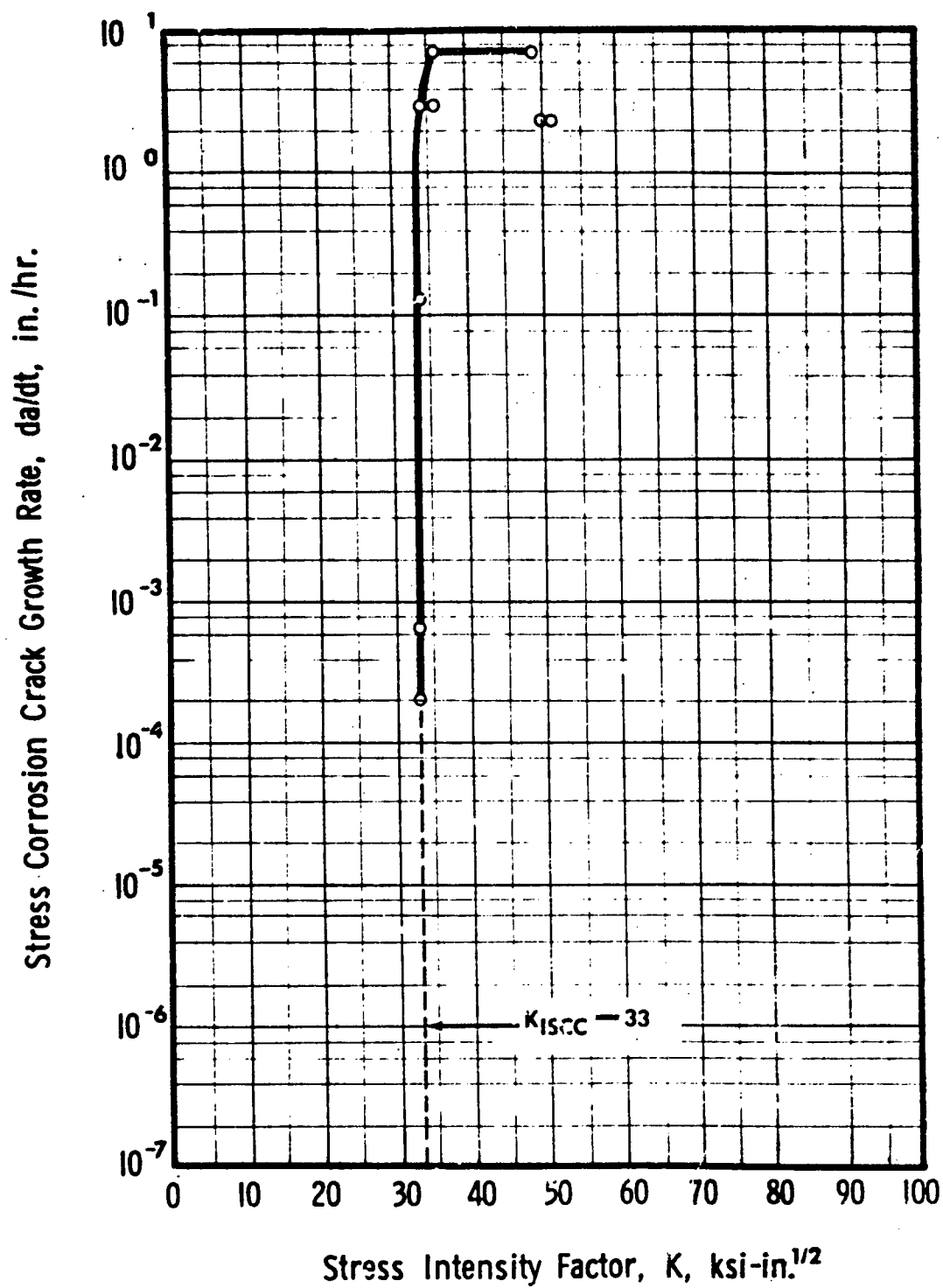


Figure 67 Environmental Crack Growth Rate Data for Ti-6Al-4V Base Metal, 1.0-in. MA Plate, T-L Direction, in 3.5 Percent NaCl at 175° F (CTT Specimen: B = 1.00 in.; W = 2.55 in.; H/W = 0.486)

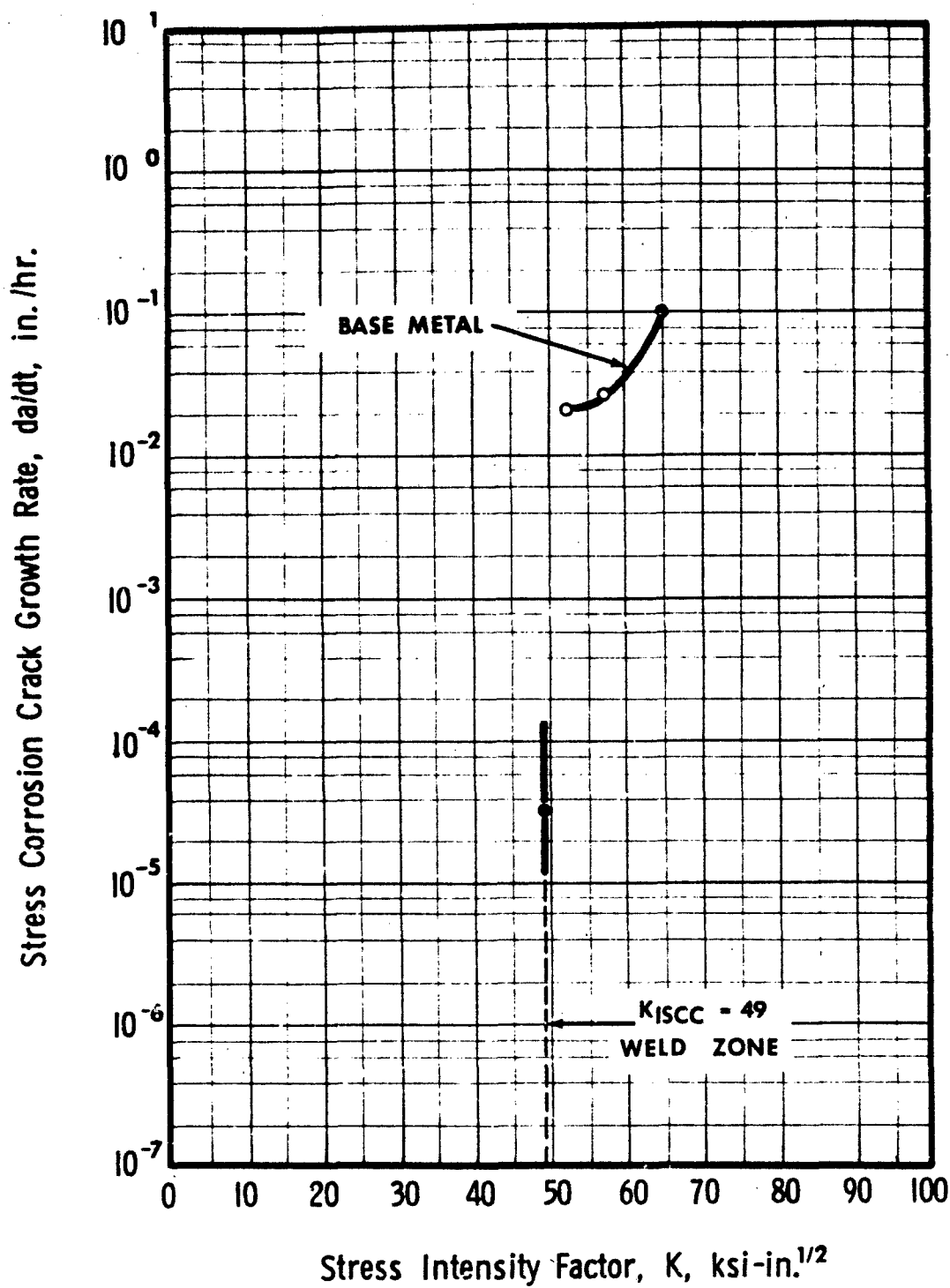


Figure 68 Environmental Crack Growth Rate Data for Ti-6Al-4V Base Metal, 1.0-in. MA Plate, T-L Direction, in JP4 at Room Temperature (CTT Specimens: $B = 1.00$ in.; $W = 2.55$ in.; $H/W = 0.486$)

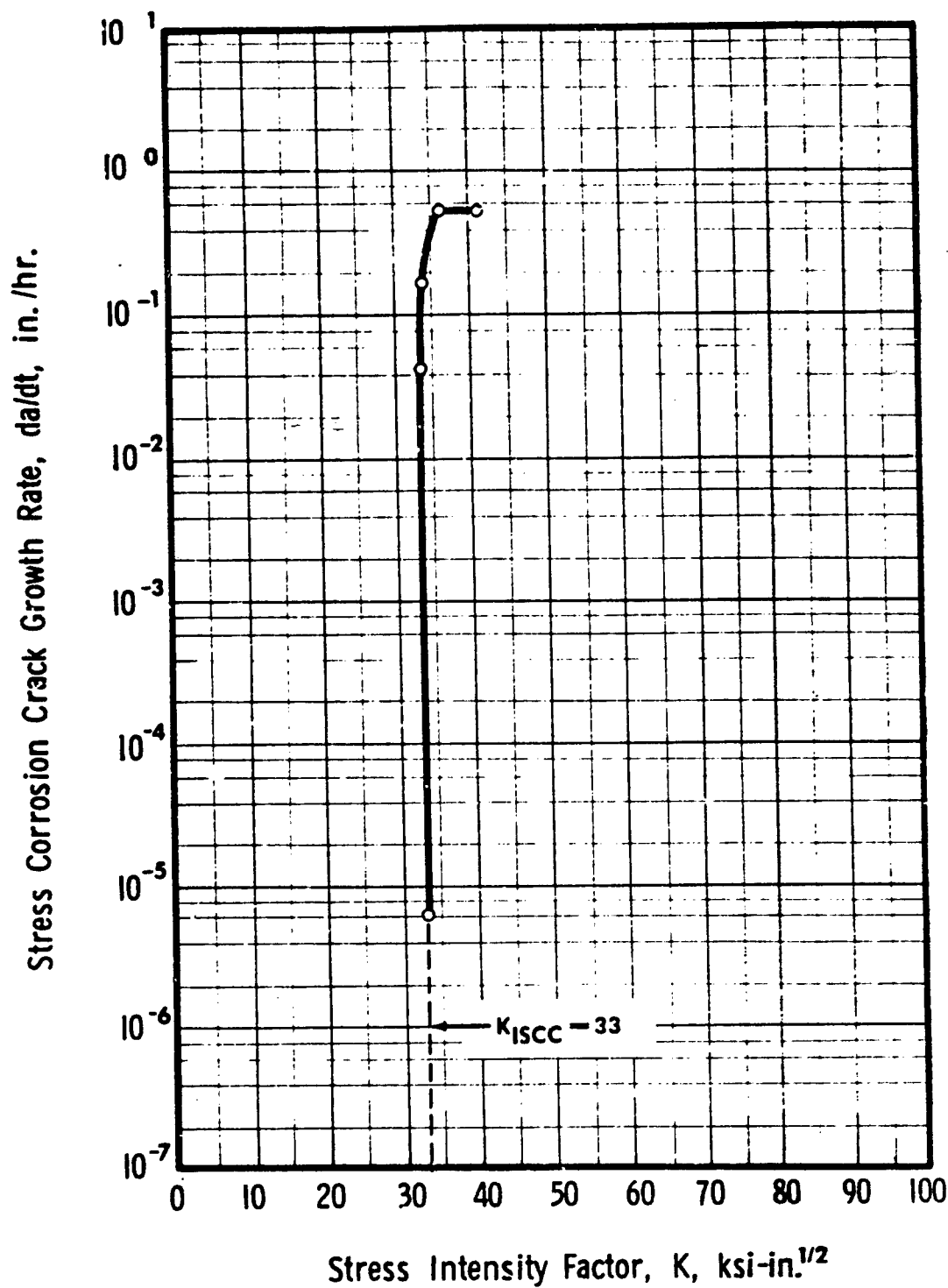


Figure 69 Environmental Crack Growth Rate Data for Ti-6Al-4V E.B. Weldment, SR, 1.0-in. Plate, HAZ, T-L Direction, in 3.5 Percent NaCl at Room Temperature (CTT Specimen; $B = 1.00$ in.; $W = 2.55$ in.; $H/W = 0.486$)

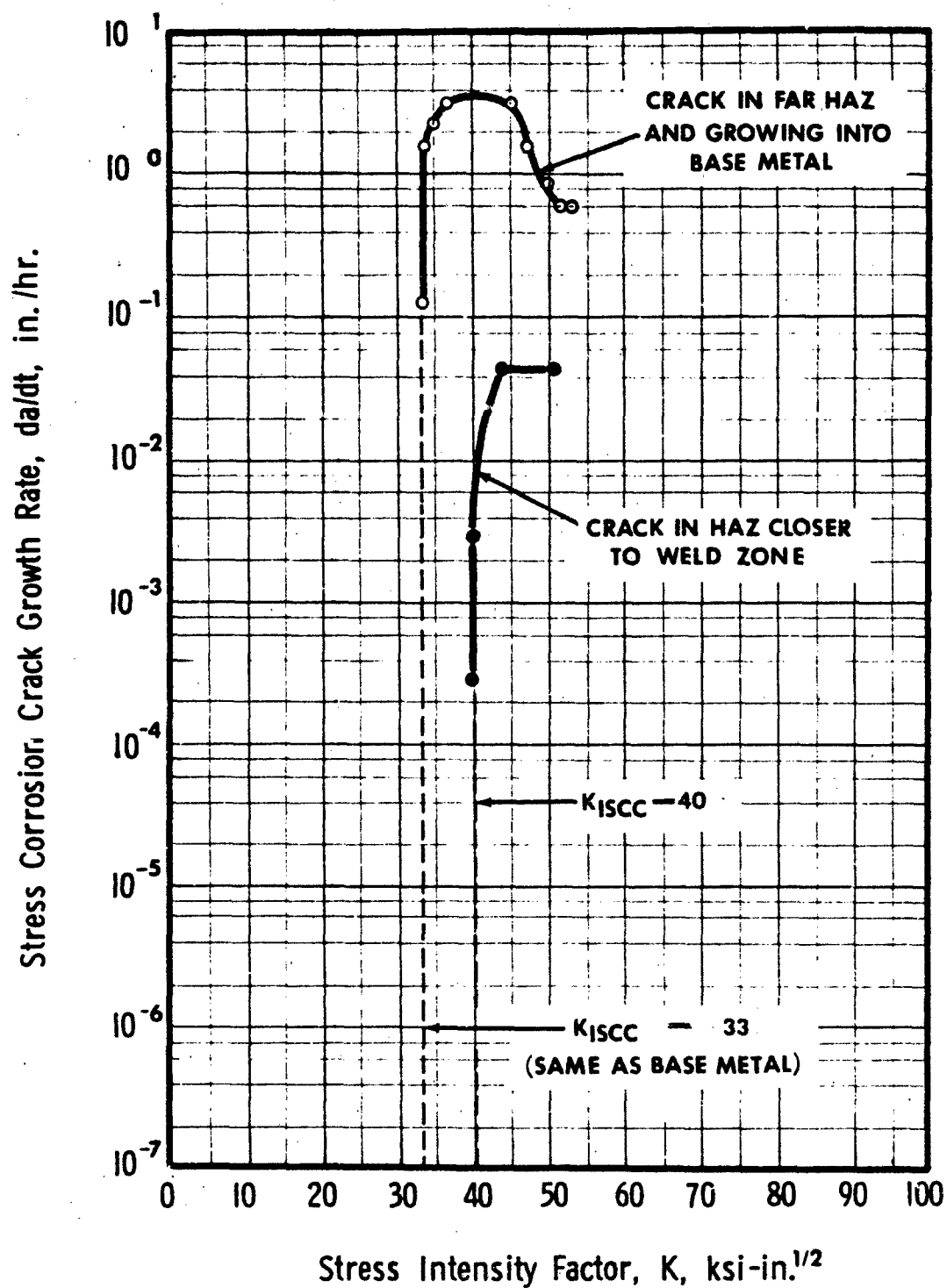


Figure 70 Environmental Crack Growth Rate Data for Ti-6Al-4V E.B. Weldment, SR, 1.0-in. Plate, HAZ, T-L Direction, in 3.5 Percent NaCl at 175°F (CTT Specimen; $B = 1.00$ in.; $W = 2.55$ in.; $H/W = 0.486$)

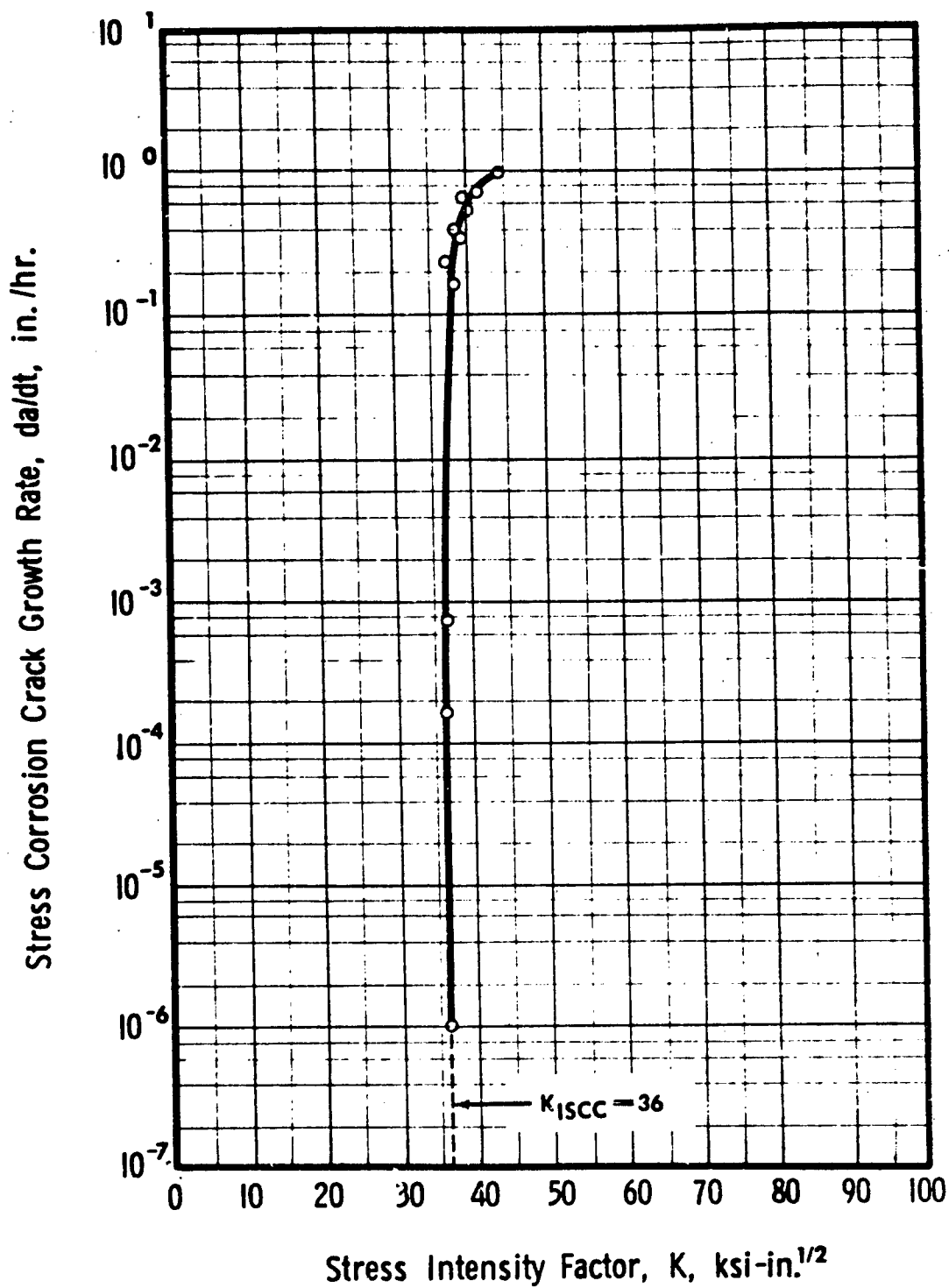


Figure 71 Environmental Crack Growth Rate Data for Ti-6Al-4V E.B. Weldment, SR, 1.0-in. Plate, WZ, T-L Plate Directions, in 3.5 Percent NaCl at Room Temperature (CTT Specimens; $B = 1.00$ in.; $W = 2.55$ in.; $H/W = 0.486$)

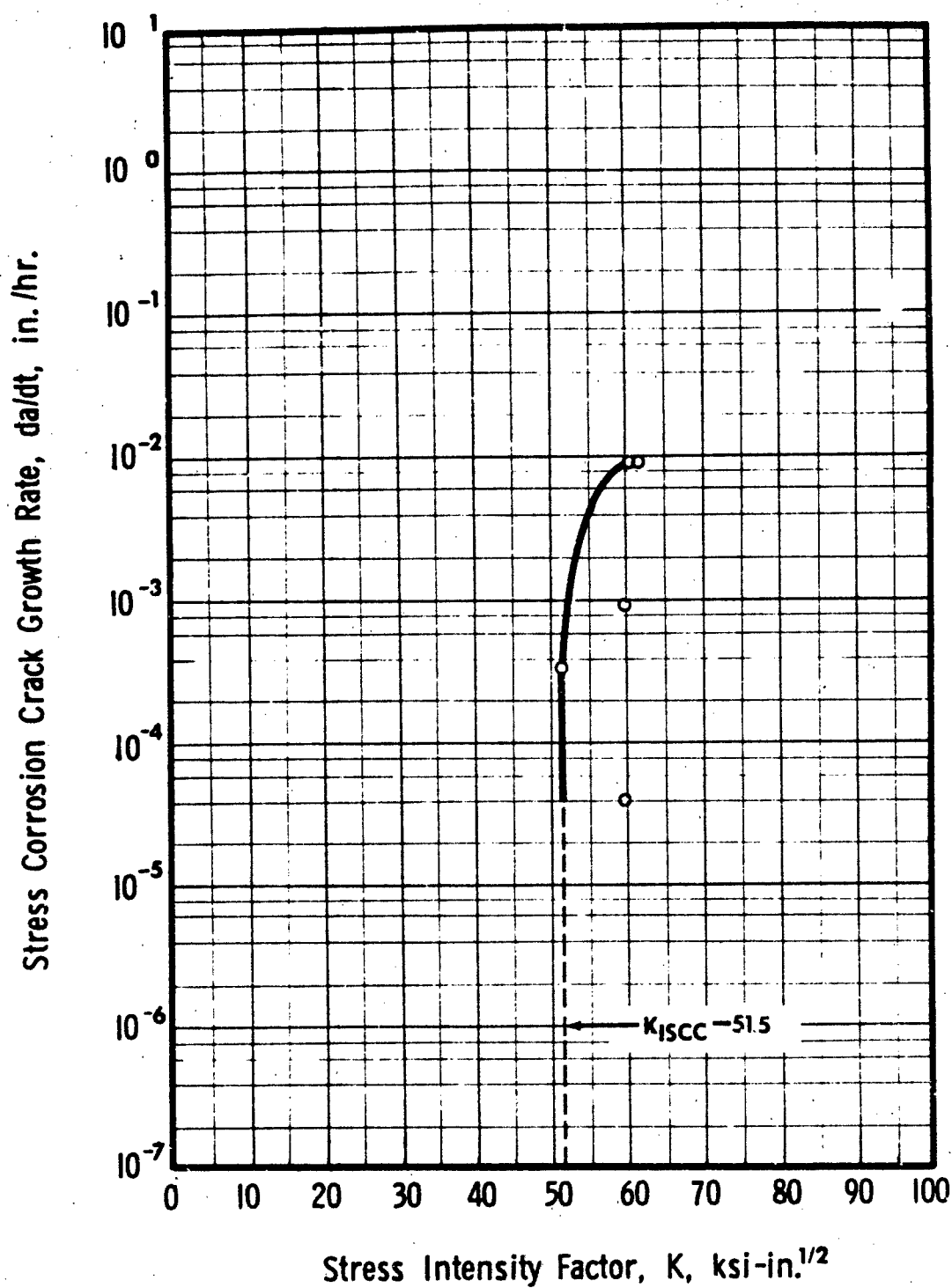


Figure 72 Environmental Crack Growth Rate Data for Ti-6Al-4V E.B. Weldment, SR, 1.0-in. Plate, WZ, T-L Plate Directions, in 3.5 Percent NaCl at 175°F (CTT Specimens: $B = 1.00$ in.; $W = 2.55$ in.; $H/W = 0.486$)

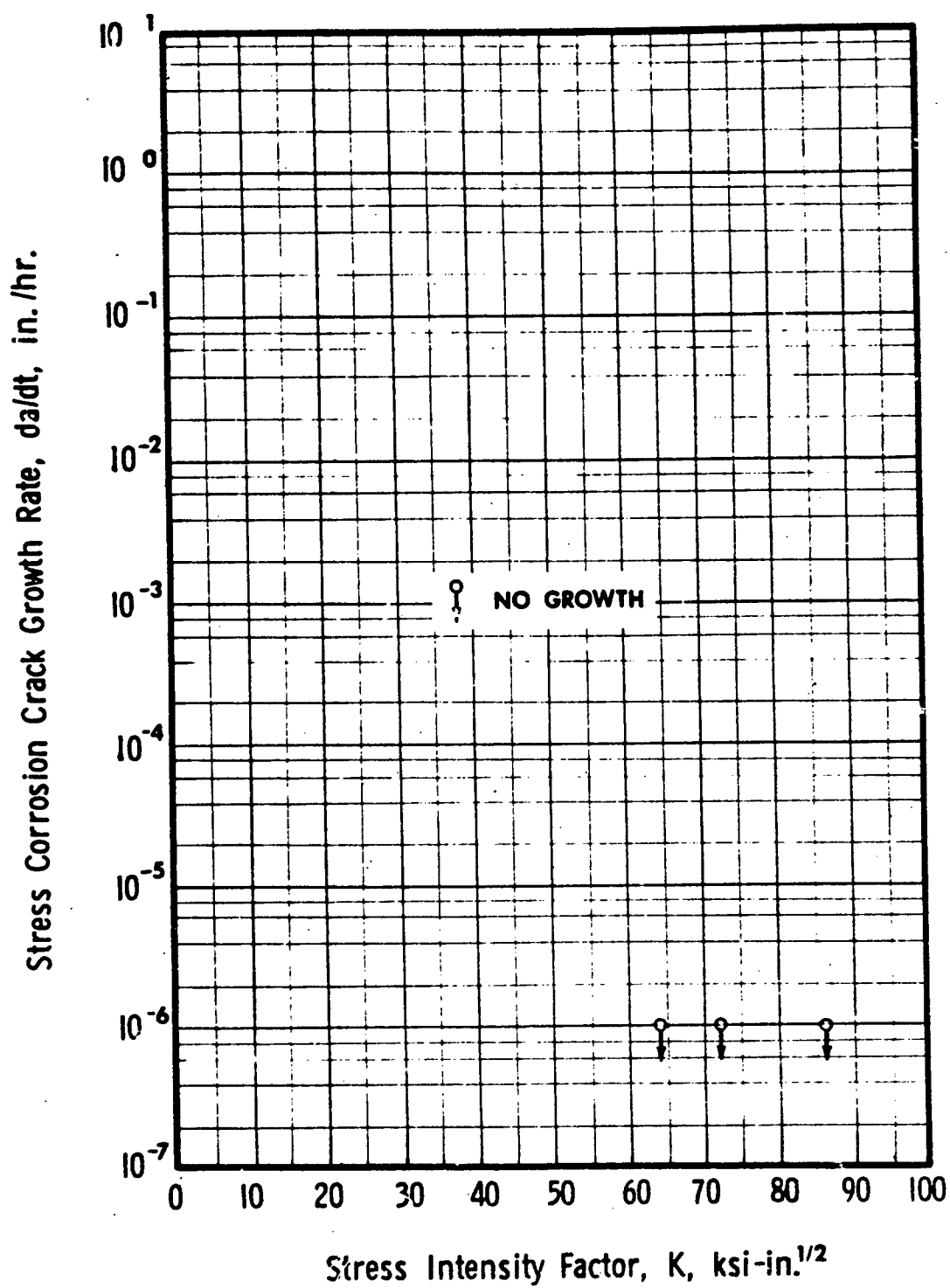


Figure 73 Environmental Crack Growth Rate Data for Beta III Titanium Base Metal, 1.0-in. STA Plate, T-L Direction, in 3.5 Percent NaCl at Room Temperature (CTT Specimen: $B = 1.00$ in.; $W = 2.55$ in. $H/W = 0.486$)

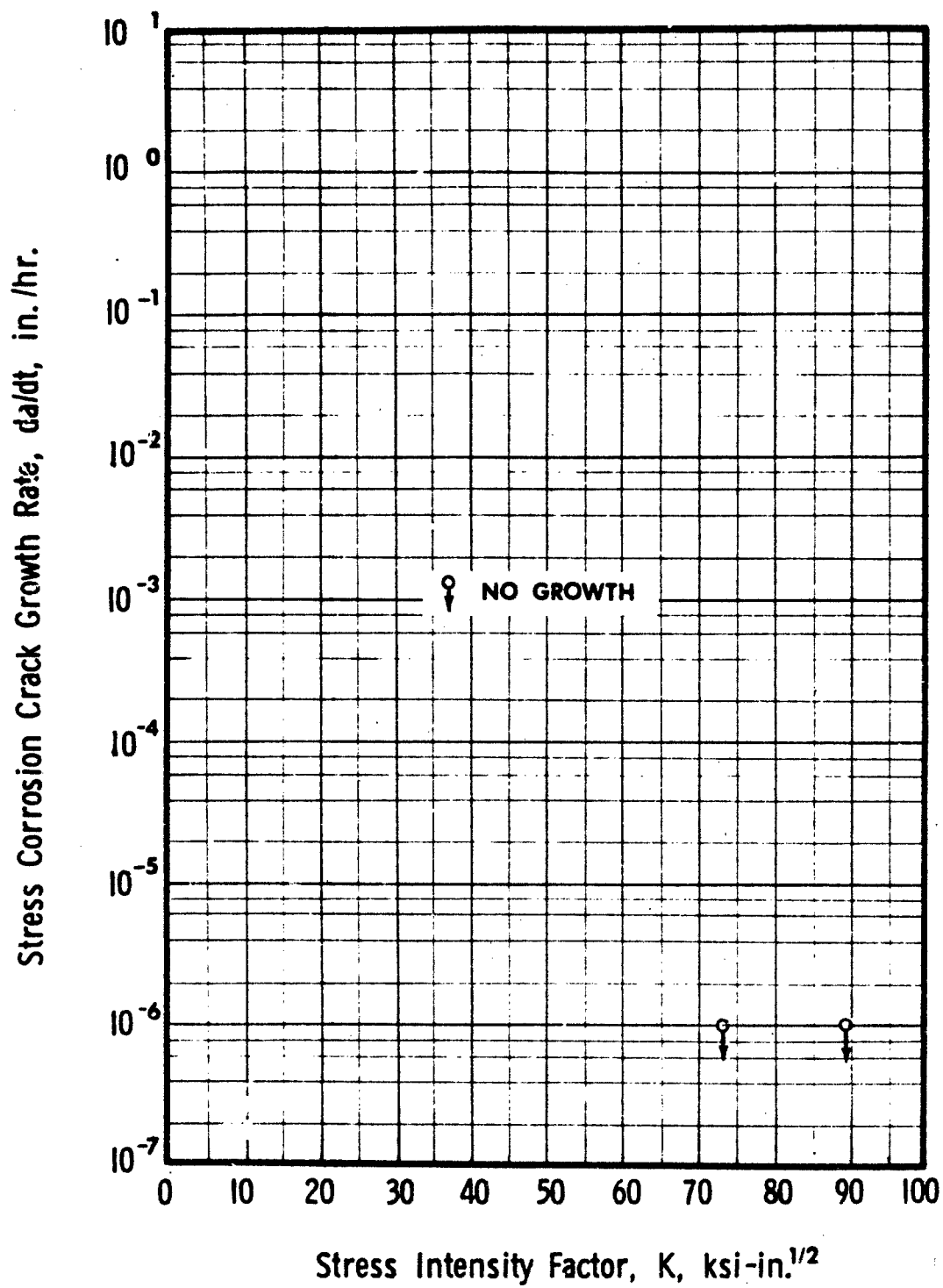


Figure 74 Environmental Crack Growth Rate Data for Beta III Titanium Base Metal, 1.0-in. STA Plate, T-L Direction, in 3.5 Percent NaCl at 175°F (CTT Specimen: B = 1.00 in.; W = 2.55 in.; H/W = 0.486)

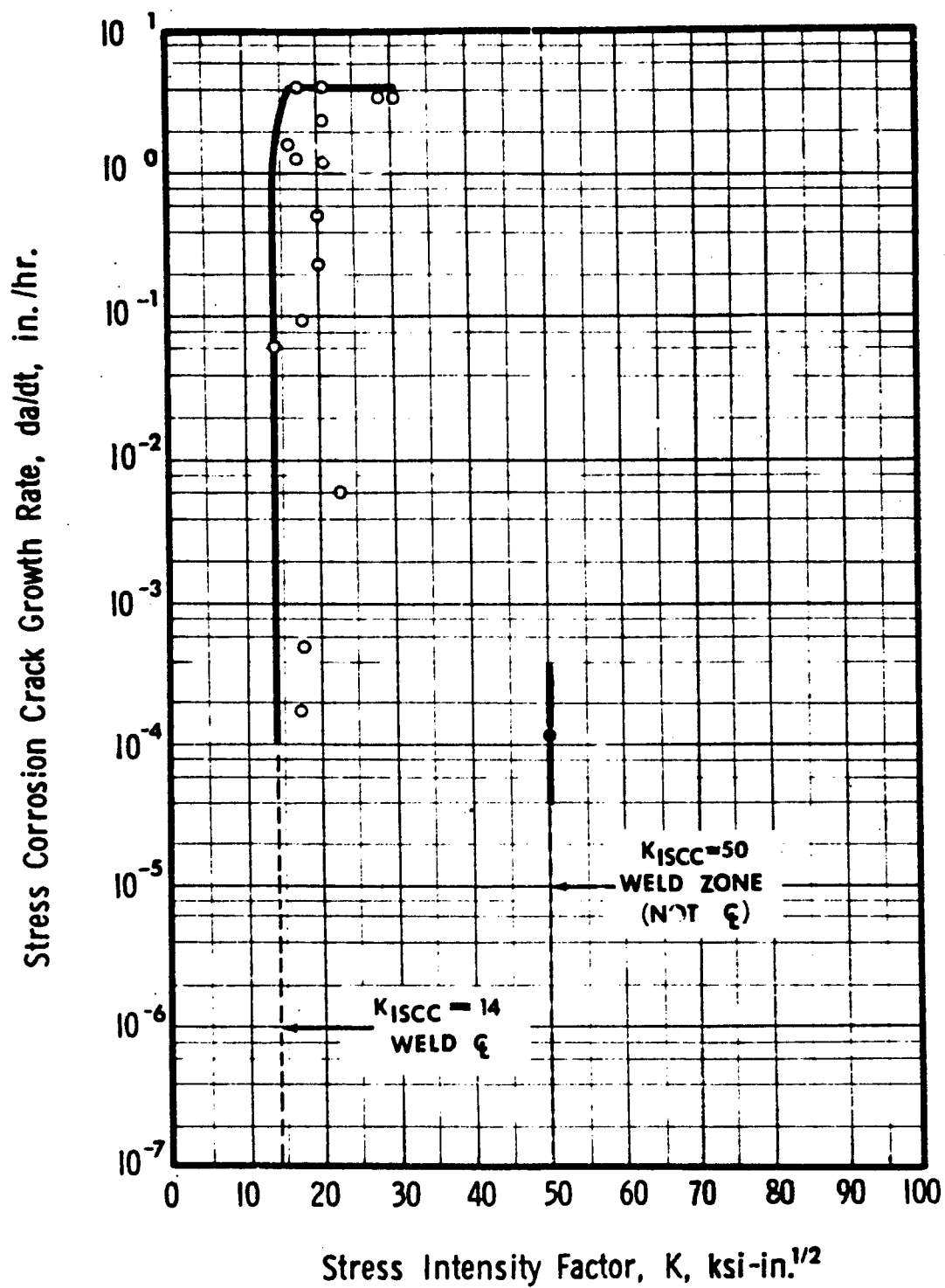


Figure 75 Environmental Crack Growth Rate Data for Beta III Titanium E.B. Weldment, STA, 1.0-in. Plate, WZ, T-L Plate Directions, in 3.5 Percent NaCl at Room Temperature (CTT Specimen; $B = 1.00$ in.; $W = 2.55$ in.; $H/W = 0.486$)



SPECIMEN: HEAT-AFFECTED ZONE, HAZ-9

PHOTO MAG. 4X

PRECRACK DEPTH: $a_o = 0.1145$

SPECIMEN THICKNESS: 0.251

PRECRACK LENGTH: $2c_o = 0.2093$

SPECIMEN WIDTH: 1.500

$a_o/2c_o = 0.547$

$a_o/t = 0.456$

FAILURE

30TH LAYER OF 21ST BLOCK

(a)



SPECIMEN: HEAT-AFFECTED ZONE, HAZ-8

PHOTO MAG. 4X

PRECRACK DEPTH: $a_o = 0.0821$

SPECIMEN THICKNESS: 0.260

PRECRACK LENGTH: $2c_o = 0.1469$

SPECIMEN WIDTH: 1.502

$a_o/2c_o = 0.56$

$a_o/t = 0.3157$

FAILURE

34TH LAYER OF 38TH BLOCK

(b)

Figure 76 Fracture Surfaces and Spectrum Fatigue Results for Ti-6Al-4V E.B. Weldment, SR, 1.0-in. Plate, Heat-Affected Zone, T-S Direction, PTT Specimens, Precracks Outlined on White: (a) Specimen HAZ-9, deep precrack, failed in the 30th layer of the 21st block; (b) Specimen HAZ-8, shallow precrack, failed in the 34th layer of the 38th block.



SPECIMEN: WELD FUSION ZONE, WZ-5

PHOTO MAG. 4X

PRECRACK DEPTH: $a_o = 0.0536$

SPECIMEN THICKNESS: 0.250

PRECRACK LENGTH: $2c_o = 0.1274$

SPECIMEN WIDTH: 1.500

$a_o/2c_o = 0.42$

$a_o/t = 0.2144$

FAILURE

34TH LAYER OF THE 48TH BLOCK

(a)



SPECIMEN: WELD FUSION ZONE, WZ-2

PHOTO MAG. 4X

PRECRACK DEPTH: $a_o = 0.0801$

SPECIMEN THICKNESS: 0.278

PRECRACK LENGTH: $2c_o = 0.1512$

SPECIMEN WIDTH: 1.503

$a_o/2c_o = 0.53$

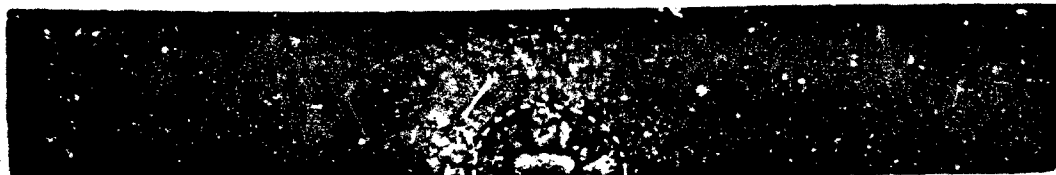
$a_o/t = 0.288$

FAILURE

34TH LAYER OF THE 49TH BLOCK

(b)

Figure 77 Fracture Surfaces and Spectrum Fatigue Results for Ti-6Al-4V E.B. Weldment, SR, 1.0 in. Plate, Weld Fusion Zone, T-S Direction, Shallow Pre-cracked PTT Specimens, Precracks Outlined in White: (a) Specimen WZ-5 failed in the 34th layer of the 48th block; (b) Specimen WZ-2 failed in the 34th layer of the 49th block.



SPECIMEN: WELD FUSION ZONE, WZ-3

PHOTO MAG. 4X

PRECRACK DEPTH: $a_0 = 0.1134$

SPECIMEN THICKNESS: 0.253

PRECRACK LENGTH: $2c_0 = 0.2309$

SPECIMEN WIDTH: 1.504

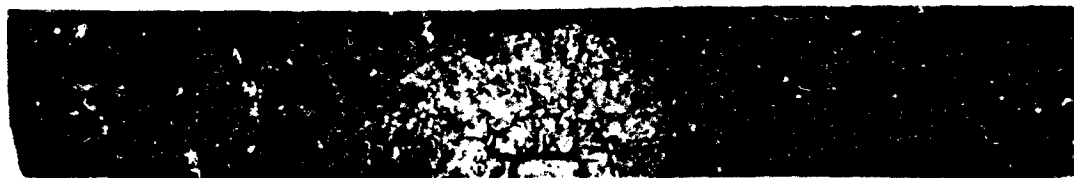
$a_0/2c_0 = 0.49$

$a_0/t = 0.448$

FAILURE

45TH LAYER OF THE 15TH BLOCK

(a)



SPECIMEN: WELD FUSION ZONE, WZ-4

PHOTO MAG. 4X

PRECRACK DEPTH: $a_0 = 0.1145$

SPECIMEN THICKNESS: 0.251

PRECRACK LENGTH: $2c_0 = 0.1866$

SPECIMEN WIDTH: 1.498

$a_0/2c_0 = 0.614$

$a_0/t = 0.456$

FAILURE

34TH LAYER OF THE 20TH BLOCK

(b)

Figure 78 Fracture Surfaces and Spectrum Fatigue Results for Ti-6Al-4V E.B. Weldments, SR, 1.0 in. Plate, Weld Fusion Zone, T-S Direction, Deep Precracked PTT Specimens, Precracks Outlined in White: (a) Specimen WZ-3 failed in the 45th layer of the 15th block; (b) Specimen WZ-4 failed in the 34th layer of the 20th block.

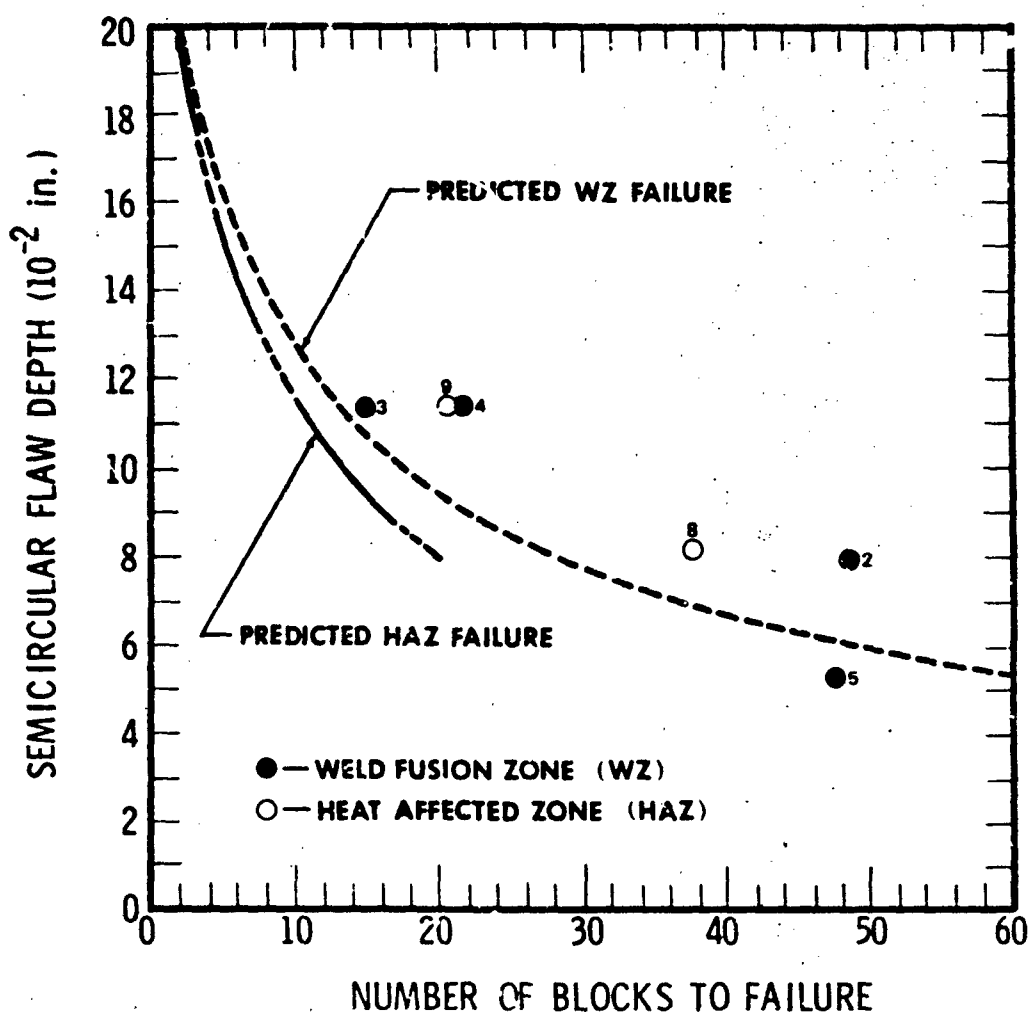


Figure 79 Spectrum Fatigue Results With Predicted Life Curves. See text for basis of prediction curves.

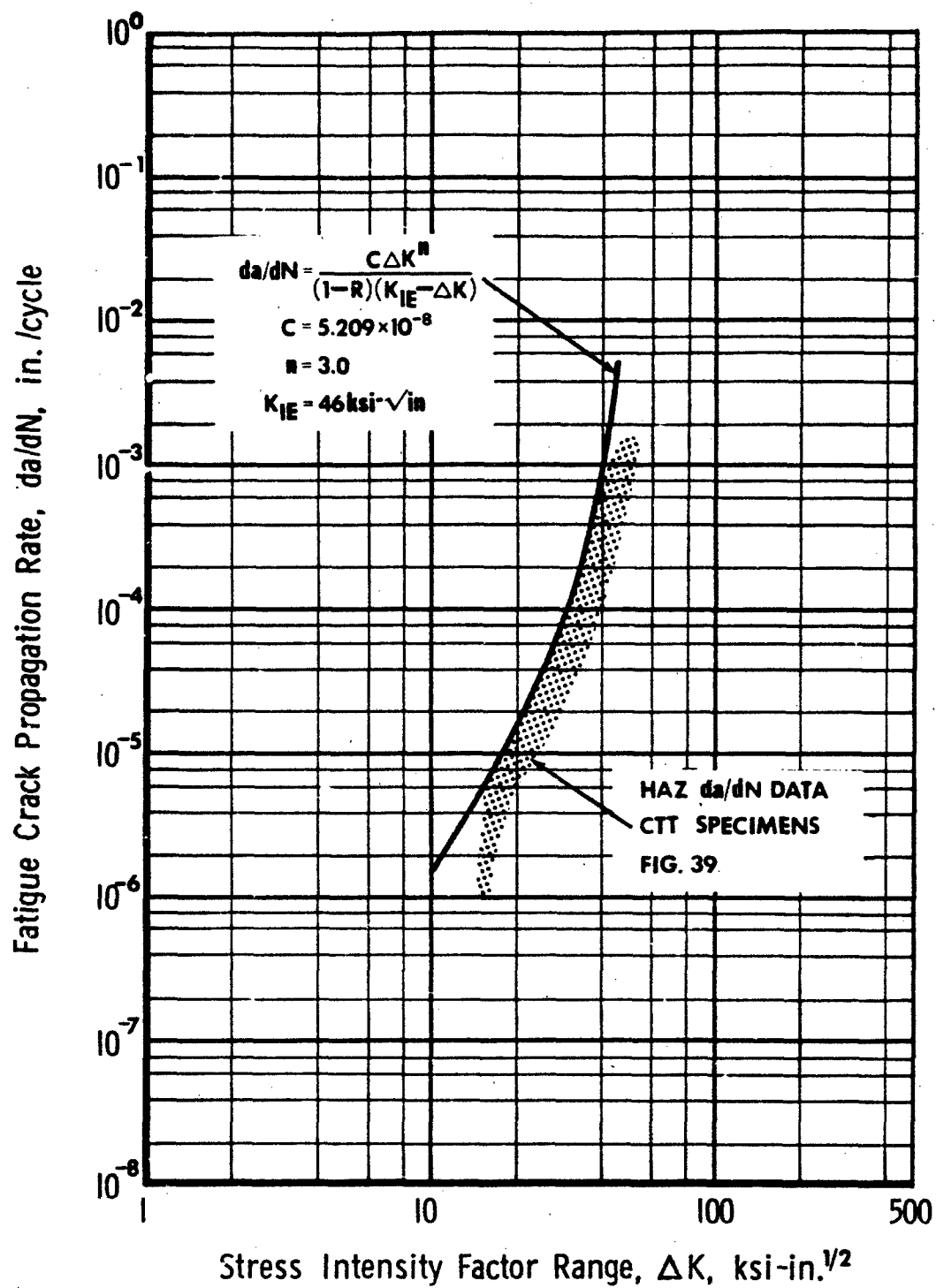


Figure 80 Crack Growth Rate Equation for Fatigue Life Prediction Model in Heat-Affected Zone

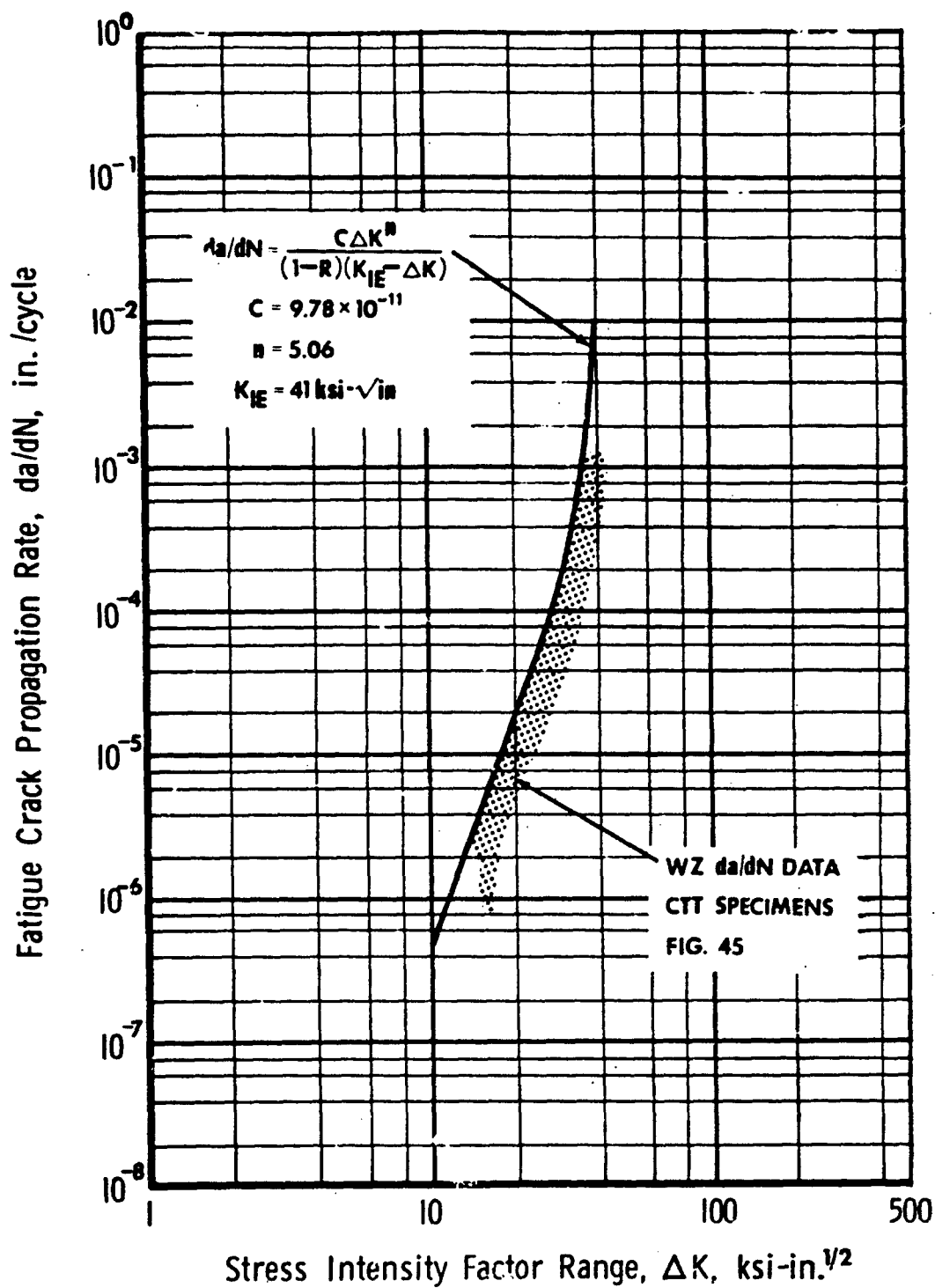


Figure 81 Crack Growth Rate Equation for Fatigue Life Prediction Model in Weld-Fusion Zone

Table I
VENDOR CERTIFICATION DATA OF TEST MATERIALS

Ti-6Al-4V
Mill Annealed

(G.O. Carlson, Inc., Thorndale, Pa.)

Heat No.	Composition (wt.%)							Mechanical Properties		
	C	N	Fe	O ₂	H ₂	Al	V	Ultimate Strength (ksi)	Yield Strength (ksi)	Elongation (%)
A41642-1	0.023	0.016	0.13	0.15	0.0008	6.48	4.29	T 150.0	T 130.0	T 11.0
								L 143.7	L 128.8	L 13.0
HC-442-1B	0.017	0.012	0.20	0.14	0.0018	6.34	4.13	T 138.9	T 125.4	T 16.0
								L 133.3	L 121.6	L 16.0

Beta III Titanium Alloy
Solution-Treated

**(Colt Industries, Crucible, Inc.,
Stainless Steel Division
Midland, Pa.)**

Heat No.	Composition (wt.%)								Mechanical Properties		
	C	N ₂	Fe	Sn	Zr	Mo	O ₂	H ₂	Ultimate Strength (ksi)	Yield Strength (ksi)	Elongation (%)
K-50776	0.02	0.014	0.03	4.7	5.8	10.2	0.13	0.0074	T 133.9	109.7	14.2
									L 131.8	110.9	11.5

Table II
SCHEDULE FOR ELECTRON BEAM WELDING OF Ti-6Al-4V AND
BETA III ALLOY 1-IN. PLATE

Material:	Ti-6Al-4V, Beta III
Thickness:	1.00 in.
Voltage:	36.5 kV
Beam Current:	375 mA
Travel Speed:	44 ipm
Focus-Current:	4.6 A
Dial:	700
Gun to Work Distance:	7 in.
Gun Slope (angle):	normal
Vacuum:	10^{-4} to 10^{-5} mm
Wash Pass:	
Voltage:	25.0 kV
Beam Current:	200 mA
Travel Speed:	44 ipm
Focus-Current:	3.0 A
Dial:	630
Gun to Work Distance:	7 in.
Gun Slope (angle):	normal
Vacuum:	10^{-4} to 10^{-5} mm
Unit:	Sciaky 60kV - 30 kW w/triode gun design

Table III
SCHEDULE FOR ELECTRON BEAM WELDING OF Ti-6Al-4V 2-IN. PLATE

Material:	Ti-6Al-4V
Thickness:	2.00 in.
Voltage:	45.0 kV
Beam Current:	450 mA
Travel Speed:	26 ipm
Focus-Current:	5.7 A
Microdial:	675
Gun to Work Distance:	7 in.
Gun Slope (angle):	10° (drag)
Vacuum:	10^{-4} to 10^{-5} mm
Wash Pass:	none
Unit:	Sciaky 60kV - 30 kW w/triode gun design

Table IV
AGING RESPONSE OF 1-IN.-THICK BETA III TITANIUM PLATE

Condition	Tensile Strength (ksi)	Yield Strength 0.2% Offset (ksi)	Elongation in 2 Inches (%)
As received	151.0	143.6	11
950°F (8 hr)	171.2	164.0	8
1000°F (8 hr)	162.5	157.4	14
1045°F (8 hr)	162.5	157.5	9.5
1100°F (8 hr)	155.6	152.5	13

The long direction of tensile specimens was transverse to the rolling direction of the plate.

TABLE V
SCHEDULE OF SPECIMENS TESTED

Type of Test	Plate		Specimen	Location	Environment	Temperature (°F)					
	Thick. (in.)	Orient.				Sub		RT		175	
						G-1	B-III	G-1	B-III	G-1	B-III
Tensile	1	T	ASTM	WZ	Lab Air	4		4		4	
	2	T	ASTM	WZ	Lab Air			4			
	1	L	ASTM	BM	Lab Air	4		4		4	
	1	T	ASTM	BM	Lab Air	4	2	4	4	4	2
	2	L	ASTM	BM	Lab Air			4			
	2	T	ASTM	BM	Lab Air			4			
K _{IC}	2	L	1-1/2-in CTT	HAZ	Lab Air			4			
	2	T	1-1/2-in CTT	HAZ	Lab Air	3		4		3	
	2	ST	1-1/2-in CTT	HAZ	Lab Air			4			
	2	T	1-1/2-in CTT	WZ	Lab Air	3		3		4	
	1	T	1-1/2-in CTT	WZ	Lab Air			3	1		
	1	T	1-5/8-in PTT	HAZ	Lab Air			3			
	1	T	1-5/8-in PTT	WZ	Lab Air			3			
	1	T	1-5/8-in PTT	BM	Lab Air			3			
	1	L	1-1/2-in CTT	BM	Lab Air			3			
	2	T	1-1/2-in CTT	BM	Lab Air	3		4		3	
	2	ST	1-1/2-in CTT	BM	Lab Air			4			
	1	T	1-1/2-in CTT	HAZ	Lab Air				1		
	1	T	1-1/2-in CTT	BM	Lab Air				1		
K _{IC}	1	T	1-5/8-in SEN	WZ	Lab Air	3	1	3	1		
	1	T	1-5/8-in SEN	WZ	Lab Air	3	1	3	1		
	1	T	1-1/2-in SEN	WZ	Lab Air	3	1	4	1		
K _{ISCC} and da/dN	1	T	1-1/2-in CTT	WZ	1.5%NaCl			2	1	2	1
	1	T	1-1/2-in CTT	WZ	JP-1			1		1	
	1	T	1-1/2-in CTT	HAZ	1.5%NaCl			2	1	2	1
	1	T	1-1/2-in CTT	HAZ	JP-1			1			
	1	T	1-1/2-in CTT	BM	1.5%NaCl			2	1	2	1
	1	T	1-1/2-in CTT	BM	JP-1			1			
da/dN	1	T	1-1/2-in CTT	WZ	Lab Air	2	1	4	1	2	1
	1	T	1-1/2-in CTT	WZ	H ₂ O			2		1	
	1	T	1-1/2-in CTT	WZ	1.5%NaCl			2	1	1	
	1	T	1-1/2-in CTT	WZ	JP-1			2			
	1	T	1-1/2-in CTT	HAZ	Lab Air	2	1	4	1	2	1
	1	T	1-1/2-in CTT	HAZ	H ₂ O			2		1	
	1	T	1-1/2-in CTT	HAZ	1.5%NaCl			2	1	1	
	1	T	1-1/2-in CTT	HAZ	JP-1			2			
	1	T	1-1/2-in CTT	BM	Lab Air	1	1	2	1	2	1
	1	T	1-1/2-in CTT	BM	1.5%NaCl			2	1	1	
	1	T	0.75-in PTT	WZ	Lab Air			4			
	1	T	0.75-in PTT	WZ	1.5%NaCl			2			
	1	T	0.75-in PTT	HAZ	Lab Air			4			
	1	T	0.75-in PTT	HAZ	1.5%NaCl			2			
1	T	0.75-in PTT	BM	Lab Air			4				
1	T	0.75-in PTT	BM	1.5%NaCl			2				
Axial Fatigue	1	T	Reduced Section Round	WZ	Lab Air			11			
	1	T	Reduced Section Round	BM	Lab Air			9			
Spectrum Fatigue	1	T	0.75-in PTT	WZ	Lab Air			4			
	1	T	0.75-in PTT	HAZ	Lab Air			2			
Natural Defect	1	T	Reduced Section Tensile	WZ	Lab Air			4			

CTT - Compact Tension Type
PTT - Part-Through Thickness
SEN - Single-Edge Notch

WZ - Weld Fusion Zone
HAZ - Heat-Affected Zone
BM - Base Metal

G-1 - T1-621-W
B-III - Beta III

TABLE VI

TENSILE PROPERTIES OF Ti-6Al-4V TWO-INCH PLATE (MA) BASE METAL AT R. T.

SPECIMEN IDENT.	ORIENT.	0.2% YIELD STRENGTH (KSI)	ULTIMATE STRENGTH (KSI)	ELONGATION (%)	R OF A (%)	MODULUS OF ELASTICITY (KSI)
2-BM-L-21	L	127.3	136.3	13.1	16.2	17.2
-22	L	125.8	133.4	12.4	17.5	16.9
-24	L	128.0	135.4	11.5	12.5	17.3
Average Values		126.9	135.0	12.3	15.4	17.1
2-BM-T-41	T	125.4	136.5	9.0	8.1	17.1
-43	T	124.7	135.8	7.5	8.2	16.7
-44	T	126.6	135.9	10.3	12.7	17.1
Average Values		125.6	136.1	8.9	9.7	17.0

TABLE VII
TENSILE PROPERTIES OF Ti-6Al-4V TWO-INCH PLATE (MA) E. B. WELDMENTS AT R.T.

SPECIMEN IDENT.	ORIENT.	0.2% YIELD STRENGTH (KSI)	ULTIMATE STRENGTH (KSI)	ELONGATION (%)	R OF A (%)	MODULUS OF ELASTICITY (KSI)
2-W-T-55	T	125.1	133.7	10.7	18.4	17.5 (1)
		125.1		5.0		16.3 (2)
2-W-T-11	T	-	130.3	10.8	20.6	16.9 (1)*
		120.7		4.6		15.7 (2)
2-W-T-22	T	127.6	134.2	8.5	17.4	16.3 (1)
		124.0		4.6		16.4 (2)
2-W-T-44	T	126.3	134.0	8.7	16.3	18.0 (1)
		126.3		4.0		15.8 (2)
Average Values		126.3	133.1	9.5	18.2	17.2
		124.0		4.6		16.2

* Strain gage malfunction - no yield load determination.

(1) Yield and modulus determinations from strain data from a 1/8-inch SR-4 gage in weld fusion zone. Percent elongation in 2 inches.

(2) Yield and modulus determinations from strain data from a 1/2-inch, B-1 extensometer placed symmetrically across weld fusion zone. Percent elongation in 1/2-inch across weld fusion zone.

(3) All failures were in base metal except where noted otherwise.

TABLE VIII

TENSILE PROPERTIES OF Ti-6Al-4V ONE-INCH PLATE (MA) BASE METAL AT R. T.

SPECIMEN IDENT.	ORIENT.	0.2% YIELD STRENGTH (KSI)	ULTIMATE STRENGTH (KSI)	ELONGATION (%)	R OF A (%)	MODULUS OF ELASTICITY (KSI)
1-BM-L-2	L	132.4	140.1	13.9	15.4	17.7
-X1	L	131.8	139.9	15.1	14.9	16.8
- 4	L	132.7	140.1	14.5	23.0	18.1
Average Values		132.3	140.0	14.5	17.8	17.5
1-BM-T-0	T	140.9	147.9	13.3	21.3	19.0
-1	T	140.5	148.8	15.0	23.9	19.7
-5	T	141.5	148.7	12.6	21.4	19.5
Average Values		141.0	148.5	13.6	22.2	19.4

TABLE IX

TENSILE PROPERTIES OF Ti-6Al-4V ONE-INCH PLATE (MA) BASE METAL AT -65° F

SPECIMEN IDENT.	ORI.	0.2% YIELD STRENGTH (KSI)	ULTIMATE STRENGTH (KSI)	ELONGATION (%)	R OF A (%)	MODULUS OF ELASTICITY (KSI)
1-BM-L-1	L	149.9	154.5	13.3	21.3	16.5
-X4	L	147.1	153.2	11.0	20.4	16.5
-12	L	155.9	160.2	12.7	22.9	17.0
-11	L	155.8	160.1	13.8	24.4	17.1
Average Values		152.2	157.0	12.7	22.3	16.8
1-BM-T-2	T	158.2	164.7	10.9	13.4	19.0
-6	T	156.2	163.2	11.5	14.1	19.1
-8	T	157.8	164.4	11.0	18.2	19.0
Average Values		157.4	164.1	11.1	15.2	19.2

TABLE X

TENSILE PROPERTIES OF Ti-6Al-4V ONE-INCH PLATE (MA) BASE METAL AT 175° F

SPECIMEN IDENT.	ORIENT.	0.2% YIELD STRENGTH (KSI)	ULTIMATE STRENGTH (KSI)	ELONGATION (%)	R OF A (%)	MODULUS OF ELASTICITY (KSI)
1-BM-L-X2	L	114.5	125.2	17.8	26.4	16.1
1-BM-L-3	L	116.6	126.8	16.9	27.7	15.9
1-BM-L-X3	L	112.7	124.9	19.1	25.6	15.9
1-BM-L-21	L	113.0	125.3	16.6	28.1	15.7
Average Values		114.2	125.6	17.6	27.0	15.9
1-BM-T-4	T	125.1	137.4	17.0	29.0	18.4
1-BM-T-6	T	124.3	137.0	15.8	23.4	19.0
1-BM-T-7	T	124.3	136.5	15.5	23.5	18.1
Average Values		124.6	137.0	16.1	25.3	18.5

TABLE XI

TENSILE PROPERTIES OF Ti-6Al-4V ONE-INCH PLATE E. B. WELDMENTS AT R. T.

SPECIMEN IDENT.	ORIENT.	0.2% YIELD STRENGTH (KSI)	(3) ULTIMATE STRENGTH (KSI)	ELONGATION (%)	R OF A (%)	MODULUS OF ELASTICITY (KSI)
1-W-T-9	T	138.3	148.4	12.9 7.2	18.0	18.4 (1)* 16.7 (2)
1-W-T-10	T	139.5	147.9	13.8 7.4	20.8	17.4 (1)* 15.7 (2)
1-W-T-8	T	138.5	146.9	6.7 8.6	6.1	17.3 (1)* 17.2 (2)**
1-W-T-11	T	137.1	148.3	16.1 10.6	22.5	17.1 (1)* 17.7 (2)
Average Values		138.4	147.9	14.3 8.5	20.4	17.6 16.8

* Strain gage malfunction - no yield load determination.

** Specimen failed in weld zone. Elongation value not included in averages.

(1) Yield and modulus determinations from strain data from a 1/8-inch SR-4 gage in weld fusion zone. Percent elongation in 2 inches.

(2) Yield and modulus determinations from strain data from a 1/2-inch, B-1 extensometer placed symmetrically across weld fusion zone. Percent elongation in 1/2-inch across weld fusion zone.

(3) All failures were in base metal except where noted otherwise.

TABLE XII

TENSILE PROPERTIES OF Ti-6Al-4V ONE-INCH PLATE E. B. WELDMENTS AT -65° F

SPECIMEN IDENT.	ORIENT.	0.2% YIELD STRENGTH (KSI)	(3) ULTIMATE STRENGTH (KSI)	ELONGATION (%)	(3) R OF A (%)	MODULUS OF ELASTICITY (KSI)
1-W-T-5	T	151.0 157.4	166.0	11.0 6.4	16.8	17.8 (1) 16.5 (2)
1-W-T-6	T	152.5 156.3	166.2	9.3 6.0	14.4	17.5 (1) 17.8 (2)
1-W-T-7	T	-	131.7	1.8	2.1	17.7 (1)*
Average Values		151.8 156.9	166.1	10.2 6.2	15.6	17.7 (1) 17.2 (2)

* Strain gage malfunction and extensometer slipped - no yield load determination.

(1) Yield and modulus determinations from strain data from a 1/8-inch SR-4 gage in weld fusion zone.

Percent elongation in 2 inches.

(2) Yield and modulus determinations from strain data from a 1/2-inch, B-1 extensometer placed symmetrically across weld fusion zone. Percent elongation in 1/2-inch across weld fusion zone.

(3) All failures were in base metal except where noted otherwise.

TABLE XIII

TENSILE PROPERTIES OF Ti-6Al-4V ONE-INCH PLATE E.B. WELDMENTS AT 175° F

SPECIMEN IDENT.	ORIENT.	0.2% YIELD STRENGTH (KSI)	(3) ULTIMATE STRENGTH (KSI)	ELONGATION (%)	R OF A (%)	MODULUS OF ELASTICITY (KSI)
1-W-T-4	T	119.5 125.8	136.8	13.4 6.0	23.7	16.1 (1) 16.0 (2)
1-W-T-2	T	123.0 120.4	136.4	13.4 6.1	26.4	16.7 (1) 16.1 (2)
1-W-T-3	T	118.4 122.0	136.7	14.9 11.0	24.1	16.7 (1) 16.9 (2)
Average Values		120.3 122.7	136.6	13.9 7.7	24.7	16.5 16.3

(1) Yield and modulus determinations from strain data from a 1/8-inch SR-4 gage in weld fusion zone. Percent elongation in 2 inches.

(2) Yield and modulus determinations from strain data from a 1/2-inch, B-1 extensometer placed symmetrically across weld fusion zone. Percent elongation in 1/2-inch across weld fusion zone.

(3) All failures were in base metal except where noted otherwise.

TABLE XIV

TENSILE PROPERTIES OF BETA III TITANIUM ONE-INCH PLATE (STA) ^{*} BASE METAL AT R. T.

SPECIMEN IDENT.	ORIENT.	0.2% YIELD STRENGTH (KSI)	ULTIMATE STRENGTH (KSI)	ELONGATION (%)	R OF A (%)	MODULUS OF ELASTICITY (KSI)
B-BM-T-5	T	166.6	171.6	9.6	13.3	15.3
B-BM-T-9	T	164.1	169.1	9.5	17.3	15.7
B-BM-T-31	T	166.7	172.9	10.1	15.1	15.1
B-BM-T-33	T	167.3	173.0	9.2	13.0	15.2
Average Values		166.2	171.7	9.6	14.7	15.3
B-BM-L-1	L	150.3	157.0	12.0	21.3	14.9
B-BM-L-3	L	150.7	157.2	11.7	20.7	14.6
B-BM-L-4	L	146.9	153.0	12.2	22.6	14.6
Average Values		149.5	155.7	12.0	21.5	14.7

^{*} Solution treated and aged at 1045° F for 8 hours.

TABLE XV
TENSILE PROPERTIES OF BETA III TITANIUM ONE-INCH PLATE (STA) * BASE METAL AT -65° F

SPECIMEN IDENT.	ORIENT.	0.2% YIELD STRENGTH (KSI)	ULTIMATE STRENGTH (KSI)	ELONGATION (%)	R OF A (%)	MODULUS OF ELASTICITY (KSI)
B-BM-T-1	T	190.0	197.1	7.2	13.2	15.7
B-BM-T-8	T	189.3	196.9	8.3	14.1	15.1
B-BM-T-10	T	187.2	193.3	7.8	13.7	15.3
Average Values		188.8	195.8	7.8	13.7	15.4

* Solution treated and aged at 1045°F for 8 hours.

TABLE XVI

TENSILE PROPERTIES OF BETA III TITANIUM ONE-INCH PLATE (STA) BASE METAL AT 175° F

SPECIMEN IDENT.	ORIENT.	0.2% YIELD STRENGTH (KSI)	ULTIMATE STRENGTH (KSI)	ELONGATION (%)	R OF A (%)	MODULUS OF ELASTICITY (KSI)
B-BM-T-2	T	149.9	158.5	10.5	17.3	15.0
B-BM-T-6	T	149.9	158.0	10.2	17.7	14.8
B-BM-T-7	T	149.8	158.9	10.7	19.1	15.5
Average Values		149.9	158.5	10.5	18.0	15.1

* Solution treated and aged at 1045°F for 8 hours.

TABLE XVII
TENSILE PROPERTIES OF BETA III TITANIUM ONE-INCH PLATE (STA) E. B. WELDMENTS AT R. T. *

SPECIMEN IDENT.	ORIENT.	0.2% YIELD STRENGTH (KSI)	(3) ULTIMATE STRENGTH (KSI)	ELONGATION (%)	R OF A (%)	MODULUS OF ELASTICITY (KSI)
B-W-T-3	T	162.2 159.7	163.7	7.9 4.6	16.9	14.7 (1) 15.4 (2)
B-W-T-4	T	164.3 162.2	165.3	8.3 4.8	19.4	14.9 (1) 15.4 (2)
B-W-T-5	T	162.7 162.7	164.2	8.8 4.0	22.4	14.7 (1) 16.5 (2)
B-W-T-7	T	- -	170.7	8.4 3.2	19.9	14.1 (1)** 15.3 (2)
Average Values		163.1 161.5	166.0	8.4 4.2	19.7	14.6 15.7

* Solution treated and aged at 1045°F for 8 hours.

** Strain gage malfunction and extensometer slipped - no yield load determination.

(1) Yield and modulus determinations from strain data from a 1/8-inch SR-4 gage in weld fusion zone.

Percent elongation in 2 inches.

(2) Yield and modulus determinations from strain data from a 1/2-inch, B-1 extensometer placed symmetrically across weld fusion zone. Percent elongation in 1/2-inch across weld fusion zone.

(3) All failures were in base metal except where noted otherwise.

TABLE XVIII

TENSILE PROPERTIES OF BETA III TITANIUM ONE-INCH PLATE(STATE)*E. B. WELDMENTS AT -65°F

SPECIMEN IDENT.	ORIENT.	0.2% YIELD STRENGTH (KSI)	(3) ULTIMATE STRENGTH (KSI)	ELONGATION (%)	R OF A (%)	MODULUS OF ELASTICITY (KSI)
B-W-1	T	183.5 184.3	187.1	7.5 4.0	18.0	15.1 (1) 15.3 (2)
B-W-2	T	- 183.2	187.7	7.1 3.0	17.1	- (1)** 15.3 (2)
B-W-8	T	179.2 179.2	181.8	7.0 3.2	17.6	14.8 (1) 15.0 (2)
Average Values		181.4 182.2	185.5	7.2 3.4	17.6	15.0 15.2

* Solution treated and aged at 1045°F for 8 hours.

** Strain gage malfunction - no yield load determination.

(1) Yield and modulus determinations from strain data from a 1/8-inch SR-4 gage in weld fusion zone. Percent elongation in 2 inches.

(2) Yield and modulus determinations from strain data from a 1/2-inch, B-1 extensometer placed symmetrically across weld fusion zone. Percent elongation in 1/2-inch across weld fusion zone.

(3) All failures were in base metal except where noted otherwise.

TABLE XIX
TENSILE PROPERTIES OF BETA III TITANIUM ONE-INCH PLATE (STA)* E. B. WELDMENTS AT 175°F

SPECIMEN IDENT.	ORIENT.	0.2% YIELD STRENGTH (KSI)	(3) ULTIMATE STRENGTH (KSI)	ELONGATION (%)	(3) R OF A (%)	MODULUS OF ELASTICITY (KSI)
B-W-T-10	T	150.5	155.8	10.2 5.0	26.6	15.4 (1) 14.6 (2)**
B-W-T-6	T	152.1 150.6	156.2	9.8 6.0	27.0	14.3 (1) 14.4 (2)
B-W-T-9	T	147.6 147.6	154.2	10.0 4.4	27.0	14.8 (1) 15.1 (2)
Average Values		150.0 149.1	155.4	10.0 5.1	26.9	14.8 14.7

* Solution treated and aged at 1045°F for 8 hours.

** Extensometer slipped - yield load not determined.

(1) Yield and modulus determinations from strain data from a 1/8-inch SR-4 gage in weld fusion zone. Percent elongation in 2 inches.

(2) Yield and modulus determinations from strain data from a 1/2-inch, B-1 extensometer placed symmetrically across weld fusion zone. Percent elongation in 1/2-inch across weld fusion zone.

(3) All failures were in base metal except where noted otherwise.

TABLE XX
AXIAL FATIGUE LIFE OF Ti-6Al-4V ONE-INCH PLATE (MA) BASE METAL

SPECIMEN IDENT.	ORIENT.	MAXIMUM STRESS (KSI)	STRESS RATIO (R)	FREQUENCY (Hz)	CYCLES TO FAILURE
1-BM-T-0	T	146.1	0.1	4	3,773
1-BM-T-2	T	144.0	0.1	4	4,315
1-BM-T-6	T	139.2	0.1	8	10,862
1-BM-T-3	T	129.2	0.1	10	33,810
1-BM-T-8	T	120.0	0.1	12	208,330
1-BM-T-9	T	109.3	0.1	12	495,110
1-BM-T-4	T	103.6	0.1	20	783,460
1-BM-T-7	T	88.7	0.1	24	1,533,890
1-BM-T-5	T	80.0	0.1	24	5,148,100

TABLE XXI
AXIAL FATIGUE LIFE OF E. B. WELDED Ti-6Al-4V ONE-INCH PLATE

SPECIMEN IDENT.	ORIENT.	MAXIMUM STRESS (KSI)	STRESS RATIO (R)	FREQUENCY (Hz)	CYCLES TO FAILURE
1-W-T-3	T	169.7	0.1	-	1
1-W-T-4	T	161.1	0.1	8	930
1-W-T-11	T	152.8	0.1	8	4,296
1-W-T-6	T	144.3	0.1	8	10,002
1-W-T-7	T	135.8	0.1	10	31,625
1-W-T-2	T	127.2	0.1	15	184,540
1-W-T-5	T	118.7	0.1	18	303,430
1-W-T-10	T	110.3	0.1	24	128,110
1-W-T-1	T	100.2	0.1	22	377,470
1-W-T-9	T	79.9	0.1	24	1,313,790
1-W-T-8	T	65.0	0.1	30	7,070,650

TABLE XXII
ASTM E399-72 CRITERIA FOR A VALID PLANE STRAIN
FRACTURE TOUGHNESS RESULT

<u>Code</u>	<u>E399 Section</u>
a. a_c and $B \geq 2.5 (K_Q/F_{TY})^2$ -----	7.1.1
b. $0.45 \leq a/W \leq 0.55$ -----	7.2.1
c. $N \leq W/16$ -----	7.2.2
d. $(a_f - a_i) \geq 0.05 a_c$ or 0.05 in. -----	7.2.3
e. $K_{f \max}/E \leq 0.002 \text{ in.}^{1/2}$ -----	7.4.2
f. $K_{f \max} \leq 0.6 K_Q$ (last 0.025 a_c)-----	7.4.2
g. $\Delta K_f \geq 0.9 K_f$ -----	7.4.3
h. $K_{f \max T_1} \leq 0.6 (F_{TY T_1}/F_{TY T_2}) K_{Q T_2}$ -----	7.4.4
i. Size Tolerances-----	8.2
j. $ a_{1/4} - a_{1/2} , a_{1/4} - a_{3/4} , a_{1/2} - a_{3/4} \leq 0.05 a_c$ -----	8.2.3
k. $(a_{any} - a_o) \geq$ larger of 0.05 $a_{avg.}$ or 0.05 in. -----	8.2.3
l. a_l or $a_r \geq 0.9 a_{avg.}$ -----	8.2.3
m. $\theta \leq 10^0$ -----	8.2.4
n. $30 \text{ ksi-in}^{1/2}/\text{min.} \leq K/\Delta t \leq 150 \text{ ksi-in}^{1/2}$ -----	8.4
o. Alignment-----	8.4
p. $P_{max}/P_Q \leq 1.1$ -----	9.1.2

TABLE XXIII
FRACTURE TOUGHNESS OF Ti-6Al-4V TWO-INCH PLATE (MA) BASE METAL AT R. T.

SPECIMEN IDENT.	ORIENT.	SPECIMEN DIMENSIONS		$K_{I(\text{MAX})}$ (KSI-IN ^{1/2})	K_Q (KSI-IN ^{1/2})	K_{Ic} (KSI-IN ^{1/2})	$2.5(K_{Ic}/E_{TV})^2$ (IN)	ASTM E-399 VIOLATIONS
		THICK. (B) (IN)	CRACK LENGTH ($a_{(AVE)}$) (IN)					
1-4	T-L	2.002	2.038	19.7	98.7	98.7	1.54	-
3-1	T-L	2.002	2.048	19.9	105.5	105.5	1.76	-
4-2	T-L	2.002	2.097	20.7	112.4	112.4	2.00	-
		Average Values			105.5	105.5		
2-2	L-T	2.004	2.197	27.0	105.0	105.0	1.75	j
3-3	L-T	2.002	2.150	17.7	118.8	-	2.23	a, j
4-4	L-T	2.003	2.137	17.6	112.1	112.1	1.99	-
		Average Values			112.0	108.6		
4	S-L	0.835	0.810	25.3	83.0	-	1.07	a
5	S-L	0.836	0.820	26.6	88.6	-	1.22	a
7	S-L	0.834	0.797	25.5	96.0	-	1.43	a
6	S-L	0.837	0.880	29.7	84.2	-	1.10	a
		Average Values			88.			

TABLE XXIV

FRACTURE TOUGHNESS OF Ti-6Al-4V TWO-INCH PLATE (MA) BASE METAL AT -65° F

SPECIMEN IDENT.	ORIENT.	SPECIMEN DIMENSIONS		$K_{I(\max)}$ (KSI-IN ^{1/2})	K_Q (KSI-IN ^{1/2})	K_{Ic} (KSI-IN ^{1/2})	$2.5(K_{Ic}/F_{TY})^2$ (IN)	ASTM E-399 VIOLATIONS
		SPECIMEN THICK. (B) (IN)	CRACK LENGTH (a(AVE)) (IN)					
1-2	T-L	2.003	1.990	19.0	88.2	88.2	0.99	-
2-1	T-L	2.002	1.980	18.4	85.7	85.7	0.94	-
2-3	T-L	2.004	1.970	18.8	89.7	89.7	1.03	-
Average Values					87.9	87.9		

TABLE XXV

FRACTURE TOUGHNESS OF Ti-6Al-4V TWO-INCH PLATE (MA) BASE METAL AT 175° F

SPECIMEN IDENT.	ORIENT.	SPECIMEN DIMENSIONS		$K_{I(\max)}$ (KSI-IN ^{1/2})	K_Q (KSI-IN ^{1/2})	K_{Ic} (KSI-IN ^{1/2})	$2.5(K_{Ic}/E_{TV})^2$ (IN)	ASTM E-399 VIOLATIONS
		THICK. (B) (IN)	CRACK LENGTH (a(AVE)) (IN)					
1-3	T-L	2.004	2.103	20.8	117	-	2.58	a
2-4	T-L	2.002	1.993	19.0	118	-	2.63	a
3-4	T-L	2.002	2.053	20.0	116	-	2.54	a
Average Values					117			

TABLE XXVI

HEAT-AFFECTED ZONE FRACTURE TOUGHNESS OF E. B. WELDED Ti-6Al-4V TWO-INCH PLATE AT R. I.

SPECIMEN IDENT.	ORIENT.	SPECIMEN DIMENSIONS		K_{Ic} (KSI-IN ^{1/2})	K_Q (KSI-IN ^{1/2})	K_{Ic} (KSI-IN ^{1/2})	$2.5(K_{Ic}/E_v)^{1/2}$ (IN)	ASTM E-399 VIOLATIONS
		THICK. (B) (IN)	CRACK LENGTH ($a_{(AVE)}$) (IN)					
1-3	L-T	1.991	2.346	25.8	117.9	-	2.22	a, b, j & m
1-2	L-T	1.992	2.263	32.8	109.1	109.1	1.90	b, d, & k
1-1	L-T	1.990	1.920	28.4	126.6	-	2.56	a, d, j, k, l & m
	Average Values				117.9	109.1		
6	T-L	1.899	2.280	25.5	128.5	-	2.64	a, b, d, k, l & m
3	T-L	1.989	1.727	19.9	101.1	100.1	1.60	b, d, j
2	T-L	1.960	2.207	23.1	130.8	-	2.74	a, d, k, l & m
	Average Values				119.8	100.1		
1	S-L	0.836	0.893	30.4	99.3	-	1.57	a, l
2	S-L	0.836	1.000	51.0	78.5	-	0.986	a, b, e & m
3	S-L	0.836	0.913	31.4	89.4	-	1.28	a, l & m
	Average Values				89.1			

TABLE XXVII

HEAT-AFFECTED ZONE FRACTURE TOUGHNESS OF E. B. WELDED Ti-6Al-4V TWO-INCH PLATE AT -65° F

SPECIMEN IDENT.	ORIENT.	SPECIMEN DIMENSIONS		$K_{I(\max)}$ (KSI-IN ^{1/2})	K_Q (KSI-IN ^{1/2})	K_{Ic} (KSI-IN ^{1/2})	$2.5(K_{Ic}/E_{TV})^2$ (IN)	ASTM E-399 VIOLATIONS
		THICK. (B) (IN)	CRACK LENGTH (a _(AVE)) (IN)					
8	T-L	1.949	2.160	30.7	119	119	1.81	d, k, l & m
5	T-L	1.970	1.770	16.6	110	110	1.54	b, d, j, k & m
2	T-L	1.926	1.683	20.0	95	95	1.15	b, d, j, k & m
Average Values								108 108

TABLE XXVIII

HEAT-AFFECTED ZONE FRACTURE TOUGHNESS OF E. B. WELDED Ti-6Al-4V TWO-INCH PLATE AT 175°F

SPECIMEN IDENT.	ORIENT.	SPECIMEN DIMENSIONS		$K_{I(\max)}$ (KSI-IN ^{1/2})	K_Q (KSI-IN ^{1/2})	K_{Ic} (KSI-IN ^{1/2})	$2.5(K_{Ic}/F_{TY})^2$ (IN)	ASTM E-399 VIOLATIONS
		THICK. (B) (IN)	CRACK LENGTH ($a_{(AVE)}$) (IN)					
9	T-L	1.988	2.300	21.7	135	-	3.45	a, c, d, j, & l
7	T-L	1.958	2.100	21.2	150	-	4.25	a, k, & l
1	T-L	1.867	1.765	30.5	123	-	2.86	a, b, k & m
Average Values					136			

TABLE XXIX

WELD ZONE FRACTURE TOUGHNESS OF E. B. WELDED TI-6Al-4V TWO-INCH PLATE AT R. T.

SPECIMEN IDENT.	ORIENT.	SPECIMEN DIMENSIONS		$K_{Ic(max)}$ (KSI-IN ^{3/2})	K_Q (KSI-IN ^{1/2})	K_{Ic} (KSI-IN ^{1/2})	$2.5(K_{Ic}/E_{TV})^{1/2}$ (IN)	ASTM E-399 VIOLATIONS
		SPECIMEN THICK. (B) (IN)	CRACK LENGTH ($a_{(AVE)}$) (IN)					
4-3	T-L	1.994	2.327	25.3	91.7	91.7	1.35	b, & j
4-1	T-L	1.915	2.463	30.2	84.9	84.9	1.15	b, d, j & p
5-3	T-L	2.002	2.733	39.3	71.3	71.3	0.813	b, e & p
Average Values					82.6	82.6		

TABLE XXX

WELD ZONE FRACTURE TOUGHNESS OF E. B. WELDED T1-6Al-4V TWO-INCH PLATE AT -65° F

SPECIMEN IDENT.	ORIENT.	SPECIMEN DIMENSIONS		$K_{I(max)}$ (KSI-IN ^{1/2})	K_Q (KSI-IN ^{1/2})	K_{Ic} (KSI-IN ^{1/2})	$2.5(K_{Ic}/E_T)^{1/2}$ (IN)	ASTM E-399 VIOLATIONS
		THICK. (B) (IN)	CRACK LENGTH ($a_{(AVE)}$) (IN)					
3-4	T-L	2.001	2.700	37.8	66.1	66.1	0.557	b, e, l & p
4-4	T-L	2.002	2.380	24.2	88.0	88.0	0.988	b & l
3-2	T-L	1.980	2.233	32.2	125*	-	1.993	b, d, k, l & m
Average Values					93	77		

TABLE XXXI

WELD ZONE FRACTURE TOUGHNESS OF E. B. WELDED Ti-6Al-4V TWO-INCH PLATE AT 175° F

SPECIMEN IDENT.	ORIENT.	SPECIMEN DIMENSIONS		$K_{I(\max)}$ (KSI-IN ^{1/2})	K_Q (KSI-IN ^{1/2})	K_{Ic} (KSI-IN ^{1/2})	$2.5(K_{Ic}/E_{TV})^2$ (IN)	ASTM E-399 VIOLATIONS
		THICK. (B) (IN)	CRACK LENGTH (a _(AVE)) (IN)					

5-2	T-L	1.974	2.753	40.0	114.7	-	2.49	a, b, e, l & m
4-2	T-L	1.998	2.717	38.8	114.0	-	2.46	a, b, e & l
5-1	T-L	1.996	2.735	39.6	105.0	-	2.08	a, b, e, l & m

Average Values 111.2

TABLE XXXII

WELD ZONE FRACTURE TOUGHNESS OF E. B. WELDED TI-6Al-4V ONE-INCH PLATE AT R. T.

SPECIMEN IDENT.	ORIENT.	SPECIMEN THICK.	DIMENSIONS		$K_{I(\text{MAX})}$ (KSI-IN ^{1/2})	K_Q (KSI-IN ^{1/2})	K_{Ic} (KSI-IN ^{1/2})	$2.5(K_{Ic}/F_{TV})^2$ (IN)	ASTM E-399 VIOLATIONS
		(B) (IN)	CRACK LENGTH (a(AVE)) (IN)						

1	T-L	1.000	1.067	30.3	52	52	0.355	d, j, k & l
2	T-L	1.001	1.180	36.6	47.6	47.6	0.297	b, d, e, l & m

3	T-L	1.002	1.080	30.6	72.6	72.6	0.692	l
---	-----	-------	-------	------	------	------	-------	---

Average Values 57.4 57.4

TABLE XXXIII
FRACTURE TOUGHNESS OF BETA III TITANIUM ONE-INCH PLATE (STA) BASE METAL
AND E. B. WELDMENTS AT R. T.

SPECIMEN IDENT.	ORIENT.	SPECIMEN DIMENSIONS		$K_{I(\max)}$ (KSI-IN ^{1/2})	K_Q (KSI-IN ^{1/2})	K_{Ic} (KSI-IN ^{1/2})	$2.5(K_{Ic}/F_y)^2$ (IN)	ASTM E-399 VIOLATIONS
		THICK. (B) (IN)	CRACK LENGTH (a(AVE)) (IN)					
Base metal	T-L	1.005	0.977	25.9	85.7	85.7	0.666	-
	T-L	0.991	0.917	24.2	42.2	42.2	0.170	-
Heat-affected zone	T-L	0.996	0.930	24.9	76.3	76.3	0.555	-

TABLE XXXIV

WELD ZONE SINGLE-EDGE NOTCH FRACTURE TOUGHNESS OF E. B. WELDED Ti-6AL-4V

ONE-INCH PLATE AT R. T.

SPECIMEN IDENT.	ORIENT.	SPECIMEN DIMENSIONS			CRITICAL STRESS INTENSITIES			FRACTURE PATH
		THICK. (t) (IN)	WIDTH (W) (IN)	CRACK LENGTH (a) (IN)	K _{POPIN} (KSI-IN ^{1/2})	K _Q (KSI-IN ^{1/2})	K _{MAX} (KSI-IN ^{1/2})	
4	T-L	0.994	3.000	1.548	-	59.5	61.7	W _Q
6	T-L	0.935	3.000	1.548	-	55.3	58.4	W _Q
		Average Values				57.4	60.1	
9	T-L	0.504	5.014	1.730	64.2	67.6	81.3	B. M.
7	T-L	0.499	5.008	2.040	52.1	54.3	71.8	B. M.
12	T-L	0.505	5.014	2.190	59.9	59.9	80.5	B. M.
		Average Values				58.7	77.9	
6	T-L	0.250	4.804	1.520	71.0	71.0	90.7	B. M.
5	T-L	0.248	5.002	2.110	-	72.9	106.8	B. M.
1	T-L	0.242	4.999	2.530	-	78.7	101.4	B. M.
		Average Values				71.0	99.6	

TABLE XXXV

WELD ZONE SINGLE-EDGE NOTCH FRACTURE TOUGHNESS OF E. B. WELDED Ti-6AL-4V
ONE-INCH PLATE AT -65°F

SPECIMEN IDENT.	ORIENT.	SPECIMEN DIMENSIONS			CRITICAL STRESS INTENSITIES			FRACTURE PATH
		THICK. (t) (IN)	WIDTH (W) (IN)	CRACK LENGTH (a) (IN)	K _{POPIN} (KSI-IN ^{1/2})	K _Q (KSI-IN ^{1/2})	K _{MAX} (KSI-IN ^{1/2})	
2	T-L	0.979	3.009	1.740	42.3	42.3	42.3	W _Q
1	T-L	0.907	2.999	1.730	45.1	45.1	45.1	W _Q
3	T-L	0.958	2.999	1.750	-	53.3	54.0	W _Q
	Average Values				43.7	46.9	47.1	
8	T-L	0.497	5.006	2.010	-	61.7	70.9	B. M.
11	T-L	0.498	4.859	2.160	52.0	50.7	71.4	B. M.
10	T-L	0.499	5.012	2.540	53.2	51.9	65.3	B. M.
	Average Values				52.6	54.8	69.2	
3	T-L	0.259	4.995	1.750	48.6	48.6	48.6	B. M.
4	T-L	0.243	4.999	2.310	75.1	66.5	79.9	B. M.
2	T-L	0.255	4.997	3.040	-	47.7	76.9	B. M.
	Average Values				61.9	54.3	68.5	

TABLE XXXVI

WELD ZONE SINGLE-EDGE NOTCH FRACTURE TOUGHNESS OF E. B. WELDED BETA III TITANIUM
ONE-INCH PLATE AT R. T.

SPECIMEN IDENT.	ORIENT.	SPECIMEN DIMENSIONS			CRITICAL STRESS INTENSITIES			FRACTURE PATH
		THICK. (t) (IN)	WIDTH (W) (IN)	CRACK LENGTH (a) (IN)	K _{POPIN} (KSI-IN ^{3/2})	K _Q (KSI-IN ^{3/2})	K _{MAX} (KSI-IN ^{3/2})	

11	T-L	0.997	3.000	1.450	-	-	28.7	Broke in fatigue
3	T-L	0.504	4.998	2.160	77.0	78.9	79.4	WE & B.M.
1	T-L	0.254	4.999	2.510	41.8	43.8	47.2	WE

TABLE XXXVII

WELD ZONE SINGLE-EDGE NOTCH FRACTURE TOUGHNESS OF E. B. WELDED BETA III TITANIUM
ONE-INCH PLATE AT -65°F

SPECIMEN IDENT.	ORIENT.	SPECIMEN DIMENSIONS			CRITICAL STRESS INTENSITIES			FRACTURE PATH
		THICK. (t) (IN)	WIDTH (W) (IN)	CRACK LENGTH (a) (IN)	K _{POPIN} (KSI-IN ^{1/2})	K _Q (KSI-IN ^{1/2})	K _{MAX} (KSI-IN ^{1/2})	

10 T-L 0.985 3.000 1.510 29.6 29.6 29.6 W_Q

4 T-L 0.506 4.888 2.120 65.1 65.1 69.4 W_Q

2 T-L 0.266 4.973 2.440 28.1 28.1 29.9 W_Q

TABLE XXXVIII

PART-THROUGH THICKNESS FRACTURE TOUGHNESS OF TI-6AL-4V ONE-INCH PLATE BASE METAL
AND E. B. WELDMENTS AT R. T.

SPECIMEN IDENT.	CRACK LOCATION	SPECIMEN DIMENSIONS				FAILURE STRESS (σ_F) (KSI)	NET STRESS (σ_N) (KSI)	K_{IE} (KSI-IN ^{1/2})	VIOLATIONS*
		THICK. (t) (IN)	WIDTH (w) (IN)	DEPTH (a) (IN)	CRACK LENGTH (2c) (IN)				
1	HAZ	0.249	1.500	0.1345	0.2702	100.1	108.4	46.6	-
3	HAZ	0.251	1.499	0.1256	0.2557	122.3	131.0	56.0	(1.)
7	HAZ	0.250	1.506	0.1056	0.2443	127.5	134.8	57.3	(1.)
Average Values									
10	WZ	0.249	1.500	0.1156	0.2365	94.6	100.4	41.1	-
4	BM	0.251	1.500	0.1054	0.2624	127.5	135.3	59.3	(1.)

* CRITERIA FOR VALIDITY OF K_{IE} RESULTS:

1. $\sigma_N \leq 0.9 F_{TY}$
2. $2c \leq W/4$
3. $t-a \geq \pi/16 (K_{IE}/F_{TY})^2$

TABLE XXXIX

NATURAL DEFECT RESULTS

SPECIMEN IDENT.	THICKNESS (in.)	WIDTH (in.)	GROSS AREA (in. ²)	FLAWED AREA (in. ²)	FAILURE LOAD (kips)	GROSS FAILURE STRESS (ksi)	NET FAILURE STRESS (ksi)	COMMENTS
1	0.497	0.987	0.4905	0.3203	5.95	12.13	24.96	
2	0.510	0.987	0.5034	-----	-----	-----	-----	No Failure 90% of Yield
3	0.504	0.994	0.5001	-----	-----	-----	-----	No Failure 90% of Yield
4	0.499	0.999	0.4985	0.3585	11.45	22.97	104.1	
5	0.501	1.010	0.5060	0.3080	7.05	13.93	35.6	
6	0.508	1.007	0.5116	-----	-----	-----	-----	No Failure 90% of Yield

APPENDIX

DATA UTILIZATION FOR SPECIFICATION REVISIONS

1. GENERAL CONSIDERATIONS

MIL or NAS specifications for raw materials or weld accept/reject criteria do not incorporate fracture mechanics data as a measure of material quality or useful weld properties. Presently, there is no requirement for K_{IC} at any temperature for thick section titanium plate. The widely used weld accept/reject specification NAS-1514 does not recognize any crack tolerance in any class of weld.

Clearly, new criteria, based on the real behavior of actual material, including weldments, are needed. The type of fracture property and crack growth resistance data developed in this program can serve as the basis for formulating specification revisions that will rectify present inadequacy of the prevailing specifications.

It was originally intended to prepare such a revised specification on thick-section electron-beam welded Ti-6Al-4V alloy as an appendix to the report. For reasons that will become apparent, however, a standard that specifies a single allowable flaw size or range of flaw sizes for all intended applications of the weldment is as impractical as the original standard that fails to specify any allowable crack to any degree. Consequently, the steps required in utilizing the fracture data to formulate or draft a useful specification for any specific application are described in general terms in this appendix. Also presented are some incidental findings that may be of merit in revising some existing specifications.

2. BASE METAL

It is usually desirable to have titanium base metal with the best combination of yield strength and fracture toughness possible. Once it is shown that titanium base metal with a given minimum yield strength can attain a desired value of fracture toughness with some consistency, these values and the metallurgical factors that make them possible then can be adopted as standards.

Flaw tolerance of base-metal plate, although important, is less a concern than that of the weldments. This is chiefly so because the probability of potentially detrimental flaws in base-metal plate thicknesses of established alloys is quite low. In all likelihood, the size of structural discontinuities that may exist is beyond the inspectability limits of the more common methods of

nondestructive inspection (NDI). Consequently, in those infrequent situations where an NDI confirmation of a flaw is established, the plate should be rejected, or the material area surrounding the flaw should be excluded from further structural consideration.

a. Ti-6Al-4V

The results of the present program indicate the dominant role of microstructure in the flaw tolerance of a base metal of given chemical composition. An example is the fracture toughness superiority of the relatively isotropic microstructure in the 2-in. material over the crystallographically textured microstructure in the 1-in. plate. Since the main objective of this program did not deal with the evaluation of microstructural effects on flaw tolerance, sufficient data to base recommendations affecting metallurgical specifications of Ti-6Al-4V base metal are lacking.

b. Beta III Titanium

Because of its limited utilization to date, Beta III titanium in thick-section plate has not had the opportunity to establish a record of structural consistency. During ultrasonic inspection of this material, it appeared to be very "noisy". Apparently, density variations - due possibly to incomplete homogenization of the microstructure during processing - cause an excessive amount of ultrasonic scattering. At times, these anomalous reflections of ultrasonic energy are sufficient to feign the presence of unacceptable flaw-like defects. As a result of this characteristic and its lack of an established reputation, 100 percent radiographic inspection of Beta III titanium should be mandatory prior to any thick-section airframe structural application.

3. WELDMENTS

Flaws and defects are not uncommon occurrences in weldments even in the most carefully performed welding operations. Much of the data necessary to show the influence of these flaws and defects on the structural properties of thick-section, electron-beam welded titanium were generated in this program. Properly utilized, these data can lead to determination of the largest possible initial flaw size an electron-beam welded service structure can tolerate without its planned lifetime being affected. Once determined, this flaw size can serve to formulate an accept/reject NDI inspection criteria and set a basis for quality control of the weldments.

The guaranteed safe-life operation of any airframe structure will depend upon the implementation of a reliable fracture control plan in which the weldment specification must assume an integral and important role.

a. Ti-6Al-4V

From the test data produced in this program - particularly the spectrum

fatigue results - it can be shown that the largest initial flaw size a weldment can tolerate depends primarily upon the intended application. For instance, a highly stressed but statically loaded weldment can successfully endure a much larger flaw than a structure subject to cyclic stresses of much lower amplitude. Also, a flaw of a given size in a fatigue-loaded weldment will fail sooner in a salt-water environment than in air. A similar situation will prevail in statically loaded structures if the combination of sustained stress and flaw size exceeds the threshold combination. As is obvious from these unsophisticated examples, specifying a solitary crack size or even a range of crack sizes for every intended application or type of application is not feasible. Revision of the existing standards to account for the presence of cracks requires specification of different tolerable crack sizes for each intended application of the weldment.

One of the methods for determining the allowable crack size in a structure is illustrated in Figure 79. Here the intended application of the weldment would be a given number of blocks or, that is, flights. The prediction curves show the relationship between allowable initial flaw sizes and the number of flights. Also, other more detailed procedures are available and can be employed to determine the tolerable flaw size (13, 14, 15). Although these references are concerned with structures other than airframes, the procedures are general and can be applied to any structural component. Essential to the meaningful determination of an allowable initial crack size - in conjunction with the flaw behavior data - is the reliable knowledge of the intended operating loads, temperatures, and environments of the electron-beam welded component.

For the more general case, where the understanding of the operating conditions is qualitative, conservative estimates of the allowable flaw sizes are possible. These estimates can be derived from the integration of the equation or equations describing fatigue crack growth. The integrated crack growth equations permit the calculation of the initial flaw size required to grow the crack to a specified size in a given number of cycles. Two examples, one for an inert service environment, e.g., air or JP4, and the other for an environment of 3.5 percent salt water, are shown in Figures A-1 and A-2.

For conservative estimates of the allowable flaw size, the endurance limit stress, i.e., extrapolated S-N stress at 10^7 cycles in Figure 31, and a stress ratio of zero were used in the calculations. In the examples, the criteria for failure were the critical stress intensity value in Figure A-1 and the threshold stress intensity value in Figure A-2.

In the log-log data plots of Figures 39, 40, 45, and 47, straight line relationships of the form

$$da/dN = C \Delta K^n \quad (A-1)$$

were used to represent crack growth. Three of the four test conditions ex-

hibited in these figures required more than one straight line segment for an adequate da/dN description. The constant, C, and the exponent, n, for each set of data and for each curve segment within the set are presented in Tables A-I and A-II.

The general form of the equation relating applied cyclic stress, crack size, and stress intensity for the most logical crack configuration, i.e., surface flaw, is

$$K = \sigma \sqrt{a\pi s} \quad (A-2)$$

where $a = 1.2/Q$ to give the Irwin relationship. The parameter, Q, equals $[\phi^2 - 0.212 (\sigma/F_{TY})^2]$ and ϕ^2 is 2.46 for a semicircular flaw.

When $R = 0$, the equation (A-1) becomes

$$da/dN = CK^n \quad (A-3)$$

Substituting equation (A-2) into equation (A-3) and letting k equal σ/F_{TY} , then

$$da/dN = Ck^n F_{TY}^n (a\pi)^{n/2} a^{n/2} \quad (A-4)$$

Integration of equation (A-4)

$$\int_{a_1}^{a_2} a^{-n/2} da = Ck^n F_{TY}^n (a\pi)^{n/2} \int_{N_1}^{N_2} dN \quad (A-5)$$

between the initial crack size, a_1 , at N_1 cycles and the new crack size, a_2 , at N_2 cycles can lead to the following convenient expression for the required number of cycles to grow a crack from one value of stress intensity to another

$$\Delta N = \frac{2 \left[(K_I)_2 / F_{TY} \right]^2}{(n-2) C k^2 a \pi (K_I)_2^n} \left\{ \left[\frac{(K_I)_2}{(K_I)_1} \right]^{n-2} - 1 \right\} \quad n \neq 2 \quad (A-6)$$

Also included in Figures A-1 and A-2 are the qualitative estimates of the probability of detecting all of the flaws in the size ranges indicated by the current state-of-the-art production NDI techniques. This type of representation serves to illustrate the shortcoming of a specification that permits no flaws. Chance detection of a flaw in the size range where the probability of detection is low and its subsequent repair results in unwarranted expense and enhances the possibility of the cure having a more detrimental effect on performance than the original flaw.

b. Beta III Titanium

The test results indicate that Beta III titanium should not be joined by electron-beam welding until some procedures can be developed to produce a more desirable fusion zone microstructure.

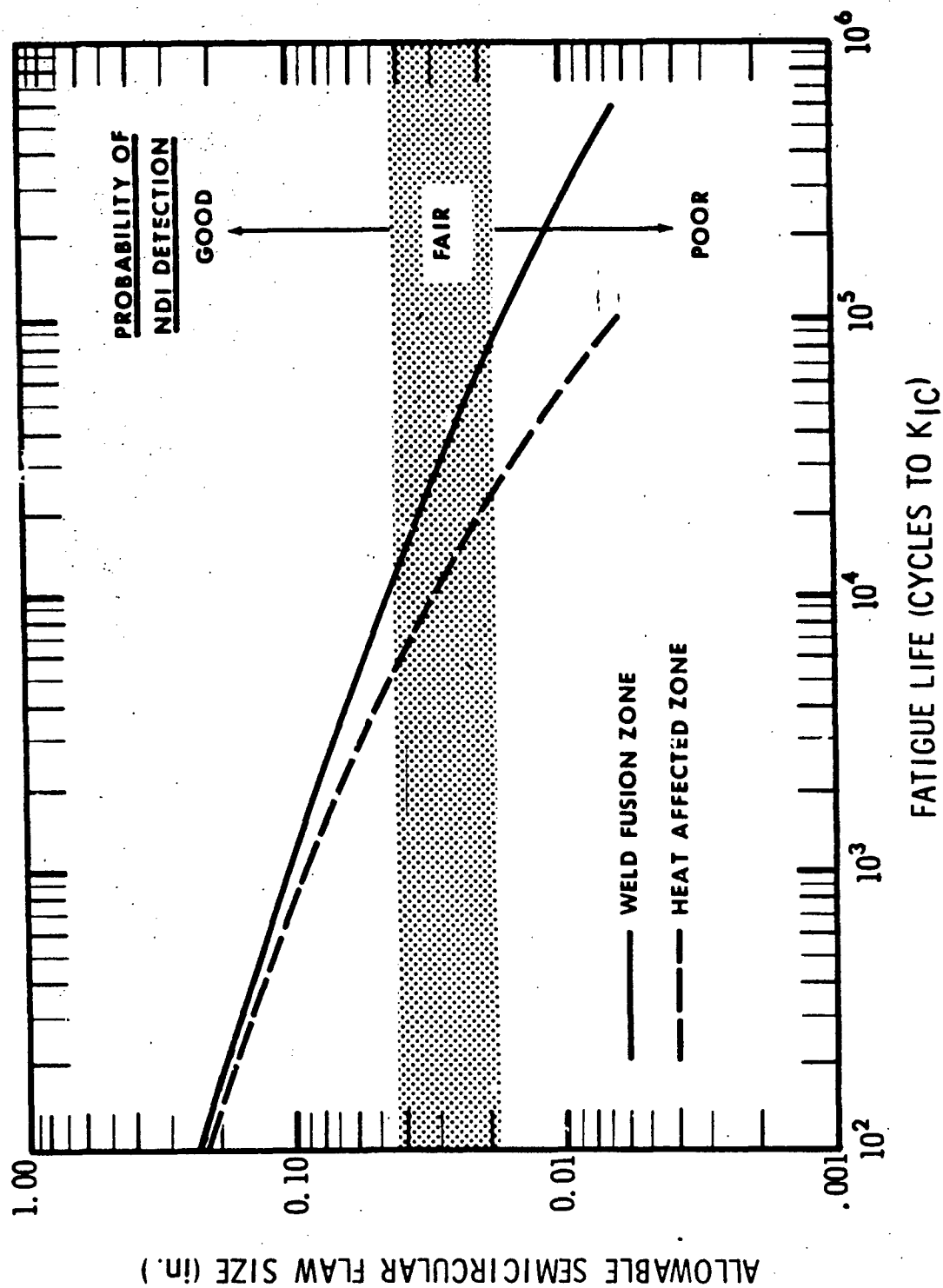


Figure A-1 Allowable Flaw Sizes in 1-in. Thick Ti-6Al-4V E. B. Weldments for Inert Service Environments

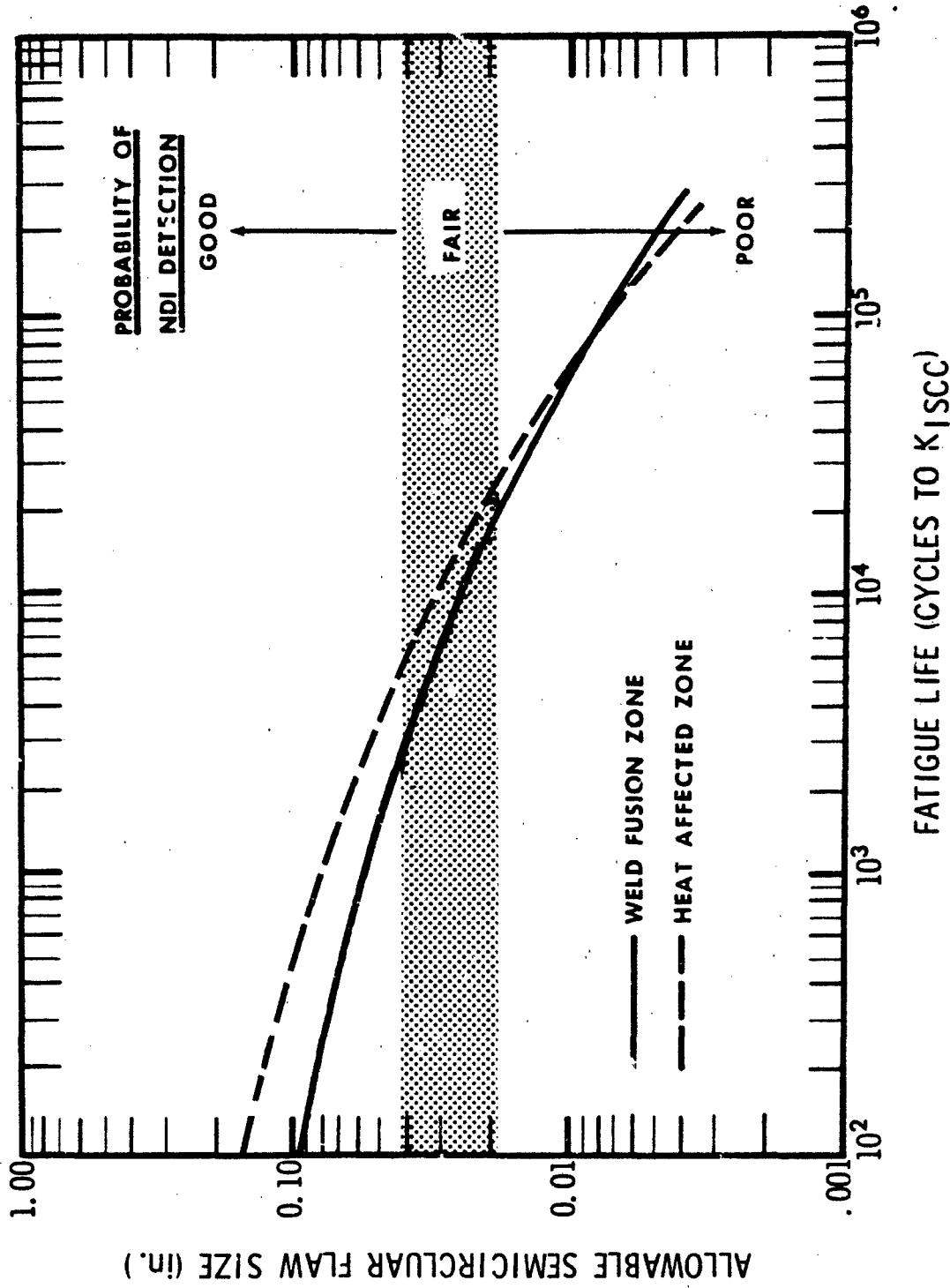


Figure A-2 Allowable Flaw Sizes in 1-in. Thick Ti-6Al-4V E. B. Weldments for a Service Environment of 3.5 Percent NaCl

TABLE A-1

FATIGUE CRACK GROWTH PARAMETERS IN INERT ENVIRONMENTS

General Crack Growth Equation

$$da/dN = C \Delta K^n; \text{ For } R = 0, da/dN = C K^n$$

MATERIAL:

Ti-6Al-4V Heat-Affected Zone (From Figure 39)

From 10 ksi-in^{1/2} to 57 ksi-in^{1/2} (K_{IC})

$$n = 5.106$$

$$C = 1.093 \times 10^{-27} (\text{in.}^{3/2}/\text{lb})^n \text{ in./cycle}$$

Ti-6Al-4V Weld Fusion Zone (From Figure 45)

Curve Segment #1

From 10 ksi-in^{1/2} to 30 ksi-in^{1/2}

$$n = 5.166$$

$$C = 5.1946 \times 10^{-28} (\text{in.}^{3/2}/\text{lb})^n \text{ in./cycle}$$

Curve Segment #2

From 30 ksi-in^{1/2} to 57 ksi-in^{1/2} (K_{IC})

$$n = 9.3346$$

$$C = 1.1297 \times 10^{-46} (\text{in.}^{3/2}/\text{lb})^n \text{ in./cycle}$$

TABLE A-II

FATIGUE CRACK GROWTH PARAMETERS
IN 3.5 PERCENT NaCl SOLUTION

General Crack Growth Equation

$$da/dN = C \Delta K^n; \text{ For } R = 0, \quad da/dN = C K^n$$

MATERIAL:

Ti-6Al-4V - Heat-Affected Zone (From Figure 40)

Curve Segment #1 - From 10 ksi-in.^{1/2} to 29 ksi-in.^{1/2}

$$n = 5.208$$

$$C = 3.68078 \times 10^{-28} (\text{in.}^{3/2}/\text{lb})^n \text{ in./cycle}$$

Curve Segment #2 - From 29 ksi-in.^{1/2} to 33 ksi-in.^{1/2}

$$K_{ISCC} = 33 \text{ ksi-in.}^{1/2}$$

$$n = 19.0467$$

$$C = 6.4896 \times 10^{-90} (\text{in.}^{3/2}/\text{lb})^n \text{ in./cycle}$$

Ti-6Al-4V - Weld Fusion Zone (From Figure 47)

Curve Segment #1 - From 10 ksi-in.^{1/2} to 20.5 ksi-in.^{1/2}

$$n = 5.235$$

$$C = 3.215 \times 10^{-28} (\text{in.}^{3/2}/\text{lb})^n \text{ in./cycle}$$

Curve Segment #2 - From 20.5 ksi-in.^{1/2} to 28 ksi-in.^{1/2}

$$n = 16.566$$

$$C = 4.473 \times 10^{-77} (\text{in.}^{3/2}/\text{lb})^n \text{ in./cycle}$$

Curve Segment #3 - From 28 ksi-in.^{1/2} to 36 ksi-in.^{1/2}

$$K_{ISCC} = 36 \text{ ksi-in.}^{1/2}$$

$$n = 5.031$$

$$C = 8.884 \times 10^{-26} (\text{in.}^{3/2}/\text{lb})^n \text{ in./cycle}$$